

Decellularised extracellular matrices as instructive microenvironments for bone marrow derived stem cells

DISSERTATION

Zur Erlangung des Akademischen Grades

Doctor rerum naturalium

(Dr. rer. nat.)

vorgelegt

der Fakultät Mathematik und Naturwissenschaften

der Technischen Universität Dresden

von

M.Sc., Marina Prewitz

geboren am 29.04.1983 in Räckelwitz

Eingereicht am 29.07.2011

Die Dissertation wurde in der Zeit von August 2007 bis Juli 2011

am Leibniz-Institut für Polymerforschung Dresden e.V.,

am Max Bergmann Zentrum für Biomaterialien

angefertigt.

Contents

Danksagung	III
Abstract	V
Nomenclature	VI
1 Introduction	1
1.1 Motivation	1
1.2 Objective	4
2 Fundamentals	7
2.1 The extracellular matrix as biological scaffold	7
2.1.1 Structure and composition	7
2.1.2 Function and regulatory cues	11
2.2 Bone marrow residing stem cells	14
2.2.1 Mesenchymal and haematopoietic stem and progenitor cells	14
2.2.2 Microenvironments and niches	17
2.3 Stem cell bioengineering - current concepts	20
2.4 Decellularisation - creating native ECM environments	23
2.4.1 Decellularisation of tissues and organs	25
2.4.2 Decellularised cell cultures	27
3 Materials and Methods	31
3.1 Surface preparation	31
3.1.1 Polymer functionalised surfaces	31
3.1.2 Immobilisation of bioactive molecules to polymer supports	32
3.1.3 Decellularised extracellular matrix substrates	33
3.2 Cell culture	35
3.2.1 Mesenchymal stromal cell isolation and culture	35

3.2.2	Hematopoietic stem and progenitor cell isolation and culture	38
3.3	Proteomic analysis of extracellular matrices	41
3.3.1	Protein extraction	41
3.3.2	Protein separation and mass spectrometry	42
3.4	Microscopy techniques	43
4	Results and Discussion	47
4.1	Human bone marrow analysis	47
4.2	Stromal cell-generated decellularised matrices	50
4.2.1	Stabilisation of MSC-secreted ECM	50
4.2.2	Characteristics of decellularised matrices	55
4.3	Proteomic composition of ECM substrates	60
4.4	Decellularised matrices as artificial <i>in vitro</i> niches	68
4.4.1	MSC culture on ECM substrates	68
4.4.2	HSPC culture on ECM substrates	80
5	General Discussion	87
5.1	Summary and conclusions	87
5.2	Outlook	96
	Bibliography	105
A	Full list of MS-identified proteins	125
	Selbstständigkeitserklärung	143

Danksagung

Die vorliegende Dissertation wurde am Leibniz-Institut für Polymerforschung Dresden e.V. in der Arbeitsgruppe Biofunktionelle Polymermaterialien am Max Bergmann Zentrum für Biomaterialien angefertigt.

Ganz herzlich bedanken möchte ich mich bei Prof. Dr. Carsten Werner für die Aufnahme in seine Forschungsgruppe und für seine wissenschaftliche Unterstützung und Förderung während der Anfertigung dieser Promotion. Für die vielen motivierenden und kritischen Gespräche und für sein stetes Interesse am Fortgang dieser Arbeit bin ich ihm sehr dankbar. Ich habe das freundschaftliche und konstruktive Arbeitsklima in seiner Gruppe sehr genossen.

Mein weiterer Dank gilt Prof. Dr. Martin Bornhäuser für seine freundliche Betreuung und seine hilfreichen Hinweise während der Anfertigung dieser Arbeit, sowie für seine außerordentliche Unterstützung bei der Bereitstellung von humanem Spendermaterial für die Durchführung der hier gezeigten Untersuchungen.

Ganz besonders möchte ich mich bei Dr. Philipp Seib für seine fachliche, instruktive und freundschaftliche Betreuung bedanken. Seine stete Unterstützung und seine hilfreichen Hinweise und Kommentare sowie kritische Diskussionen haben den Fortschritt dieser Arbeit in hohem Maße unterstützt.

Ich danke der 'Dresden International Graduate School for Biomedicine and Bioengineering' (DIGS-BB) für die Möglichkeit der Teilnahme an weiterführenden Kursen und Lehrveranstaltungen im Rahmen dieses Programmes, und für die Organisation des 'Thesis Advisory Committee' bestehend aus Prof. Carsten Werner, Prof. Martin Bornhäuser und Dr. Konstantinos Anastassiadis. Allen Mitgliedern dieses Komitees möchte ich danken für ihre hilfreichen Kommentare und für die kritischen Hinweise während des Verlaufs dieser Promotion.

Ich bedanke mich bei Prof. Dr. Tilo Pompe, Dr. Uwe Freudenberg für ihre kritischen und fachlichen Anregungen und ihren technischen Beitrag an dieser Arbeit. Den Kollegen und Mitarbeitern des Forschungsbereiches Biofunktionelle Polymermaterialien danke ich für die gute Zusammenarbeit und ihre Unterstützung beim Entstehen dieser Arbeit. Insbesondere danke ich Martina Franke, Juliane Drichel und Kati Mittasch für ihre Hilfe bei Zellkulturversuchen und deren Vorbereitung, bei Andrea Zieris und Silvana Prockop für die Hilfe bei der Durchführung von ELISA Analysen, bei Ina Kurth und Manfred Maitz für die Einführung in die Durchflussszytometrie und bei den Praktikanten Katrin Taetz und Monique Marx für ihre Unterstützung beim Fortschritt dieser Arbeit. An dieser Stelle möchte ich mich auch ganz herzlich bei Aline Stifel bedanken für die tatkräftige und unermüdliche Unterstützung bei der Vorbereitung von Zellkulturversuchen und hunderten von Polymerträgern.

Ich danke Armin Springer für die Unterstützung bei der Probenvorbereitung und für die fachkundige Einweisung in die Elektronenmikroskopie. Ich danke Jean-Marc Verbavatz (MPI-CBG, Electron Microscopy Facility) für die Durchführung der Transmissionselektronenmikroskopie. Bei Dr. Jens Friedrichs möchte ich mich für die hilfreiche und fachliche Durchführung der raster-

kraftmikroskopischen Messungen bedanken. Weiterhin danke ich den Kollaboratoren Prof. Dr. Bernard Hoflack, Christian Niehage und Steffi Lenhard am Biotechnologischen Zentrum der TUD für die Durchführung der Massenspektrometrie und die Bereitstellung der Daten.

Dank gilt auch den Mitarbeitern der Arbeitsgruppe um Prof. Martin Bornhäuser am Medizinisch Theoretischen Zentrum (MTZ) der TUD. Hier möchte ich mich besonders bei Katrin Müller bedanken, für die Vorbereitung und Bereitstellung von MSC-Spendermaterial und für die Unterstützung bei Zellversuchen und deren Auswertung. Weiterhin möchte ich mich bei Fernando Fierro, Manja Wobus, Duohui Jing und Regina Duryagina für kritische Diskussionen und hilfreiche technische Hinweise bedanken.

Für die angenehme Arbeitsatmosphäre und für die darüber hinaus sehr freundschaftliche Unterstützung auch während der schwierigen Zeiten im Verlauf dieser Arbeit möchte ich mich bei Babette Lanfer, Katja Schneider, David Sebing, Andreas Ofenbauer, Marion Fischer, Uwe Freudenberg, Lars Renner und Philipp Seib bedanken.

Abschließend möchte ich mich bei meiner Familie bedanken. Ganz besonderer Dank gilt meiner Mutter Kerstin Schichtel gemeinsam mit Wolfgang Schichtel und meiner Schwester Katrin Tuazon, für ihre liebevolle Unterstützung und Motivation während der Anfertigung dieser Arbeit. Bei meinen Freunden Denise Stenzel, Eva Pollmer, Christiane Menzfeld, Nicole Gensch, Matthias Pinkert, Janine Thiele, André Tschentscher, Kristin Dürschke, Danielle Borg und Maria Grazia Magro bedanke ich mich für unzählige herzliche gemeinsame Stunden und für die vielen aufbauenden Gespräche und ihr Verständnis für manche Ausnahmesituation im Verlauf der letzten 4 Jahre.

Abstract

The regenerative potential of adult stem cell populations within the human body bears great promises for their use in regenerative medicine. The bone marrow (BM) harbours two different types of adult stem cells, haematopoietic stem and progenitor cells (HSPCs) and multipotent mesenchymal stromal cells (MSCs), which are tightly regulated in their distinct anatomically defined niches by multiple cues such as cytokines, cell-cell contacts, the extracellular matrix (ECM) and the physical microenvironment. The *ex vivo* expansion of these cells for applications in regenerative therapies is of great interest and several biomaterial approaches attempt to mimic the natural BM niche and its components to control stem cell maintenance and differentiation. However, as of now the complexity of such stem cell niches is hard to recapitulate. Towards this goal, this work was focussing on the ECM environment of BM stem cells and was set out to engineer improved *in vitro* culture systems. MSC themselves are one of the most important cell types within the BM that secrete and construct ECM-networks and thereby shape the microenvironment of the residing cells. The potential of primary human BM-MSC to secrete ECM *in vitro* has been exploited to generate niche-like ECM surrogates in a robust and versatile format. Application of decellularisation regimes allowed the fabrication of complex matrices which demonstrated suprastructural, compositional and physicochemical properties comparable to those of the native BM-ECM environment. Reliable stability and reproducibility was achieved by a dedicated procedure of maleic anhydride co-polymer-mediated covalent binding of fibronectin and subsequent anchorage of cell-secreted ECM molecules. As a result of the high reproducibility, a complete proteomic register of ECM molecules was obtained in combination with determining the complex fibrillar and soft gel-like characteristics of MSC-derived matrices. Based on the established BM niche-like substrate, the impact of extracellular matrices on MSC and HSPC *ex vivo* behavior has been explored. Both cell types demonstrated strong adhesion to ECM substrates and depicted a changed cellular morphology upon contact with native ECM structures compared to standard culture substrates or simple ECM protein coatings, indicating an intense interplay between the cell and the microenvironment. MSC that re-grew into their own matrices have shown advantageous proliferation and cytokine secretion levels as well as enhanced differentiation intensity (upon differentiation induction) compared to MSC that were cultured on less complex substrates. Similarly, HSPC were also instructed for enhanced expansion on MSC-derived matrices without exhaustion of stem cell-marker expressing progenitor cells. The efficiency of these matrices was related to their ability to mimic the native composite suprastructure, ligand nano-topography, molecular composition and physical properties of natural BM ECM environments. The data obtained within this thesis set the ground for a more rational design of artificial stem cell niches with defined and distinct properties, offering exciting options for the in-depth analysis and understanding of stem cell regulation by exogenous cues.

Nomenclature

2D	Two-dimensional
3D	Three-dimensional
aaECM	Ascorbic acid-stimulated extracellular matrix
Ang-1	Angiopoietin-1
CPD	Cumulative population doublings
ECM	Extracellular Matrix
ERK/MAPK	Extracellular Matrix Related Kinase / Mitogen Activated Protein Kinase
FAK	Fokal Adhesion Kinase
FBS	Fetal Bovine Serum
Flt-3	FMS-Related Tyrosine Kinase-3
GAG	Glycosaminoglycan
G-CSF	Granulocyte-colony stimulating factor
HSA	Human Serum Albumin
HSC	Haematopoietic Stem Cells
HSPC	Haematopoietic Stem and Progenitor Cells
HSPG	Heparan Sulfate Proteoglycans
IL	Interleukin
MDM	MSC-Derived Extracellular Matrices
MMP	Matrix Metalloproteinase
MNC	Mononuclear Cells
MS	Mass Spectrometry
MSC	Mesenchymal Stem Cells
osteoECM	osteogenic-induced extracellular matrix
PBS	Phosphate Buffered Saline
PEG	Poly(ethylene glycol)
PI3-K	Phosphatidylinositol 3-Kinase
POMA	Poly(octadecene <i>alt</i> maleic anhydride)
PTP	Plasma-Treated Polystyrene (Tissue Culture Plastic)
RGD	Arginine-Glycine-Aspartate
SCF	Stem Cell Factor
SDF-1	Stromal Cell-Derived Factor -1
SEM	Scanning Electron Microscopy
Tpo	Thrombopoietin

Chapter 1

Introduction

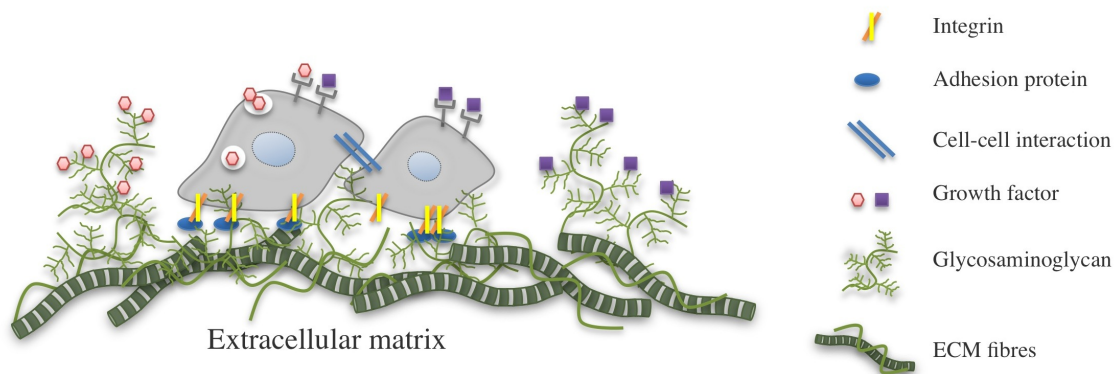
1.1 Motivation

Increasing demand for the treatment of tissue loss and organ failure following traumatic, degenerative or malignant destruction is a major concern of today's health care systems. The traditional treatment for tissue reconstruction is autologous or allogeneic harvest of a variety of tissues or organs from a healthy donor site and transplantation into the diseased patient (e.g. kidney or bone marrow transplants) [1]. Implantation of mechanical devices such as heart valves, stents or prostheses are a practicable alternative [2]. However, the lack of organ-donor availability and complications such as graft-rejection, donor site morbidity, and the risk of implant infection or thromboembolism are major limitations. Regenerative medicine offers a different direction of new therapeutic strategies, which have the potential to overcome these limitations of classical reconstruction and transplantation therapies.

Regenerative medicine is an interdisciplinary field of stem cell biology, bioengineering, tissue engineering and cellular therapies which aims at the development of biological substitutes that are able to restore, maintain or improve tissue and organ function [3]. Combined principles of life sciences and engineering are applied to develop *in vivo* and *ex vivo* cellular treatments involving genetic manipulation, molecular and pharmaceutical treatment, and seeding cells onto functionalised and 3-dimensional scaffolding materials. The possibilities within the field of regenerative medicine lead to high aspirations for current biomedical research. Research strategies include endogenous regeneration of degenerated tissues by means of gene therapy or cell transplantation, but also more complex strategies such as complete replacement and reconstruction of disfunctional or damaged tissues by application of fabricated tissue engineering constructs [3]. However, the required specialised and functional cell types can mostly not be harvested from the diseased organ or are not available in sufficient numbers to mediate regenerative efforts. New approaches make use of the body's endogenous system of regeneration and repair via stem and progenitor cells. These cells can be found in almost every type of tissue and they are a valuable cell source with the capacity for self-renewal and differentiation into various specialised lineages [4]. Within the last decade, research has put a lot of effort

into the establishment of regenerative therapies that use the potential of embryonic and adult stem cells to generate replacement tissues or to improve tissue function. Despite their widespread potential and steady progress towards clinical use, a major drawback is the difficulty to increase tissue-specific stem cell numbers without loss of stem cell potential and to control stem cell fate towards a specialised and functional cell type of interest. This is in contrast with the *in vivo* potential of those cells, where they exhibit extensive self-renewal capacity and facilitate the offspring of numerous mature cells throughout the lifetime of an individual. The general concept behind this phenomenon is the idea that adult stem cells reside in specialised microenvironments - so called niches - that coordinate self-renewal (the process of cell division that creates two identical stem cell type daughter cells without differentiation) and initiation of differentiation (the process of altering the cells genotype causing specialisation towards a mature cell type). Microenvironments regulate growth, self-renewal and cell-fate by an interplay of four signalling sources, namely (i) soluble growth factors, (ii) cell-cell interactions, (iii) insoluble extracellular matrices and (iv) environmental stress and physical cues [5]. Importantly the combined interplay between all these signalling sources is pivotal to the efficient and correct stimulation of cellular response and regulates proliferation, migration, survival, self-renewal and differentiation. A fundamental unit that controls this interplay is the extracellular matrix (ECM), which builds up a 3-dimentional scaffold for directed cell-cell interaction and spatial presentation of soluble growth factors and adhesion ligands, as represented in figure 1.1.1.

Figure 1.1.1: The extracellular matrix provides an instructive microenvironment



Fibrous structures of the ECM provide topographical features and trigger morphogenesis. Incorporated adhesion molecules (for example fibronectin and laminin) contain recognition sequences to interact with transmembrane integrin receptors of the cell to activate intracellular signalling pathways, which regulate cellular behaviour. Glycosaminoglycans (such as hyaluronic acid and heparan sulphate) serve as a depot for soluble growth factors and cytokines and aid their functional presentation. Graphic adapted from [6].

Today's most successful clinical application of stem cell therapies is the use of bone marrow stem cells for the treatment of haematological disorders, malignancies and bone defects [7, 8]. The human bone marrow harbours two types of adult stem cells, namely multipotent mesenchymal

stromal cells (MSC) and haematopoietic stem cells (HSC). Both cell types offer an enormous regenerative potential and are tightly regulated in their distinct anatomically defined niches [9]. Bone marrow niches are the most intensely studied stem cell microenvironments [10, 11]. To pursue the advanced use of bone marrow stem cells in regenerative medicine, the availability of *ex vivo* expanded or pre-differentiated cells would be enormously beneficial, but implies a detailed control of stem cell behaviour. Intrinsic to the therapeutic stem cell concept is the field of stem cell bioengineering. This “endeavor focusses on quantitative description of stem cell fate processes and the use of this information for the development of clinically and industrially relevant cell-based technologies” [12]. Therefore, the study of microenvironmental conditions for the control of stem cell behaviour is one critical step towards controlled manipulation of cells outside and inside the human body. As it was mentioned above, the extracellular matrix is the native surrounding of cells and serves as a guiding structure for cellular regulation and tissue development. The mimicry of extracellular matrix properties of the microenvironment is the gold standard for biomaterials approaches in regenerative stem cell biology [13].

Biologic and artificial materials have been used to create tissue engineering substrates that mimic ECM components and control stem cell fate [14, 15, 16]. These approaches include (i) the use of synthetic components without the addition of bioactive components, (ii) biopolymer based strategies using native ECM components (iii) biohybrid systems with combined synthetic and biomolecular components and (iv) biohybrid systems that use synthetic materials in combination with bioactive sequences. Conventional synthetic materials like nylon meshes, silicone scaffolds, or poly(ethyleneglycol) gels have the advantage to create highly reproducible scaffolds with control over the materials properties, but they allow only little control over cell behaviour and lack biological activity. Biopolymer based approaches facilitate isolated or recombinant components of the extracellular matrix and have been used to create extracellular microenvironments by immobilisation of single or combinatorial ECM molecules or for example by reconstitution of natural collagen assemblies. Materials with dual character combine synthetic substances with incorporated biomolecular functionalities to mimic structural and functional aspects of the natural ECM in conjunction with stimulation of cellular receptors. For example, cellular recognition sequences or receptor binding domains, growth factors and signalling ligands, enzyme sensitive peptides and glycosaminoglycans are incorporated into synthetic polymers such as poly(ethylen glycol) [17]. Such materials that are designed to mimic the stem cell niche and control stem cell behaviour have been able to directly link extracellular cues to a cellular response [18].

Although a lot of engineering effort is put towards mimicking the natural environment these materials can not compete yet with the ability of biologically derived materials in terms of a wholistic cellular stimulation and structural guidance. The natural ECM environment comprises a complex anisotropic topography with integrated adhesion and recognition sites for directed cellular regulation. Furthermore they are susceptible to cellular proteolytic degradation and remodelling of the growing tissue. Most realistic similarities in ECM composition, microstructure and biomechanical properties have been conducted with decellularised extra-

cellular matrix products. These have the ability to most naturally reconstitute a functional tissue environment. Advantageous is the possible use of allogeneic or even xenogenic decellularised donor material, which can be seeded with autologous cells and omits the need for immuno-suppression post transplantation [19]. Next to the use of decellularised organs also decellularised *in vitro* cultures have become more and more interesting for the study of cellular behaviour in a native 3-dimensional environment. Cell-generated decellularised matrices have been used to analyse the regulation of stem cell functions. For example, embryonic stem cells that are routinely cultured together with a layer of feeder cells have been cultured on matrices derived from embryonic fibroblasts. Human embryonic stem cells could be maintained in a self-renewing and pluripotent state when they were cultured on these matrices [20]. This demonstrates the power of decellularised matrix substrates for the culture and expansion of stem cells *ex vivo* and for the detailed analysis of stemness maintaining conditions. Importantly, the composition and character of the extracellular microenvironment is characteristic for each tissue specific ECM and demands the generation of tissue-specific extracellular matrices to mimic particular stem cell niches [19].

For a better understanding of the regulatory interplay between the extracellular matrix of the bone marrow niche and the residing stem cells a culture system needs to be established and characterised that closely resembles the native microenvironment. As it was mentioned above, decellularised matrices of tissues, organs and cultured cells have the highest potential to resemble native ECM environments. The concept of decellularisation has been used successfully for the creation of tissue engineering scaffolds for medical applications, but also for the creation of cell-type specific cell culture substrates that resemble tissue-specific ECM compositions. MSC and their differentiated progeny of the bone marrow have been used to create decellularised ECM coatings for implant materials, or to enhance differentiation into the osteogenic lineage [21, 22]. However, the use of MSC-generated ECM for the creation of a stem cell niche that can promote self-renewal and expansion of primitive progenitors for both bone marrow stem cell types - MSC and HSPC - still remains an open challenge. Furthermore, the creation of stable, reproducible matrices made by bone marrow MSC, which can be analysed for all their constituents and physicochemical characteristics would serve a great advancement for the study of stem cell behaviour within their niches.

1.2 Objective

The niche of multipotent mesenchymal and haematopoietic stem and progenitor cells (MSC and HSPC) is regulated by close interaction with the extracellular matrix. To generate extracellular matrices that resemble the bone marrow environment the idea was to use MSC themselves, since they are known to be major regulators of the niche and produce large amounts of ECM within the marrow cavities [23, 24]. The aim of this study was to generate naturally derived ECM scaffolds and utilise them as a versatile stem cell culture substrate. The matrices should be prepared in a way that their complex molecular composition could be analysed in detail and

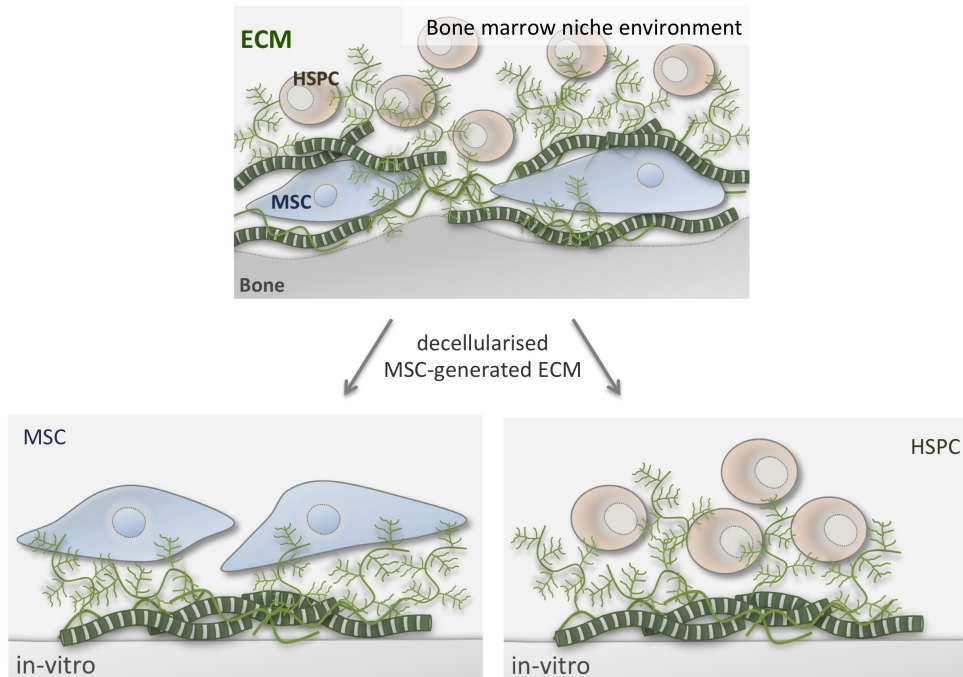
therefore allow to dissect the different cues influencing a certain response of scaffold-cultivated stem cells. In fact, in 1995 Klein et al. have tried to analyse the intricate composition of the bone marrow environment and managed to reveal some of the extracellular players of the niche [23]. Since then many other studies have followed this approach, but a comprehensive description of bone marrow extracellular niche characteristics and their functional mechanisms is still elusive. Kleins statement of 1995 is still valid today: “*Since it is becoming more and more evident that the extracellular matrix is far more complex, a refined analysis of the extracellular matrix production by these stromal cell lines will be necessary*”. Thus, this study is aiming at using *human primary* MSC to generate decellularised matrices in the most possible *in vivo*-like manner and to make them applicable as well-defined and adaptable scaffolds for *ex vivo* culture of bone marrow derived stem cells.

The strategy to reconstruct the interplay of bone marrow MSC and HSPC with their natural extracellular microenvironment *in vitro* is shown in figure 1.2.1. It illustrates the action of the extracellular matrix as key instructor of cellular phenotype and behaviour. The whole complexity of ECM intrinsic characteristics, such as suprastructural topography and physico-chemical properties can be presented best by natural structures such as decellularised matrices to reveal their full potential for bone marrow stem cell engineering. Specifically, decellularised culture substrates can provide physiological and complex extracellular environments to study authentic cell-matrix interactions and regulation of cellular behaviour. Thus, in an effort to create potent culture systems based on decellularised cell-made scaffolds for the expansion and differentiation of bone marrow stem cells, the following main goals had to be addressed within this thesis:

- (A) Establishment of a robust and reproducible decellularised matrix substrate that mimics the tissue-specific extracellular environment of the bone marrow; generated by primary bone marrow MSC *in vitro*.
- (B) Identification of the molecular constituents of decellularised matrices and analysis of their topographical and physical properties, to elucidate the mechanisms of action of the material.
- (C) Probe the potential of bone marrow specific decellularised matrices for support and expansion of tissue specific MSC and HSPC outside the human body, accompanied by the analysis of cellular behaviour.

Finally, this study could help to open new perspectives towards efficient cellular treatments within stem cell-based regenerative medicine approaches.

Figure 1.2.1: Reconstruction of bone marrow stem cell microenvironments *ex vivo*



The natural in vivo situation of the human bone marrow stem cell niche serves as a guiding and starting point from where to engineer in vitro stem cell microenvironments for the control of stem cell self-renewal and differentiation.

Chapter 2

Fundamentals

This chapter gives an overview of the fundamental background information needed to understand the scope of this thesis. First, the structure, composition and functions of the extracellular matrix are introduced. Next, bone marrow and residing stem cells are presented together with their regulation by the *in vivo* niche. Following, current concepts of bone marrow stem cell bioengineering will be introduced, focussing on biomaterials to direct stem cell fate. Finally, strategies for decellularisation of extracellular matrices and their use in regenerative medicine and stem cell biology are presented.

2.1 The extracellular matrix as biological scaffold

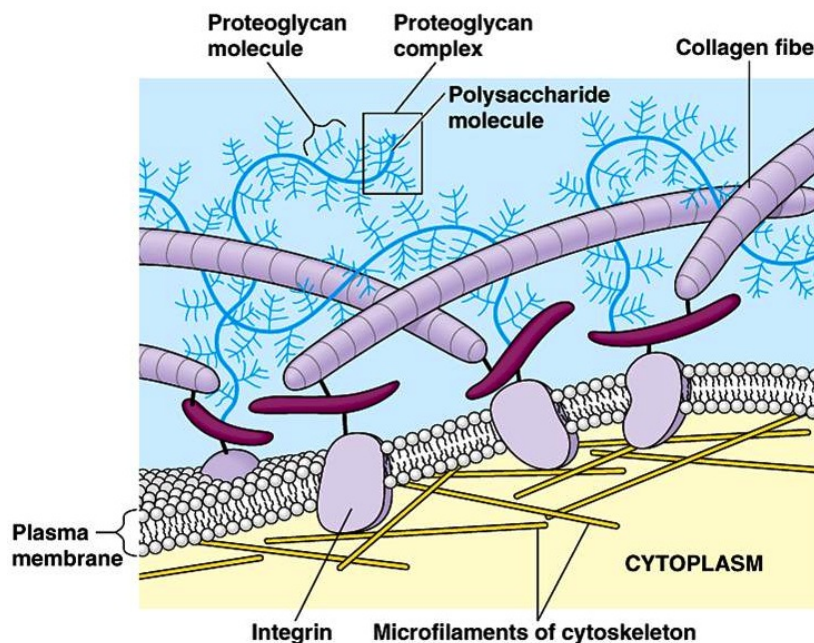
For the successful development of artificial stem cell niches it is crucial to recapitulate the natural environmental conditions that control stem cell fate. *In vivo*, cells derive a continuous flow of information from their surrounding extracellular environment. The extracellular matrix (ECM) encloses and separates cells within their tissue and instructs the fulfillment of specific genetic programmes which determine cell and tissue behaviour. Artificial scaffolds that aim at reconstruction of stem cell niches must be able to take on this instructive role in order to control cell behaviour as if they were in their native environment. The natural ECM scaffold is the master-guideline for the design and engineering of scaffolds for regenerative medicine [25]. The following section will introduce components and functions of native ECM and describe its role as natural biological scaffold.

2.1.1 Structure and composition

The ECM is an intricate three-dimensional network composed of a variety of structural and functional molecules that include the collagen family, elastic fibres, proteoglycans and glycosaminoglycans (GAG), and adhesive glycoproteins [26] (Figure 2.1.1). The ECM is the secreted product of tissue resident cells and different combinations, immobilisation, and spatial organisation of these secreted molecules gives rise to unique and characteristic tissue-specific scaffolds

[27]. The ECM serves as structural support, provides mechanical strength and guides cell-cell and cell-ECM signalling events. Intrinsic to its structure and composition, the ECM provides adhesion sites for cell surface receptors and serves as a reservoir for morphogens and growth factors. Thereby, the ECM acts as a key regulator of a variety of cellular processes, such as proliferation, survival, differentiation, migration and overall tissue homeostasis [26]. The components of the ECM can be categorised into two main classes of molecules. One, fibrous and adhesion proteins, which mediate mechanical stability and facilitate spatially defined and chemically specific adhesion sites. And two, proteoglycans and glycoproteins, which are commonly composed of a core protein that is posttranslationally modified with mucopolysaccharide chains (GAG), offering hydration and pressure resistance to the ECM. Furthermore, proteoglycans also support cell adhesion and function as a depot for growth factors within the ECM [26].

Figure 2.1.1: The extracellular matrix



The extracellular matrix consists of structural proteins, adhesion proteins and proteoglycans. Graphic adapted from [28].

It is to note that many ECM molecules have overlapping functions, which does not allow a strict division into structural and functional groups. The interplay between ECM molecules imparts further diversity and functionality to the extracellular environment and changes in response to environmental cues. The bidirectional flow between cells and their ECM triggers constant reorganisation, degradation and synthesis of ECM structures. All these molecular interactions prime cellular responses towards differentiation, proliferation, migration, wound healing or apoptosis [27, 29].

Fibrous proteins

Fibrous proteins within the ECM are collagens, elastin, fibrillin and fibulin. The most prominent fibrous protein is collagen. Collagen is also the most abundant protein in the vertebrate body, comprising more than 90% weight of the ECM from most tissues and organs [30]. This heterogeneous class of proteins contains up to 20 different collagens which exhibit different biological functionalities [27]. Collagens contain three polypeptide α -chains, displaying a triple helical conformation which is the characteristic feature of the collagen superfamily. Each polypeptide chain has a repeating Gly-XY triplet in which glycyl residues occupy every third position and the X and Y positions are frequently occupied by proline and 4-hydroxyproline, respectively [30]. The collagen family is categorised into subfamilies, that are fibrillar collagens (type I, II, III, V, XI), fibril-associated collagens with interrupted triple helices (FACIT) (type IX, XII, XIV), transmembrane (type XIII, XXV), network forming (collagen VIII, X) or basement membrane collagens (collagen type IV), according to their supramolecular assembly. In addition to their mechanical and structural functions, collagens play important roles in determining cell attachment and spreading as well as influential roles in cell migration and differentiation [27]. Along with collagen, elastin is another major structural ECM protein. Individual tropoelastin subunits are crosslinked together to form the mature elastin fibre. Elastin co-fibrils together with fibrillin inherit reversible extensibility and are responsible for the flexibility of many tissues [31].

Adhesive glycoproteins

Adhesive glycoproteins are a class of ECM molecules that occur in several variant forms and offer multiple binding domains which are capable of binding collagens, proteoglycans and cell surface receptors. Members of this class of ECM molecules are fibronectin (FN), laminin, vitronectin, thrombospondin, tenascin and others [32]. Fibronectin is the most studied adhesive glycoprotein. It is secreted as a disulfide-bonded dimer and is assembled into insoluble fibrils via a cell-mediated process. Variant forms of FN exist, which arise from alternative splicing of the mRNA precursor. Both dimers are nearly identical and contain FN type I, type II and type III repeats which possess specific recognition sequences for cellular interaction and interaction with other ECM proteins [33]. Sequences that are responsible for cell binding are RGD (Arg-Gly-Asp), RGDS (Arg-Gly-Asp-Ser), LDV (Leu-Asp-Val), and REDV (Arg-Glu-Asp-Val) [26], whereby the RGD sequence is a very frequent recognition sequence also present in many other ECM proteins. Due to its binding sites that can activate cell surface integrin-receptors, FN is a key player for cell attachment, cell movement, differentiation and multiple developmental processes [34]. FN is not only a mediator of diverse cell-matrix interactions, it also contains binding sites for other ECM molecules such as collagen, fibrin and heparan sulfate proteoglycans, thereby playing a major role in organising the components of the ECM [29].

Glycosaminoglycans and Proteoglycans

GAGs are long unbranched polysaccharides existing of repeating disaccharide units, which are either a hexose or hexuronic acid, linked to a hexosamine. Depending on the type of hexosamine, hexose or hexuronic acid (e.g. glucuronic acid, iduronic acid, galactose, galactosamine, glucosamine) and the geometry of the glycosidic linkage different types of GAGs include the galactosaminoglycans, chondroitin sulfate and dermatan sulfate and the glycosaminoglycans heparan sulfate, heparin, and keratan sulfate [35]. All GAGs can be associated to a core protein backbone and thereby appear as so-called proteoglycans. Hyaluronan is an exception to this and is also the only GAG that does not occur in a sulfated state. The net negative charge of proteoglycans attracts water molecules and mediates their ECM hydration functionality. Examples of proteoglycans and their core proteins are glypicans, syndecans, perlecan, versican, aggrecan and decorin. Proteoglycans and GAGs can occur associated to the cell surface or interact between each other and other ECM components, such as laminin, collagen and fibronectin. Another key structural role of proteoglycans is their contribution to the ECM architecture and permeability and their functional importance in combination with other ECM molecules to influence coupling, release and presentation of specific growth factors and morphogens [36].

ECM proteases

Cell movement and tissue remodelling are important processes which require ECM degradation [37]. These mechanisms are accomplished by ECM proteases, which can be divided in the family of matrix metalloproteinases (MMP), the family of A disintegrin and metalloproteinase with thrombospondin motif (ADAMTS) and the heparan sulfate-degrading enzyme heparanase [29]. In mammals 24 MMP proteins have been identified as either membrane bound, transmembrane-proteins or secreted proteins. The majority of ECM degradation is carried out by cell-associated MMPs [38]. To maintain tissue homeostasis, their activity is highly regulated at the level of transcription, by requirements for proteolytic processing before they become active, or by tissue inhibitors of metalloproteinases (TIMPs). ADAMTS are similarly regulated and together with MMP play important roles for processing membrane bound precursor proteins such as Notch, Delta and other growth factors to release active molecules [39]. Apart from protein degradation also heparan sulfate ECM components can be degraded. Heparanase is an endoglucuronidase that is crucial to the removal of heparan sulfate crosslinkers of ECM proteins, to release heparan sulfate-bound growth factors, and to release oligosaccharides from heparan sulfate to regulate protein-protein binding [29].

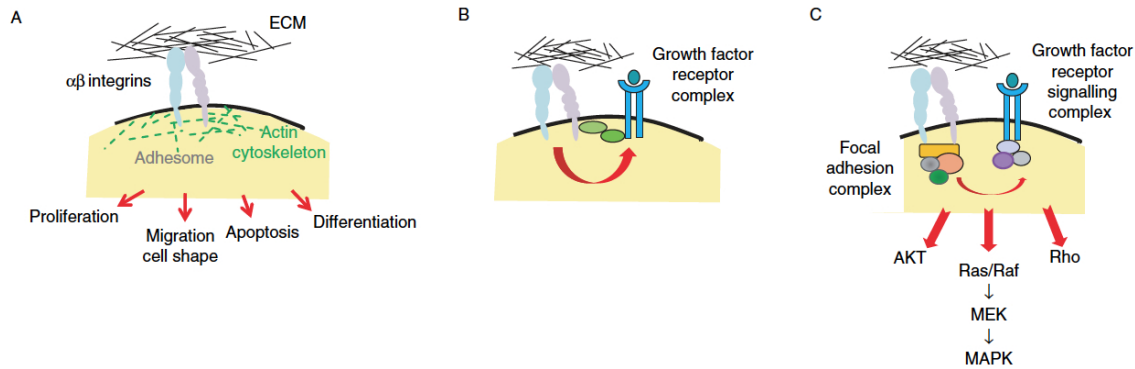
2.1.2 Function and regulatory cues

The described biochemical, structural and mechanical properties of the ECM are essential to the regulation of cellular functions such as cell adhesion, proliferation, migration, differentiation and cell death by their respective tissue-specific ECM surroundings [40]. ECM biochemical cues mostly comprise biomolecules, which are involved in binding and activation of cell membrane receptors to control downstream signalling events and ultimately cellular phenotype, and mediate the storage functionality for soluble signalling molecules. Mechanical, structural and physical characteristics of the ECM govern tensile strength, cushioning and filter functions as well as geometric and topographical guidance for cellular growth and tissue formation [40]. In fact, it is very difficult to distinguish the biomolecular and physical cues since they often occur in combination with each other, represented by complex interwoven ECM assemblies. This section will discuss separate and combinatorial instructive effects of the ECM.

Biochemical signals

Most of the ECM molecules contain multiple adhesion and recognition sites for specific cell-ECM crosstalk [41]. Extracellular signals are transmitted into the cell via cell surface receptors which recognise specific ECM adhesion domains and display differential binding affinities towards their ligands. The most important group of cell surface receptors are integrins, which mediate the crosstalk between biochemical and mechanical cues of the ECM to the interior cytoskeleton of the cell. Integrins are heterodimeric trans-membrane receptor glycoproteins which consist of eighteen α subunits and eight β subunits, which are non-covalently assembled into 24 different combinations [42, 43]. The interplay between the cell and the ECM is dependent on the specific integrin expression pattern on the cell surface and dictates which ECM signals can be sensed from the environment. Mechanisms of integrin mediated signal transduction are presented and described in figure 2.1.2. Furthermore, non-integrin cell surface receptors exist, which are transmembrane proteoglycans like syndecan, CD44 and laminin receptors. In response to the received signals of the ECM the cell can alter its phenotype or return the received information in an inside-out signal transduction fashion via changes in cell surface receptor expression or secretion of ECM proteases which results in active remodelling of the ECM environment [37]. Another mechanism based on the molecular composition of ECM is the interaction between growth factors and growth factor-binding proteins with extracellular molecules, which regulates cell behaviour on various levels. Proteoglycans and their GAG side chains play a crucial role in mediating the binding and mobilisation of growth factors, cytokines and morphogens for their functional presentation to the cell. Biological activity, spacial distribution, local concentrations and concentration gradients of growth factors are controlled by direct binding to the ECM [44, 45]. Reciprocally, transcription, translation and post-translational modification of ECM macromolecules are regulated by various growth factors [46]. The collaboration between growth factors and ECM molecules is an important aspect of distinct cellular environments or niches and regulates cellular genotype and phenotype.

Figure 2.1.2: ECM and integrin signalling

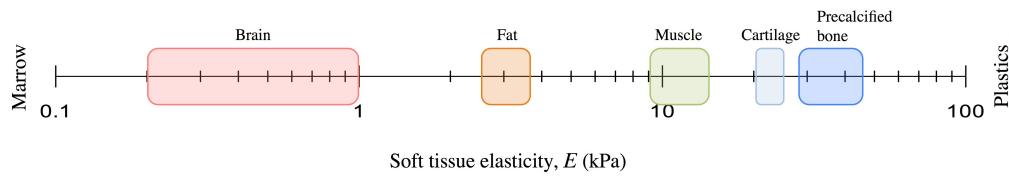


Simplified schematic of signal-transduction events via transmembrane integrin receptors. (A) A specific repertoire of $\alpha\beta$ -integrins is expressed on the cell surface of a particular cell type and can specify which signalling pathways are activated upon differential binding affinity to ECM ligands and recognition sequences. ECM stiffness and topography are further important regulators to initiate signalling pathways. Clustering of integrin/actin complexes strengthens focal adhesions and initiates the assembly of adhesomes. (B) The cytoplasmic domains of integrin receptors recruit adapter proteins to the plasma membrane which can regulate growth factor signalling in conjunction with other growth factor receptors. (C) In response to growth factor stimulation, integrins co-localise with growth factor receptors at focal adhesion sites associated with cytoskeletal molecules such as paxillin, talin and vinculin, and signalling molecules like focal adhesion kinase. Eventually downstream effectors such as AKT-Kinase, MAPKinase and Rho GTPases are activated which transmit signals usually via phosphorylation-signalling cascades to the nucleus. Graphic adapted from [29].

Mechanical signals

Physicochemical cues of the ECM are mechanical and structural signals which act on the residing cells within a tissue [47]. Tissue elasticity is the product of precise ECM composition and structural processing of ECM molecules. Each tissue harbours its own specific tissue-stiffness and thereby is representative for the mechanical environment of the embedded cells and their mechanical instructions. Varying tissue elasticities are shown in figure 2.1.3. On the cellular micrometre level, elasticity is conducted by the flexibility and extensibility of ECM molecules such as collagens or elastins. Most of the mechanical interactions between the cell and the ECM are integrin-mediated cell adhesion and mechanotransduction processes, which link the mechanical properties of the ECM to the cellular cytoskeleton, where cytoskeletal stresses are propagated into cellular motility which can evoke additional mechanical signals. In response, cells can take on differential morphologies and rearrange the ECM by means of tensile forces [48, 49]. Cycles of mechanosensing of a local force geometry, mechanotransduction via integrin receptors and mechanoresponse by intracellular transduction of tensegrity into biochemical signals result in responses that regulate cell growth, differentiation, shape changes and cell death and ultimately tissue homeostasis [50].

Figure 2.1.3: Elasticity of tissues



ECM microenvironments are physically diverse and tissue elasticity is the product of tissue-specific ECM composition and ECM processing. Cellular response to the environment is not only dependent on biochemical cues but also on the combinatorial physico-chemical effect of the ECM which regulates tissue-specific cell fate and behaviour. Graphic adapted from [51].

Structural signals

The presented biochemical and mechanical cues of the ECM are mediated by cell surface receptors that recognise specific structural features of ECM molecules. It is very important to note that only a few specialised tasks of the ECM are reserved for isolated molecules, but in principal, proper ECM functionality relies on the presence of suprastructural elements which originate from ECM polymerisation into insoluble fibrils, micro-fibrils and networks that are assembled into regional structures (i.e. fibres or basement membranes) [52]. This suprastructural conformation determines the ligand topography by which nano-scale and macro-scale patterns of biochemical and physical cues are presented to the cell. Importantly, ECM structure and topography also actuates as contact guidance for the development, orientation, alignment and migration of cells within their 3-dimensional environment. In combination with biochemical and mechanical signals, like ECM-protease-mediated or stretch-mediated exposure of cryptic binding sites within ECM structures, more complexity is added to the versatile mechanisms of action how ECM environments regulate cellular behaviour and tissue formation [53]. The principles by which suprastructural elements control cell-functional consequences are not fully identified. Further research is necessary to understand the impact of the complex ECM suprastructural organisation on the assembly of natural cellular environments.

2.2 Bone marrow residing stem cells

Stem cells are defined as “clonogenic cells capable of both self-renewal and multilineage differentiation” [54]. The earliest and most primitive type of stem cells are embryonic stem cells, which are described as totipotent cells capable of generating all cell types of the adult body. In contrast, adult stem cells reside in most adult tissues and exhibit multipotent properties for differentiation into a range of tissue-specific cell types. Throughout development and growth they can undergo a phase of rapid proliferation and differentiation to form tissues and organs. In the adult they exist in a quiescent or dormant state for longer periods until they become activated by injury or disease to fulfill their regenerative functions. Repeated entering into the cell cycle and return to quiescence are tightly controlled by distinct cues of the stem cell microenvironment or the so called ‘niche’. Extrinsic cues such as cell-cell contacts between stem cells and niche supporting cells and their ligands, as well as stem cell interactions with the ECM regulate self-renewal and differentiation behaviour [55].

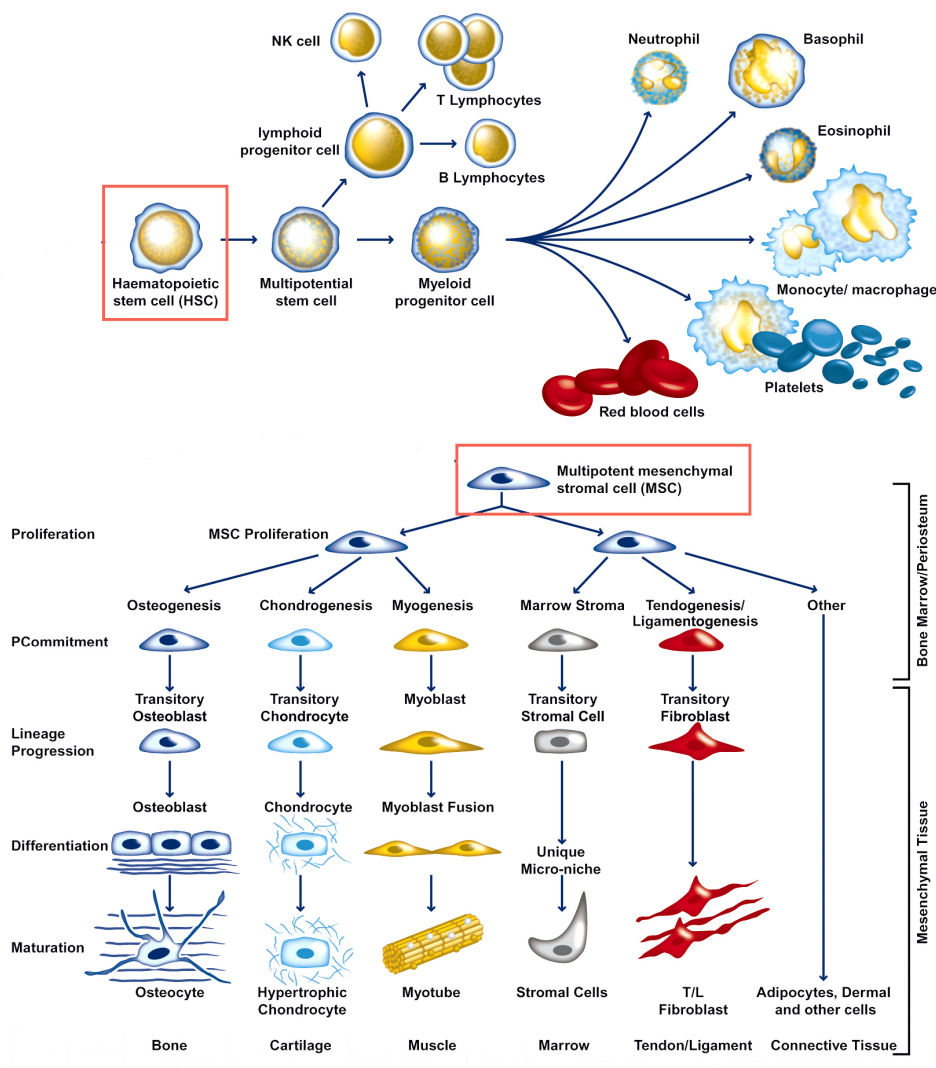
The bone marrow (BM) is one organ of the adult body that contains two types of adult stem cells with fundamental roles for homeostasis which is mediated via their enormous regenerative potential [56, 57]. These adult stem cells are haematopoietic stem cells (HSC) and mesenchymal stem cells (MSC). HSC are responsible for the BMs main function as haematopoietic organ, where developing HSC-derived progenitor cells are retained within the marrow until they have matured and are released into the vascular system. MSC also reside within the bone cavity and play important roles for skeletal development, for the formation of other mesodermal cell lineages, for mediating anti-proliferative, anti-inflammatory and immunoregulatory effects, and importantly for close interaction and support of HSC [24]. BM is distinguished into red marrow and yellow marrow, both containing numerous blood vessels and capillaries [58]. Red marrow is the place for active haematopoiesis and is found in flat bones and in the cancellous and trabecular epiphysis of long bones. This is also the place where HSC predominantly reside. Yellow bone marrow consists mainly of fat cells and is found in the medullary cavity of long bone diaphysis. With age, the amount of yellow marrow increases, but in cases of severe blood loss, yellow marrow can be reverted back into red marrow to increase blood formation. MSC are found in both marrow types where they contribute to BM stroma, consisting of reticular cells, perivascular cells, osteoblasts, osteoclasts and adipocytes [11, 56]. This following section will introduce the characteristics of both stem cell types and their interplay and regulation within BM stem cell niches.

2.2.1 Mesenchymal and haematopoietic stem and progenitor cells

The definition of adult stem cells claims their multipotent character with the ability to differentiate into specialised cell types. MSC and HSC have this ability and can generate mature cell types with various properties, as shown in figure 2.2.1. HSC are the most primitive haematopoietic cells and are the precursor for all mature blood cells. HSC differentiate into myeloid

or lymphoid progenitor cells, and controlled regulation of gene expression drives onward differentiation into cells with more and more specialised functions. These two branches of progenitor cells lead to the production of cells such as macrophages, neutrophils, erythrocytes, eosinophils, monocytes, basophils, megakaryocytes and platelets in the case of myeloid progenitor cells; and T cells, B cells and natural killer cells in the case of lymphoid progenitor cells. Since myeloid progenitors are very short lived their supply from HSC is imperative [59]. MSC have the ability to differentiate into a range of mesenchymal tissue cell types, including bone, cartilage, stroma, tendon, adipose and evidence suggested even greater plasticity for differentiation into non-mesenchymal tissues including muscle, liver, heart, skin and nervous tissues [60, 61].

Figure 2.2.1: Multipotency of HSC and MSC



Bone marrow hematopoietic stem cells (HSC) and mesenchymal stem cells (MSC) and their differentiation lineages. Graphic adapted from abcam.com.

Mesenchymal stem cells

The first time MSC were identified as multipotent stromal precursor cells was in 1970 by Friedenstein et al.. He described the isolation of mononuclear cells (MNC) from bone marrow, which were adherent spindle-shaped clonogenic cells that he termed colony-forming unit fibroblasts (CFU-F) [62]. Later in 1991, Caplan coined the term 'mesenchymal stem cell' to describe BM-derived stromal cells and their multipotency[63]. Various other synonyms can be found in the literature including mesenchymal stromal cells (MSC), bone marrow stromal cells (BMSC), marrow-isolated adult multipotent inducible cells (MIAMI), multipotent adult progenitor cells (MAPC) and many more [64]. MSC can also be isolated from other tissues like adipose tissue or cartilage [65], but BM is the predominant source for MSC research. The commonly accepted proof for identification of MSC includes formation of CFU-F in culture, multi-lineage potential (in particular osteogenic, chondrogenic and adipogenic) and expression of a set of surface markers [61]. However, so far no consensus has been reached for the proof of MSC self-renewal and for the definition of a specific set of phenotype markers to identify MSC from the heterogeneous stromal cell population. Minimal criteria for defining MSC have been postulated by the International Society for Cellular Therapy [66]. MSC isolated from bone marrow or other tissues must exhibit plastic adherence in standard culture conditions, multipotent differentiation as mentioned above, and >95% of the population must show expression of CD73 (ecto-5' nucleotidase), CD90 (Thy-1) and CD105 (endoglin) and less than 2% are allowed to express haematopoietic or endothelial markers CD45 (pan-leukocyte marker), CD11b (monocyte) or CD14 (macrophage), CD19 or CD79 α (B-cells) and HLA-DR (marker for stimulated MSC) [66]. Other markers that have been identified on MSC include CD271 (low-affinity nerve growth factor receptor) [67] and CD146 (MCAM) [68]. CD146 identifies a population of subendothelial cells with osteogenic, adipogenic and chondrogenic potential which can support the haematopoietic environment. The functions of BM-MSC involve formation of skeletal tissue within the marrow cavity, secretion of soluble factors involved in haematopoietic development, pericyte functions in support of BM sinusoids and maintenance of the structural environment by secretion and remodeling of ECM [69]. All these functions demonstrate the crucial role of MSC for the formation of BM microenvironments that control tissue-specific cells and importantly also HSC [70, 71] (see section 2.2.2).

Haematopoietic stem and progenitor cells

More than 40 years ago HSC have been recognised as blood forming cells [72]. The enormous potential of these primitive stem cells has been shown by the fact that only one single HSC is able to regenerate the entire haematopoietic system of an organism [73]. The majority of adult HSC resides within the BM, but also at lower frequencies in extramedullary tissues such as the spleen [74]. Similar to MSC, the cell surface phenotype for HSC specifies different subsets of stem cell populations, but has not been determined to such accuracy to be able to define 'true' stemness of HSC. Most of these definitions are available for murine HSC. For human

HSC a surface marker profile of CD34 (transmembrane sialomucin), CD133 (prominin-1) and CD90 and the absence of CD38 (cyclic ADP ribose hydrolase) and lineage markers describes a fairly homogenous population of human HSC [75, 76, 77]. HSC can leave the BM and circulate the peripheral blood upon injury and mobilisation, and in return they can home to the bone marrow instructed by signal gradients from the niche. Stromal cell-derived factor 1 (SDF-1, also called CXCL12) is expressed by stroma and endothelial cells and interaction with its receptor CXCR4 (CXC-motive-chemokine receptor 4) expressed on HSC plays a key role in human HSC trafficking to the BM microenvironment [78]. Signalling pathways that are involved in HSC self-renewal within the niche are for example Notch signalling, Wnt/ β -catenin signalling, BMP and TGF- β signalling or prostaglandin signalling [79, 80]. Signal transduction via these pathways results in molecular changes of transcription factor interaction with DNA sequences of HSC-regulatory genes. Thus, the gene expression profile responsible for self-renewal can be altered or maintained in response to the environment. Furthermore, HSC can be influenced by a variety of cytokines, which regulate haematopoietic development at various stages [81]. The ones that have been found useful for the support of *ex vivo* expansion of self-renewing HSC are, interleukin-3 (IL-3), IL-6, thrombopoietin (Tpo), stem-cell factor (SCF) and fms-related tyrosine kinase 3 (Flt-3) [82, 83, 84].

2.2.2 Microenvironments and niches

The concept of the stem cell niche was first described by Schofield in 1978 [85]. His model postulated that the conditions within the niche support stem cell activity and self-renewal by maintaining quiescence or promoting differentiation in response to environmental cues. Today this model has been extended, and the decision between self-renewal or differentiation upon environmental stimulation is thought to be regulated via symmetric or asymmetric cell division. Cell-divisional asymmetry (one daughter cell contains cell-fate determinants towards differentiation) and environmental asymmetry (one daughter cell is relocated from the niche) prompt the cell into self-renewal or into a specialised cell-fate [75]. The process of cell division however stays at the end of a long cascade of signalling events that arise from the varying stimuli of the niche. Both MSC and HSPC possibly share environmental niches, and for the case of MSC, they are an integral part for the formation of such. The balanced interaction with the niche thereby controls stem cell quiescence or activation, migration and mobilisation, as well as differentiation or apoptosis [86].

MSC self-renewal and lineage commitment is regulated via interaction with other cell types, autocrine or paracrine soluble growth factors and via ECM proteins. In terms of MSC interaction with the ECM, genes have been identified that are involved in regulation of MSC stemness, which are Thy-1 glycan, decorin and thrombospondin-1 [87]. Furthermore, MSC have been suggested to reside in perivascular niches associated with blood vessels in almost all adult tissues [68, 88]. As mentioned above, data exist which claim that MSC and pericytes are actually one and the same cell type, and that virtually all MSC-activity is found within the pericyte population [89]. The hypothesis that MSC reside in perivascular niches throughout the whole

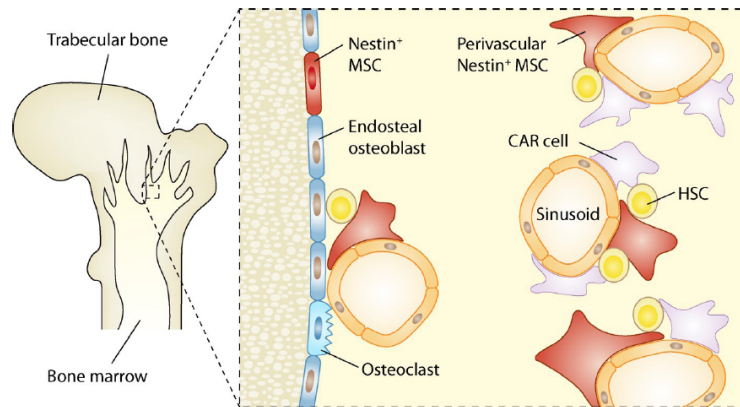
body enhances their capability to migrate to local or distant sites of injury or pathogenesis in response to systemic signals [64]. However, up to now fairly little is known about the exact origin of MSC and the detailed regulation of MSC self-renewal within their niches. In contrast the regulation of HSC by their niche has been studied in far more detail than that of MSC. Two distinct sites have been suggested and heavily discussed to contribute to HSC niches within the BM [75, 55, 74], which are the endosteum (endosteal niche) and the region around sinusoids (vascular niche). Sinusoids are reticular fenestrated venules that allow cells to pass in and out of circulation. There is evidence that individual dormant HSC are located more in niches at the endosteum, whereas activated HSCs are in close contact to sinusoids of the BM microvasculature [90, 91, 92]. In recent years the term 'niche-stem-cell-synapse' has been introduced [75], which describes the close interaction between MSC or differentiated niche osteoblasts with HSC. Signals that are exchanged through this synapse include cell-cell signals (e.g. N-cadherin interaction, membrane bound SCF and c-kit receptor interaction, Jagged ligand and Notch receptor interaction, VCAM1 and VLA4 interaction), MSC secreted signals (e.g. angiopoietin-1, SDF-1, Wnt-ligands) and secreted ECM molecules (e.g. FN-integrin signals, hyaluronic acid and osteopontin interaction with HSC CD44 glycoprotein receptors). The latest breakthrough has been presented by a landmark study by Méndez-Ferrer et al. [93]. They have identified nestin-expressing MSC populations closely associated with HSC. These strictly perivascular cells are tightly associated with adrenergic nerve fibres and regulate HSC mobilisation. Strikingly, nestin⁺ MSC expression levels of HSC maintenance factors were higher than those of any other stromal cell type including osteoblasts. Nestin⁺ cells show several similarities to so called CAR cells (MSC progenitors identified as CXCL12-abundant reticular cells), which are more abundant within the marrow and also show close interaction to HSC [94, 95]. Figure 2.2.2 gives a schematic overview over the locations and components of HSC niches.

Extracellular matrix of the bone marrow niche

Early work in the 1980s by Klein et al. and others have investigated the constituents of BM ECM [23, 96, 97]. Cytoadhesive components of the BM microenvironment have been identified and suggested for haematopoietic progenitor regulation, such collagen type-VI, thrombospondin and tenascin [98, 99, 100]. The close interaction between cells of the BM stroma and HSC have been studied *in vitro* using so called Dexter cultures [101]. Dexter et al. introduced this culture system in the 1970s to culture adherent stroma cells with mixed haematopoietic cell population, and later with more purified HSC populations. By the help of this culture method various ECM molecules have been identified to be secreted by MSC stroma [102, 103]. MSC-secreted GAGs and proteoglycans play a crucial role for the maintenance of HSC within the niche, either by direct interaction with HSC, or via the presentation of cytokines to HSC (i. e. control of growth factor sequestration and establishment of gradients) [104, 105, 106]. Within the last 20 years our knowledge about BM ECM and its functional role for residing stem cells has dramatically increased. However, the detailed mechanisms govern maintenance, growth and differentiation are still largely elusive. The here presented study of the intricate interaction of BM stem

cells with the broad spectrum of ECM-mediated extracellular signals will add further valuable information to the understanding of MSC and HSC regulation within their microenvironments.

Figure 2.2.2: HSC niches in trabecular bone cavities



Several locations and interactions with environmental cells have been proposed for HSC regulation. HSC can be found at the endosteum, where they are in contact with osteoblasts that can promote HSC maintenance (the endosteum can also be remodeled by osteoclasts). Vascular sinusoids are often localised at greater distance to the endosteal region, where HSC are in contact with perivascular cells. Sinusoids can also be found close to the endosteum. The assumption that HSC reside in two different niches (the endosteal niche and the perivascular niche) is still the current concept for HSC niche locations. However, the presence of HSC-promoting nestin+ MSC and CXCL12-abundant reticular (CAR) cells in both locations might indicate that both niches may not be as distinct as it was assumed. Yet, the osteoblast niche is thought to harbour more dormant HSC and the perivascular niche houses self-renewing HSC. Graphic adapted from [11].

The need for *ex vivo* control of bone marrow stem cells in artificial niches

HSC are the one stem cell source that has been successfully used for therapeutic applications for more than 30 years [107]. Autologous obtained HSC can be used for rescuing the patient following high doses of chemotherapy or for targeted application of gene-therapy vectors. Allogeneic HSC transplants are useful for the treatment of malignancies by replacing the malignant haematopoietic system with healthy cells. On top of treating malignancies such as lymphoma, myeloma and leukaemia by HSC therapy, also other diseases like β -thalassaemia and sickle-cell anaemia have been successfully treated. Each year approximately 45,000 patients are treated by HSC transplantation [107]. Present and future therapeutic applications of MSC involve repair of osteogenic or chondrogenic defects, treatment of graft-versus-host-disease, treatment of myocardial infarction defects and support of treatments to cure diabetes [60, 69]. The need for expandable MSC and HSC sources is a pressing issue that urges the development of *ex vivo* culture conditions which can support stem cell self-renewing proliferation. The next section describes stem cell bioengineering approaches, which are aiming at a detailed understanding of niche regulatory cues for the deconstruction and reconstruction of artificial microenvironments that support the advancement of regenerative therapies.

2.3 Stem cell bioengineering - current concepts

The key function of stem cell niches is maintenance of a constant stem cell population during homeostasis by directed control of stem cell activation or quiescence. Upon injury or disease stem cells can migrate to other microenvironments or the site of tissue damage and start proliferating and differentiating to regenerate the lost tissue function. However, the mechanisms by which microenvironmental cues induce this directed behaviour remains poorly understood. Within their niche, stem cells are exposed to a spatially controlled mix of soluble cytokines and growth factors (mainly presented via ECM-GAG structures), insoluble receptor ligands and furthermore fibrillar and adhesion-type ECM proteins. In order to understand the underlying mechanisms of stem cell regulation within their niches, several approaches in stem cell bioengineering are aiming to study isolated components of this complex system. Technologies such as biomaterials design, microfabrication and microfluidics allow tunable and variable investigation of influential parameters of stem cell fate, in a systematically manner [15, 16]. Most stem cell research is carried out on rigid plasma treated polystyrene (tissue culture plastic) substrates. This culture environment is very different from the natural cellular environment of the body, where the cells are surrounded by a mixture of anchored molecules which are presented in close proximity and structural complexity. Additionally, gradients of chemokines, calcium and oxygen have been shown to be involved in the regulation of niche dynamics. One approach to create improved cell culture conditions is the use of ECM-protein-coated substrates or the use of cell culture conditions on top of hydrogels which are made from ECM components (for example Matrigel or collagen gels). Such 2-dimensional (2D) biomaterial culture systems have the advantage of simplification towards deconstructing the niche. Individual niche components can be assessed in their effectiveness for controlling stem cell fate decisions. On top of this, other bioengineering approaches are set out to mimic 3-dimensional (3D) conditions as they are imposed on stem cells within their natural environments. These systems are more complex and allow instruction of polarised cellular morphology and activation of 3D related signalling events [51, 108]. Taking the engineering approach even further, the use of individual peptide sequences or epitopes of ECM molecules is one example of a more reductionist approach to model basic physicochemical properties of the ECM. Hybrid biomaterials which consist of synthetic and natural components can make the need of complex ECM materials redundant, but only if they can accomplish the functional presentation of critical biological cues in a non-natural way [6, 109].

For the control of bone marrow stem cells within artificial stem cell niches, 2D and 3D bioengineering approaches have been developed to probe individual cues or combinations of cues on MSC and HSPC self-renewal and differentiation *ex vivo*.

Engineered 2-dimensional artificial stem cell niches

Systematic identification and analysis of biomolecules and their relevance for stem cell regulation is one critical step for the definition of niche regulatory factors. Soluble or tethered molecules have been tested separately or in combination of various patterns and concentrations. In addition, growth factors and cytokines are usually presented in a spatially immobilised manner via proteoglycans and receptor ligands are presented via the cell membrane. The immobilisation of soluble or receptor ligands is proposed to play a critical role for protein stability and for persistent receptor clustering and signalling [110]. For example, covalent immobilisation of the Notch1 receptor Delta-1 has been shown to maintain human cord-blood CD133+ HSPC. Compared to soluble Delta-1, the immobilised receptor resulted in an increase of CD133+ cells that were capable of reconstituting the haematopoietic system of irradiated mice [111]. Similarly, another Notch ligand, Jagged-1, has been shown to expand lineage-negative murine bone marrow HSPC via immobilisation of Jagged1 on Sepharose beads [112]. In an attempt to analyse the degree of HSPC adhesion to components of the ECM, Franke et al. have used immobilised ECM proteins to investigate HSPC adhesion areas. Strongest adhesion was observed on fibronectin surfaces compared to less intense adhesion to heparin, heparan sulfate or co-fibrils thereof with collagen-I. The separate analysis of each ECM component revealed integrin $\alpha 5 \beta 1$ -specific adhesion to fibronectin and selectin-mediated adhesion to heparin [113]. Fibrillar collagen-I matrices have also been used to probe the influence on HSPC maintenance. Collagen-I gel-type substrates enabled HSPC proliferation and such culture conditions allowed the study of HSPC gene expression profiles in response to this particular ECM component [114]. One of the glycosaminoglycans that is most frequently used in biomaterials approaches is heparin. For example, resorbable polymer scaffolds of polycaprolactone (PGL) surfaces conjugated with heparin supported high-affinity adsorption of BMP-2 (representing the cytokine-depot functionality of GAGs) and promoted enhanced adhesion and proliferation of a murine MSC cell line [115]. Functionalisation of polyethylene glycol (PEG) hydrogels with heparin was shown to enable sustained viability and osteogenesis of human MSC [116]. Hydrogels are favoured materials for bioengineering approaches because of their tunable material properties, such as hydrogel elasticity. As it was mentioned before, each tissue within the body has its own tissue-specific elasticity (see figure 2.1.3). A pioneering study by Engler et al. demonstrated that modulation of polyacrylamide hydrogel stiffness according to the elasticity of brain, muscle and bone initiated a differentiation process of altered morphology and gene expression of human MSC into the respective tissue-specific cell types [117]. Another example for stem cell regulation is the manipulation of cell shape via differentially sized adhesion regions. MSC stem cell differentiation was shown to be affected by differentially-sized patterns of fibronectin islands. MSC took on the shape of the fibronectin island, either small and round or large and spread, and in turn were committed towards differentiation into the adipocyte or osteoblast fate, respectively [118]. One example of topography-modulated regulation of umbilical cord CD34+ HSPC was shown by the use of aminated polyethersulfone (PES) nanofibres. HSPC adhered and adopted a spherical morphology to a much greater extent than on

standard PTP substrates. The biomaterial supported elevated expansion and engraftment potential of CD34+ cells compared to PTP-cultured HSPC [119]. For a more combinatorial and high-throughput type of screening of niche regulatory cues array systems have been developed to test multiple molecules at the same time in parallel. Langer and co-workers have used such an approach to identify synthetic polymers that can support attachment and proliferation of MSC [120]. These examples show how the presentation of particular ECM proteins, or the immobilisation of receptor ligands or biomaterial stiffness and substrate topography can influence stem cell behaviour in a 2D culture setting. These well controlled systems allow the analysis of minimal sets of niche components. The application of artificial 3D culture scenarios is aiming at deconstructing a more complex and tissue-like environment.

Engineered 3-dimensional artificial stem cell niches

As mentioned for 2D artificial systems, hydrogels have become a more and more important biomaterial for the controlled fabrication of stem cell microenvironments. Due to their tunable properties in terms of physical or chemical cross-linking degree, possible biodegradability and importantly due to their controllable uptake and delivery of soluble factors, these materials offer many possibilities for stem cell engineering. However, not all properties (swelling ratio, mesh size and elasticity) can be modified independently, since they all depend on cross-linking degree. But, by the use of large scale array platforms, multiple tunable characteristics of the environment can be investigated. For example, a 3D PEG-hydrogel array system has been used to screen combinatorial effects on MSC cell behaviour [121]. Out of the investigated parameters, which were gel degradability, cell adhesion-ligand type and adhesion-ligand density, degradability and adhesion-ligand density were found to enhance MSC viability in a dose-dependent manner [121]. Another study by Anderson et al. demonstrated encapsulation of human MSC in MMP-degradable and cell-adhesive PEG-hydrogels using photopolymerization [122]. MSC were able to survive and proliferate within these gels, and biodegradability allowed higher expression levels of differentiation markers (of adipogenic and osteogenic lineage progeny) compared to MSC in non-degradable gels [122]. A similar approach using adhesion ligand-modified PEG-RGD hydrogels has shown that chondrogenic differentiation of encapsulated MSC was enhanced via a RGD-dose dependent manner [108, 123]. A different 3D-encapsulation approach for MSC included the fabrication of spherical collagen-I and agarose polymer beads via emulsification of a liquid MSC-matrix suspensions in a silicone fluid phase and subsequent gelation to form hydrogel beads. Cell viability could be maintained for 8 days in culture and MSC adhesion and spreading increased with increasing collagen concentration [124]. Although these encapsulation concepts are promising strategies for manipulation of MSC fate and for protected delivery of stem cells, these systems are limited in terms of effective nutrient and oxygen supply and removal of cellular waste products. The interwoven fibrous 3D microstructure of stem cell environments can be mimicked by techniques like electrospinning or self-assembly of natural and synthetic molecules. Electrospinning allows the deposition of continuous fibres with high porosity and spatial interconnectivity. For example, biocompatible polymeric electrospun

fibres fabricated from natural chitosan have been presented as a sequential BMP-2/BMP-7 (bone morphogenic proteins) delivery system for bone tissue engineering [125]. However, one disadvantage of electrospinning is the limited variability of fibre diameter, which ranges at the upper limit of those seen in natural ECM (50-500nm). Microscale mold-based biomaterials are another way to probe 3-dimensionality in a well-plate or bioreactor sized setting. For example, fabrication and functionalisation of 10-50 μ m scale poly(dimethylsiloxane) (PDMS) microcavities with fibronectin revealed that smaller sized environments promote HSPC-marker expression and supported a quiescent cellular phenotype [126]. In an approach to model the microscale sponge-like 3D bone marrow microenvironment *in vitro* Nichols et al. have used synthetic silicone scaffolds of inverted colloidal crystal geometry [127], resulting in a microporous environment that was seeded with a bone marrow stromal cell line. The dimension of the system allowed 28-day culture of human CD34+ cells within this bone marrow model system. The haematopoietic cells were able to proliferate and differentiate along the B-lymphocytic lineage. Although, this system has been able to recapitulate parts of the bone marrow niche, it is not practicable for use in larger dimensions due the lack of vascular support. A very similar approach used stromal cell-free 3D inverted colloidal crystal acrylamide hydrogels functionalised with Delta-1 and was able to support the *ex vivo* T-cell development of human HSPC [128].

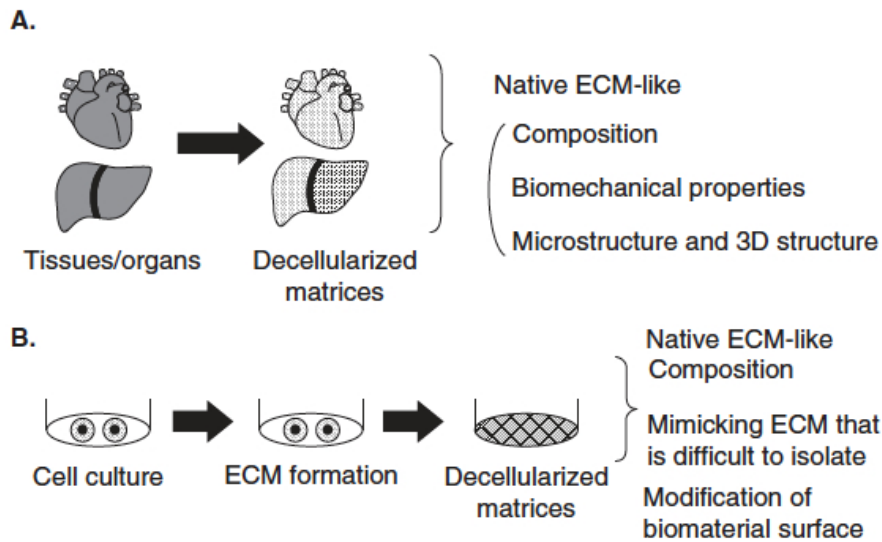
The use of both natural (protein and polysaccharide) and synthetic polymers allowed material scientists to engineer patterns of adhesion, composition, growth factor gradients, elasticity, degradation rates and geometry. The mechanisms of cellular interaction and subcellular signalling within these artificial environments still need to be better described and understood [129]. The field of biomaterial-engineering will continue to investigate particular components of the stem cell microenvironmental niche, and thereby promote the development of defined regulatory stem cell systems. However, ultimately it will be desirable to mimic and analyse the role of comprehensive cellular environments, which would allow the study of a more complete set of variables. Furthermore, the observed effects in terms of stem cell expansion vary in intensity and require further optimisation to yield efficient cell numbers for clinical applications. Decellularised natural ECM environments are one possible approach to study the control of stem cells in a physiologically, topographically and physicochemically more natural 3D environment.

2.4 Decellularisation - creating native ECM environments

Biomaterials and ECM mimicking scaffolds have been shown to enable some degree of constructive recreation of tissue properties and ECM functionalities. However, the natural composition of the ECM is far more complex than artificial systems are able to imitate. A different route for the creation of functional ECM scaffolds with intricate compositional and structural properties is decellularisation of tissues and organs, as well as decellularisation of cell cultures. Several reasons indicate the superior potential of decellularised ECM systems. ECM molecules are arranged in a tissue specific and ultrastructural manner and provide an ideal support for tissue residing cells. To make the situation even more complex, the ECM composition and

structure is constantly undergoing remodelling by the cells of the environment to procreate the mechanical demands and the prevailing niche conditions [130]. This dynamic reciprocity is a major advantage of natural scaffolding material and highlights the importance of maintaining appropriate ultrastructure and tissue-specific composition. Native ECM scaffolds that have been derived from tissues and organs retain many of the tissue intrinsic structures. It has been suggested that ultrastructural topography together with ligand spacing and alignment of ECM molecules within decellularised scaffolds provides a defined landscape that directs and supports appropriate cell attachment and differentiation [131, 132, 133]. These dynamic ultrastructural characteristics of the natural ECM are important players for modulation of cellular behaviour. The ECM environment facilitates the cell's ability to attach and migrate into specific regions within the scaffold and influences tissue-specific phenotypic differentiation [130]. Decellularisation of tissues, organs and cell cultures is the most natural way to create ECM environments that truly resemble the native ECM situation. The most classical approach is decellularisation of whole tissues and organs to create scaffolds for tissue engineering. Additionally, more recently also decellularised cell-made matrices *in vitro* have been investigated for their regulatory functions towards stem cells control (see figure 2.4.1). Thus, decellularised matrices are not only useful for tissue engineering and medical therapy but also for basic biological and bioengineering research [19].

Figure 2.4.1: Decellularised matrices from tissues/organs and cultured cells



(A) Decellularised matrices from tissues and organs. Native ECM composition, microstructure and biochemical properties as well as tissue morphology and shape are maintained. (B) Decellularised matrices from cultured cells. Matrices of cultured cells can mimic the structure and composition of native ECM from different cell types. Also biomaterial surfaces can be modified with cell-made decellularised matrices. Graphic from [19].

2.4.1 Decellularisation of tissues and organs

Decellularisation of tissues and organs is one promising approach for generation of highly functional tissue engineering scaffolds. Such scaffolds provide not only the initial support of re-seeded cells, they also help migration and localisation of cells towards the appropriate spaces, combined with optimal physical and biochemical cues for adhesion, proliferation and differentiation. Following tissue assembly, the propagated cells can remodel the scaffold and replace the scaffold with their own matrices during the regeneration process. Many studies have investigated the potential of decellularised tissues and organs as scaffolds for tissue engineering [19, 134]. A number of human or animal decellularised tissue scaffolds have been created, which include heart [135] and heart valves [136], blood vessels [137], small intestinal submucosa [138], lung [133], trachea [139], skin [140], nerve [141], cornea [142], oesophagus [143], liver [144], kidney [145], bladder [146], cartilage [147], ligament [148], adipose tissue [149] and amniotic membrane [150]. The intricate vessel and airway network and the 3D organ structure are almost impossible to reconstruct with conventional technology. Some of these decellularised scaffolds have already been commercialised for therapeutic applications, such as intestinal submucosa and skin-derived products.

As mentioned above, the tissue residing cell population is responsible for the orchestrated appearance and composition of a tissue specific ECM. Therefore, organ-specific ECM is used to stimulate cell types that are naturally harboured within the respective environment. Furthermore, decellularised matrices from specific tissues or organs can be utilised in a soluble form as culture substrate or as injectable gel-type matrices. The advantage is that injectable matrix mixtures can fit into any 3-dimensional space, instead of using whole constructs of decellularised ECM scaffolds [136]. Furthermore, such extracted and reconstituted ECM mixtures of decellularised tissue-specific ECM have been shown to support native cellular phenotypes and cellular functionality, when used as a coating for cell culture substrates [151]. Zhang et al. demonstrated that skin, liver and muscle specific cell types show better proliferation and differentiation on substrates that were coated with ECM from their own tissue of origin [151].

Decellularisation techniques

The use of appropriate processing techniques for the purpose of decellularising a tissue or an organ allows preservation of the native composition, ultrastructure and 3-dimensional architecture of the derived scaffold. Diverse methods have been developed to remove all cellular component from an extracellular tissue or organ scaffold [152]. These methods include, physical, chemical and enzymatic treatments (see figure 2.4.2). Physical treatments use agitation, sonication, mechanical massage, pressure or freezing and thawing to cause disruption of the cell membrane and to release intracellular contents. Chemical treatments utilise alkalis, acids, detergents, organic solvents, chelating agents, hypotonic solutions or hypertonic solutions to disrupt cell membranes and additionally the bonds that are responsible for intercellular and extracellular adhesions. Enzymatic treatments use protease or nuclease to cleave peptide or

nucleotide bonds. All of these methods have their respective advantages and disadvantages. A trade-off has to be found between efficient removal of cellular remnants such as nuclei, actin and cell membranes, and the optimal maintenance of biological activity and biomechanical properties. However, it is extremely difficult to achieve complete decellularisation, and mostly the remaining ECM material retains some residual DNA and other cytoplasmic and nuclear material [153]. Especially for fragile scaffolds physical decellularisation methods which disrupt cell membranes via intracellular ice crystals or mechanical cell lysis, are not appropriate since they can easily disrupt or fracture the ECM architecture. Enzymatic treatments such as trypsinisation, which cleaves peptide bonds can disrupt ECM structure and remove laminin, fibronectin, elastin or GAG structures. Chemical treatments utilising Sodium dodecyl sulfate or Sodium deoxycholate solubilise cytoplasmic and nuclear membranes but also tend to denature proteins and have been shown to disrupt tissue structure, remove GAGs and damage collagen. [152]. The method used in this thesis was application of a non-ionic detergent: Triton X-100. It disrupts lipid–lipid and lipid–protein interactions, while leaving protein–protein interactions intact. Decellularisation efficiency of Triton X-100 has shown mixed results dependent on the tissue. Mild effects on GAG removal have also been observed. However, the adverse affects of these different methods also depend on the exposure time of the respective treatment. In general, a combination of these methods aims at maximising complete decellularisation while minimising any adverse effects, and is applied in a selective manner for the tissue of interest [134]. The same techniques and principles of decellularisation also apply for *in vitro*-generated ECM by cultured cells.

Figure 2.4.2: Decellularisation techniques for tissues and organs

Physical	Enzymatic	Chemical
Mechanical agitation	Trypsin	Alkaline/acid Hypotonic and hypertonic solutions EDTA/EGTA
Freeze/thaw	Endonucleases	
Sonication	Exonucleases	<i>Nonionic detergents</i> Triton X-100
		<i>Ionic detergents</i> Sodium dodecyl sulfate (SDS) Triton X-200
		<i>Zwitterionic detergents</i> CHAPS Tri(n-butyl)phosphate

Examples of techniques used to decellularise tissues and organs. Abbreviations: CHAPS, 3-[(3-cholamidopropyl)dimethylammonio]-1-propanesulfonate; EDTA, ethylene diamine tetraacetic acid; EGTA, ethylene glycol tetraacetic acid. Graphic adapted from [134].

2.4.2 Decellularised cell cultures

Three-dimensional decellularised scaffolds of tissues and organs have demonstrated their vast potential for tissue engineering and medical applications. But for the purpose of *in vitro* investigation and manipulation of stem cells and somatic cells, native and multifunctional decellularised ECM culture substrates have become more and more important. Optimal culture conditions for the purpose of bioengineered stem cell niches should have the capacity to expand primitive progenitor cells to a maximum amount without changing their phenotype and characteristics. The special requirements that are demanded of culture scaffolds or substrates can be supplied by the help of tissue or niche intrinsic cells which secrete and modulate ECM molecules in a natural way. Along this line, *in vivo*-like 3-dimensional matrices can be created that allow the convenient *in vitro* study of cell-ECM interactions in a physiologically relevant manner and potentially support microenvironmental induced cell morphology, function and signalling.

When cells are kept in culture (usually on tissue culture plastic substrates), they start to secrete ECM proteins and deposit a layer of structurally and enzymatically processed extracellular material onto the culture carrier [154, 155]. Exploiting this aspect, an ECM-surrogate substrate can be created *in vitro* and serve as culture scaffold for re-seeded cell types. Very early studies by Hedman et al. isolated matrices of human fibroblasts and used them as novel cell culture substrates [156]. Very complicated ECM structures such as basement membrane could be recreated by the use of alveolar epithelial cells [157, 158]. Compared to the standard basement membrane model, which is Matrigel, primary hepatocytes were able to survive longer and maintain their differentiated functionalities such as albumin secretion at higher levels when they were cultured on decellularised basement membrane culture substrates [159]. Early studies by Cukierman et al. have demonstrated the difference between cell-matrix adhesions on conventional 2D *in vitro* substrates and cell-made 3D matrices as they appear *in vivo* [160, 161]. By the use of fibroblast cell lines, naturally deposited extracellular matrices were generated with 3D characteristics. For comparison, cell-matrix adhesion was also probed on mechanically compressed 2D fibroblast-matrices or more simple 2D ECM substrates such as laminin or collagen coated surfaces. The observed 3D matrix interactions and adhesions differed to those of 2D substrate interactions in their content of $\alpha_5\beta_1$ and $\alpha_v\beta_3$ integrins, paxillin, cytoskeletal components and phosphorylation of FAK [160]. The investigated matrix adhesions supported *in vivo*-like cell morphology and cell migration. Differences between classic *in vitro* substrates and cell-made 3D substrates indicate the advanced biological relevance for mimicking living organisms. This highlights again the importance of the above mentioned ultrastructural topography and ligand spacing landscape of native extracellular matrices.

In an effort to elucidate stem cell regulation and function, cell-made decellularised matrices have been studied to control stem cells maintenance and directed stem cell differentiation. For example, embryonic stem cells are usually cultured on a layer of feeder cells to maintain their pluripotent character. Decellularised matrices prepared from mouse embryonic fibroblasts enabled the establishment of human feeder-free cell lines with the ability to maintain self-renewal

[20]. This indicates the potential of extracellular matrices to instruct a cellular phenotype and shows that the presence of a cellular feeder-layer is dispensable. On the other hand, directed stem cell differentiation is another important aspect for the use of embryonic stem cells for tissue engineering. Higuchi et al. demonstrated that a basement membrane derived from HEK293 cells (which stably express basement membrane laminin-511) allowed directed sequential differentiation of mouse embryonic stem cells or induced pluripotent stem cells into definitive endoderm, pancreatic progenitor cells and finally insulin secreting pancreatic β -cells [162]. Decellularised matrices have also been used to direct differentiation of adult multipotent stem cells. As mentioned before, the multipotent character of MSC makes them interesting candidates for applications in bone remodelling and osteogenic therapy. Especially in the field of MSC-osteogenesis several groups have tried to utilise the possibilities of decellularised matrices for the stimulation of osteogenic bone formation. Synthetic biomaterials such as titanium scaffolds have been surface modified with cell-deposited decellularised matrices. Osteogenic cell lines and rodent MSC have been cultured on titanium scaffolds coated with decellularised matrices and have demonstrated enhanced bone formation capacity of these cells [21, 22, 163]. To study the stepwise tissue-development of MSC into the osteogenic or adipogenic lineage, decellularised matrices were created at each step of the differentiation process [164, 165]. Individually tailored systems like these allow the targeted analysis of stem cell differentiation processes under natural ECM-microenvironmental conditions. Table 2.4.1 summarises the use of cell culture-generated decellularised matrices for the investigation and manipulation of somatic cells and stem cells.

Table 2.4.1: Cell-made decellularised matrices *in vitro*

Cell source	Application	Ref.
Fibroblast	Cell culture substrate	[155, 156]
Alveolar epithelial cells	basement membrane model, cell culture substrate	[157, 158, 159]
Fibroblast	Study of cell-matrix adhesion	[160, 161]
Stromagenic fibroblasts	Tumor-associated stromal cell cultures	[166, 167]
Embryonic fibroblast	human embryonic stem cell maintenance	[20]
HEK293	differentiation of embryonic stem cells into pancreatic lineage	[162]
SAOS-2 / osteogenic MSC	ECM coating of titanium scaffolds for osteogenesis of MSC and bone implantation	[21, 22, 163]
adipogenic/osteogenic MSC	matrix preparation at each step of adipogenesis/osteogenesis	[164, 165]

Table partially adapted from [19].

The above mentioned studies have all addressed the potential supportive functionality of decellularised cell culture matrices. In particular, these approaches have demonstrated how native ECM-scaffolds can mimic stem cell niche environments and instruct self-renewal or differentiation *in vitro*. However, firstly no conceptual strategy has been applied to facilitate biologically defined and reproducible anchorage of decellularised matrices to the culture carrier, to prevent delamination processes (upon decellularisation procedure) which hamper the robust generation of cell-free matrices. Secondly, this lack of reproducibility has impeded the extensive and elaborate characterisation of structure and composition of the ECM scaffolds in detail, thus robust information about the complex interplay of ECM-structure and composition and the subsequent cell response is still missing. Furthermore, so far the use of decellularised culture substrates as BM niche surrogates for the maintenance of both MSC and HSPC BM stem cell populations has not been addressed. Based on these facts, the research in this thesis will address these issues and work towards the generation of reliably stabilised and reproducible decellularised matrices and towards the establishment of a human primary MSC-generated ECM substrate that can be analysed in detail for its constituents and for the support of MSC and HSPC behaviour within their niche. Appreciating the potential supportive functions of other decellularised *in vitro* systems, the use of tissue-specific MSC-made niches for the support of primitive MSC and HSPC cell types is very promising.

Chapter 3

Materials and Methods

3.1 Surface preparation

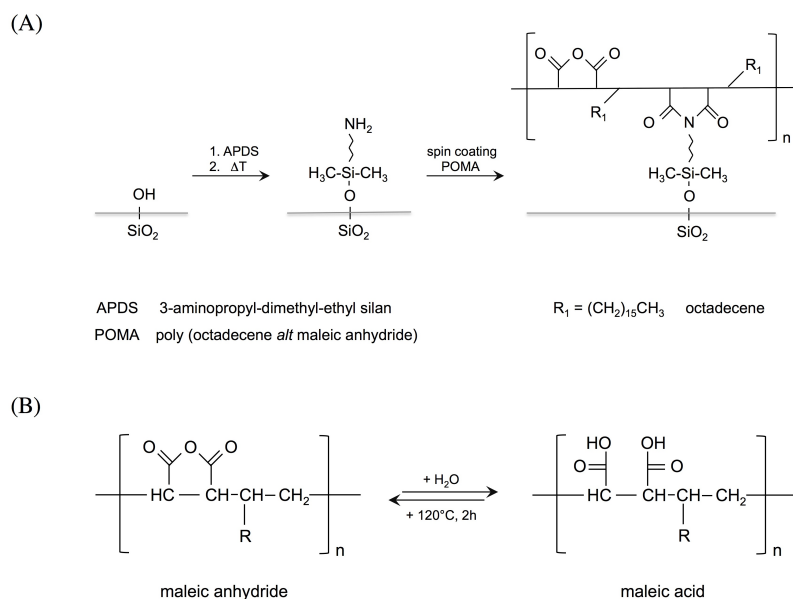
The mechanism and procedure for surface immobilisation of reactive copolymers and ECM molecules has been described in detail by Pompe et al. and Salchert et al. [168, 169, 170, 171]. The techniques that were used in this work for surface immobilisation of polymers and proteins as well as the procedure for creating decellularised cell-made ECM substrates are described in the following sections.

3.1.1 Polymer functionalised surfaces

Maleic acid copolymer thin films are a versatile platform for the bio-functionalisation of surfaces [168]. Within this work the copolymer poly(octadecene *alt* maleic anhydride) (POMA) was used. POMA has a molecular weight of 40.000 g/mol, is very hydrophobic (water contact angle of 100°) and has a thin film thickness of ~5nm. Covalent attachment of the copolymer to a planar silicon dioxide substrate was achieved via aminosilane chemistry. The maleic anhydride moiety can be converted into carboxylic acid groups by hydrolysis in aqueous solution. This conversion is reversible by annealing the surface at 120°C for 2h. Figure 3.1.1 demonstrates the copolymer platform and its functionality.

Thin films of POMA (Polysciences Inc., Warrington, PA) were created by spin-coating a 0.16wt% solution in tetrahydrofuran (Fluka, Germany) onto circular glass coverslips (Menzel-Gläser, Germany), at 4000rpm for 30s. Prior to polymer coating the coverslips were freshly oxidised in a mixture of aqueous solution of ammonia (Acros Organics, Belgium) and hydrogen peroxide (Merck, Germany) in a 5:1:1 ratio. To allow covalent binding of the copolymer thin films, the glass substrates were surface-modified with 3-aminopropyl-triethoxy-silane (ABC, Germany) before the copolymer solution was applied. Stable bonding of the polymer to the glass surface was achieved by annealing at 120°C for 2h. POMA coated coverslips were prepared in various sizes depending to their later use in tissue culture well-plates.

Figure 3.1.1: Maleic acid copolymer platform

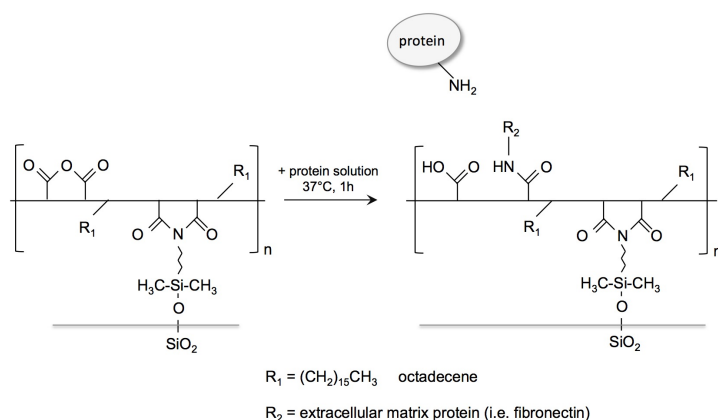


(A) schematic representation of the maleic acid copolymer platform, covalently immobilised on a silicon dioxide surface via an aminosilane functionality, (B) maleic anhydride repeating unit and its hydrolysis in water and the reversible annealing at 120°C for 2h (schematic adapted from [168])

3.1.2 Immobilisation of bioactive molecules to polymer supports

With the help of the maleic acid copolymer platform it is possible to covalently bind proteins and other compounds to polymer support surfaces. Figure 3.1.2 shows the mechanism of binding proteins from solution to annealed maleic anhydride substrates. Proteins bind to the anhydride moieties of the copolymer via free aminogroups, usually through lysine residues.

Figure 3.1.2: Binding of ECM molecules to POMA-functionalised surfaces



Fibronectin (FN) (Roche, Germany) was bound to POMA-coated surfaces at a concentration of 50 μ g/ml in PBS for 1h at 37°C. FN-POMA surfaces were rinsed in PBS to remove excess FN, yielding a monolayer of covalently bound FN. Collagen coated surfaces were prepared using bovine dermal collagen I solution (purified and pepsin-solubilized in 0.012 N HCl, PureCol, USA) either as fibrillar collagen structures, or as tropocollagen (as described by Lanfer et al. [172, 173]). For fibrillar collagen substrates collagen was brought to physiological pH by mixing eight parts of the acidic collagen solution (3.0mg/ml) with one part of 10-fold concentrated PBS and one part 0.1M NaOH. All components were kept in an ice bath before and after mixing. Appropriate volumes of chilled 1x PBS were added to adjust the final concentration of the collagen solution to 1.2mg/ml. The solution was placed onto annealed POMA-coated coverslips and fibril formation was initiated at 37°C. After 90min the bulk phase collagen gel was removed from the surface by two PBS washes leaving a thin collagen layer on the substrate. Tropocollagen surfaces were created by diluting the acidic collagen stock solution to 0.1mg/ml in 0.012N HCl. This solution was applied to POMA-coated coverslips and allowed to dry onto the surface over night at room temperature. The next day the surfaces were washed in PBS twice. Poly-L-lysine polymers (pLL) (Sigma, Germany) can be applied to make surfaces more adhesive. In this work a 0.01% pLL solution (MW 150.000-300.000) was covalently attached to POMA-coated surfaces to create a pLL layer for cell and ECM attachment. The solution was incubated for 1h at 37°C and unbound polymer was rinsed off by two PBS washes. Matrigel is a processed solubilised mixture of basement membrane, extracted from Engelbreth-Holm-Swarm mouse tumor, which is rich in ECM proteins. The major components are laminin, collagen IV and heparan sulfate proteoglycans [174]. Matrigel was used to compare the MSC-generated ECM with another complex mixture of ECM proteins. Ice cold Matrigel (BD Biosciences, Germany) was diluted in cold PBS to 50 μ g/ml to prevent Matrigel from forming a gel. The solution was incubated on POMA-coated coverslips for 1h at 37°C and subsequently rinsed in PBS yielding a stable Matrigel/POMA surface. Since POMA-coated surfaces are very hydrophobic the amount of protein solution used was minimised by simultaneously coating two coverslips in a sandwich-like manner to aid the distribution of the solution over the whole surface. At the end of the incubation time both coverslips were floated apart with an excess of PBS and transferred to tissue culture plates in the right orientation. Bioactively functionalised surfaces were used immediately or were stored under PBS at 4°C for up to 48h.

3.1.3 Decellularised extracellular matrix substrates

Decellularised ECM substrates were created *in vitro* by the use of primary human primary MSC. The procedure was adapted from a protocol by Beachman et al. [155]. Details on MSC culture are given in section 3.2.1. First, passage 1 MSC were expanded in 75cm² culture flasks to obtain sufficient cell numbers for ECM production. To create cell-secreted ECM layers passage 2 MSC were plated at 10.000 cells/cm² onto covalently bound FN/POMA surfaces and cultured for 24-48h until they have reached confluence. Two different types of ECM were

created by varying the stimuli subjected to MSC during the ECM secretion phase. Ascorbic acid was added to the culture to enhance collagen biosynthesis and to stimulate cells to secrete elevated levels of collagen. This ECM was termed ascorbic acid ECM (aaECM). To mimic the osteogenic environment of the bone marrow MSC were fed with osteogenic induction medium (as also described in section 3.2.1). This ECM was termed osteogenic ECM (osteoECM). At the onset of MSC confluence the medium was changed to either aaECM medium or osteoECM medium as described in table 3.1.1 (all reagents Sigma, Germany). MSC were allowed to secrete ECM for 10 days with a medium change every second day.

Table 3.1.1: Media formulations for aaECM and osteoECM production

aaECM	osteoECM
50µg/ml ascorbic acid	100nM dexamethasone
(280mM)	10mM β-glycerol-phosphate
	50µM 2-phospho-ascorbic acid

Supplements were added to standard MSC medium (see section 3.2.1)

At day 10 MSC-ECM layers were decellularised with warm PBS pH 7.4 containing 0.5% Triton X-100 and 20mM ammonium hydroxide (Sigma-Aldrich) by gentle agitation and 2min incubation at 37°C. ECM layers were washed 3 times with an excessive volume of PBS, whereby care was taken not to disturb the ECM layer by turbulent PBS flow. ECM substrates were stored in PBS supplemented with 100U/ml Penicillin and 100µg/ml Streptomycin (Sigma, Germany) at 4°C for up to 3 months. The quality and integrity of the ECM substrates was verified by phase contrast microscopy prior to each experiment. For the culture of HSPC on decellularised ECM, residual cytokines were washed off by a 5s wash in 2M NaCl, 20mM HEPES, pH7.4 containing protease inhibitors (inhibitor mix M, Serva, Germany) to release growth factors bound via hydrostatic interaction with the ECM (adapted protocol from Reichert et al. [175]).

Quantification of Collagen and sulphated GAG

Total amounts of collagen and sulphated glycosaminoglycans (sGAG) present in decellularised ECM preparations were quantified using the Sircol collagen assay and Blyscan sGAG assay (Biocolor, UK), according to the manufacturers instructions (reagents provided by the assay kit).

Briefly, collagen was extracted from decellularised ECM layers by acid-pepsin solubilisation. At a pepsin concentration of 0.5mg/ml in 0.5M acetic acid (Sigma, Germany) the enzyme was effective in removing the terminal non-helical telopeptides to release collagen into solution. After an over night incubation at 4°C samples were concentrated by first neutralising the

extracted sample (in Tris-HCl and NaOH) and concentrating all collagen by incubation in polyethylene glycol in Tris-HCl, pH7.6 at 4°C over night. The centrifuged collagen pellet was incubated with collagen dye reagent (sirius red in picric acid), which binds to the helical structures of collagen and forms a collagen-dye-complex that precipitates. After a second centrifugation step the collagen pellet was washed in ice-cold acid/salt wash-solution (acetic acid and sodium chloride) and was reconstituted in 0.5M sodium hydroxide to release the bound dye. Absorbance was measured at 540nm in duplicate using a microplate reader (Tecan GENios, Tecan Ltd., Switzerland). Sample concentrations were obtained from a collagen standard curve generated from a collagen type I solution (provided by the assay).

Sulphated GAG were detected in papain extracted decellularised ECM samples. First, ECM substrates were incubated in papain extraction reagent (0.2M sodium phosphate buffer pH6.4 containing 0.1M sodium acetate, 0.01M Na₂EDTA, 0.005M cysteine HCl and 0.2mg/ml papain) (all Sigma, Germany) at 65°C for 3h to break up the ECM sample. An aliquot of the solubilised sample was mixed with sGAG dye reagent (1,9-dimethyl-methylene blue) which specifically binds sulphated polysaccharide components of proteoglycans or the proteins free sulfated GAG chains. The centrifuged pellet was incubated with dissociation reagent (the sodium salt of the anionic surfactant) and the dissociated dye was measured spectrophotometrically at 660nm (Tecan GENios) in duplicate. A reference standard curve was generated from chondroitin 4-sulfate (provided by the assay) which was used to calculate sample sGAG concentrations.

3.2 Cell culture

3.2.1 Mesenchymal stromal cell isolation and culture

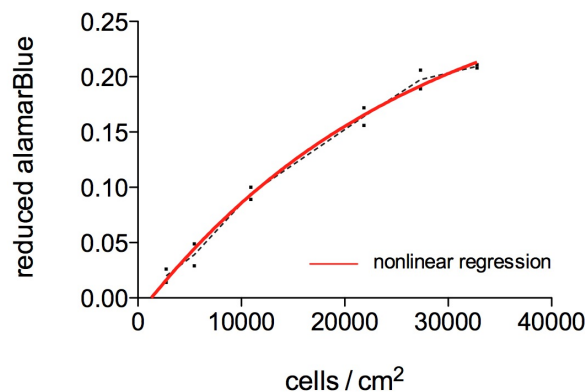
MSC were isolated from male human bone marrow (BM) aspirates (donor age 20-40 years), kindly provided by the University Hospital Carl Gustav Carus, Dresden. Primary MSC were isolated, expanded and characterised as described previously [176, 177, 178, 179]. The study was approved by the local institutional review board. Briefly, 5-7 ml BM aspirate was diluted 1:5 in PBS containing 0.5% human serum albumin (HSA) (Sigma, Germany). A 20ml aliquot was layered over a Percoll solution ($d = 1.073\text{g/ml}$) (Biochrom, Germany) and centrifuged at 900g for 30min at room temperature. Mononuclear cells (MNC) at the interface were recovered and washed twice in PBS 0.5% HSA. Primary MNC were plated into 75cm² flasks. Cells were maintained in a humidified atmosphere of 5% carbon dioxide at 37°C and were cultured in low-glucose Dulbecco's modified Eagle medium containing GlutaMAX (DMEM, Gibco, Germany) supplemented with 10% fetal bovine serum (FBS) (Gibco, Germany) and 100U/ml Penicillin and 100µg/ml Streptomycin. This medium is referred to as standard MSC medium. Nonadherent cells were removed after 24 hours by a PBS wash. The medium was changed every 3-4 days. Primary MNCs adherent to tissue culture plastic (one criterium that defines them as MSC [66]) were left to proliferate until they have reached first confluence. Cells were recovered using 0.25% Trypsin-EDTA (ethylenediaminetetraacetic acid) (Sigma, Germany) and replated at a density

of 6.000-10.000 cells/cm² as passage 1 (p1) cells. At this point cells were also cryo-conserved in standard medium supplemented with 10% dimethylsulfoxid (DMSO) (Sigma, Germany) and an additional 10% FBS in liquid nitrogen. The initial frequency of colony forming units fibroblast (CFU-F) and the cells ability to differentiate into the osteoblast and adipocyte lineage, as well as surface marker expression of CD (cluster of differentiation) antigens via flow cytometry (positive for CD166, CD105, CD90, CD73, CD146 and negative for CD34, CD45, CD14) was evaluated. Isolation of MSC and all initial tests for MSC characterisation were kindly provided from the Medical Theoretical Centre (MTZ) by the laboratory of Professor Martin Bornhäuser. All following experiments in this work were performed with passage 1 or 2 MSC.

Proliferation studies

Short term proliferation was measured indirectly via the metabolic activity of MSC using the alamarBlue proliferation assay (Invitrogen, Germany). In this assay, the reagent resazurin, a non-fluorescent indicator dye, is converted to bright red-fluorescent resorufin via the reduction reactions of metabolically active cells. The amount of fluorescence produced is proportional to the number of living cells. The data were related to a standard curve of defined MSC cell numbers from 2 independent MSC donor experiments to calculate experimental cell numbers from fluorescence values (see figure 3.2.1).

Figure 3.2.1: Calibration curve of alamarBlue reduction over MSC cell number



Two different MSC donors were seeded at defined cell densities and reduction of alamarBlue was measured after cell attachment (dots represent separate values, dashed line represents the average curve). A non-linear fit (red line) describes the reduction of alamarBlue as a function of cells/cm².

For long term culture of MSC, cells were cultured on the same substrate for several passages (up to 10) to determine their proliferation behaviour under constant substrate conditions for longer periods. At the beginning of each passage cells were seeded at 5.000 cells/cm². Once they have reached confluence cells were subcultured to the same starting cell density. At the end of each passage cell numbers were determined using a Neubauer haemocytometer. Adapted

from Baxter et al. [180] cumulative population doubling was calculated as follows. Population doubling within one passage was described as cell number at confluence divided by starting cell number of the same passage. Cumulative population doubling at each passaging timepoint was calculated from the population doubling of the given passage added to the population doublings of the previous passages. Absolute cell numbers (possible yield of total cells, if all cells were subcultured into the next passage) were calculated from the population doubling within each passage (percentile growth) multiplied by the total number of cells at the end of the previous passage.

Osteogenic and adipogenic differentiation of MSC

MSC differentiation studies were performed as described by Pittenger et al. [181]. Briefly, for osteogenic differentiation MSC were cultured in standard medium for 2 weeks in the presence of 100nM dexamethasone, 10mM β -glycerol-phosphate and 50 μ M 2-phospho-ascorbic acid. Adipogenic differentiation was induced by the addition of 1 μ M dexamethasone, 500 μ M 3-isobutyl-1-methylxanthine, 100 μ M Indomethacin and 1 μ g/ml insulin to standard medium for 2 weeks (all reagents Sigma-Aldrich). Control cultures received no differentiation treatment and were fed with standard MSC medium. The medium was changed every 2-3 days.

Differentiation intensity was quantified by visualising the mineralisation of osteogenic induced cultures by vanKossa staining as previously described [176]. Briefly, cell layers were fixed with 10% formalin (Merck, Germany) for 30 minutes, incubated with 2% (w/v) silver nitrate solution (Sigma, Germany) for 15 min in the dark, and developed with 1% pyrogallol (Merck, Germany). The layer was washed thoroughly with deionized water and the staining was fixed in 5% sodiumthiosulfate (Merck, Germany) for 5min. Cultures were imaged by phase contrast microscopy and mineralisation intensity was analysed using ImageJ software (ImageJ software, NIH, USA).

Adipogenic differentiation was analysed by Oil Red O staining for fat droplet accumulation and subsequent extraction and quantification of the dye (adapted from [182]). Cultures were washed in PBS and fixed in 4% paraformaldehyde, followed by 3 PBS washes. A filtered stock solution of Oil Red O (Sigma, Germany) at 0.5g/100ml isopropanol was used to prepare the working solution by dilution with water at a 3:2 ratio. Cells were incubated with the staining solution for 1h, washed in PBS twice and the walls of the culture wells were cleaned with PBS soaked cotton buds. After taking photographs for visual evaluation the Oil Red dye was extracted with isopropanol for 5min and an aliquot was used to measure the absorbance at 540nm with a microplate reader (Tecan GENios, Tecan Ltd., Switzerland).

Detection of secreted cytokines

The secretory profile of MSC grown on different culture substrates was analysed using (i) a dot blot cytokine array (Proteome profiler, panel A, R&D Systems, Germany), which allows the simultaneous detection of up to 21 growth factors and cytokines and (ii) an enzyme linked immunosorbent assay (ELISA) to quantify secreted cytokine levels of interleukin-8 (IL-8), angiopoietin-1 (Ang1) and stromal cell-derived factor 1 (SDF1) (Quantikine kit, R&D Systems, Germany). Three different MSC donors were seeded onto ECM and control substrates at 10.000 cells/cm² and conditioned medium was collected at 24h, 48h and 72h post plating and was stored at -80°C. For ELISA quantification of cytokines standard MSC culture medium was used as a background control. At the same time points as harvesting MSC supernatants reduction of alamarBlue was measured to normalise cytokine levels to cell numbers (as described under MSC proliferation studies, figure 3.2.1).

Cytokine array: For each treatment (substrate) a pool of conditioned supernatants was prepared by mixing the supernatants of 3 different MSC donors, each according to the corresponding volume equivalent to 10.000 cells. This pool of supernatants was mixed with a biotinylated detection antibody cocktail and applied to nitrocellulose membranes spotted with capture antibodies to various cytokines. After removal of any unbound material the membrane was incubated in streptavidin-horseradish peroxidase and a chemiluminescent signal was detected and imaged using a bioimager (LAS 3000 Bioimager, Fujifilm Life Sciences, USA). The signal at each spot is proportional to the amount of bound cytokine. Pixel intensity of each spot was analysed using ImageJ (ImageJ software, NIH, USA).

ELISA: Equal volumes of cell culture supernatant were assayed in parallel for 3 different MSC donors. Background cytokine levels were assayed in standard MSC medium and in standard MSC medium in contact with plain ECM substrates. The amount of cytokine quantified as pg/ml was then calculated according to the corresponding volume of 10.000 cells (pg/10.000 cells). For this quantitative sandwich enzyme immunoassay, culture supernatants were incubated on a microplate pre-coated with monoclonal antibody specific for the cytokine of inspection. Present cytokine in the sample was immobilised to the plate and an enzyme-linked monoclonal antibody specific to the same cytokine was added. After removal of unbound reagent a substrate solution was added and a color reaction developed in proportion to the amount of bound cytokine in the initial step. Optical density was measured using a microplate reader set to 450nm (Tecan GENios, Tecan Ltd., Switzerland). In parallel, a standard curve was generated from known concentrations of the detected cytokine, from which sample concentrations were calculated. All standards and all samples were assayed as single measurements.

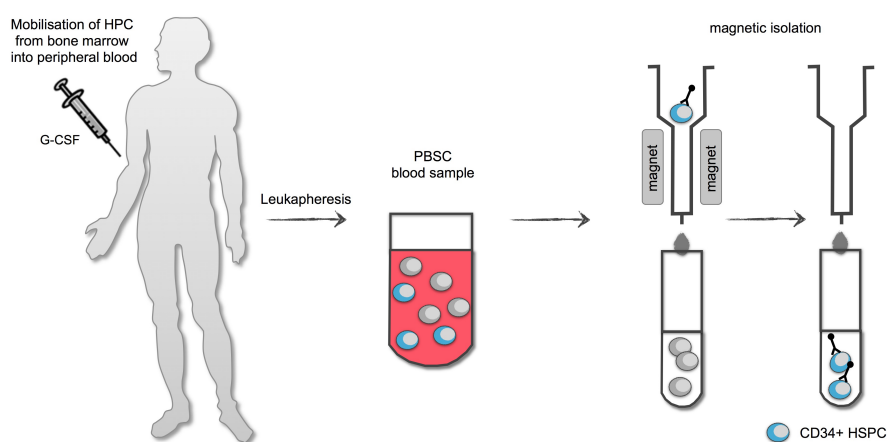
3.2.2 Hematopoietic stem and progenitor cell isolation and culture

Haematopoietic stem and progenitor cells (HSPC) were isolated from granulocyte-colony stimulating factor (G-CSF) mobilised leukapheresis products obtained from healthy donors after

their informed consent. Leukapheresis products were provided by the University Hospital Carl Gustav Carus, Dresden. CD34⁺ HSPC were selected via magnetic affinity cell sorting (MACS) using the CD34 direct isolation kit (Miltenyi Biotec, Germany), as schematically shown in figure 3.2.2.

A small sample volume (2-5ml) of leukapheresis blood was washed by the addition of 8ml isolation buffer (PBS, 2mM EDTA, 0.2% HSA), filtered through a 30 μ m nylon mesh (pre-separation filters, Miltenyi Biotec, Germany) to remove coagulated cell clumps and was centrifuged at 300g for 15min. The upper layer of blood plasma was discarded and the remaining MNC and red blood cells were resuspended in isolation buffer to a maximum volume of 3ml and processed for magnetic isolation. Larger sample volumes (6-15ml) of leukapheresis blood were mixed with ACK lysing buffer (Invitrogen, Germany) in a 1:2 ratio (2ml ACK per 1ml blood) to lyse all red blood cells. After 5min incubation at room temperature the sample was centrifuged at 300g for 5min and the supernatant was discarded. The remaining pellet of MNC was washed in 5-10ml of PBS, centrifuged, resuspended in 3-5ml of PBS and processed for subsequent magnetic isolation of CD34⁺ cells. Prior to magnetic isolation, the sample was incubated with 100 μ l/10⁸ MNC of FcR blocking reagent (to avoid unspecific labelling of cells via Fc receptors) and anti-human CD34 antibody (conjugated to 50nm sized magnetic micro beads) for 30min at 4°C. Samples were subsequently washed by addition of 10ml isolation buffer and were then separated on a MACS column in a MACS separator which generates a magnetic field that retains magnetically labelled cells within the column (Miltenyi Biotec, Germany). The flow through was discarded. After removal of the MACS column from the magnetic field, the retained CD34⁺ cells were flushed out with isolation buffer and were counted using a Neubauer haemocytometer. At the beginning of every HSPC culture the purity of the CD34⁺ population was verified by flow cytometry to range between 92-99% purity.

Figure 3.2.2: Isolation of CD34⁺ HSPC from leukapheresis products



Schematic representation of the isolation of HSPC from G-CSF-mobilised leukapheresis products by magnetic affinity cell sorting (MACS). HSPC are enriched via immunolabeling of the CD34 surface antigen with magnetic bead-conjugated antibodies.

Isolated HSPC were cultured in suspension in serum-free CellGro medium (CellGenix, Germany) supplemented with 10ng/ml human stem cell factor (SCF) (Miltenyi Biotec), thrombopoietin (TPO) and FMS-like tyrosine kinase 3 ligand (Flt-3) (both R&D Systems). For standard culture experiments a cell density of 50.000-60.000 cells/2ml were plated to 9cm² culture wells. Cells were kept in culture for one week without a medium change. At the end of culture (on ECM or control substrates) cells were harvested from the culture carrier by 2 washes with PBS, a 10min incubation in accutase (PAA, Germany) followed by a final wash in PBS. All cells from each washing step were collected in one tube and centrifuged at 300g for 5min. Cells were resuspended in a defined volume of PBS to allow quantification of total cell numbers and were kept at 4°C until proceeding with subsequent flow cytometry analysis.

Flow Cytometry

Freshly isolated HSPC and *in vitro* expanded cells were analysed for their cell surface marker expression (CD-antigens) by flow cytometry using the MACSQuant Analyser (Miltenyi Biotec, Germany). Cells were prepared for flow cytometric analysis by 15min incubation at 4°C in PBS containing FcR blocking reagent at a 1:11 dilution, 2mM EDTA and 5% BSA. Samples were split into defined volumes for various staining cocktails. To calculate absolute cell numbers of cell expansion after *in vitro* culture it was crucial to define the volume of initial cell suspension used for the final flow cytometric analysis of a given flow cytometry sample volume. Cells were labelled with up to 3 antibodies (with APC, PE and VioBlue label) at a 1:11 dilution in PBS containing 2mM EDTA and 1% BSA, for 10min at 4°C and were subsequently washed in the same buffer, centrifuged at 300g for 5min and resuspended to a final volume for flow cytometric analysis. To account for unspecific antibody binding to the cell surface control samples were labelled with isotype-control antibodies conjugated to the same fluorophore as the staining antibody. Just before sample measurement, propidium iodide (Miltenyi Biotec, Germany) was added at a 1:100 dilution to exclude all dead cells from the analysis. A list of all antibodies used for flow cytometry is given in table 3.2.1. Data were analysed and processed using FlowJo (FlowJo software, Tree Star Inc., USA).

Table 3.2.1: Flow cytometry antibodies

antibody	isotype / clone	dilution	company
CD34-magnetic micro beads	IgG1 (Qbend/10)	1:11	Miltenyi Biotec
CD34-APC / PE	IgG2a (AC136)	1:11	"
CD133-PE / APC	IgG2b	1:11	"
CD45-VioBlue	IgG2a	1:11	"
CD117-PE	IgG1	1:11	"
isotype-APC / PE	IgG2a	1:11	"
isotype-APC / PE / VioBlue	IgG2b	1:11	"
isotype-PE	IgG1	1:11	"

allophycocyanin (APC), phycoerythrin (PE)

For the analysis of HSPC expansion on ECM or control substrates, the accurate starting cell number of CD45, CD34 and CD117 cells was calculated from the flow cytometric measurement of freshly isolated cells (related to 60.000 cells that were subjected to each substrate). At the end of culture, the total cell number harvested from the surface was determined and CD45, CD34 and CD117 cells were calculated from the flow cytometric measurement. CD45 was used as a marker for total haematopoietic cell number. The fold change (expansion/decrease) in cell number was then related to that of the PTP control substrate within each experiment.

3.3 Proteomic analysis of extracellular matrices

To characterise the constituents of MSC-generated decellularised ECM substrates a proteomic approach was chosen. Via mass spectrometric analysis of fractionated protein extracts proteins present in aaECM and osteoECM substrates were identified.

3.3.1 Protein extraction

Decellularised ECM substrates were generated as described in section 3.1.3. Before decellularised matrices were processed for protein extraction, the presence of residual DNA was minimised by a DNase treatment. A 9cm² area of ECM substrate was treated with 1ml DNase buffer (50mM Tris-HCl, 10mM MgCl₂, 0.05mg/ml HSA and 50U/ml DNase I) (all Sigma, DNase I Roche, Germany) followed by two PBS washing steps. Proteins of the ECM were then extracted in 400µl 5M guanidine buffer containing 10mM dithiothreitol (DTT) (both Sigma, Germany) and protease inhibitors (protease inhibitor mix M, Serva, Germany) at 4°C overnight on a rocking platform. The next day the solubilised ECM was scraped off the culture well and ECM extracts of 5 different MSC donors were pooled together, for aaECM and osteoECM respectively, yielding a final volume of approximately 12ml. These extracts were left to solubilise further for 3h at 4°C, rotating. Samples were mechanically homogenised using an Ultra-Turrax (Ultra-Turrax T8, IKA-Werke, Germany) at level 6, followed by a 2h incubation step at 4°C, rotating. To lower the high salt concentration of the extraction buffer in the sample, a buffer exchange was performed using cellulose membrane spin columns with an exclusion size of 3kDa (AmiconUltra-4, MilliPore, Germany) against tissue protein extraction buffer (T-PER buffer, Pierce, USA) containing 25mM Bicine, 150mM sodium chloride and detergent at pH7.6 which was supplemented with 20mM β-mercaptoethanol (Sigma, Germany). First, the membrane was wetted with T-PER buffer via centrifugation at 4000g at 4°C. The total amount of protein extract was added to the column by serial centrifugation steps. Large sample volumes were split to up to 3 cellulose membrane spin columns and were combined at the end of the buffer exchange. The protein in each spin column was washed at least 3 times with 2ml T-PER buffer via centrifugation. Samples were concentrated to a final volume of 500µl in T-PER buffer. At this point protein extracts were aliquoted to appropriate volumes and frozen at -80°C.

3.3.2 Protein separation and mass spectrometry

The protein concentration of the ECM extract was determined via Bradford assay (Coomassie solution, Sigma, Germany) and the equivalent volume of 7 μ g protein was precipitated with 4 volumes of ice-cold acetone (Sigma, Germany) at -20°C for 2hr. A pellet was obtained by centrifugation at 18.000*g* and was dissolved in 20 μ l of 4x sample buffer (0.25M Tris-HCl, 6% SDS, 40% glycerol, 0.04% bromophenolblue, 20% β -mercaptoethanol). Samples were separated by sodium dodecyl sulfate polyacrylamide gel electrophoresis (SDS-PAGE) on 1mm thick, 7% acrylamide gels at 120V. Protein bands were visualised by coomassie brilliant blue stain (Coomassie G-250, Sigma, Germany). The procedure of SDS-PAGE separation was carried out following standard protocols by U.K. Laemmli [183]. SDS-PAGE gels were imaged using the LAS 3000 Bioimager (Fujifilm Life Sciences, USA) prior to subsequent processing for mass spectrometry.

All mass spectrometric analysis were done at the Mass Spectrometry Facility at the Biotechnology Center (Technical University, Dresden) in collaboration with Chrsitian Niehage and Bernard Hoflack. The following methodical description was contributed by Christian Niehage. SDS-PAGE separated extracts of aaECM and osteoECM were cut into 17-20 slices according to the major bands present in both lanes. In-gel digestion of proteins was performed using standard protocols [Shevchenko 2006]. Briefly, proteins were reduced by 10mM dithiothreitol and carbamidomethylated by 55mM iodoacetamide. Tryptic digestion was performed in an enzyme to protein ratio of 1:20 for 16h at 37°C. Peptides were eluted, dried and resuspended in 20 μ L 0.1% formic acid. LC-MS analysis were performed on an Ultimate 3000 HPLC system (Dionex, Amsterdam, The Netherlands) in front of a LTQ Orbitrap XL mass spectrometer (Thermo Scientific, Bremen, Germany), equipped with a nanoESI source (Proxeon, Odense, Denmark). 9 μ L of each peptide fraction was loaded onto a precolumn (C18, 2cm x 75 μ m, 3 μ m beads of 100Å pore size, Dionex) and separated on a 50cm column (C18, 50cm x 75 μ m, 2 μ m beads of 100Å pore size, Dionex) using a 240min linear gradient from 5% to 45% acetonitrile containing 0.1% formic acid. Top 8 peaks in mass spectra (Orbitrap, resolution 60000) were selected for fragmentation (CID, normalized collision energy 35%, activation time 30ms, q-value 0.25). Dynamic exclusion was enabled (repeat count 2, repeat duration 10s, exclusion duration 20s). MS/MS-spectra were acquired in the LTQ in centroid mode. Proteins were identified using the MaxQuant software package version 1.2.0.18 (MPI for Biochemistry Munich, Germany) [Cox 2008] and Uniprot data base version 02/2011. Carbamidomethylation of cysteine was chosen as a fixed modification, acetylation of the N-terminus, deamidation of asparagine and oxidation of methionine as variable modifications. Other parameters were: a protein FDR of 0.01, a minimum of unique peptides of 1 and a minimum of two different peptides for each protein.

3.4 Microscopy techniques

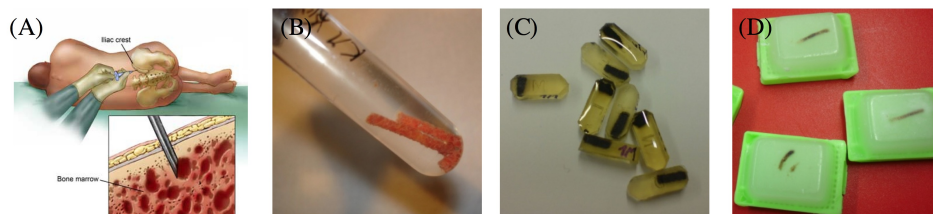
Bright field, phase contrast and and fluorescence microscopy

For standard analysis of cell cultures and for the examination of decellularised ECM substrates a Leica inverted microscope (Leica DMIL, Leica Microsystems, Germany) in combination with Leica application suite (LAS software, Leica Microsystems, Germany) was used. All images of cell cultures and decellularised ECM are greyscale phase contrast micrographs. Bright field images were taken for visualisation of MSC differentiation (Oil Red O and van Kossa stain) and for color images of histological stainings of bone marrow specimen.

Histology of paraffin-embedded bone marrow cylinders

Human bone marrow was analysed using biopsy material of the iliac crest from bone marrow aspirations (same as for MSC isolation, see section 3.2.1 and figure 3.4.1). A cylinder of trabecular bone was collected from the aspiration needle and immediately fixed in 10% formaldehyde (neutral buffered formalin, Sigma, Germany) for approximately 24h at room temperature. For better sectioning results of the hard bone specimen the samples were decalcified in 10% formic acid and 5% formaldehyde (Sigma, Germany) for 6h at room temperature. Samples were washed in distilled water and placed back into fixation solution until processed for paraffin embedding (within the same day). All subsequent embedding and histological staining procedures were performed by the Pathology department of the University Hospital Carl Gustav Carus, Dresden. Briefly, samples were dehydrated and infiltrated with paraffin, followed by sectioning of 1 μ m sections. Paraffin sections were deparaffinised and either immunostained for CD34 using a brown DAB (diaminobenzidin) color reaction to visualise CD34 expression or were stained by standard histological techniques, such as haematoxylin/eosin staining (visualising nuclear, cytoplasmic and collagenous structures) and alcian blue staining (visualising sulfated glycosaminoglycans).

Figure 3.4.1: Preparation of bone marrow cylinders for ultrastructural and histological analysis



(A) Human bone marrow specimen were collected as cylinders from the bone marrow aspiration needle. (B) Bone marrow cylinders were fixed in glutaraldehyde for electron microscopy or in formalin for histological analysis. (C) Epoxy embedded cylinders for ultra-thin sections (200nm). (D) Decalcified and paraffin embedded cylinders for micro-thin sections (1 μ m).

Immunocytochemistry for cell shape analysis

Cell shape of MSC was determined by fluorescence imaging of phalloidin stained cells to visualise the cellular cytoskeleton. To analyse cell shape during the initial contact with the various culture substrates MSC were plated at a starting density of 2.000 cells/cm². After 48h cultures were washed in PBS and fixed in 2% paraformaldehyde (Sigma, Germany) in PBS. Cell membranes were permeabilised in PBS containing 0.2% Triton X-100 (Sigma, Germany) followed by a 1h incubation with phalloidin-Alexa 488 (molecular probes, Invitrogen, Germany). Samples were washed in PBS twice and mounted onto microscope slides. Fluorescently labelled cells were imaged using the Leica DMIRE2 fluorescence microscope (Leica Microsystems, Germany). At least 10 images of each substrate were taken and cell shape was analysed from a minimum of 50 cells, using ImageJ (ImageJ software, NIH, USA). Cell shape was determined as cellular area in μm^2 and as cellular roundness (whereby 1 describes a perfect circle, $\text{roundness} = \frac{4 \cdot \text{area}}{\pi \cdot \sqrt{\text{majoraxis}}}$).

Scanning Electron Microscopy

Morphological characterisation of decellularised ECM substrates

The morphological characteristics of decellularised ECM substrates were analysed by scanning electron microscopy (SEM). To maintain the complex structure of the ECM and the attached GAGs, a fixation procedure was adapted from Wight et al. [105]. Ruthenium red is a cationic dye that allows superior visualisation of proteoglycans in combination with a post-fixation in osmiumtetroxide [184]. ECM substrates were washed in PBS and fixed in 0.1M cacodylate buffer pH 7.3 containing 2% paraformaldehyde, 2% glutaraldehyde and 0.2% ruthenium red for 1h at room temperature. Samples were rinsed for 30min in 0.1M cacodylate buffer containing 7.5% sucrose and 0.1% ruthenium red followed by postfixation in 0.1M cacodylate buffer containing 1% osmiumtetroxide and 0.05% ruthenium red (all reagents Sigma, Germany; OsO₄ by Roth, Germany). Next, the samples were washed in double distilled water and critical point dried (Bal-Tec CPD 030, Bal-Tec, Liechtenstein), sputtered with 3nm platinum (Bal-Tec SCD 500, Bal-Tec, Liechtenstein) and examined using a Zeiss scanning electron microscope (Zeiss, Ultra Plus, Zeiss Germany).

Ultrastructure of human bone marrow

Bone marrow cylinders have also been used to analyse the *in vivo* ultrastructure of stem cell microenvironments. Bone marrow specimen were collected as described for histological analysis (see figure 3.4.1). Following the collection of the bone marrow cylinder the samples were fixed in 2% glutaraldehyde in PBS for 24h at room temperature. After a PBS wash the samples underwent an over night post-fixation procedure in 2% osmiumtetroxide (Roth, Germany) to improve image contrast of fatty substances and membrane structures. Samples were dehydrated in increasing concentrations of acetone. At 50% acetone concentration the

samples were again negative stained in 1% uranylacetate (Sigma, Germany) to further add to the contrasting effect of OsO_4 for enhanced electron-scattering. After 3 cycles in 100% acetone and total dehydration the samples were embedded in epoxy resin using the modified SPURR embedding kit (Serva, Germany). After curing the resin over night the samples were trimmed and sectioned to ultra-thin sections (200nm) using a Leica ultramicrotome (Leica EM UC7, Leica Germany).

Transmission electron microscopy (TEM) was performed by the electron microscopy facility of the Max Planck Institute of Cell Biology and Genetics, Dresden. Prior to microscopical analysis the samples were again stained in uranyl acetate and lead cytrate. Bone marrow regions close to the bone surface of trabecular bone were analysed for cellular distribution of stromal cells and presence of extracellular structures.

Atomic force microscopy

Atomic force microscopy (AFM) was used to analyse the elasticity and the thickness of decellularised ECM substrates. Samples were prepared for AFM analysis by DNase treatment to remove excess adhesive material that could interfere with the interaction of the AFM-cantilever with the surface (see DNase treatment as described in section 3.3.1). All AFM measurements were performed by Jens Friedrichs using a Nanowizard II AFM (JPK Instruments) mounted on an inverted optical microscope (Observer.D1, Zeiss). For elasticity and height measurements, tipless, 200 μm long V-shaped cantilever having nominal spring constant of 0.06N/m (NP-O, Bruker) were used. Cantilever were calibrated using the equipartition theorem [Hutter, 1993].

For elasticity measurements, colloidal force probes were prepared by attaching glass beads (diameter 20 μm , Kisker Biotech) to the apex of tipless cantilever using a two-component epoxy glue (Araldit) as described [185]. To prevent non-specific adhesion to the matrices, the modified cantilevers were incubated in heat inactivated fetal calf serum (Invitrogen) for 1 hour prior to cell elasticity measurements. Force-distance curves were acquired using 500pN contact force and 5 $\mu\text{m}/\text{s}$ approach/retract velocity. The Young's Modulus was extracted from approach force-distance curves using the AFM data processing software (JPK Instruments).

To measure the thickness of hydrated ECM substrates a defined scratch was applied to the substrate to analyse the difference in height over the scratch area. To create a defined scratch ECM substrates were first dehydrated under a laminar flow of nitrogen after 3 washes in double distilled water. Using a scalpel a straight scratch was drawn into the decellularised ECM. The substrate was rehydrated in PBS and processed for AFM measurement. The height of the matrices was determined by performing a 100 μm line scan perpendicular to the scratch. Scan velocity was 1 $\mu\text{m}/\text{s}$.

Statistical analysis

Data were analysed using GraphPad Prism 5 (GraphPad Software Inc., USA). Multiple samples were analysed by one-way analysis of variance (ANOVA) and Tukey-Kramer's post hoc test or by two-way ANOVA and Bonferroni post hoc test to evaluate statistical differences among all samples. Asterisk denote statistical significance as follows: * $P < 0.05$, ** $P < 0.01$, *** $P < 0.001$. All data are presented as mean values \pm standard error of mean (s.e.m.).

Chapter 4

Results and Discussion

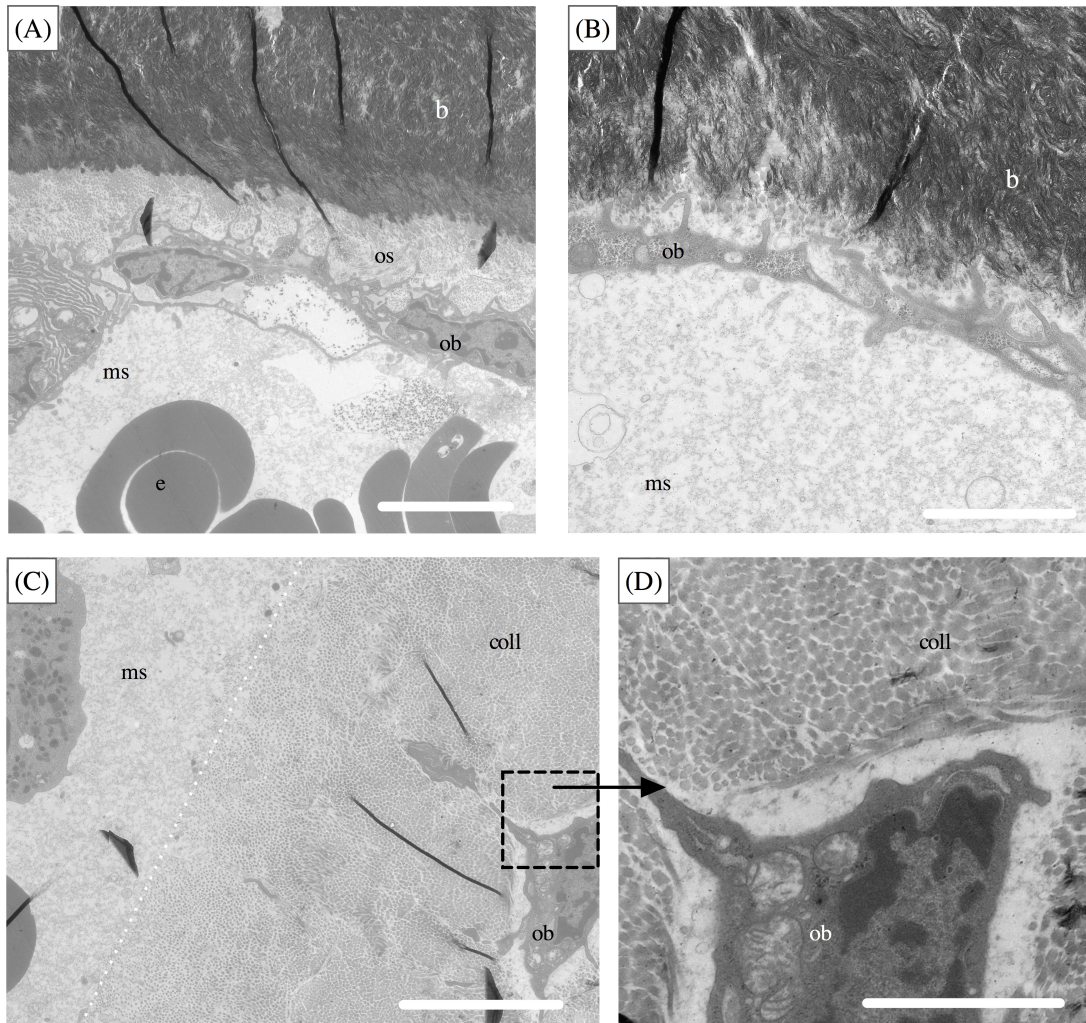
This study was set out to mimic the natural microenvironment of the BM in terms of ECM composition and architecture, to facilitate improved culture and expansion of stem and progenitor cells outside the human body. Therefore, at the beginning of this project the *in vivo* architecture of human BM was investigated to gain insight into the arrangement of ECM molecules within BM microenvironments. Next, the establishment of a stable anchorage platform for reproducible attachment of MSC-secreted matrix molecules is presented and complemented by varying stimulation of MSC during the ECM segregation phase. The established matrix substrates were further analysed for their morphology, topography, elasticity and composition. Finally, the potential for progenitor cell support and expansion was investigated by MSC and HSPC culture in contact with decellularised matrices.

4.1 Human bone marrow analysis

Trephine BM biopsy specimen from the iliac crest (drawn from the aspiration needle after BM aspiration) were used to study the histological and ultrastructural appearance of human BM. The focus was to analyse ECM structures present at BM sites which are thought to be stem cell niches, for example the osteogenic niche at the trabecular bone surface [75]. All samples were obtained from healthy donors and the overall appearance of the analysed BM specimen was in line with the common knowledge of trabecular bone anatomy. The haematopoietic BM depicted a highly vascularised reticular connective tissue, densely packed with haematopoietic cells [186]. The haematopoietic cell content relative to adipocyte content was in a normal range between 40-60% [58]. The bone surface was covered by endosteal cells, usually osteoblasts and stromal cells which secrete collagenous matrix into their environment [23]. This layer of matrix is called the osteoid, which gradually mineralises and forms the solid bone [187]. Figure 4.1.1 A and B shows transmission electron micrographs of bone lining regions. The analysed specimen were not decalcified and show a clear boundary between dark and mineralised bone areas and lightly coloured areas of osteoid (adjacent to osteoblasts). However, the specimen showed intrinsic artefacts of ruptured cells and cellular debris, caused by the aspiration and sampling

procedure. It was therefore difficult to analyse intact haematopoietic cells in close contact with the endosteal niche. Yet, it was clearly detectable that stromal cells secrete large volumes of extracellular material into their environments. Figure 4.1.1 C and D shows an osteoblast cell that secreted large amounts of collagen into the extracellular space, whereby typical patterns of collagen fibrils are visible either as longitudinal fibrils or in cross-section [188].

Figure 4.1.1: Human bone marrow ultrastructure

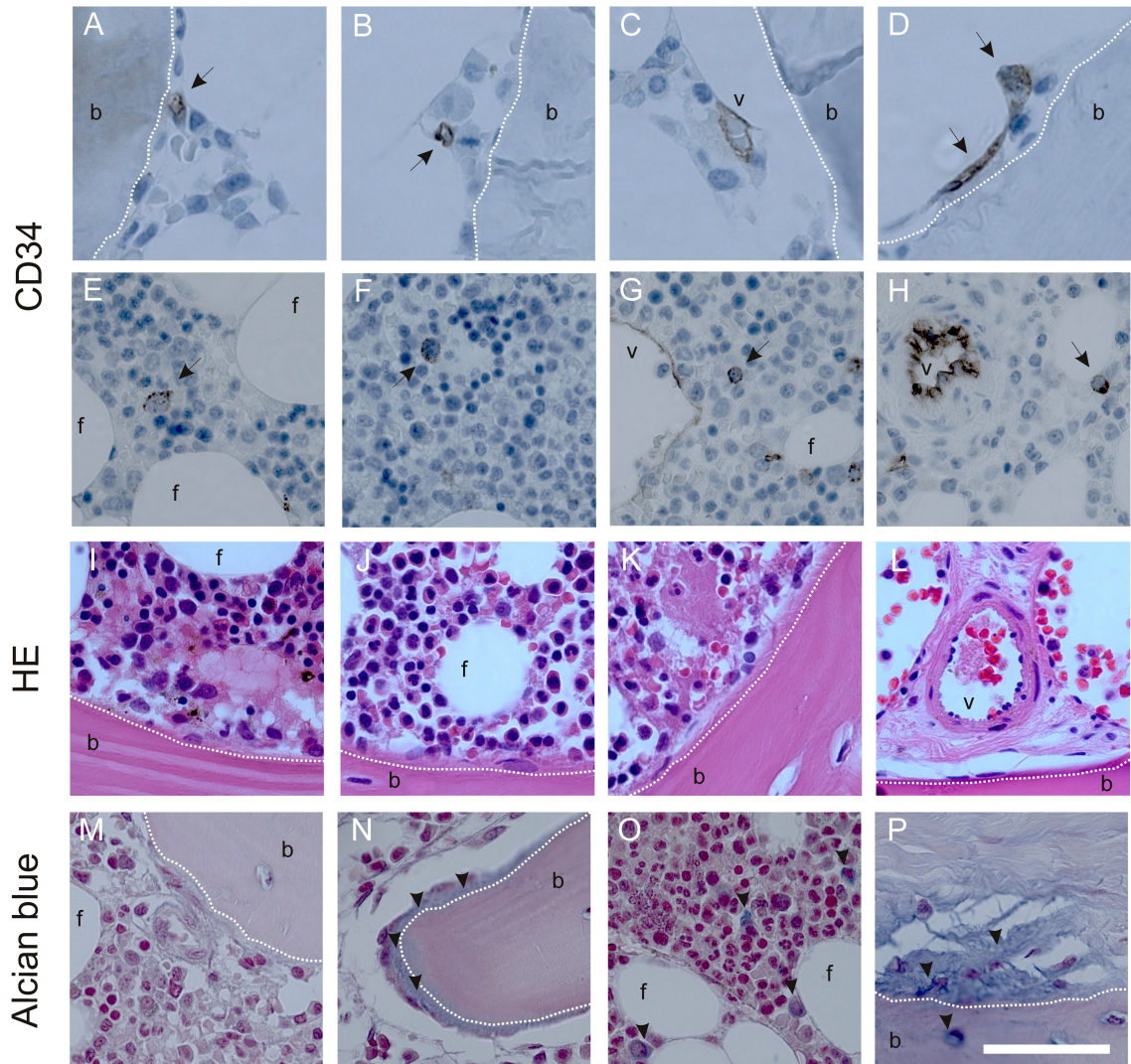


Transmission electron micrographs of human bone marrow specimen. Images show the accumulation of matrix material along the bone surface. Osteoblasts and bone lining stroma cells secrete collagenous matrix into their environment. Hematopoietic cells reside within the marrow space. (b bone, os osteoid, ob osteoblast/bone lining cell, ms marrow space, e erythrocytes, coll collagenous matrix) Scale bars at 5 μ m (A-C) and 2 μ m (D).

The marrow space provides the framework for nutritional supply and waste removal via the vascular network. Self-renewal and differentiation of precursor cells is provided by the marrow stroma [58]. BM stroma is known to be a mixture of adipocytes, fibroblasts and macrophage-like cells, as reviewed by Campbell et al. in 1988 [189]. Pioneering work in the 1980s has identified many ECM components of the bone marrow environment [96, 97,

190], including fibronectin, collagens and proteoglycans. The histological analysis of paraffin embedded samples allowed a general overview of the trabecular and vascular architecture of human BM. The paraffin specimen were also slightly damaged at the interface between bone and marrow, caused by the sectioning procedure. Figure 4.1.2 shows CD34+ cells that were detected at endosteal (panel A-D) and medullary (panel E-H) sites of the BM. Their phenotype shows a small cell shape with a low nuclear to cytoplasmic ratio.

Figure 4.1.2: Human bone marrow histology



Paraffin sections of human bone cylinders from bone marrow aspirations. (A-H) Immunohistochemical staining for CD34 cell surface antigen (brown DAB-signal). (I-L) Haematoxylin/Eosin cytoplasmic and nuclear staining. Blue color depicts nuclei, red color depicts cytoplasm and collagenous fibres, faint red depicts elastic fibres. (M-P) Alcian blue staining for sulfated glycosaminoglycans in blue. (v vessel, b bone, f fat, arrow CD34+ cells, arrow head alcian blue positive areas, dotted line marks the bone surface). Scale bar at 50 μ m.

Endothelial cells, also expressing CD34 mark the vasculature within the BM. The localisation of CD34+ HSPC was in line with proposed stem cell niches, like the osteoblastic niche [92], the reticular stromal niche [68] and the vascular endothelial niche [91]. Haematoxylin and eosin are basic and acidic dyes for the visualisation of nuclei and cytoplasm, respectively. Eosin also stains collagen and elastic fibres. Panel I-K shows densely packed haematopoietic cells in the marrow space surrounded by collagenous matrix material. Image L shows an example of a blood vessel next to the bone surface. The area around the vessel is supported by elastic and collagenous fibres. Alcian blue is a positively charged dye that binds to anionic substances like sulfated glycosaminoglycans (GAG). Panel M-P shows accumulation of GAG molecules at the bone interface. Very little glycoprotein staining was observed in the marrow space, which might be due to the processing of the sample material.

Histological and ultrastructural analysis have shown that the endosteal region in human BM harbours ECM proteins and proteoglycans. The existing ECM components are in exchange with progenitor cells by cell-ECM interactions. To mimic these interactions *in vitro* an authentic surrogate system has to be developed. Since stromal cells from the BM produce large amounts of ECM the idea was to use these cells and allow them to secrete BM-like ECM microenvironments outside the human body. The next section will discuss the establishment of stromal cell-generated ECM systems.

4.2 Stromal cell-generated decellularised matrices

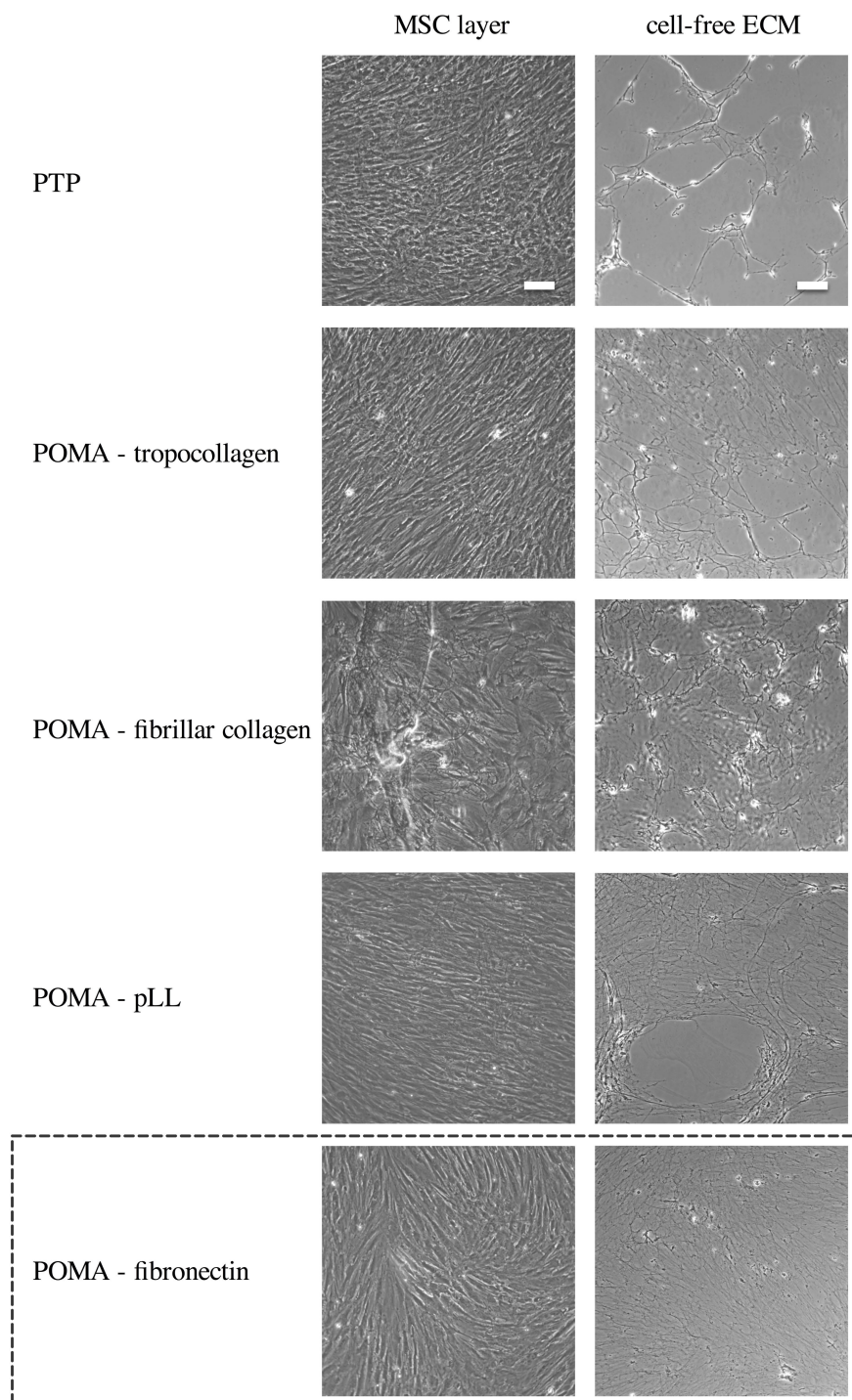
As observed by the analysis of human BM specimen, the ECM of living organisms is organised in a three-dimensional and fibrillar pattern. In order to allow better culture conditions for BM stem cells it is vital to provide the right microenvironment for cell adhesion, migration and proliferation. Previous studies by Cukierman et al. have shown the potential of 3-dimensional matrices in creating physiologically relevant cell-matrix interactions [160]. To create culture substrates that are able to closely mimic the complex nature of the *in vivo* situation primary human BM-MSC were used to generate extracellular matrices *in vitro*. The generation of 3-D matrices was adapted from a protocol by Beacham et al., which utilised primary fibroblast for the production of ECM substrates [155]. However, the main problem was the stabilisation of the secreted ECM to the culture substrate. The next section describes the stabilisation of MSC-secreted ECM to culture carriers.

4.2.1 Stabilisation of MSC-secreted ECM

To establish an *in vitro* ECM niche, early passage (p2) human MSC were allowed to deposit ECM onto the culture carrier for a period of 10 days. Subsequently, the cellular MSC layer was withdrawn from the culture by a decellularisation procedure using a detergent buffer containing Triton X-100 and ammonium hydroxide. Cultures were in short contact with the decellularisation agents and little mechanical force was applied to dislodge the MSC. The aim was to

cause minimal disruption to the underlying ECM network with tethered glycoprotein structures. However, the major drawback at that point was the delamination of freshly generated decellularised ECM sheets from the culture surface. The top panel of figure 4.2.1 shows the confluent MSC layer and the decellularised ECM network on standard polystyrene tissue culture plastic (PTP) substrates. The necessary washing steps to remove remnant cellular debris and the decellularisation reagent caused substantial displacement of the ECM layer. Beacham and colleagues described in their decellularisation protocol a procedure of surface preparation that includes gelatin coating and cross-linking of gelatin with glutaraldehyde to stabilise the attachment of matrices [155]. However, the artificial cross-linking of gelatin might hamper the natural interaction of ECM molecules with the surface and weakens the flexibility of the cell-generated ECM environment. Therefore, a dedicated approach was developed to improve interaction and anchorage of the secreted ECM with the culture surface. Reactive maleic-anhydride copolymer thin films aid the adhesive interaction between ECM and the substrate (see section 3.1.2 and [168]). Thin films of the hydrophobic polymer poly(ocadecene-*alt*-maleic anhydride) (POMA) were applied onto glass coverslips, and allowed covalent binding of biomolecules to anhydride moieties of the polymer via free aminogroups of the protein (usually by lysine residues). Covalently bound tropocollagen, fibrillar collagen, poly-L-lysine (pLL) and fibronectin (FN) was used to study which biomolecule serves best as a coupling agent to stabilise the secreted ECM sheets. Figure 4.2.1 shows culture of BM-MSC on each tested substrate and their effectiveness in stabilising decellularised ECM layers. All substrates showed decreased delamination effects during the decellularisation and washing procedure compared to PTP substrates. Tropocollagen and fibrillar collagen surfaces exhibited a thick underlying sheet of globular and fibrillar collagen, respectively [170]. Both substrates were rated as not applicable for routine stabilisation of MSC-generated ECM. Not only is tropocollagen the least effective in stabilising intact ECM layers (out of the 4 tested biomolecules), but also the artificial gel-like layer of fibrillar collagen appears to engage a large part of the decellularised ECM network instead of serving as a thin link between ECM and the substrate. The hydrophilic poly-L-lysine is a positively charged homo-polypeptide that is thought to mediate electrostatic binding of adhesion ligands to the surface. pLL was effective in stabilising ECM layers, however it did not support efficient stabilisation over longer storage periods. Thin monolayers of FN (at a concentration of 400ng/cm², [191]) showed superior ECM adhesion and anchorage to the substrate and prevented ECM perturbation during cell lysis. The remaining ECM layer appeared as a homogenous and dense sheet of complex interconnected ECM structures. The FN molecule serves as a protein-binding platform via its functional binding domains (FN domain type I, II and III) that are responsible for binding to fibrin, collagen and heparan sulphate proteoglycans [29, 34]. Multiple interactions sites between FN and secreted ECM molecules enhance the stability of the substrate and maintain a natural conformation of the matrix network. Since covalently bound POMA/FN surfaces resulted in the best stabilisation of decellularised matrices they were used for all following experiments as an anchorage platform for ECM substrates.

Figure 4.2.1: Substrates for stabilisation of secreted ECM to the culture carrier

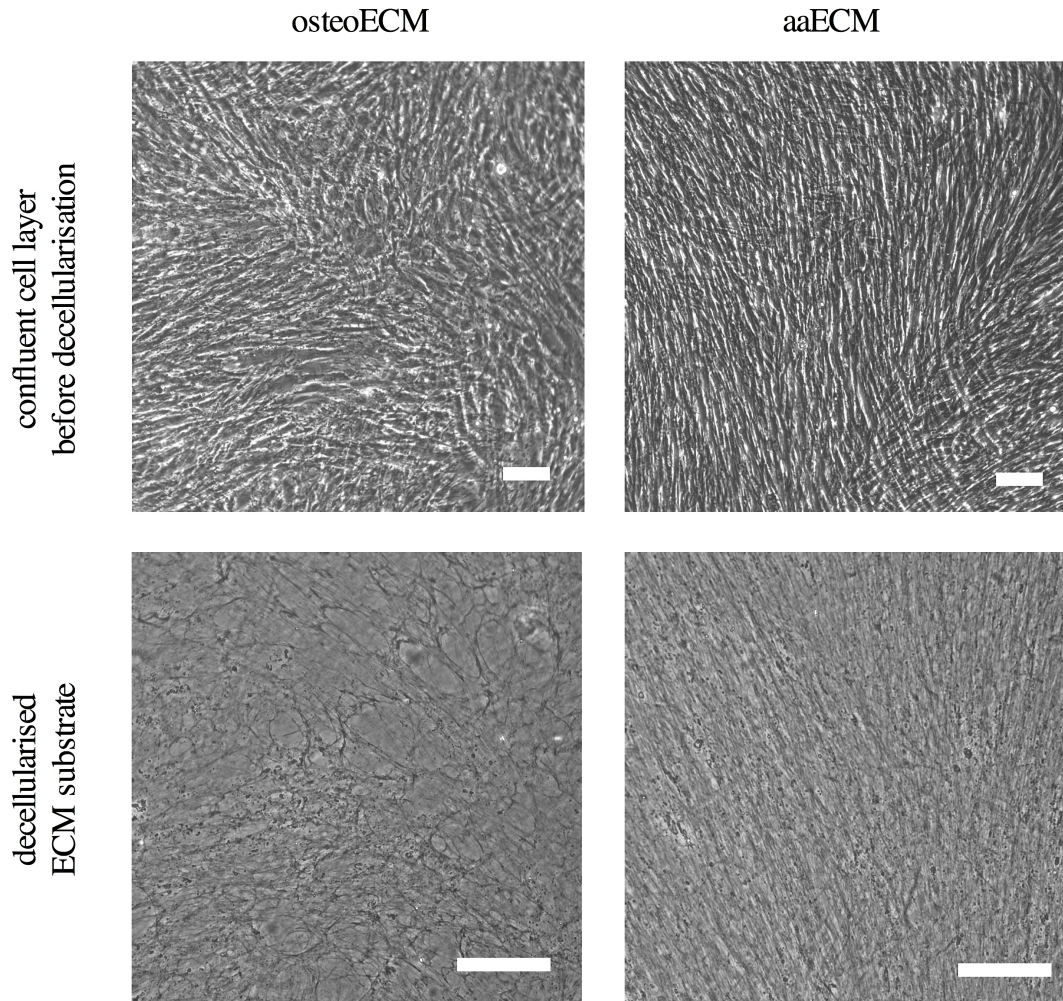


Different substrates tested for stabilisation of secreted ECM. Almost complete delamination of decellularised ECM layers from PTP culture carriers (top row). Tropocollagen, fibrillar collagen, poly-L-lysine (pLL) and fibronectin were covalently bound to POMA-coated surfaces to probe their stabilisation properties. Left column shows cells at confluence prior to the decellularisation procedure. Right column shows the cell-free ECM sheets after extensive washing in PBS. POMA-fibronectin was found to anchor the decellularised ECM most appropriate (dotted box). Images are phase contrast micrographs, scale bars at 100 μ m.

To account for the different regions of BM two kinds of ECM were generated, by applying different stimuli to the cells during the ECM production phase. The first kind of ECM substrate was created focussing on enhanced collagen secretion by BM-MSC. Collagen synthesis is dependent on the presence of vitamin C. For the conversion of procollagen into collagen, namely the hydroxylation of proline and lysine residues, ascorbic acid is needed as a cofactor [192]. Therefore, ascorbic acid effectively augments collagen biosynthesis [193]. The ECM substrates that were created by elevated ascorbic acid supplementation were termed *aaECM*. The second type of ECM that was generated by BM-MSC was thought to mimic the osteogenic microenvironment, similar to the endosteal region that is created by bone lining osteoblasts [74]. To induce MSC differentiation into osteoblasts and to trigger the secretion of osteoblast-like ECM molecules, the cultures were supplemented with osteogenic induction factors (see table 3.1.1).

The ECM substrates that were created by osteoblast differentiated MSC were termed *osteoECM*. Figure 4.2.2 shows the confluent MSC layers and the decellularised ECM of both ECM types. Morphologically, both types appeared as very complex interwoven networks of ECM proteins, fibres and GAGs. OsteoECM appeared less dense and showed an open comb-like structure resembling the arrangement of osteogenic induced MSC. In comparison, the appearance of aaECM was specified by the aligned morphology of the confluent MSC-layer and resulted in a thick and packed matrix environment left behind after decellularisation.

Figure 4.2.2: aaECM and osteoECM stabilised on FN/POMA culture carriers



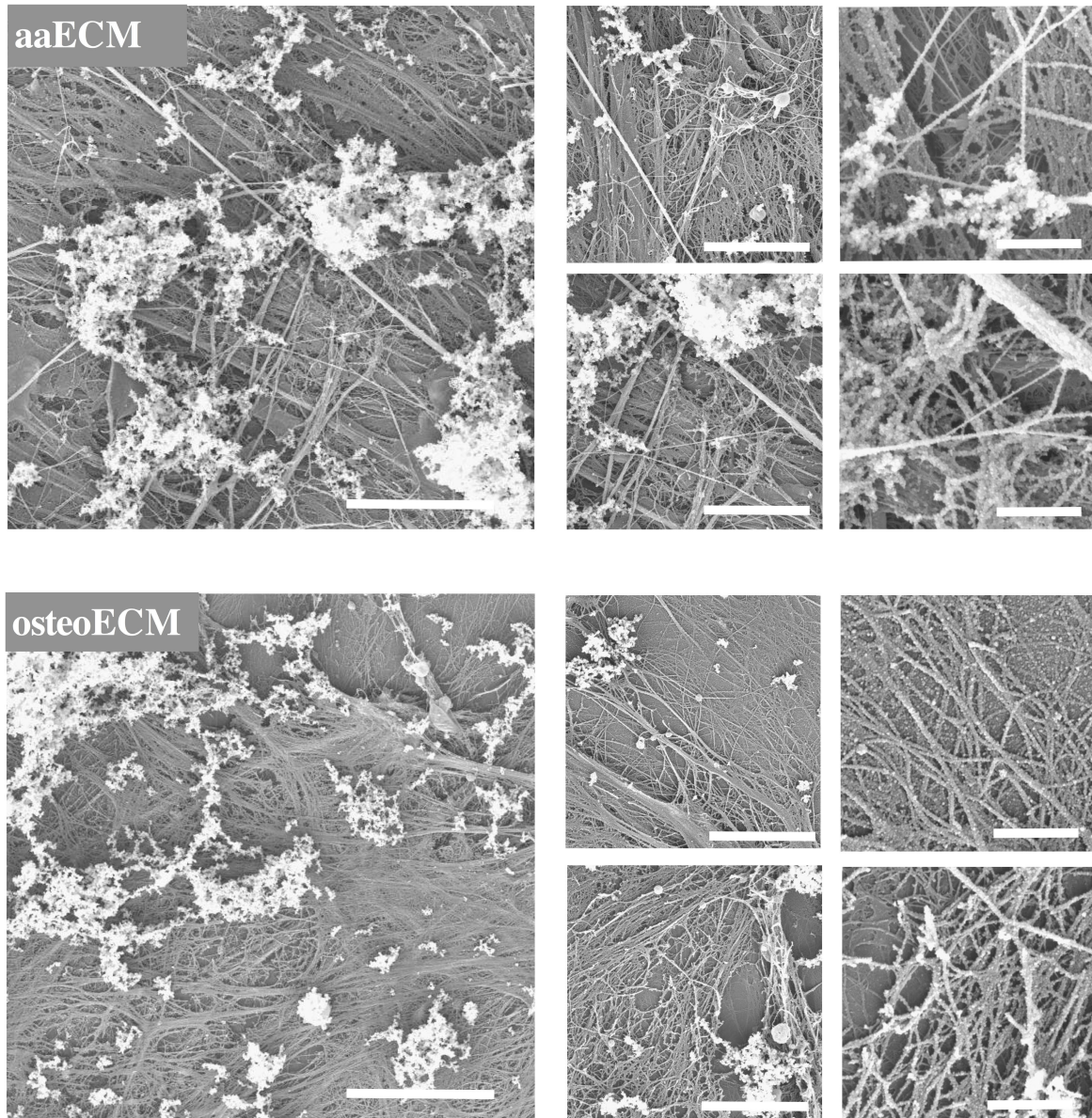
Two types of ECM substrates were generated by MSC stimulated with ascorbic acid (aaECM) or osteogenic induction media (osteoECM). MSC were cultured on FN/POMA carriers until confluence and allowed to secrete ECM for 10 days (top row). An anchored protein network was achieved throughout the decellularisation process yielding stable ECM substrates with distinct morphology for aaECM and osteoECM, respectively (bottom row). Images are phase contrast micrographs, scale bars at 100 μ m.

In summary, the procedure of creating decellularised ECM substrates has been optimised in terms of stability and variety. The application of continuous covalent attachment of coupling agents such as aminosilane, a hydrophobic reactive copolymer thin film and fibronectin permits reproducible and robust anchorage of ECM proteins to the culture surface. The idea of using BM intrinsic cells to generate ECM microenvironments was successfully conducted and resulted in the establishment of two varying types of MSC-made ECM that can serve as cell-free *in vitro* niches. These substrates were furthermore analysed for their characteristics, as discussed in the next section.

4.2.2 Characteristics of decellularised matrices

MSC-generated decellularised extracellular matrices were analysed for their ultrastructural appearance, their physical properties and for abundance of collagenous and sulphated glycosaminoglycan components. First, the ultrastructural character was analysed via scanning electron microscopy (SEM). The most striking observation when looking at decellularised matrices, is their complex architecture and fibrillar interwoven disposition. Figure 4.2.3 shows SEM micrographs of aaECM and osteoECM substrates. Both matrices have a distinct morphology. aaECM substrates depict a dense meshwork of fibrillar bundles that are connected by numerous smaller structures that span the distance between fibres. In osteoECM substrates the coverage with fibrillar structures is less dense compared to aaECM, but larger networks of fibre bundles are visible. GAG structures are detectable as white sponge-like arrangements on top of the fibrillar network [105]. The complexity of such elaborate structures deposited solely by MSC reflects the importance of cellular processing and modification of secreted ECM proteins for the creation of native extracellular environments. The advantage of decellularised matrices is the preservation of the complex suprastructure of the ECM network. The hierarchical organisation of macromolecules into fibrils, microfibrils and suprastructural networks mediates specific structural features and the overall physical properties of the extracellular environment. The efficiency of these matrices is related to their ability to exhibit structural features of the ECM that are responsible for the interaction of cells with extracellular signalling ligands [52]. ECM suprastructures are composites of more than one molecular species that differ in identity and relative abundance. Most studies focus only on singular molecular features and mechanisms, but it is important to keep in mind the importance of the orchestrated topography of enzymatically linked and processed ECM molecules for a functional interaction between the cell and the ECM. Studies by Cukierman [160, 161] have shown that decellularised matrices can serve as an effective *in vivo* surrogate to study cellular adhesion mechanisms. Other studies have shown that matrix proteins cause a different response of cells when they are either organised in filaments or displayed on a flat surface [194, 195], reflecting that cells sense nanoscale surface topographies such as spacing patterns of matrix ligands [196]. The topographical complexity of decellularised matrices produced by BM-MSC implies that these substrates have the potential to serve as valid *in vitro* model-systems for native extracellular microenvironments.

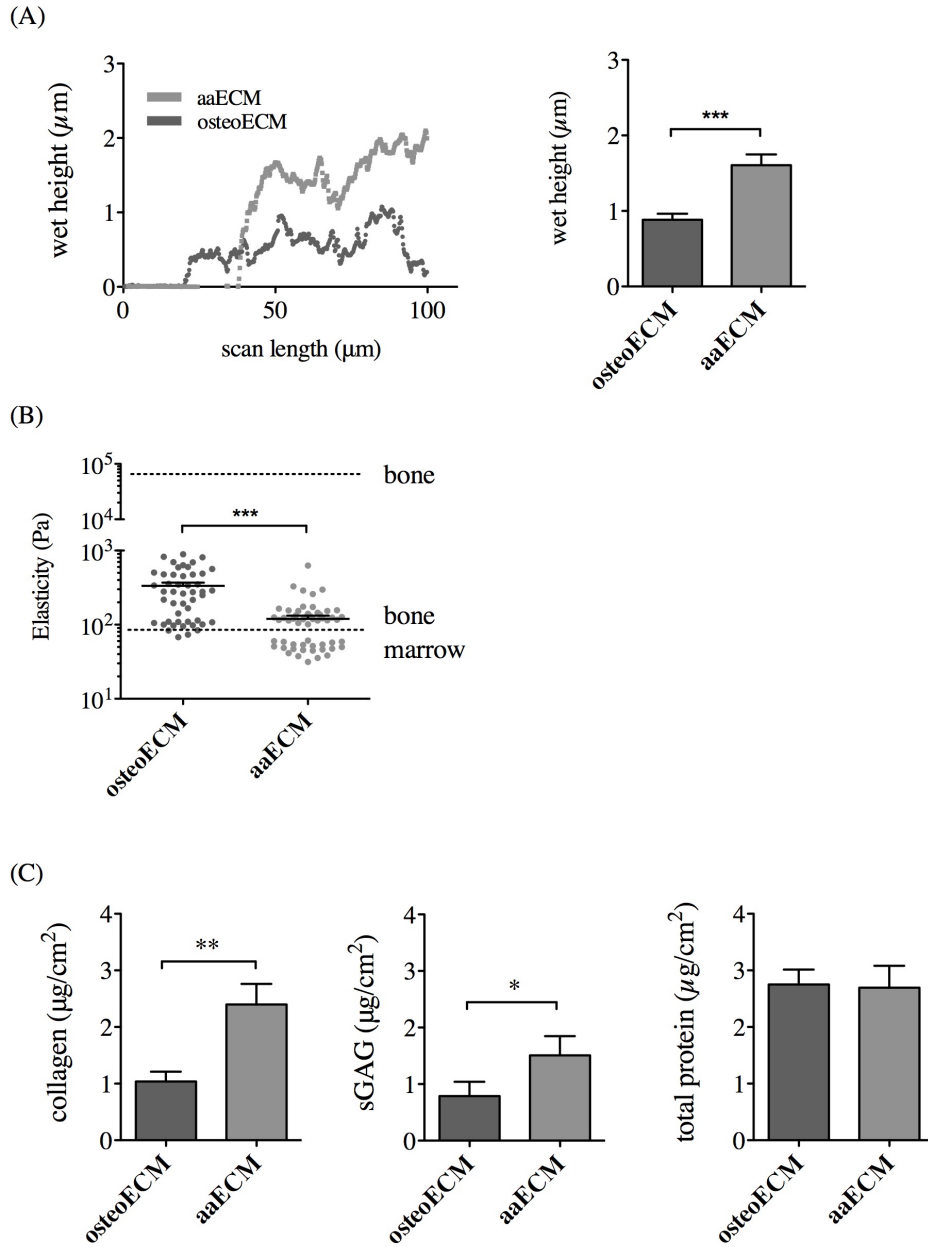
Figure 4.2.3: Suprastructural appearance of aaECM and osteoECM substrates



Scanning electron micrographs of decellularised aaECM (top panel) and osteoECM (bottom panel) substrates. Composite fibrillar structures are arranged to suprastructural ECM complexes. GAGs are visible as delicate white structures attached to the fibrillar network of ECM. Scale bars as follows: left column 10µm, center column 5µm, right column 1µm.

Figure 4.2.4 shows the characteristics of decellularised ECM in terms of substrate height, elasticity and total collagen, sGAG and protein content. The thickness of ECM substrates was measured via the difference in height over a scratch in the substrate. As already implied by SEM images (figure 4.2.3), the height of aaECM and osteoECM substrates was found to be significantly different. The height determined for aaECM was $1.607 \pm 0.14 \mu\text{m}$ ($n=39$) and for osteoECM $0.883 \pm 0.08 \mu\text{m}$ ($n=38$) ($P < 0.0001$). The 3-dimensional character of the substrates can be appreciated from the line scan plot, as the substrate depicts groves and elevations (figure 4.2.4 A left). Thereby, decellularised extracellular matrices allow some degree of 3-dimensionality in spite of the fact that they are created in a 2-dimensional culture setup. As important as it is for cells to be arranged in 3-dimensional patterns within a tissue, it is also important that they can sense and interact with the elastic properties of their environment to conduct the corresponding signalling and cell fate events [48]. The elasticity of decellularised aaECM and osteoECM substrates was determined by AFM indentation measurements. Substrate elasticity was significantly different between aaECM and osteoECM, measuring a Young's Modulus of $119.7 \pm 13.1 \text{ Pa}$ ($n=55$) and $335.0 \pm 35.17 \text{ Pa}$ ($n=50$), respectively ($P < 0.0001$) (Figure 4.2.4 B). The higher stiffness of osteoECM could result from i) the less dense, more flat and coarse-meshed morphology of osteoECM compared to aaECM, and from ii) the process of osteoblast differentiation of MSC including incorporation of calcium phosphate deposits into the ECM [197]. However, both substrates describe a very soft environment, ranging at a tissue stiffness comparable to that of BM [51] (see section 2.1.2). Initial studies with fibroblasts and tumor cells have highlighted the importance of cell-ECM mechanosensing mechanisms [198, 199]. More recent studies by Engler et al. investigating MSC differentiation, have shown that substrate elasticity can have profound effects on the outcome of cell fate [117]. The process of mechanosensing, mechanotransduction and mechanoresponse is a bi-directional process (as described in section 2.1.2). It includes integrin and ECM clustering at the cell membrane triggering transmission of Rho GTPase and MAPKinase signalling events into the nucleus that can alter gene expression patterns. Those changes in turn can change the presentation of adhesion receptors on the cell surface and cause remodelling of ECM assemblies and cell shape [50, 200]. Many biomaterial approaches are now trying to mimic different elasticities to investigate mechanotransduction processes and to develop new tissue engineering strategies [17]. The BM model system of decellularised matrices presented in this study can provide very soft, gel-like substrates for the culture of human MSC and HSPC.

Figure 4.2.4: Characteristics of ECM substrates



(A) Wet height of decellularised ECM layers. Representative height profiles of aaECM and osteoECM as measured by atomic force microscopy (AFM) over a 100 μ m scan length (left graph) and average data from 3 separate MSC donors ($n=30$) (right graph). (B) ECM substrate elasticity measured by AFM indentation. For comparison tissue elasticity of bone and bone marrow are depicted as dotted lines ($n=4$ MSC donors, min. 50 measurement spots). (C) Total collagen (left graph) and sulphated glycosaminoglycan (sGAG) (middle graph) content of ECM substrates ($n=4$ donors) compared to total protein amount of decellularised ECM (right graph, $n=8$) given as μ g/cm² substrate area. All data mean \pm s.e.m; asterisk denote statistical significance * $P<0.05$, ** $P<0.01$, *** $P<0.001$.

As mentioned in section 4.1, the BM mainly consists of collagenous and proteoglycan matrix molecules [96, 97, 189, 190]. *In vitro* generated decellularised matrices were analysed for their quantitative amount of these major ECM components (figure 4.2.4 C). Collagen was detected at a concentration of $2.399 \pm 0.361 \mu\text{g}/\text{cm}^2$ in aaECM and $1.038 \pm 0.17 \mu\text{g}/\text{cm}^2$ in osteoECM substrates. This 2-fold significant difference can be attributed to the enhanced ascorbic acid treatment and increased collagen synthesis in aaECM cultures [193]. In comparison to collagen, the total protein content of decellularised matrices is also shown in figure 4.2.4 C; ranging at approximately $3 \mu\text{g}/\text{cm}^2$ for both substrates. Regardless that both, collagen and total protein values, were determined by different quantification techniques, it indicates that indeed most of the protein that is present in decellularised matrices can be allocated to collagen. Sulfation of GAG chains is one mechanism to add various functionalities to proteoglycans, and almost all proteoglycans are sulfated (except hyaluronan). The assay used to quantify proteoglycan content in decellularised matrices specifically labelled sulfated polysaccharide components of proteoglycans or free sulfated GAG chains, such as chondroitin sulfates, keratan sulfates, dermatan sulfates and heparan sulfates. The result shows that again aaECM contains more proteoglycans than osteoECM per cm^2 culture area (sGAG content at $1.509 \pm 0.34 \mu\text{g}/\text{cm}^2$ for aaECM and $0.788 \pm 0.25 \mu\text{g}/\text{cm}^2$ for osteoECM; $n=4$; $P<0.05$). The importance of collagens and proteoglycans for stem cell function in the BM has been investigated by many studies [104, 171, 201, 202]. The next section will discuss more closely which additional components are present in decellularised ECM substrates.

It can be summarised that both ECM types describe representative characteristics of a BM microenvironment in terms of their overall collagen and glycoprotein composition, as well as depicting the appropriate elasticity and suprastructural arrangements of native extracellular environments. To more closely decipher the molecular constituents of decellularised matrices the next section will discuss the detailed proteomic composition of aaECM and osteoECM.

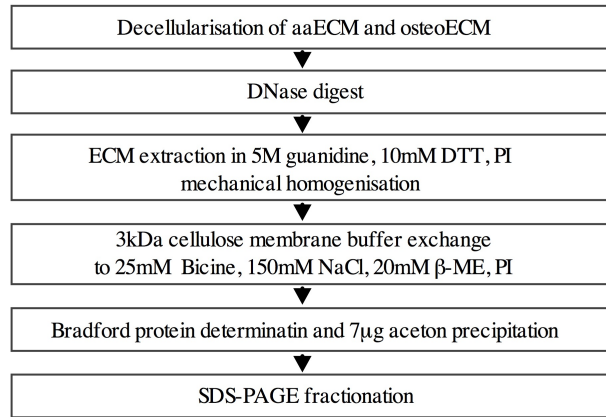
4.3 Proteomic composition of ECM substrates

The presented MSC-generated extracellular matrices termed aaECM and osteoECM that were introduced and described in section 4.2 were analysed for their detailed proteomic composition to draw conclusions about the factors that are responsible for BM niche properties. Therefore, protein extracts of ECM substrates generated by different MSC donors were separated via SDS-PAGE and fragmented for mass spectrometric analysis. Figure 4.3.1 shows the extraction procedure to create solubilised ECM extracts. Sequential runs of differing pools of ECM extracts are shown in figure 4.3.1 B. For double mass spectrometric analysis (MS-MS, termed MS²), SDS-PAGE separated samples were cut into slices for in-gel digest and MS analysis of tryptic peptides. Figure 4.3.2 shows the cutting pattern for both aaECM and osteoECM in parallel. The most dominant proteins from each slice of the SDS-gel are shown as a representative example for an aaECM sample. Both types of ECM displayed similar banding patterns of fragmented proteins, suggesting reproducible proteomic configurations. Indeed, both ECM types have a majority of proteins in common (see table 4.3.1). Unfortunately, definitive and significant differences between aaECM and osteoECM can not yet be stipulated, since only two separate matrix extraction runs have been analysed by mass spectrometry. However, the ECM components that were detected in both samples are discussed in this section.

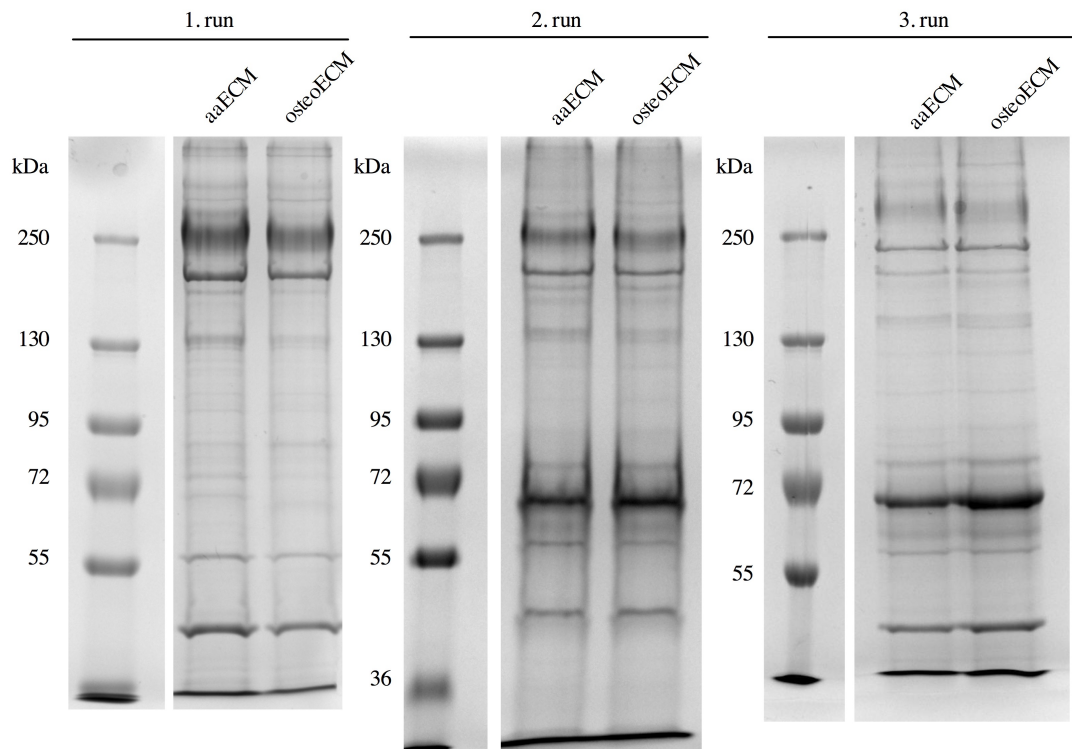
After SDS-PAGE separation of aaECM and osteoECM extracts lanes of each sample were cut into several fragments, processed for in gel tryptic digestion and subsequently analysed via mass spectrometry. The used orbitrap mass spectrometric analysis was highly sensitive and detected more than thousand proteins within each sample. It is to note that many intracellular proteins were detected in decellularised ECM extracts (for example ribosomal and cytoskeletal proteins). However, this is related to residual intracellular protein contamination resultant from the cell lysis procedure during decellularisation. Figure 4.3.3 shows the percentage of extracellular matrix annotated proteins within the whole protein extract. The number of MS² spectra are a measure for the identification frequency of protein-specific peptides (figure 4.3.3 A). Spectrum intensity is a measure for the quantitative abundance of detected protein-specific peptides (figure 4.3.3 B). Although, only 10% of all detected proteins are extracellular matrix annotated the quantitative majority of ECM substrates can be related to extracellular proteins. A full list of all identified proteins in decellularised matrices is given in appendix A.

Figure 4.3.1: Extraction and separation of decellularised ECM substrates

(A) Extraction of decellularised ECM proteins

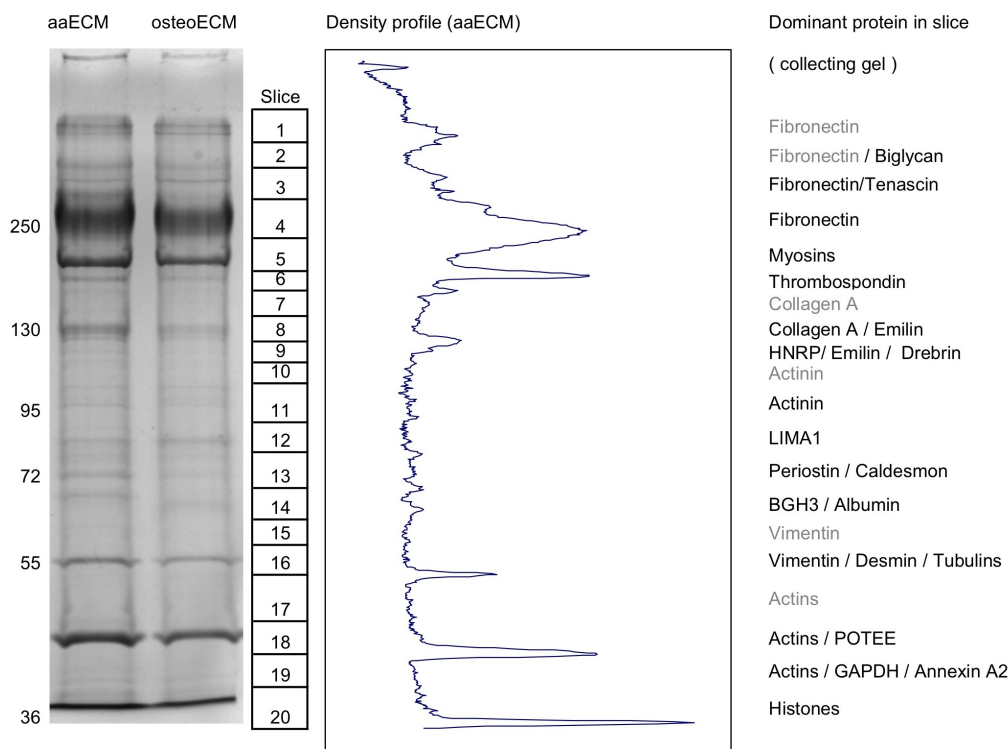


(B) SDS-PAGE separated protein extracts



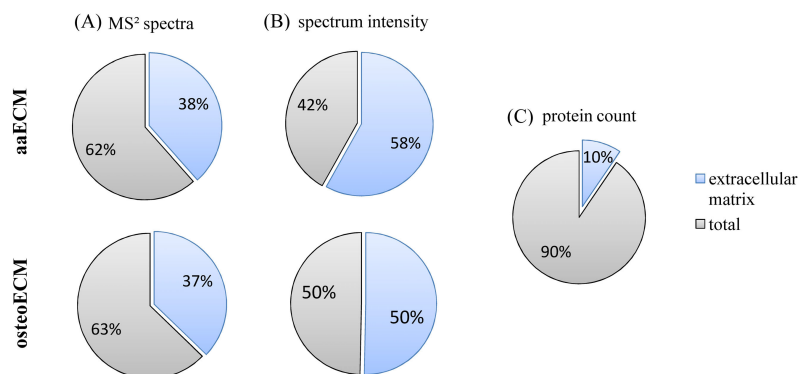
(A) Extraction procedure for ECM substrates to yield soluble extracts of ECM proteins for subsequent fractionation and mass spectrometric analysis (for details see section 3.3.1). (B) SDS-PAGE gels of 3 independent protein extraction runs. Each run describes a pool of 5 MSC donor extracts for aaECM and osteoECM, respectively. The banding pattern shows close similarities between both ECM types and between each run.

Figure 4.3.2: SDS-PAGE gels and cutting pattern for in-gel digestion



SDS-PAGE gel of protein extraction run 1 is shown as a representative example for the cutting pattern of in-gel-digestion before mass spectrometric analysis. A line scan for aaECM separated proteins shows the density profile over the whole lane. Dominant proteins from each gel slice are given next to each slice and represent the proteins from which tryptic peptides have been identified with the highest intensity.

Figure 4.3.3: Percentage of extracellular matrix annotated proteins in total sample



Percentages of extracellular matrix annotated proteins in total aaECM and osteoECM extracts are given as (A) the cumulative number of peptide-MS² spectra for each protein, (B) the normalised cumulative peptide intensities for each protein and (C) the number of identified proteins. Data are mean values of run 1 and 2 of ECM extraction.

Table 4.3.1 lists the identified components of extracted decellularised matrices that have been assigned as extracellular proteins by gene ontology annotations for subcellular localisation. More than 70 proteins are allocated to this group. As already discussed in section 4.2.2 the proteomic analysis also revealed that the majority of ECM proteins are collagens and proteoglycan core proteins. Many independent studies have analysed the composition of *in vivo* BM-ECM [23, 96] or secreted ECM proteins of BM-stroma *in vitro* [102, 103]. Other studies have analysed the transcriptome of BM-MSC and stem cell-supporting stromal cells [203, 204, 205, 206, 207]. The main proteins that frequently have been detected in almost all those studies, and which also have been detected in this work are the following. Collagen I, collagen III, collagen V, FN, tenascin, thrombospondin, perlecan, emilin-1, fibulin, versican, biglycan, syndecan, decorin, osteonectin (SPARC), vitronectin, transforming growth factor-beta-induced protein ig-h3 and connective tissue growth factor. This listing shows the amplitude of molecules that are involved in the complex organisation of native extracellular environments. Five of the most identified proteins in aaECM and osteoECM are going to be discussed in this section. Many proteins that are present at very low concentrations (that were identified less often) are not necessarily less important for the microenvironment. The power of the compiled data has to be extracted by researching known and new relationships between ECM components and cells of the environment.

Fibronectin was the most identified protein in decellularised ECM extracts. The amount of FN that was secreted by BM-MSC can not be determined since FN was also used for culture setup and anchorage of secreted ECM. Nevertheless, FN is one of the major BM-ECM components and its ample presence in decellularised matrices partially reflects the situation of the BM environment [208, 209]. As mentioned previously, FN interacts not only with cellular integrins it also contains binding sites for collagens, fibrins and heparan sulfate proteoglycans [210, 211], which also makes it an important candidate for the structural architecture of decellularised matrices.

Another glycoprotein that has been identified in large quantities in aaECM and osteoECM was thrombospondin-1. Thrombospondins (TSP) are calcium binding adhesive glycoproteins that mediate cell-cell and cell-matrix interactions. TSP-1 is involved in platelet aggregation, inflammatory response and angiogenesis [212]. It modulates angiogenesis by regulating the activity of extracellular proteases, such as matrix metalloprotease 9 and thereby is involved in remodelling of ECM structures [213]. Thrombospondin contains multiple protein domains. The amino-terminal domain has heparin-binding, cell attachment, migration and proliferation functions, and can be recognised by syndecan, HSPG and $\alpha 3\beta 1$ integrin. The type 1 domain repeats are responsible for protein binding, TGF β -activation and inhibition of proliferation, angiogenesis and apoptosis. Type 1 repeats can be recognised by HSPG and $\beta 1$ integrin. The type 3 domain repeats are calcium binding and cell binding domains that are recognised by $\beta 3$ integrins [214]. These domains also contain homology sites of procollagen, FN and von Willebrand factor [215]. TSP is cell surface associated and functions at the interface between ECM and the cell membrane. It has the ability to form multiprotein complexes that form

specialised regions for signalling cascades which involve activation of integrins, FAK and RAS for cell adhesion and migration or activation of PI3K and fascin for cytoskeletal organisation [214]. Long et al. have shown that TSP acts as a cytoadhesion molecule supporting human HSPC in the BM [100].

Collagens are a group of structural proteins that mediate tissue strength, support and elasticity. They support cell growth and contain binding domains that can initiate cell signalling [216] regulating cell adhesion and migration. Various collagens have been shown to be involved in these mechanisms in the BM [98, 102, 217]. The collagens that were detected in this study are collagens type I, III, IV, V, VI, XI, XII, XIV, XV, XVI. Collagen type I was the most identified fibrillar collagen and its importance for MSC [218] and HSPC [114] proliferation and differentiation has been shown. For example collagen I stimulated osteogenesis of human MSC by activation of ERK and Akt through PI3K/ERK pathway [218]. Another highly identified collagen is collagen VI, which forms microfibrillar structures and is assembled from three individual α (VI) chains. Klein et al. [98] have detected collagen VI in human BM microenvironments and have shown that it is a strong adhesive substrate for BM mononuclear cells. Only the triple helical domain structure could mediate adhesiveness and not purely RGD/ β 1 integrin interaction. These data indicate that clearly, collagens are one of the most important ECM proteins to consider for investigation of MSC and HSPC interaction with decellularised matrices.

Transforming growth factor-beta-induced protein ig-h3 (also termed β ig-h3 or RGD-containing collagen-associated protein) is an adhesion protein which binds to type I, II, and IV collagens and is involved in many physiological and pathological mechanisms. The most studied pathological condition involving β ig-h3 is corneal dystrophy [219]. A study with recombinant β ig-h3 has shown that it directly interacts with biglycan and decorin, promotes collagen VI aggregation, and participates in ternary complexing with these macromolecules [220]. The protein contains four tandem repeats of FAS1 domains (first identified in drosophila fascilin-1) and a carboxy-terminal RGD sequence [221]. The FAS1 domain represents an ancient cell adhesion domain and other human proteins have been identified to contain FAS1 domains. For example periostin which is also one of the most identified proteins in aaECM and osteoECM and which has been shown to be expressed by MSC [222] also contains FAS1 domains. This indicates that FAS1-integrin interactions may play an important role for communication of BM cells with the ECM. The cleavage of RGD-peptide from the c-terminal region of β ig-h3 has been suggested to facilitate apoptosis [223]. With its broad abundance within decellularised matrices and its many functions in cell adhesion and signalling β ig-h3 is an interesting candidate to study its impact on BM stem cells.

Tenascin-C is a large hexameric glycoprotein and occurs together with FN and collagen type III in human BM [99]. Each subunit consists of EGF-like repeats, FN type III-like domains and a fibrinogen-like terminal sequence. Interaction between BM mononuclear cells and the mentioned binding domains has been shown by Seiffert et al. [224]. Besides its adhesive and mitogenic properties tenascin has also been shown to be involved in migratory pathways of

haematopoietic progenitor cells [225]. As previously shown in figure 4.2.4 C, proteoglycans are present in large quantities in decellularised ECM substrates. A specific proteoglycan that has been identified in large abundance within decellularised matrices was perlecan.

Perlecan (also termed basement membrane-specific heparan sulfate core protein) is a heparan sulfate proteoglycan (HSPG) of basement membranes and pericellular matrices. It interacts with other basement membrane components such as laminin, prolargin, collagen type IV and extracellular matrix protein 1 [226, 227, 228], which are also detected in aaECM and osteoECM. Perlecan is arranged in 5 distinct domains, harbouring protein motifs involved in cell growth, adhesion and signalling [229, 230]. Many HSPG of BM are known for their ability to bind hematopietic growth factors and present them to precursor cells in their environment [201], whereat perlecan is also involved in collagen fibrillogenesis and structural stability of the skeleton [45, 231]. The ability of HSPG to establish and mediate morphogen and growth factor gradients underlines their proposed importance as building blocks for stem cell niches [232]. Many other interesting extracellular binding proteins, signalling ligands and structural proteins have been detected in MSC-generated decellularised matrices. To investigate detailed mechanisms of action for specific proteins present in decellularised matrices, the next possible steps are targeted manipulation of cellular interaction with proteins of particular interest for BM niche function.

Summarising, it can be said that many proteins that have been reported to be present in BM have also been detected in MSC-secreted decellularised matrices, validating the surrogate character of these matrices as *in vitro* BM microenvironments. It is important for future studies to identify minimal criteria, which of the ECM components are indispensable and which are dispensable for successful engineering of BM stem cell culture systems. Dissecting the functions of the proteomic components will help to break down the complexity and will be of assistance to design defined systems that mimic not only singular but also combinatorial molecular structures of BM microenvironments.

But first, the impact of the presented complex and multifunctional decellularised culture system is tested for its potential to interact with and support BM progenitor cells. In section 4.4 the impact of MSC-generated decellularised matrices on MSC and HSPC culture will be discussed.

Table 4.3.1: List of ECM proteins detected in decellularised protein extracts

log (MS2 count) aaECM	log (MS2 count) osteoECM	Protein IDs	MW [kDa]	Descriptions
4.09	3.97	P02751	262.6	Fibronectin
3.52	3.35	P12111	343.7	Collagen alpha-3(VI) chain
3.32	2.84	P24821	240.9	Tenascin
3.25	3.03	P07996	129.4	Thrombospondin-1
3.08	3.22	Q99715	333.1	Collagen alpha-1(XII) chain
3.16	2.76	P12109	108.5	Collagen alpha-1(VI) chain
3.02	2.56	P21810	41.7	Biglycan
3.00	2.58	Q15582	74.7	Transforming growth factor-beta-induced protein ig-h3
2.99	2.33	Q15063	93.3	Periostin
2.87	2.67	Q9Y6C2	106.7	EMILIN-1
2.28	2.93	P98160	468.8	Basement membrane-specific heparan sulfate proteoglycan core protein
2.86	2.49	P12110	108.6	Collagen alpha-2(VI) chain
2.72	2.52	P07355	38.6	Annexin A2
2.74	0.85	Q05707	193.5	Collagen alpha-1(XIV) chain
2.15	2.52	P51888	43.8	Prolargin
2.33	2.33	P08123	129.3	Collagen alpha-2(I) chain
2.27	2.10	P07585	39.7	Decorin
2.05	2.27	P27658	73.4	Collagen alpha-1(VIII) chain
2.26	2.05	P02452	138.9	Collagen alpha-1(I) chain
2.16	2.01	P04004	54.3	Vitronectin
1.84	2.13	P23142	77.2	Fibulin-1
1.74	1.97	P98095	126.6	Fibulin-2
1.43	1.98	Q14112	151.3	Nidogen-2
1.12	1.91	P12107	181.1	Collagen alpha-1(XI) chain
1.82	1.54	P20908	183.6	Collagen alpha-1(V) chain
1.85	1.10	P51884	38.4	Lumican
1.71	1.70	P08572	167.6	Collagen alpha-2(IV) chain
1.79	1.56	P09382	14.7	Galectin-1
1.78	1.50	P07093	44.0	Glia-derived nexin
1.40	1.70	Q76M96	108.2	Coiled-coil domain-containing protein 80
1.44	1.54	P36955	46.3	Pigment epithelium-derived factor
0.78	1.63	Q08431	43.1	Lactadherin
1.52	1.43	P05121	45.1	Plasminogen activator inhibitor 1
1.54	1.37	P39060	178.2	Collagen alpha-1(XVIII) chain
1.34	1.48	Q92626	165.3	Peroxidasin homolog
1.54	0.63	Q8IUX7	130.9	Adipocyte enhancer-binding protein 1
1.20	1.48	P13611	372.8	Versican core protein
1.40	1.33	P05997	144.9	Collagen alpha-2(V) chain
1.45	1.18	P35625	24.1	Metalloproteinase inhibitor 3
1.13	1.41	P10915	40.2	Hyaluronan and proteoglycan link protein 1
0.59	1.44	P15502	68.5	Elastin
1.17	1.35	Q7Z5L7	69.0	Podocan
0.92	1.38	Q14767	195.1	Latent-transforming growth factor beta-binding protein 2
0.50	1.32	P14543	136.4	Nidogen-1
1.14	1.19	P02765	39.3	Alpha-2-HS-glycoprotein
0.92	1.24	P29279	38.1	Connective tissue growth factor
1.17	0.57	P25940	172.1	Collagen alpha-3(V) chain
1.06	0.99	P02462	160.6	Collagen alpha-1(IV) chain
0.39	1.17	P11047	177.6	Laminin subunit gamma-1

Table 4.3.1 is continued overleaf.

log (MS2 count) aaECM	log (MS2 count) osteoECM	Protein IDs	MW [kDa]	Descriptions
1.11	0.81	P02461	138.6	Collagen alpha-1(III) chain
1.10	0.80	Q16610	60.7	Extracellular matrix protein 1
0.56	1.13	Q7Z7G0	118.6	Target of Nesh-SH3
0.90	1.01	Q96S86	40.9	Hyaluronan and proteoglycan link protein 3
0.99	0.91	P09486	34.6	SPARC
0.59	1.09	Q9UHI8	105.4	A disintegrin and metalloproteinase with thrombospondin motifs 1
0.45	1.03	Q6ZMP0	112.5	Thrombospondin type-1 domain-containing protein 4
1.00	0.48	P39059	141.7	Collagen alpha-1(XV) chain
0.66	0.99	Q07092	157.8	Collagen alpha-1(XVI) chain
0.87	0.66	O43294	49.8	Transforming growth factor beta-1-induced transcript 1 protein
0.00	0.89	P08493	12.4	Matrix Gla protein
0.52	0.84	Q9GZM7	52.4	Tubulointerstitial nephritis antigen-like
0.65	0.65	O75487	62.4	Glypican-4
0.50	0.80	Q9H1J7	40.3	Protein Wnt-5b
0.00	0.80	Q9H4F8	48.2	SPARC-related modular calcium-binding protein 1
0.72	0.45	Q14766	186.8	Latent-transforming growth factor beta-binding protein 1
0.82	0.76	P35555	312.2	Fibrillin-1
0.62	0.75	P28300	46.9	Protein-lysine 6-oxidase
0.52	0.69	Q9UBX5	50.2	Fibulin-5
0.24	0.66	P07942	198.0	Laminin subunit beta-1
0.39	0.60	Q6PCB0	46.8	von Willebrand factor A domain-containing protein 1
0.00	0.56	P55268	196.0	Laminin subunit beta-2
0.39	0.39	Q96CG8	26.2	Collagen triple helix repeat-containing protein 1
0.35	0.30	Q32P28	83.4	Prolyl 3-hydroxylase 1
0.35	0.24	Q16363	202.5	Laminin subunit alpha-4

Proteins listed were selected via gene ontology annotations for the subcellular localisation set to extracellular matrix. Log transformed counts of MS^2 spectra of aaECM and osteoECM are given as a measure for the identification frequency of protein-specific peptides. The represented data were drawn from run 1 and 2 of separated protein extracts (see figure 4.3.1).

4.4 Decellularised matrices as artificial *in vitro* niches

Both matrices, aaECM and osteoECM have been analysed for their morphology and characteristics. To investigate their potential as artificial *in vitro* niches for BM stem cells BM-MSCs and G-CSF-mobilised peripheral blood HSPC have been cultured on decellularised matrices compared to standard culture condition. The next two sections describe the observed effects of the ECM culture model on both progenitor cell types.

4.4.1 MSC culture on ECM substrates

For MSC culture on decellularised matrices matching MSC donors were used for the preparation of ECM substrates and for subsequent re-seeding of MSC. First, MSC short-term and long-term proliferation and expansion was investigated accompanied by cell shape analysis of cells growing on differing culture substrates, as shown in figure 4.4.1 and 4.4.2. Control substrates in use were standard plasma treated polystyrene (PTP) and covalently bound FN and Matrigel (as described in section 3.1.2). The first striking observation when culturing MSC on decellularised matrices is their different cell shape compared to control substrates. Figure 4.4.1 and figure 4.4.2 A shows cells in contact with ECM and control surfaces and their altered morphology. Especially upon first contact with decellularised matrices MSC adapt a small, elongated and fibroblast like phenotype compared to widespread and bulky cells on control substrates. Throughout the culture period MSC on aaECM and osteoECM substrates maintained this phenotype and at confluence displayed a densely packed MSC layer with aligned growth directions corresponding to the underlying fibril direction (Figure 4.4.2 A). MSC on control substrates displayed a change in morphology towards confluence. While the cells secrete extracellular matrix into their environment cell shape changes and adopts a more elongated and aligned pattern. This process was observed at earlier timepoints on protein pre-coated FN and Matrigel substrates than on plain PTP. Figure 4.4.1 shows quantitative results for different cell morphologies, analysed at day 3 post plating. Cell area was significantly different between decellularised matrices and control substrates FN and PTP. Cells on PTP were 4-times and on FN 2-times bigger than on ECM substrates. Also between PTP and FN significant differences in cell area were observed. These differences between PTP and FN were not observed for cellular roundness. On both substrates cells displayed a spread (more round) morphology than significantly more elongated cells on aaECM and osteoECM. Figure 4.4.2 B, shows a representative growth curve for one MSC donor. Differences in cell shape are also reflected by cell number at confluence. MSC on aaECM and osteoECM substrates proliferate faster and reach confluence at an earlier timepoint than MSC in control cultures. Furthermore, due to their smaller cell shape total cell number of expanded MSC was higher at confluence on ECM substrates (see dotted lines in growth curve plot). In comparison, MSC on control substrates reached confluence at later timepoints and contained less cells at the confluent state. As early as day 6 significant differences in cell number were observed between decellularised matrices and PTP. Although aaECM and osteoECM showed very similar results, proliferation was slightly

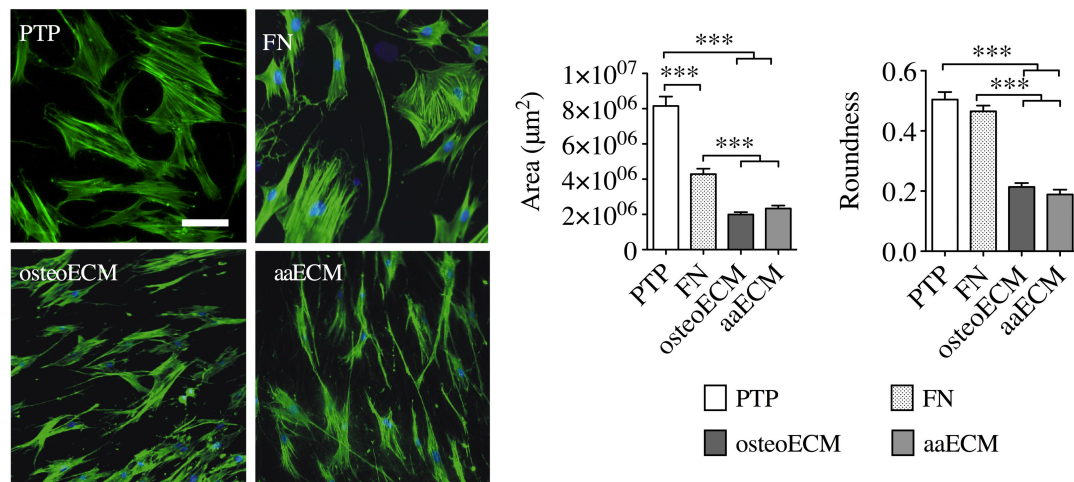
increased on osteoECM compared to aaECM substrates (Figure 4.4.2 B, not significant). Long-term expansion of MSC was investigated by serial subculture of MSC into the same substrate condition once they have reached confluence. Figure 4.4.2 C shows 3 MSC donors and their culture progression for up to 80 days. Different donors displayed varying proliferative capacities, reaching 7-11 passages within 60-90 days. Cumulative population doubling (CPD) was determined and shows the same trend as observed for short term culture within one passage. Each donor displayed best proliferation results on aaECM and osteoECM substrates. FN and Matrigel substrates supported proliferation less effective than ECM substrates but still more than on PTP. Especially with increasing passage number MSC on PTP lost their ability to proliferate and went into growth arrest. On average, the cumulative population doubling for all 3 donors was significantly 3-4-fold higher on ECM and 2-3-fold higher on FN and Matrigel substrates compared to PTP. CPD between ECM substrates and FN or Matrigel substrates was also significantly different. Since MSC on PTP slowly declined their proliferation rate over the first 5 passages, relative differences in CPD did increase for the other substrates because of their stable growth rates. Only at later timepoints relative CPD declined because growth rates on other substrates also started to decline (Figure 4.4.2 C, average graph). Table 4.4.1 shows hypothetical absolute numbers of MSC expansion if all cells were subcultured into the next passage at each passaging step.

The presented results for MSC culture on decellularised ECM reflect the superior character of 3-dimensional and native environments over FN coated substrates or 2-dimensional globular protein mixtures such as Matrigel. A review by Hidalgo-Bastida et al. [233] summarised that MSC show increased surface attachment to single protein coatings such as laminin, vitronectin, collagen IV, collagen I and FN surfaces (in order of increasing adhesion). However, as previously mentioned, studies by Cukierman et al. have highlighted the role of 3D-matrices for authentic matrix adhesion of cells [160]. Requirements for appropriate cell adhesion included 3-dimensionality, fibronectin and other matrix components, $\alpha 5 \beta 1$ integrin and pliability of the substrate. Cell morphologies that were detected in their study on FN and 3D-matrices resemble very much the findings in this work. This concept of force-induced and adhesion-topography-dependent mechanosensing has also been shown by Grinnell et al. [50, 195]. Culturing fibroblast cells in either collagen matrices or on collagen-coated coverslips induced distinct cell morphology of dendritic projections or flat spreaded cells, respectively (similar to figure 4.4.2 D). Mechanotransduction and the resulting cellular deformation activates downstream signalling events, for example MAP-kinase pathway, which has been shown to enhance MSC proliferation [234]. Another study has shown that proliferation and cell cycle of various cells is controlled in a conserved way by matrix elasticity [235] via adhesion mediated mitogenic events. Lindner et al. have shown that culture of MSC on Matrigel coated surfaces resulted in improved proliferation and differentiation [236]. However, as shown by this work, decellularised matrices have been able to augment the proliferative potential of BM-MSC to a greater extent than Matrigel substrates. Conventional *in vitro* expansion of MSC implies extended cell culture on PTP substrates. Baxter et al. have shown that this results in rapid cell aging and growth arrest

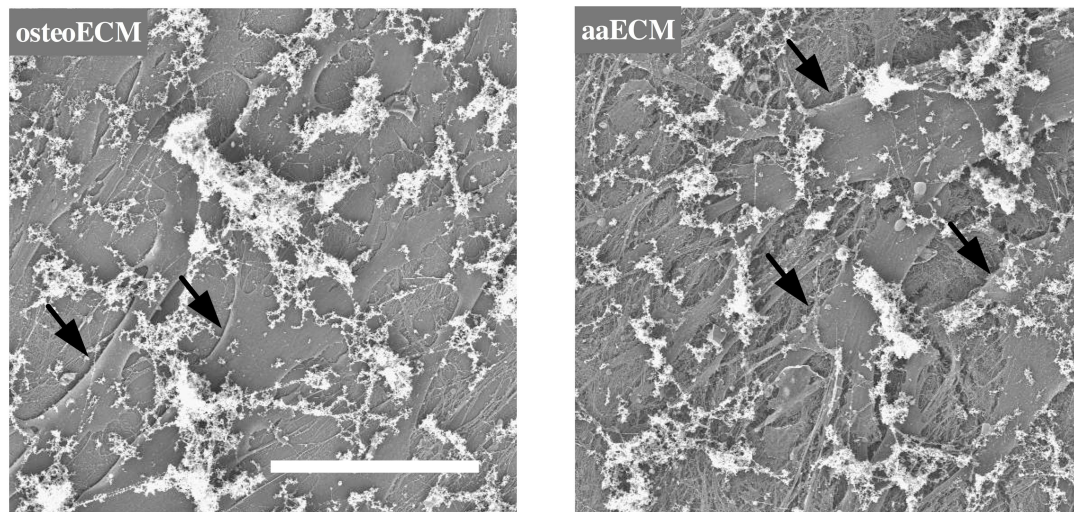
involving telomere shortening [180]. The presented culture system of decellularised matrices has been able to delay this aging process, while supporting appropriate cell morphology and long-term proliferation.

Figure 4.4.1: Cell shape of MSC cultured on decellularised matrices

(A) Cell shape analysis



(B) SEM micrographs of MSC in close contact with decellularised ECM



Cell shape analysis of MSC grown on ECM and control substrates. The cellular cytoskeleton is labelled with phalloidin at day 3 post plating. Cell area (μm^2) and cell roundness (1 describes a perfect circle) were analysed graphically ($n=\text{min. } 50$ cells). SEM images show MSC in close contact with the ECM fibres and with GAG structures (white structures). Black arrows point out cells that are intermerged within the 3D-matrix. Scale bar on fluorescence images at $100\mu\text{m}$, and on SEM images at $50\mu\text{m}$. All data mean \pm s.e.m; asterisk denote statistical significance $***P<0.001$.

Figure 4.4.2: MSC culture on decellularised ECM substrates

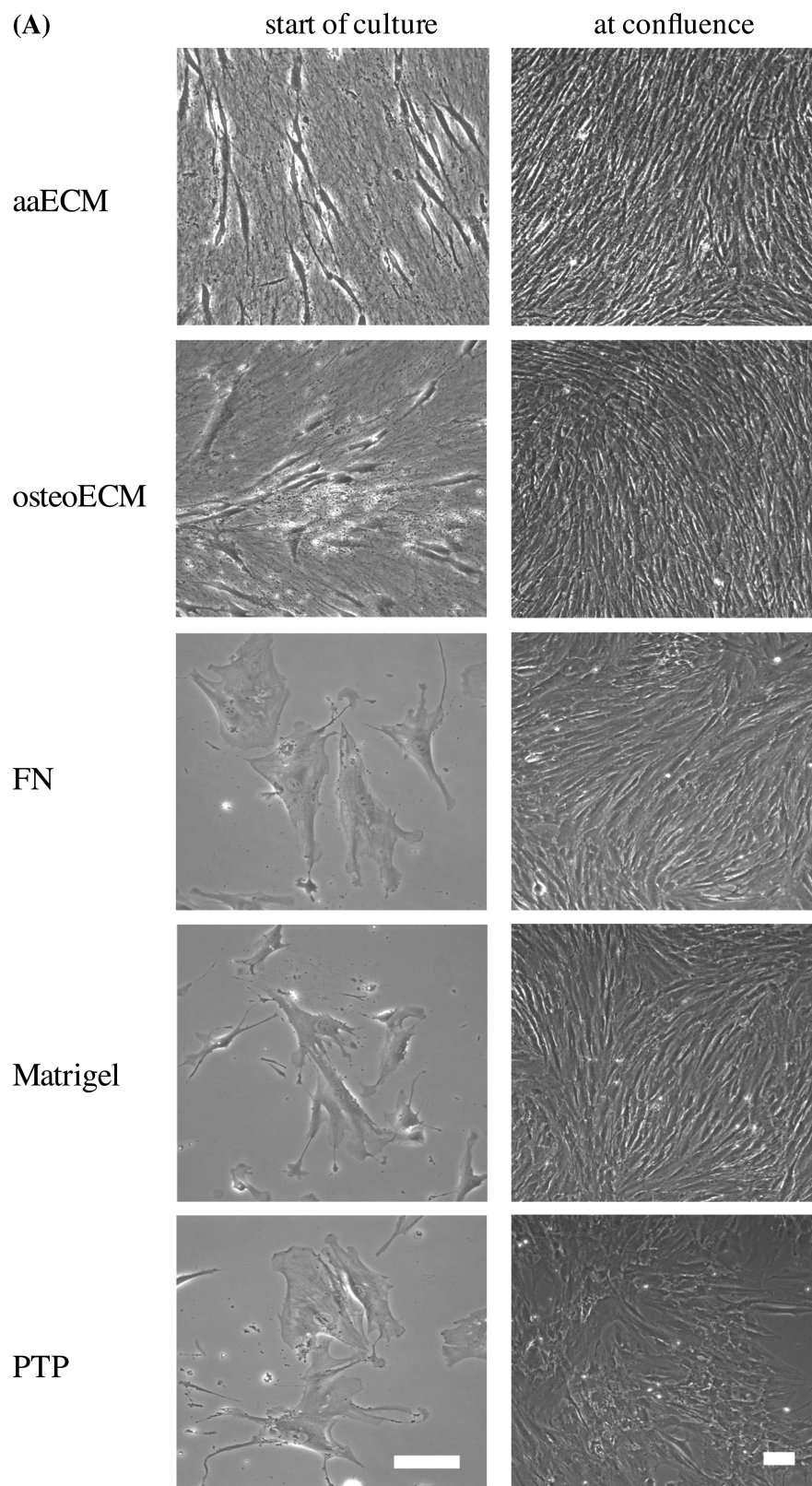
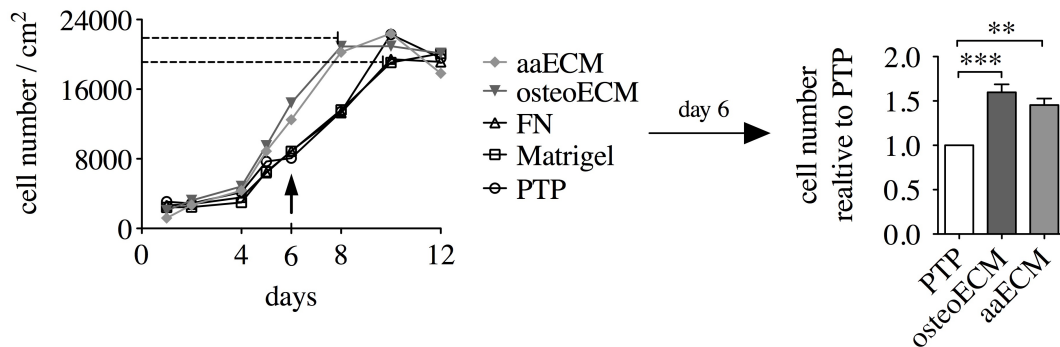
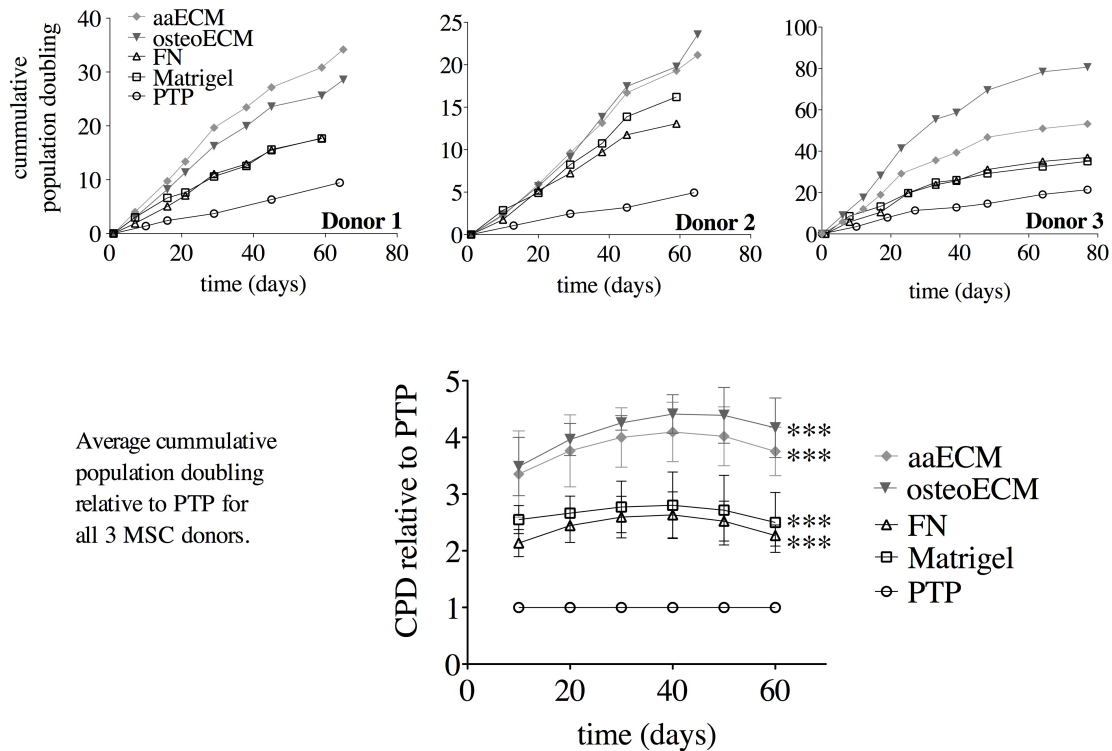


Figure 4.4.2 is continued overleaf.

(B) Short-term culture of MSC on decellularised ECM and control substrates



(C) Long-term expansion of MSC on decellularised ECM and control substrates



(A) MSC of passage 2 cultured on control substrates PTP, Matrigel and FN and on aaECM and osteoECM at the onset of culture 3 days post plating (left column) and at confluence (right column). Scale bars at 100µm. (B) Short-term culture of MSC over the period of one passage (p2), representative for one MSC donor. MSC grown on ECM substrates reach confluence at an earlier timepoint and reach higher cell numbers than control cultures (dotted lines). As early as day 6 significant differences in total cell number/cm² were observed ($n=3$ donors). (C) Long-term culture of MSC over 7-10 passages, as shown by 3 independent MSC donor experiments, as cumulative population doubling (CPD) over time. Cells were subcultured at confluence to the same plating density. Average CPD relative to PTP substrate was analysed for all 3 donors at 10 day intervals. Significance is given relative to PTP. All data mean \pm s.e.m; asterisk denote statistical significance ** $P<0.01$, *** $P<0.001$.

Table 4.4.1: Expansion of MSC

	PTP	Matrigel	Fibronectin	osteoECM	aaECM
DONOR 1					
final passage	p7	p9	p9	p10	p10
total cell number	0.008×10^8	0.2×10^8	0.3×10^8	10×10^8	49×10^8
DONOR 2					
final passage	p6	p8	p8	p9	p9
total cell number	0.001×10^8	0.2×10^8	0.04×10^8	2.2×10^8	1×10^8
DONOR 3					
final passage	p9	p10	p10	p11	p11
total cell number	0.8×10^8	22×10^8	41×10^8	55676×10^8	2319×10^8

Each donor was cultured for the same duration of time on the given substrates. The starting cell number at the beginning of culture (p2) was 54,000 cells for all donors on all substrates. Cells were only subcultured at confluence and the final passage states the maximum of passages that were reached within the given time. Total cell number describes the possible yield of expanded cells calculated from the cumulative population doubling over the given time period. (See also figure 4.4.2 C)

One criterium of MSC is their ability to differentiate along the various mesenchymal lineages. To study the potential of decellularised matrices to support MSC differentiation, MSC of passage 2 were induced to differentiate into osteoblasts and adipocytes while cultured on ECM and control substrates for 2 weeks. Figure 4.4.3 shows quantification of differentiation intensity. Osteogenic differentiation was determined by van Kossa staining for mineral deposition (Figure 4.4.3 A). Adipogenic differentiation was determined via Oil Red O staining for fat droplet accumulation (Figure 4.4.3 B). After the given differentiation time significant differences in differentiation intensity were observed for both osteogenic and adipogenic differentiation between cultures on decellularised ECM and control substrates. Osteogenic induction of MSC caused intense mineralisation in aaECM and osteoECM substrates. Both significantly higher than all control substrates. But aaECM also showed significantly higher mineralisation values than osteoECM. In all cultures no mineralisation was observed when cultured with control medium containing no osteogenic inducers. This indicates that ECM environments alone (for example osteoECM matrices) do not induce osteogenic differentiation. Also for adipogenic differentiation decellularised matrices have shown very similar results. ECM substrates have shown enhanced numbers of adipocytes with intense fat droplet accumulation compared to control substrates. A significant difference in adipogenic differentiation was also observed between aaECM and osteoECM. This shows that osteoECM is less supportive for adipogenic differentiation, which might be correlated to the osteogenic environment of osteoECM. Cultures without adipogenic induction did not show any adipocytes or fat droplet accumulations. Within control substrates (between PTP and FN or Matrigel) no difference in differentiation behaviour was observed, which validates the importance of native ECM environments for differentiation processes.

MSC are also a source of many secreted factors which stimulate and regulate the behaviour of cells in their environment or of themselves. Therefore, the secretory profile of MSC un-

der different culture conditions was investigated. MSC of passage 2 were cultured for 3 days on decellularised ECM and PTP substrates and conditioned medium was collected for detection of secreted cytokines. By the use of a cytokine dot blot array pooled and normalised supernatants of 3 MSC donors were analysed (see figure 4.4.4 A). Pixel intensity of positive dots was determined and is a measure for the cytokine level in MSC culture supernatants. Interleukin-6 (IL-6), Interleukin-8 (IL-8) , and serpin E1 were detected with high intensity. Interleukin-13 (IL-13) and stromal cell-derived factor 1 (SDF-1) were detected at lower intensities. Unfortunately, background levels for serum contamination by the cell culture medium could not be subtracted. Therefore, more precise quantitative measurements were performed via ELISA for IL-8 and other known MSC-secreted cytokines that play important roles in the niche, namely angiopoietin-1 (Ang-1) and SDF-1. Figure 4.4.4 B shows detected amounts of cytokine as pg/10.000 cells, whereat serum background levels have been subtracted. IL-8 secretion was significantly different between PTP and ECM substrates on day 1, and secretion levels dropped down in all culture conditions the following days. Ang-1 has shown elevated secretion levels for all 3 days by MSC cultured on osteoECM substrates compared to PTP. During the first 2 days of culture also a significant differences to aaECM Ang-1 levels have been detected. SDF-1 secretion by MSC steadily increased over the 3 day culture period. On day 1 and 3 MSC cultured on aaECM showed significantly higher SDF-1 secretion levels than cells on PTP and osteoECM. The amount of cytokine that has been detected in supernatants that were only in contact with plain ECM substrates was very low, indicating that the decellularised ECM substrates do not contain or do not release large amounts of cytokine.

Figure 4.4.3: MSC differentiation on ECM and control substrates

(A) Osteogenic differentiation - vanKossa staining for mineralisation

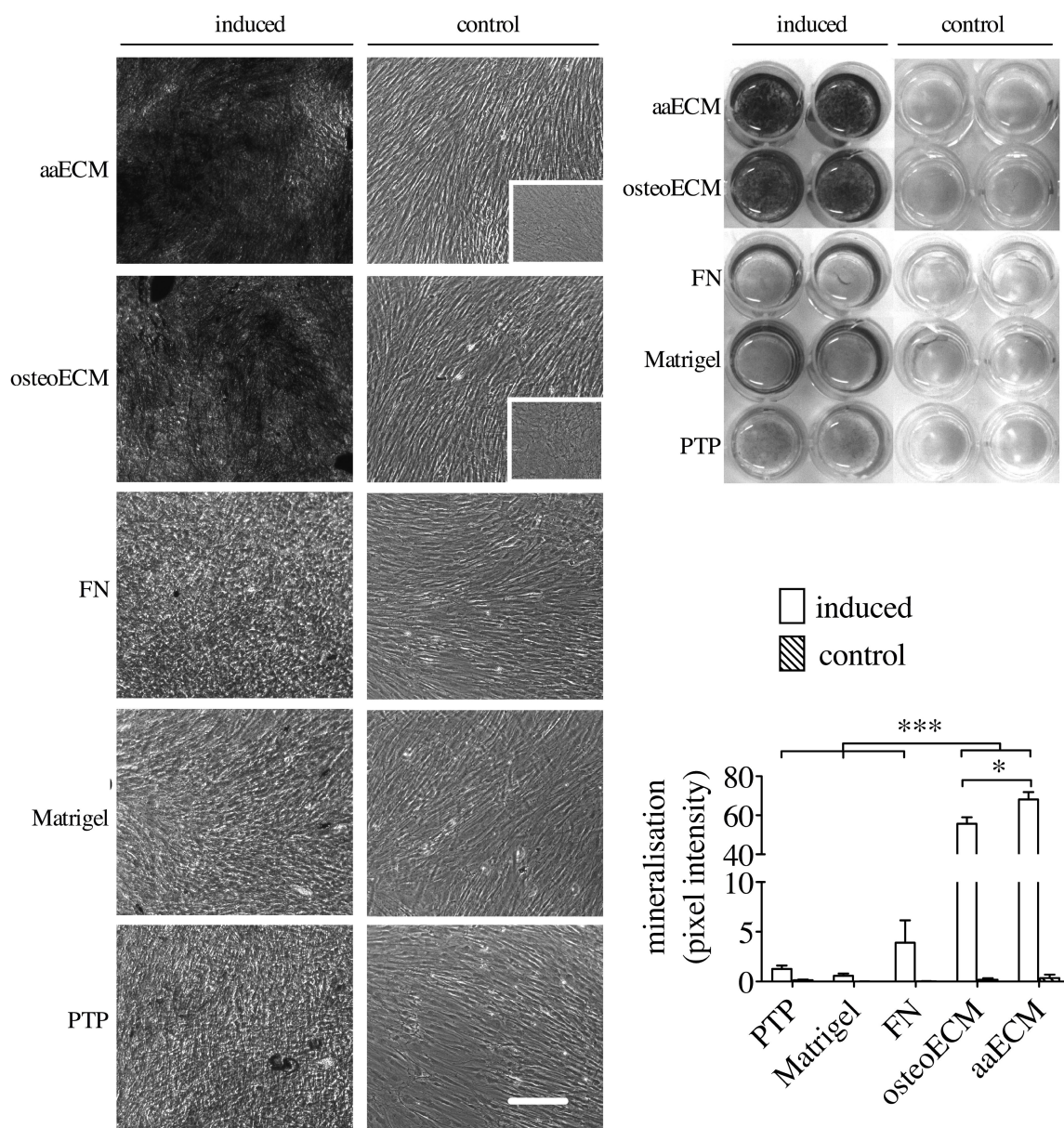
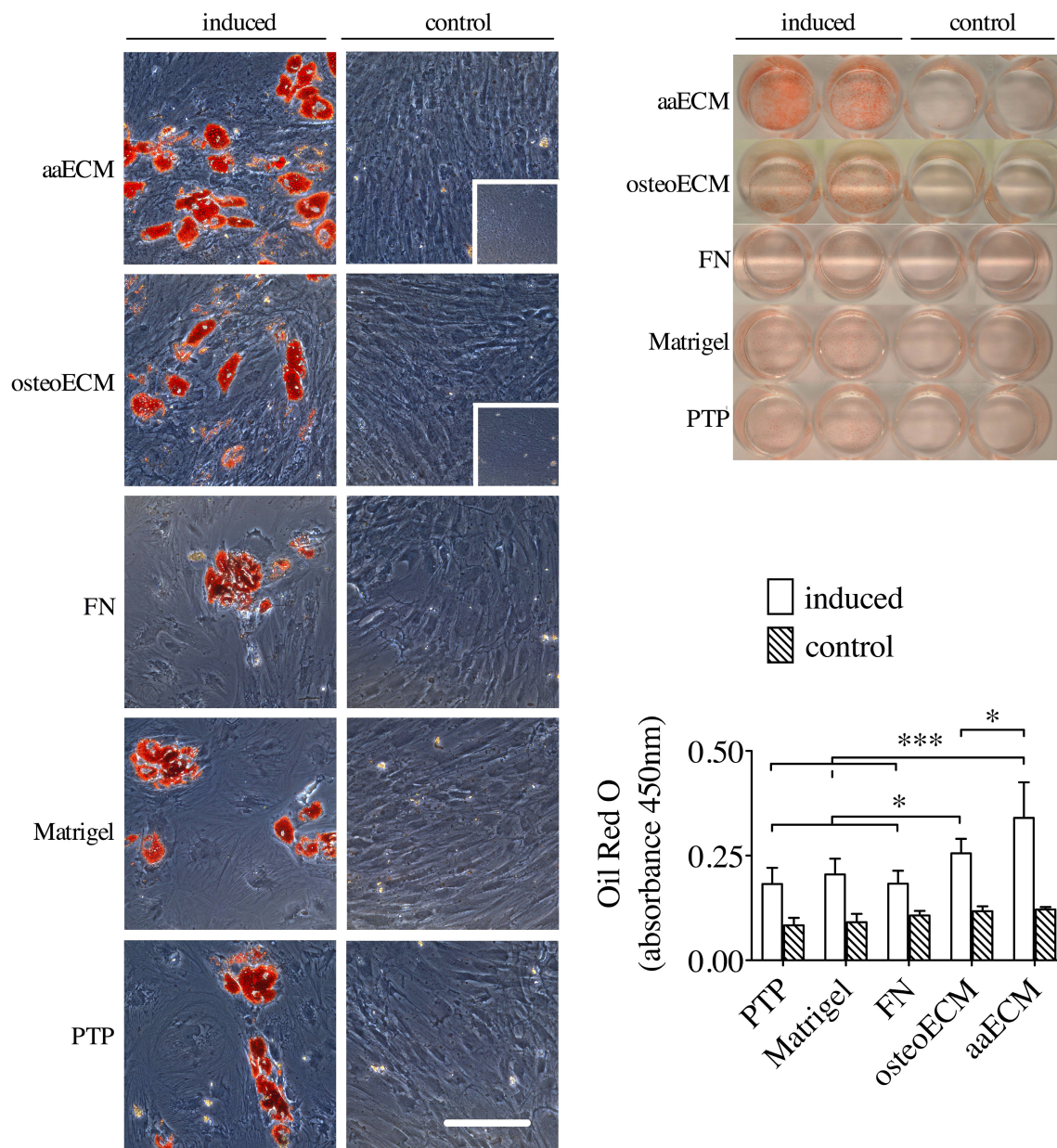


Figure 4.4.3 is continued overleaf.

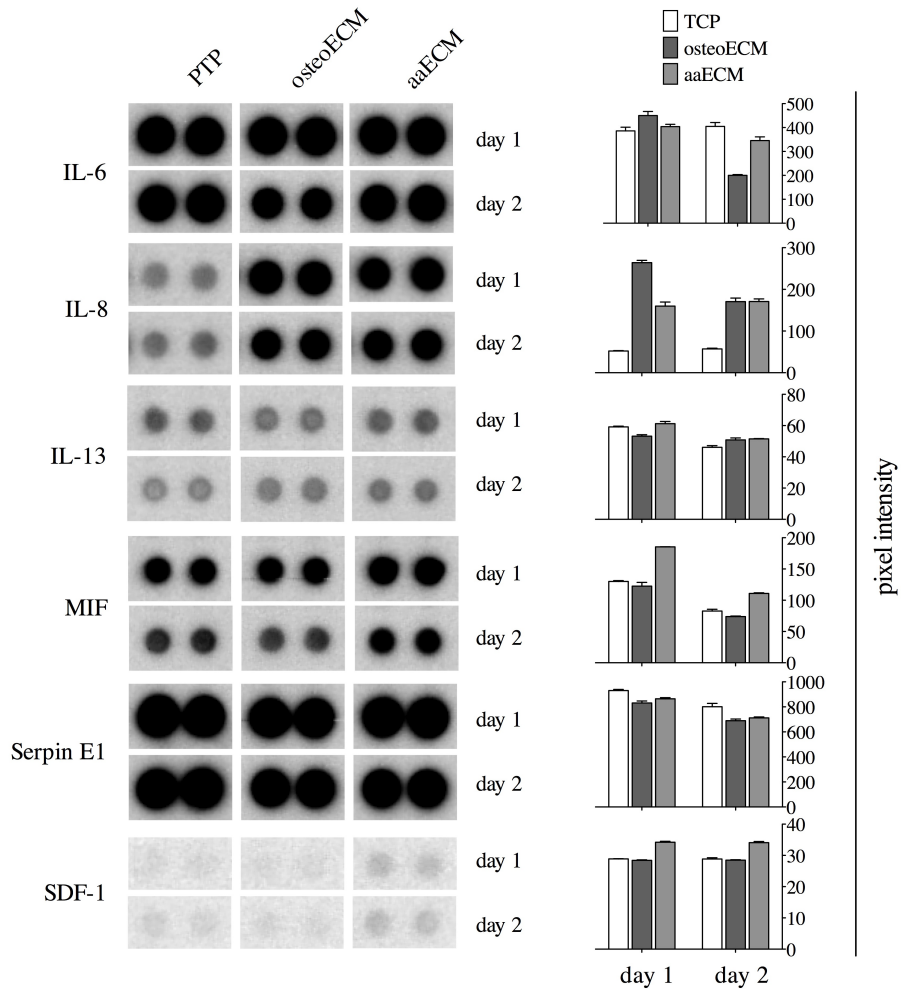
(B) Adipogenic differentiation - Oil Red O staining for fat droplet accumulation



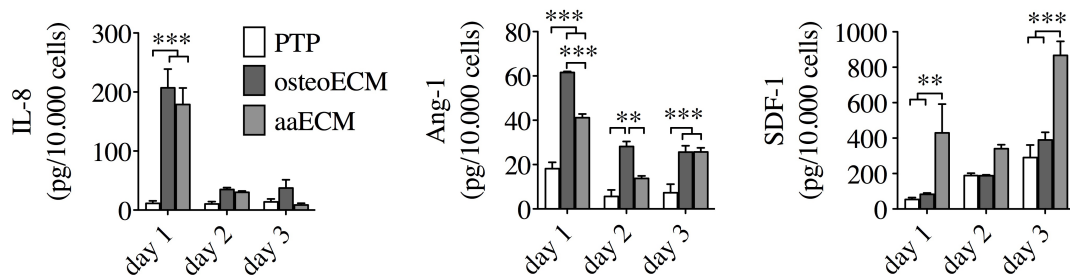
Osteogenic (A) and adipogenic (B) differentiation of MSC on ECM and control substrates visualised by vanKossa staining for mineral deposition and by Oil Red O staining of cellular fat droplet accumulation, respectively. Differentiation (induced) and control (standard MSC medium) treatment are visualised microscopically (left panel) and macroscopically by plate view (right panel), representative for one MSC donor. Insets in ECM control images depict staining of plain ECM substrates. Quantification of differentiation intensity represents data from 3 independent experiments with 3 different MSC donors. Scale bars at 100µm; all data mean \pm s.e.m; asterisk denote statistical significance * P < 0.05, *** P < 0.001.

Figure 4.4.4: MSC cytokine secretion

(A) Cytokine dot blot array



(B) ELISA-quantification for IL-8, Ang-1 and SDF-1



Secreted cytokine levels in conditioned media of MSC in contact with PTP, osteoECM and aaECM, analysed at day 1,2 and 3 post initial contact with the substrate. (A) Detected cytokines on a dot blot membrane from MSC cell culture supernatants pooled from 3 different MSC donors (normalised to 10.000 cells). Cytokine levels were analysed as pixel intensity of duplicate dots. (B) Quantitative analysis of IL-8 (left graph), Ang-1 (middle graph) and SDF-1 (right graph) cytokine levels from separate supernatants (n=3 donors) given as pg/10.000 cells. All data mean \pm s.e.m, asterisk denote statistical significance *P<0.05, **P<0.01, ***P<0.001.

Previous data by Seib et al. [237] have shown that artificial constructs of individual ECM proteins (tropocollagen, fibrillar collagen, collagen/hyaluronic acid and collagen/heparin) had rather limited effects on the cellular behaviour of BM stem cells in comparison to standard PTP substrates. For example the secretion level of Ang-1 and SDF-1 was not affected by the culture substrates and even less than on PTP substrates. The detected cytokines secreted by BM-MSC were also identified by another study, such as IL-6, IL-13 and SDF-1 [70]. Seib et al. also showed that the secretory profile of MSC is dependent on matrix elasticity [238]. Although much stiffer substrates were used in that study similar cytokine secretion was detected in comparison to this work. Due to their elevated secretion levels of pro-angiogenic factors such as IL-8, SDF-1 and Ang-1 [239], MSC expanded on decellularised substrates are a viable cell source for use in tissue engineering and cell therapy approaches.

Differentiation of MSC on decellularised matrices has shown drastic increase in mineralisation of osteogenic induced cultures. The potential of ECM substrates to aid osteogenic mineralisation is intrinsic to its character as nucleation network for calcium phosphate deposition [197]. For example, identified components of decellularised ECM such as thrombospondin [240] and periostin [222] are known for their role in extracellular matrix mineralisation. Other studies have investigated the pre-coating of tissue engineering scaffolds with rat osteoblast-generated matrix layers and found that culture of MSC on such scaffolds dramatically increased their bone formation capacity [21, 22]. This indicates that decellularised matrices are useful for application in various biomaterials concepts to guide differentiation of MSC into the osteogenic phenotype and aid mineralised bone formation. In a recent review by Engler and Reilly [241] intrinsic ECM properties such as structural, biochemical and mechanical cues were directly linked to cellular phenotype of MSC. MSC differentiation is regulated by integrin mediated adhesion to tissue specific ECM molecules. Additionally to the right set of adhesion sites, ECM topography and elasticity also causes changes in cell shape associated with force generation within the cell which activates differentiation signalling cascades and alters gene expression [241]. Decellularised matrices exhibit those mentioned regulators more appropriate and demonstrated more effective MSC differentiation and proliferation than control substrates, which lack critical parameters of this multifunctionality. MSC are furthermore conditioned by their extracellular environment and pre-destined to follow certain lineage pathways once they have adapted to signals of their environment. Irreversible epigenetic changes prime the cell to respond in particular ways to further stimuli [242] which diminishes their multipotentiality. Here may lie one of the reasons why MSC expansion or differentiation on PTP, FN or Matrigel substrates displayed impaired culture outcome. This indicates the importance of the culture environment for maintenance of a functional cellular phenotype for subsequent use in specific cellular assays or applications that require cellular plasticity.

Very recent studies by Chen and colleagues have used a very similar approach of cell-free ECM substrates for MSC culture [243]. They could show that culture of murine [244] or human [245] BM-MSC on decellularised MSC matrices also supported rapid expansion of cell numbers and improved differentiation into adipocytes and osteoblasts compared to PTP cultures.

Transplantation of ECM expanded murine cells generated 5-times more bone and 8-times more hematopoietic marrow compared with cells expanded on plastic. Furthermore, they have shown similar results for transplantation of human MSC expanded on cell-free ECM substrates. After expansion for multiple passages cells retained their capacity for skeletogenesis compared to dramatically diminished bone formation capacity of cells expanded on PTP. In conjunction with these studies, Sun et al. [246] found that decellularised matrices generated by young murine femoral cells (3 months old mice) were able to restore defects in self-renewal and bone formation capacity of old MSC (from 18 months old mice). ECM substrates prepared from old MSC were not able to support MSC self-renewal and osteogenesis. These findings are in line with the results from this study and approve the functionality of long-term expanded MSC. Analysis of global gene expression patterns of human MSC cultured on ECM substrates compared to PTP revealed that most of the genes that were differentially up-regulated on ECM substrates were genes involved in cell cycle processes, mitosis, cytoskeleton and cytoskeleton-dependent intracellular transport [245]. Another gene expression study by Song et al. identified decorin and thrombospondin-1 as one of the genes involved in MSC self-renewal and multipotency [87]. Together with the data obtained by mass spectrometry of decellularised matrices the mechanisms of MSC self-renewal can be elucidated by analysing specific interactions between ECM and MSC.

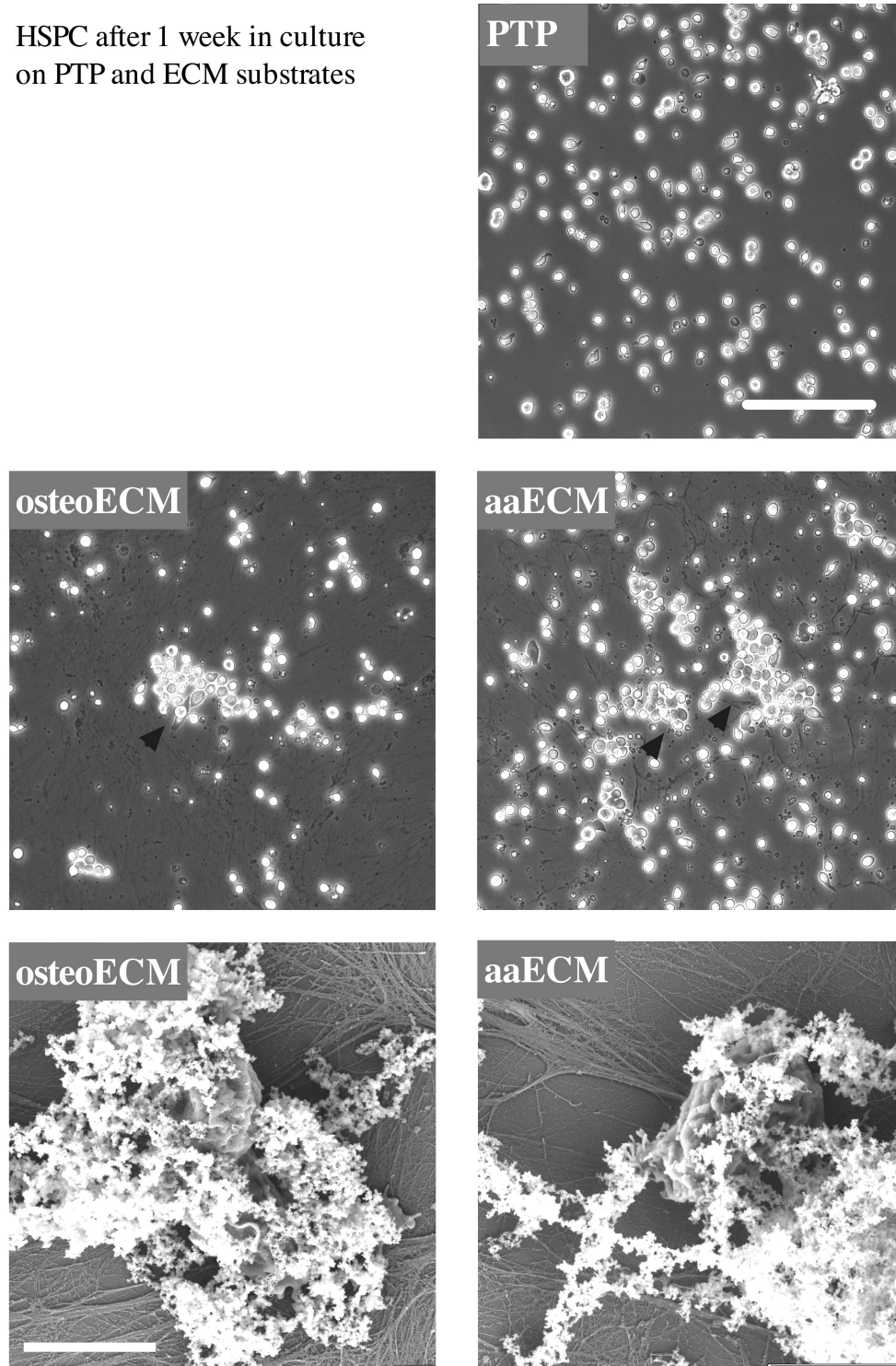
Taken together, BM-MSC have shown to react to a great extend to decellularised ECM substrates compared to standard culture conditions on either protein coated FN and Matrigel or PTP substrates. The pre-deposited proteins, fibrils and GAGs served as guiding structures for growth and migration of MSCs. Both types of decellularised matrices, aaECM and osteoECM, were able to significantly improve cytokine secretion, proliferation and differentiation capacity of primary MSCs *ex vivo*.

4.4.2 HSPC culture on ECM substrates

The complex interaction between MSC and HSPC within the BM regulates stemness of both stem cell types. Previous MSC-HSPC co-culture studies have revealed the potential of such culture systems in terms of HSPC self-renewal and expansion [70, 93, 247, 248]. This study applied a minimal co-culture system, using only the extracellular residues of MSC as a culture environment for HSPC. Peripheral blood CD34-isolated human progenitor cells were cultured for a period of one week in contact with aaECM, osteoECM, FN and PTP substrates to investigate the potential of MSC-made ECM to support and expand HSPC. Figure 4.4.5 shows progenitor cells cultured on PTP and decellularised matrices. Cells appeared in close interaction with the underlying ECM substrates, indicating an adhesive inter-communication between the matrix substrate and progenitor cells. Cells were analysed via flow cytometry for cell surface marker expression, as shown in figure 4.4.6 C. It was found that CD34+ HSPC were able to proliferate and expand on ECM substrates. Total expansion of the HSPC population was significantly higher when in contact with aaECM and osteoECM environments, compared to PTP and FN substrates (Figure 4.4.6 A). Table 4.4.1 shows absolute values for expansion of CD34+ and CD34/CD133 double positive cells. Allowing an up to 3-fold expansion of CD34+ cells, aaECM was the most potent substrate in supporting HSPC maintenance *and* expansion. OsteoECM allowed a duplication of CD34+ cells in relation to the starting cell number. PTP substrates maintained the initial population size, whereat on FN substrates cell numbers declined. Although, on control substrates cell numbers were only steady or declined, the amount of dead cells in the final population was not significantly different between all culture substrates; analysed by propidium iodide live/dead staining (PTP $2.92 \pm 0.6\%$ and FN $2.85 \pm 0.6\%$ compared to osteoECM $1.7 \pm 0.3\%$ and aaECM $1.62 \pm 0.3\%$). Also the percentage of CD34, CD133 and CD177 expressing cells was not significantly different between cell populations from all different substrates (Figure 4.4.6 B). Only between PTP and aaECM a significant difference was observed for the percentage of CD34+ cells in the total population. This is most likely related to the enhanced expansion of progenitor cells (and subsequent appearance of CD34-differentiated progenitors) in aaECM cultures, compared to the non-proliferating cell population in PTP cultures. The described experiments were performed with cytokine-washed ECM substrates (see section 3.1.3 for preparatory details). It was tested if decellularised matrices contained active amounts of residual signalling molecules such as growth factors and cytokines. Figure 4.4.7 shows expansion of HSPC on native and cytokine-washed decellularised matrices. Both conditions yielded the same expansion of progenitors, indicating that none or ineffective amounts of cytokines remained within the ECM. The amount of soluble factors released by the washing procedure was below the detection limit of ELISA quantifications for IL-8, SDF-1 and Ang-1 (data not shown), as previously described to be secreted by MSC (see figure 4.4.4). This indicates that decellularised matrices (native or cytokine-washed) are mostly free of remaining cytokines, but it is thought that they have the potential to bind and present cytokines (for example present in culture medium, or individually applied) via proteoglycans and glycoproteins in a more efficient way than plain PTP substrates (discussed further down in this section).

Figure 4.4.5: HSPC cultured on ECM and PTP substrates

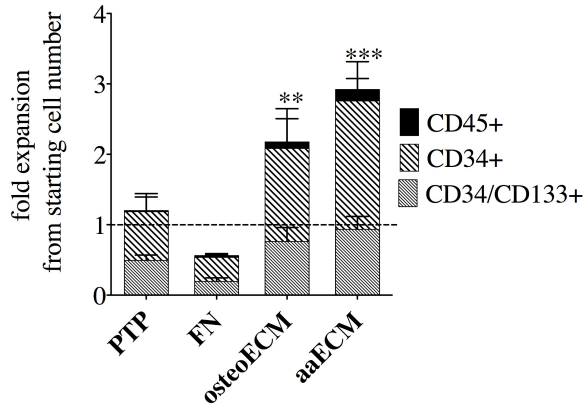
HSPC after 1 week in culture
on PTP and ECM substrates



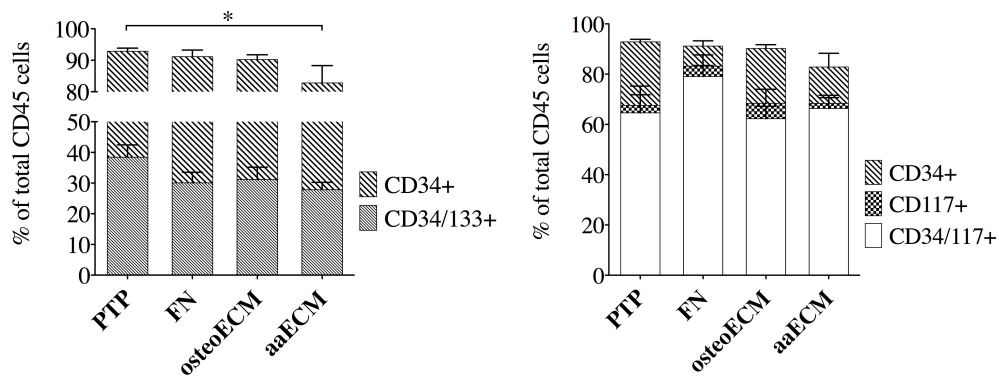
Culture of peripheral blood G-CSF-mobilised CD34+ HSPC on decellularised aaECM and osteoECM substrates and on control PTP substrate at day 7. Phase contrast images (upper three) show all cells in suspension on PTP surfaces. Note the close interaction of HSPC with the decellularised ECM layer and the flat morphology of adherent HSPC (arrow heads). SEM micrographs (lower panel) show interaction of HSPC with the surrounding ECM and especially with GAG structures, pictured as white structures around the cell. Scale bars at 100µm on phase contrast, and at 5µm on SEM images.

Figure 4.4.6: Culture of HSPC on ECM substrates

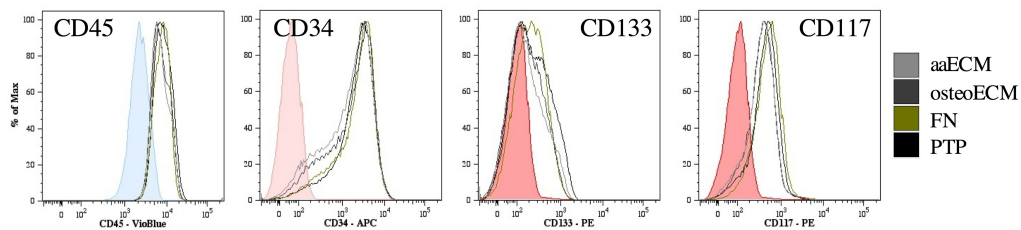
(A) Fold expansion of HSPC on ECM and control substrates



(B) Percentage of progenitor cells in total cell population



(C) Flow cytometric analysis for CD45, CD34, CD133 and CD117 surface antigens



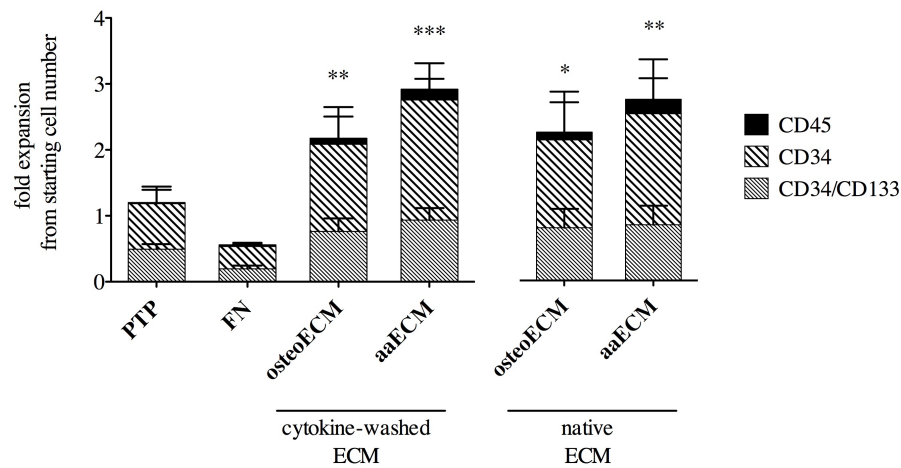
(A) Overall expansion of HSPC cultured for 1 week in low cytokine conditions (10ng/ml SCF, Tpo, Flt-3) on cytokine-washed decellularised matrices, PTP and FN substrates. Expansion of CD45+ and CD34+ (but not CD34/CD133+) cells was significantly higher on matrix substrates compared to PTP. (B) Percentage of progenitor cells in the total cell population. Expression of surface markers was not significantly different between substrate conditions, except CD34 expression between aaECM and PTP. (C) Example of flow cytometric analysis for CD45, CD34, CD133 and CD117. Tinted plots represent unspecific isotype control antibodies conjugated to the respective fluorophor. Almost no difference in expression intensity of surface markers between cells from different substrates was observed. All data mean \pm s.e.m, asterisk denote statistical significance * $P < 0.05$, ** $P < 0.01$, *** $P < 0.001$.

Table 4.4.2: Expansion of HSPC on ECM substrates

	PTP	Fibronectin	osteoECM	aaECM
final cell number CD34+ cells	$6.7 \pm 1.3 \times 10^4$	$3.0 \pm 0.8 \times 10^4$	$11.7 \pm 2.5 \times 10^4$	$14.9 \pm 2.3 \times 10^4$
fold expansion CD34+ cells	1.2 ± 0.2	0.5 ± 0.1	2.1 ± 0.4	2.8 ± 0.3
fold expansion CD34/CD133+ cells	0.5 ± 0.1	0.2 ± 0.1	0.8 ± 0.2	0.9 ± 0.2

The starting cell number for all HSPC culture experiments was set to $5-6 \times 10^4$ cells/ 9cm^2 culture area. Total expansion of CD34+ cells over the time course of one week is given in row one. Rows two and three quote the fold-expansion of CD34+ and CD34/133 double positive cells. Data for PTP, osteoECM and aaECM $n=6$; for FN $n=3$.

Figure 4.4.7: Comparison of cytokine-washed and native ECM



Expansion of CD34+ HSPC cultured for 1 week in low cytokine conditions (10ng/ml SCF, Tpo, Flt-3) on native and cytokine-washed decellularised matrices, PTP and FN substrates. Expansion of CD45+ and CD34+ (but not CD34/CD133+) cells was significantly higher on matrix substrates compared to PTP. No significant difference between native and cytokine-washed ECM substrates was detected in terms of HSPC expansion.

The application of cytokines for *ex vivo* expansion of HSPC has been investigated by many studies. For instance, early cultures of human BM-, peripheral blood- and cord blood-derived stem cells with various cytokine combinations (mainly SCF, Flt-3, IL-6, IL-3 and Tpo) resulted in 2- to 5-fold expansion of long-term repopulating cells after 4 to 21 days in culture [249, 250, 251, 252, 253]. But as the field of HSCP culture advanced, more sophisticated culture systems emerged. Physical immobilisation of the extracellular domain of the Notch ligand Delta1 in combination with FN fragments and soluble cytokines for the culture of human cord blood HSPC led to a nearly 16-fold increase in NOD/SCID repopulating cell frequency [254, 255, 256]. In this study hematopoietic progenitor cells were cultured at very low cytokine concentrations, and the repopulation ability of the expanded progenitor cells still remains to

be analysed in ongoing experiments. But, using decellularised matrices in conjunction with elevated concentrations and refined mixtures of cytokines might enhance the effect of stem cell expansion.

Several previous studies have examined the role of single ECM molecules and their interaction with cell surface receptors for haematopoietic stem cell maintenance. Adhesion receptors of HSPC sense and regulate the interaction between the cell and the extracellular environment [257]. For example, HSPC culture on planar FN substrates initiated direct adhesion of progenitor cells via $\alpha 4$ -integrin receptors to the heparin binding domain of FN and inhibited HSPC proliferation [258], similar to the finding in this study (see figure 4.4.6 A). ECM molecules like fibronectin [259], laminin [260], fibrillar collagen I [114] and heparan sulfate GAGs [201] have been shown to support primitive HSPC maintenance *in vitro*. On the other hand, inhibition of collagen deposition by stroma cultures prevented haematopoiesis in long-term BM cultures [217], fostering the importance of secreted extracellular structures. One important aspect of decellularised matrices is that ECM components, and especially GAG components, can bind and present cytokines and signalling molecules in a biologically active manner. Studies with BM stromal cell heparan sulphates demonstrated the importance of GAG-mediated cytokine presentation for HSPC maintenance [104, 231, 232]. Potentially, the cytokine cocktail used in this study was presented in a more functional way, or was preserved for longer periods on decellularised matrices than on PTP or FN substrates. However, the SCF receptor CD117 was not differentially expressed on progenitor cells in contact with extracellular matrices compared to control substrates (Figure 4.4.6 D). This might be related to the finding that membrane bound SCF is more effective in active and prolonged signalling into HSPC [261]. The application of higher amounts of SCF or in depth analysis of subsequent signalling events after CD117 activation might reveal differences in SCF interaction with HSPC on ECM or PTP substrates.

In this study, HSPC were exposed to an orchestrated mixture of ECM factors and extracellular signalling molecules. Many components that were detected via mass spectrometric analysis of decellularised matrices (see table 4.3.1) have been shown to play important roles in HSPC regulation. A few examples are discussed to show the versatile influence of ECM components on HSPC. Tenascin is a large glycoprotein which plays an important role as a cytoadhesive component within the haematopoietic microenvironment. Klein et al., have shown that stromal cells strongly express tenascin and that it is co-distributed with fibronectin and collagen type III around maturing haematopoietic cells in the BM [99]. The glycoprotein thrombospondin showed similar effects, influencing cell-cell and cell-matrix adhesion of haematopoietic progenitor cells [100]. Fibulins are glycoproteins that can associate with elastic fibres such as elastin and fibrillin [262]. Gu et al. reported that fibulin-1 and fibulin-2 associate with fibronectin in BM stroma and adhere to haematopoietic cells via $\beta 3$ integrins [211]. The dual impact of fibronectin and laminin on murine BM cells was examined by Sagar et al., and was shown to enhance expansion of primitive stem cells and improve BM engraftment in mice [260]. One example of a secreted signalling molecule detected in decellularised ECM extracts is Wnt-5b. Wnt (Wingless) signalling has been shown to limit proliferation and preserve the stem cell

character of HSPC within the niche [263, 264, 265]. Collectively, all these molecules influence haematopoietic progenitor cells via activation of cell surface receptors and cause subsequent initiation of signalling cascades. Furthermore, the collective behaviour of extracellular matrices also describes a physical microenvironment that exerts stimuli towards the responding cell type. As mentioned previously for MSC, also HSPC are influenced by the elasticity of the substrate. Holst et al. [266] were able to show a 3-fold tropoelastin-dependent expansion of human CD34⁺/CD38⁻ HSPC. The effect was related to the extensional elasticity of tropoelastin, indicating that HSPC can sense and react to physical properties of their environment. The importance of 3-dimensionality was shown by Kurth et al., where spatial constraints of progenitor cells in FN-coated microcavities caused cellular quiescence [126]. Along that line, differences in expansion intensity between aaECM and osteoECM substrates might arise from the difference in physical properties of both substrates (see figure 4.2.4). aaECM exhibited a thicker (more 3-dimensional) and more elastic phenotype than osteoECM. But the detailed mechanisms of action still need to be investigated to draw conclusions about the functionality of both ECM types. Further indications for differential regulation of HSPC via aaECM and osteoECM substrates can be expected from the statistical analysis of the proteomic composition of ECM extracts, which is ongoing.

Hines et al. tried to summarise the complex nature of haematopoietic stem cell niches including cell adhesion molecules, growth factors, cytokines and chemokines [267]. Many components of the extracellular space that are listed as crucial factors for a functional niche have also been detected in this study. For example, glypican, collagens, decorin, FN, hyaluronic acid, laminins, nidogens, tenascin, thrombospondin and vitronectin were all found in aaECM and osteoECM extracts. The function of additionally detected components, as either important factors for the assembly of extracellular structures or as adhesion sites for stem cell signalling has to be investigated. The obvious complexity of the decellularised ECM system exerts its supportive effect on HSPC most likely through multiple gateways. This system permits investigation of activated or inhibited signalling pathways, which direct HSPC into the observed phenotype. To proof the functionality of ECM-expanded HSPC, repopulation and BM engraftment studies are on the way at present. These experiments will show the true potential of decellularised matrices in expanding primitive haematopoietic progenitor cells with the ability to home to the BM and produce mature haematopoietic cells. Identification of adhesion receptors and gene expression profiles will help to gain more insight into mechanosensing, proliferation, cell-cycle and self-renewal signalling events of HSPC. Thereby, this system of decellularised ECM will be invaluable for the establishment of tissue-specific culture environments that facilitate control of cell fate for therapeutic applications.

Chapter 5

General Discussion

5.1 Summary and conclusions

Among the factors that regulate cellular phenotype and cell behaviour the extracellular matrix is inarguable one of the most important. All cells within the body are surrounded by organ and tissue-specific extracellular material that bears superordinate functionalities, such as regulation of cell shape, migration, gene expression and subsequent maintenance or changes in cellular response. Over the past decade more light has been shed on the impact of ECM properties such as suprastructure, molecular interaction between ECM components, physicochemical signals and mechanisms of mechanotransduction. In the field of stem cell biology the concept of specific extracellular microenvironments, so called 'niches', which control self-renewal and cell fate arose. Along that line, this thesis was set out to mimic the multifunctional character of cellular microenvironments to establish a culture systems that supports adult stem cells *in vitro*.

In the frame of this work a novel and highly complex surrogate culture model has been developed to mimic the *in vivo* ECM environment of human bone marrow. Primary human bone marrow stromal cells were successfully utilised for secretion of extracellular matrix components in a native and functional manner. The presented *in vitro* culture system can exhibit diverse characteristics and implies versatile options for its use as a stem cell niche model. Bone marrow stem and progenitor cells - MSC and HSPC - have been successfully stimulated by the surrogate culture substrate for expansion and differentiation, involving complex interactions with decellularised extracellular matrices.

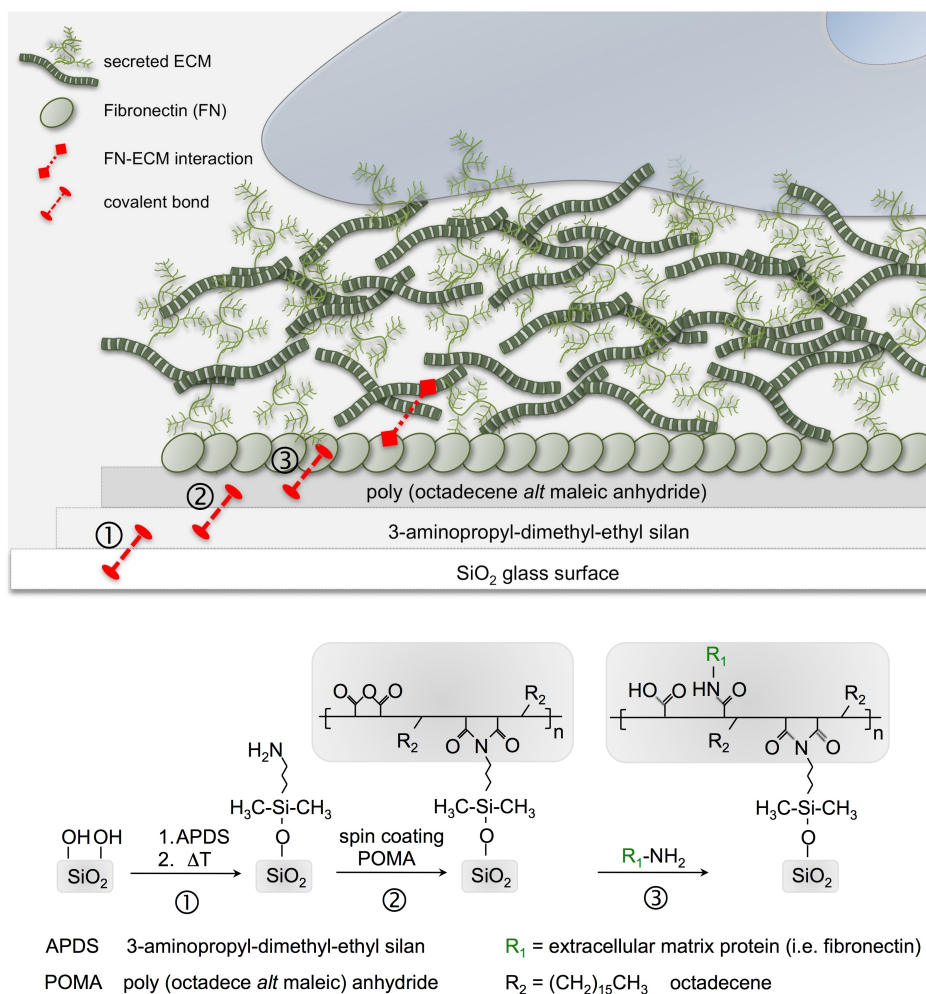
Decellularisation of tissues and cell cultures is a practicable strategy to investigate the impact of the ECM and study cellular behaviour upon contact with extracellular molecules. However, unlike decellularised organs decellularised cell cultures have not extensively been used as model systems for the study of authentic and methodical cell-ECM interactions [19]. One of the reasons for this discrepancy, and one major drawback of these systems is the difficulty of yielding intact and homogeneous extracellular matrix structures following the decellularisation

procedure. A critical accomplishment in the beginning of this work was the reliable and secure anchorage of cell-secreted matrix components to the culture carrier. Adsorptive binding of secreted ECM to hydrophobic plasma treated surfaces alone is not sufficient, and a common drawback during fabrication of decellularised matrices is delamination of freshly formed ECM sheets from the culture carrier. This results in unsatisfactory recovery rates of homogenous and suitable matrix substrates for cell culture applications. Therefore, a novel approach was developed that facilitates covalent binding of coupling agents to preserve the link between ECM and substrate. The newly established method involved integrated covalent attachment of (1) aminosilane, (2) poly(octadecene *alt* maleic anhydride) thin films and (3) human fibronectin and thereby allowed incorporation and anchorage of cell-secreted ECM into the coupling layer, as shown in figure 5.1.1. Fibronectin was an ideal binding platform for cell-secreted extracellular molecules as it has the ability to interact with collagen, heparin and fibrin via internal binding domains (fibronectin type I, II and III domains). Also the hydrophobic character of poly(octadecene *alt* maleic anhydride) and its long alkyl chains mediated hydrophobic interactions between secreted matrix molecules and the substrate surface. Beneficial effects were not only appreciable during ECM deposition, but especially throughout the processing of decellularised matrix layers and their subsequent use in culture experiments. Thus, this novel binding system permits long-term cross-linkage of segregated ECM networks and is invaluable for the reliable establishment of decellularised extracellular matrices.

It was the aim of this study to develop *in vitro* cell culture systems that mimic extracellular matrix structures found in the natural human bone marrow microenvironment. Pioneering work by Cukierman et al. has demonstrated the effect of fibroblast-generated decellularised matrices on *in vivo*-like cellular adhesion mechanisms and cell morphology. However, tissue specific decellularised matrices for the bone marrow have not been extensively described. Therefore, mesenchymal stromal cells were chosen for the creation of extracellular matrix substrates as they are known for their properties as matrix secreting cells and major regulators of bone marrow stem cell niches [24, 93]. Early passage human MSC were cultured on FN-coated adhesive surfaces and were allowed to secrete ECM components. Within 10 days human primary BM-MSC have produced dense and homogenous sheets of extracellular matrix material. The presented coupling strategy resulted in stable and processable MSC-derived matrices (from now on termed *MDM*). Furthermore, the outcome of fabricated matrices was tuneable by means of differential MSC-stimulation over the period of matrix secretion. Two types of MSC-secreted matrices have been developed according to specific characteristics of the bone marrow. Collagen is the most abundant ECM protein in bone marrow and in the whole body and is important for tissue integrity and stability. In dependence of ascorbic acid MSC have shown elevated segregation of collagen into their environment. Matrices that were generated under ascorbic acid stimulation were termed aaECM and yielded collagen rich extracellular matrices. Osteoblasts are progeny of MSC with supposed regulatory functions towards haematopoietic progenitor cells within the osteogenic stem cell niche of trabecular bone [92]. Stimulated osteoblast differentiation of MSC during their ECM secretion phase resulted in osteogenic extracellular matrices

that were termed osteoECM. Although different primary MSC donor populations were used for repeated matrix segregation, the individual and characteristic appearance of both matrix types was largely consistent. Taken together, the first aim of this thesis was accomplished by the establishment of a method that allows stable, variable and reproducible construction of surrogate bone marrow ECM *in vitro*.

Figure 5.1.1: Stabilisation of MSC-secreted ECM



Schematic representation of the coupling strategy for improved anchorage of MSC-secreted ECM to the substrate surface.

Based on this first accomplishment, the next goal was to characterise such *in vitro* microenvironments. The surrogate nature of decellularised aaECM and osteoECM substrates was substantiated by analysis of their compositional, topographical and elastic properties. Molecular and physicochemical cues direct cellular morphology, migration, proliferation and survival. Therefore, it is crucial that MDM have the ability to mimic these properties in a functional and native manner.

Many studies have been able to demonstrate the importance of single or multi-component

matrix preparations on cellular behaviour [232, 268, 269]. But, these approaches involve limitations as they cannot address the complex interaction of manifold ECM molecules towards the cell [237]. Microarray analysis have tried to decipher which genes are activated in early MSC, including secreted extracellular matrix components [203, 205]. However, a detailed proteomic identification of extracellular molecules secreted by MSC has not been done so far. In this study the complex composition of decellularised extracellular matrices was revealed by highly sensitive mass spectrometric analysis of complete protein extracts. Unlike identification of only a hand full of proteins via proteomic studies involving 2-dimensional electrophoresis techniques, here more than 70 proteins with gene ontology annotations for extracellular matrix classification have been identified. Many of the identified proteins can be allocated to the family of either collagens or proteoglycans. This implies that among many others, functionalities such as structural guidance and growth factor presentation are crucial to the microenvironment. In dependence of varying stimuli both MDM types demonstrated differing abundance of these major ECM components, validating their distinct characteristics. aaECM reflected a higher abundance for collagens and sulfated glycosaminoglycans than osteoECM, which arised from the elevated ascorbic acid treatment. However, in consideration of their overall proteomic composition, both ECM types demonstrate very similar results. This indicates that MSC secrete a consistent set of fundamental BM-specific ECM components and upon external stimulation or differentiation into osteoblasts their quantitative abundance is changed. Definitive differences between aaECM and osteoECM in absolute abundance of selective proteins have to be elucidated by further statistical analysis of mass spectrometric data (3rd repetition currently on the way). Thereby, differences in aaECM and osteoECM properties can be addressed more specifically. In general, the appearance of MDM is highly complex in its composition. Many of the identified proteins are involved in the assembly of micro- and supra-structural elements of extracellular matrices. For example proteins like fibulin aid formation of fibronectin-containing matrix fibres. Others are involved in enzymatic post-translational processing of extracellular molecules, such as hydroxylation of collagen or deamination of collagen or elastin. Metalloproteinases and their inhibitors are important regulators of ECM remodelling and were also detected in decellularised matrices. In the same way, but though very rare, soluble signalling ligands like the Wnt-protein 5b were also detected at low frequencies and demonstrate that functional components such as growth factors and cytokines are present too. In conjunction, the entity of proteins in the system comprises all necessary parameters for cell adhesion, cell migration and activation of cell signalling events. The most frequently identified components such as collagens, fibronectin, thrombospondin, tenascin and others have been categorised as major constituents of the natural bone marrow extracellular environment [23, 96]. This demonstrates that the secretory behaviour of primary MSC *in vitro* has been very similar to their natural behaviour *in vivo*, and argues for the close resemblance of the established MDM substrates with native extracellular BM conditions.

The varying stimuli used for the creation of different ECM types also resulted in varying topography and elasticity of MDMs. As it can be derived from the compositional complexity of

matrix extracts, the cell-free extracellular matrices harbour capabilities to reflect supramolecular structures of native ECM assemblies. Cell-made matrices have the advantage that processes like post-translational modification, active fibrillogenesis, aligned deposition and remodelling of matrix molecules is conducted in a physiological manner. The established MDM substrates comprise complex suprastructural elements of natural matrix assemblies. Large fibres are associated with smaller fibrils and tethered glycosaminoglycans were layered down in an oriented fashion according to the cellular orientation. After decellularisation the structural aspect of the ECM remained and contained some degree of 3-dimensionality. Osteogenic type ECM demonstrated large and coarse-meshed fibre structures but resembled a rather flat morphology. In contrast, aaECM revealed dense fibre-networks with numerous fibrillar interconnections and a thickness of about 2 μ m, including topography changes at a sub-cellular range. The morphology of the fibre network, fibre cross-linking and non-covalent interactions with other matrix proteins also contributes to matrix elasticity. Bone marrow is a highly viscous tissue ranging at a very small elasticity of 0.1kPa. Here, the Young's Modulus of decellularised substrates demonstrated a similar and very soft character, ranging at 0.1 and 0.3kPa, for aaECM and osteoECM respectively. The soft elasticity of matrices secreted by MSC undergoing osteoblast differentiation might be due to the short differentiation time and limited mineral deposition. The given characterisation of MDM implies that these cell-made ECM systems have the ability to mimic and display most functional aspects of *in vivo* ECM systems, such as presentation of adhesion sites within ECM molecules, mechanical stability and elastic extensibility and presentation of growth factors and soluble ligands by glycoproteins and proteoglycans. In comparison to other bioengineered culture systems, which systematically present only single aspects of the microenvironment, this system allows to probe all these multiple parameters at the same time for their potential to synergistically support BM stem cell expansion *in vitro*. In conclusion, the second goal of this work has been accomplished by identifying the molecular composition, the topographical architecture and the elastic properties of MDM. The presented ECM substrates resemble the physicochemical properties of complex bone marrow microenvironments.

The next goal was to support and expand BM stem cells *ex vivo* by the help of the developed surrogate microenvironment culture system. Figure 5.1.2 summarises the findings of MSC and HSPC culture and their response to MDM.

The study of MSC culture on MSC-ECM demonstrated that the proliferative behaviour of these cells was notably influenced by the culture substrate. Although preparation of 2D fibronectin and Matrigel surfaces demonstrated superior long-term expansion than plain tissue culture plastic, MDM substrates have been able to go beyond this effect. Enhanced proliferative behaviour was accompanied by altered cell shape (smaller and more elongated than cells on control substrates) and by increased secretion of cytokines such as IL-8, Ang-1 and SDF-1. Maintenance of a small and spindle shaped morphology has been associated with higher proliferation rates [270] and demonstrates that the extracellular environment of decellularised matrices bears considerable advantages in comparison to simple ECM preparations of ECM components. Furthermore, MDM also promoted enhanced proliferation into adipocytes and

osteoblasts upon stimulation into both lineages. The absence of residual cytokines from MDM (as observed by ELISA analysis of cytokine washes from the matrix) implies that the supportive function of the substrate is not due to the release of remaining growth factors but more likely due to the adhesive properties and subsequent regulatory processes. For the possible purpose of clinical application not only large numbers of MSC are important but also the secretion of cytokines and growth factors is crucial for MSC functionality. Most of the therapeutic beneficial effects of MSC are exerted via paracrine mechanisms [271]. The presented culture system demonstrated that cytokine secretion can be stimulated when MSC are in contact with MDM. The finding of enhanced growth factor secretion is one indication that ECM stimulation alters global MSC behaviour. Furthermore, paracrine stimulation between MSC via self-secreted morphogens is most likely guided by the local presentation of cytokines via ECM molecules of MDM. The extracellular microenvironment influences the physiological presentation of soluble signalling ligands and controls their sequestration, thereby influencing the outcome of cell fate. For example, controlled binding and release of TGF- β by biglycan and decorin proteoglycans directs controlled proliferation and survival of marrow stromal cells. Absence of these molecules leads to excess levels of TGF- β which in turn binds directly to its receptor and overactivates the signalling pathway resulting in apoptosis and reduced numbers of marrow stromal cells [272]. Another aspect of environmental cell fate control is the conditioning of MSC by their niche. Once the cells are adapted to signals of their environment they are pre-destined to follow certain lineage specifications. Irreversible epigenetic changes prime the cell to respond in particular ways to further stimuli [242] which diminishes their multipotentiality. Here lies one of the reasons why MSC cultures on plain plastic substrates or simple and flat Matrigel preparations resulted in impaired culture outcome. This strengthens the importance of the culture environment for maintenance of functional cellular phenotypes. This is especially important if the expanded cell population is intended for subsequent use in specific cellular assays or for applications that require cellular plasticity.

Another aspect that is included in this phenomenon is the alteration of cell shape on MDM. The underlying substrate determines cell shape by topographical patterning of adhesion sites. Furthermore, cell shape is altered by transduction of external elasticity into intracellular tensegrity, dependent on the resilience of the substrate. Pioneering work by the Chang laboratory [118] indicated that culture surface modification by presentation of micro-patterned ECM molecules dictates cell shape and MSC cell fate into osteoblasts or adipocytes. Similarly the group around Spatz et al. [196] has shown that activation of integrins via nanopatterned adhesive surfaces controls the formation of focal adhesion sites and actin stress fibres, leading to altered cell shapes and cellular responses. These processes are thought to be myosin-driven, generating traction forces against the matrix. Also mechanisms of force-sensitive protein conformational changes (at focal adhesion sites or within the ECM) are thought to control cell shape-mediated cell fate decisions [241]. In contrast to the speculated elasticity driven differentiation of MSC [51, 117], the very soft characteristics of MDM did not induce differentiation of MSC under standard culture conditions (unless differentiation was specifically induced). This may be re-

lated to the fact that both ECM substrates demonstrated a Young's Modulus ranging below the usually tested elasticities by Discher and co-workers and harbours a different effect of very soft matrices towards MSC. As mentioned above, the BM is one of the softest tissues in the body, and the here presented MDM were able to take on this characteristic. The property of this very viscous matrix material should be considered for the establishment of artificial BM stem cells culture scaffolds. In conclusion, the natural topographical presentation of adhesion sites within MDM is a key advantage of these substrates in comparison to Matrigel or even simpler fibronectin or plastic surfaces. Under these premises, the observed differences between aaECM and osteoECM in supporting MSC differentiation might be attributed to their differential elasticity and or topography.

Analysing the potential of BM cell-generated extracellular matrices as *in vitro* niches for MSC has become fashionable. Shortly after this thesis was initiated, studies by Chen and co-workers demonstrated similar effects of MSC proliferation and differentiation behaviour on MDM as described in this thesis. *In vivo*-transplantation into mice revealed that the bone formation capacity of long-term ECM-expanded cells is dramatically enhanced in comparison to less potent cells that were expanded on tissue culture plastic [243, 245, 246]. Another very recent work by Pei et al. indicates that the beneficial effect of MDM is transduced into MSC by activation of integrin $\alpha 2$ and $\beta 5$ and by activation of proliferation related ERK1/2 and cyclin D1 pathways [273]. In line with these findings cell-cycle control has been shown to be regulated via matrix elasticity and activation of ERK and FAK [235]. In conjunction, the here presented support of MSC expansion and differentiation, and the mentioned findings by other groups, point out that adhesion processes and mechano-transduction of signalling events are key mechanisms by which MDM conduct their functionality towards MSC. Taken together, decellularised ECM substrates function as supportive environmental niches for BM-MSC and are potent culture systems for MSC expansion, differentiation and stimulation of cytokine secretion.

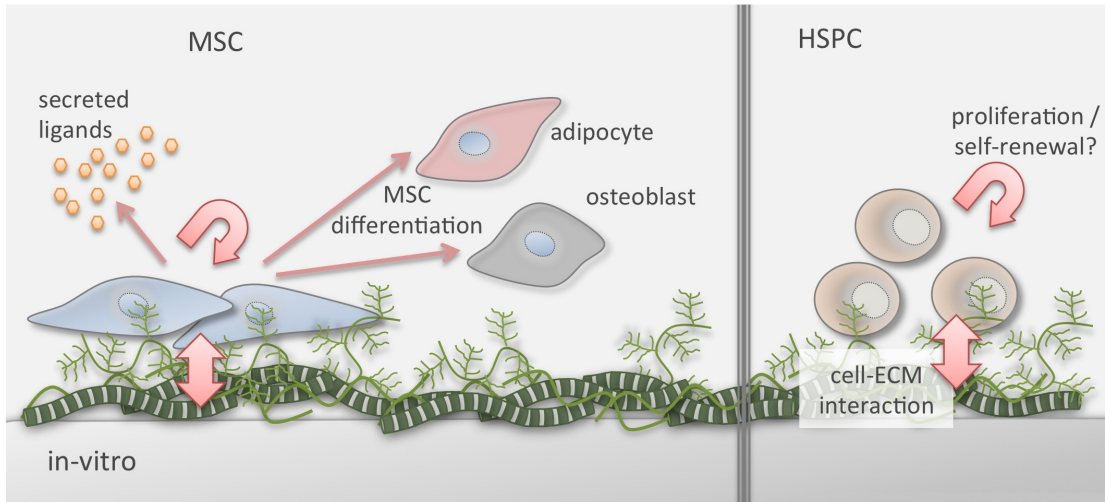
Unlike the recent interest in MSC culture on decellularised MDM, the expansion of HSPC by such systems has not been investigated. In the past, the standard culture condition that was used to maintain and expand haematopoietic stem cells was the so called Dexter Culture System, which is a co-culture of stromal feeder cells together with a mix of progenitor and premature haematopoietic cells or with enriched HSPC. As described by the hypothesis of the stem cell synapse [75], the supportive function of feeder-based cultures is not only the direct cell-cell contact between stromal cells and HSPC but also the secretion of HSPC-supporting factors by stromal cells (soluble and ECM ligands). Today, HSPC are mainly cultured in suspension with little opportunity for cell attachment, only controlled by the addition of cytokines. In this study, MDM provide a matrix for cell attachment of HSPC and thereby provide more natural cues for stem cell regulation. The data from this thesis demonstrate that MDM have the potential to support the expansion of CD34+ progenitor cells by upto 3-fold (for aaECM substrates). Thereby, a constant number of progenitor cells was maintained expressing early stem cell markers CD34 and CD133 in comparison to an exhaustion of those cells on tissue culture plastic or fibronectin coated substrates. Although not significantly different, osteoECM

substrates did not support HSPC as robust as aaECM, which indicates that the properties of osteoECM are not as optimal for HSPC culture as those of aaECM. Analysis of the differential effects of both substrates might help to identify the mechanisms by which HSPC can be stimulated for enhanced 'self-renewing' proliferation. The true stem cell phenotype of HSPC is classically demonstrated, not only by cell surface marker expression, but moreso by their ability to reconstitute the haematopoietic system in lethally irradiated recipient mice after transplantation of *ex vivo* manipulated cells. Ongoing transplantation experiments of human ECM-expanded HSPC into SCID (severe combined immunodeficiency) mice will reveal the amount of true stem cells expanded or maintained by the MDM system.

On both culture substrates, HSPC demonstrated close interaction and strong adhesion to the underlying matrices. For a fraction of cells this adhesion was accompanied by a change in cell shape, demonstrating a more flat and cobblestone-like morphology. A recent study by Jing et al. [247] investigated MSC-HSPC co-cultures and found that the fraction of more immature progenitor cells exhibited a flat morphology and was located underneath the stromal cell layer in close contact with the underlying matrix. Similarly, 3D culture systems of HSPC, for example in ECM functionalised microcavities also presented more adhesion sites to progenitor cells and resulted in stem cell maintenance [126]. The close contact of HSPC to MDM can also be explained by the presence of the chemoattractant SDF-1 in MDM substrates. As shown in Appendix A, SDF-1 has been detected in MDM, but is was listed as extracellular matrix annotated although it is a secreted product of MSC [274]. SDF-1 has been shown to control stem cell homing from the circulation back to the niche via interaction with CXCR4 receptors on the cell surface of HSPC [78]. The presence of SDF-1 in MDM indicates that homing-related signals are an important aspect for *ex vivo* HSPC-supportive substrates to spatially present migratory gradient-signals which are able to cause directed stem cell interaction with the niche. SDF-1 has also been suggested to mediate HSPC expansion [248], which could be one of the responsible factors for the detected elevated proliferation levels of HSPC on MDM. By interaction with MDM presented SDF-1, receptor levels of CXCR4 on HSPC might change and cause different signalling events that determine further behaviour of the cells in culture, which would be absent in control cultures due to the lack of the ligand. As it was already stressed for the regulation of MSC, the MDM substrate provides an adhesive environment that contains binding sites for HSPC cell surface receptors and thereby enables the specific interaction between HSPC and ECM components. As many studies have highlighted the regulation of HSPC by stromal cell proteoglycans [45], the here presented culture substrate includes all molecular aspects to mediate cytokine adhesion and interaction with progenitor cells. Only small amounts of cytokines have been added into the medium and resulted in a measureable difference between MDM and control substrates. Application of even higher doses of growth factors might augment the proliferative capacity even further. These findings indicate that close interaction of HSPC with the ECM substrate stimulate signalling cascades that can maintain HSPC stemness. This hypothesised maintenance of early progenitors within the ECM compartment probably leads to reduced exhaustion of stem cells irrespective of extensive proliferation.

In conclusion, also the third aim of this thesis was successfully accomplished. Taken together, many ECM intrinsic factors are involved and are necessary for the composition of native extra-cellular environments. The use of optimal physiological substrates may replace or complement existing approaches to support and expand stem cells *ex vivo*. The here presented system of decellularised bone marrow-surrogate matrices is one route to achieve optimal culture conditions for MSC and HSPC in a controllable and tuneable way.

Figure 5.1.2: Response of bone marrow stem and progenitor cells to decellularised matrices



Mesenchymal and haematopoietic stem and progenitor cells cultured on MSC-generated decellularised matrices demonstrate intense cell-substratum interactions, accompanied by morphological changes and enhanced proliferative activity. MSC secrete elevated levels of soluble ligands and show robust differentiation into adipocytes and osteoblasts upon inductive stimulation.

From the presented work in this thesis four important conclusions can be drawn:

- ❖ The reliable use of decellularised matrix substrates can be highly improved by appliance of polymer-mediated covalent binding of fibronectin and subsequent anchorage of cell-secreted extracellular matrix molecules.
- ❖ Generation of decellularised matrices is variable by means of cellular-stimulation during the process of matrix segregation. Furthermore, the system can be transferred to other cell types for tissue-specific generation of decellularised ECM substrates.
- ❖ Detailed analysis of decellularised matrix extracts and its characteristics demonstrates the intricate and complex nature of BM-MSK extracellular constituents. Combined presence of all ECM intrinsic properties determines substrate functionality.
- ❖ Niche-like decellularised MDM can support expansion and differentiation of tissue-specific stem and progenitor cells (MSC and HSPC) *in vitro* and permit insight into control mechanisms of stem cell self-renewal and cell fate decisions. The system can be exploited to produce defined artificial stem cell niches in an *ex vivo* setting.

This brings us back to the initial idea of this project. The ability of the extracellular matrix to instruct cellular phenotype should not be underestimated when thinking how artificial environments orchestrate stem cell function. The extracellular matrix should be regarded as an entity with versatile, but yet specific functions. The presented studies have highlighted that progenitor cells of the bone marrow are regulated by the complex interplay with the ECM in a more natural manner when using organ specific ECMs than by standard culture regimes or reconstituted ECM preparations with no organ specificity.

The results gained within this thesis work are promising but also imply the requirements for further research strategies. To fully understand the mechanisms by which extracellular matrices regulate stem cell self-renewal, survival and cell fate more detailed analysis have to follow. The outlook in this last section will give ideas and possibilities how to continue facilitating this system for further research applications.

5.2 Outlook

The establishment of BM-specific decellularised matrices and their detailed characterisation is the starting point for manifold following investigations exploiting the value of this culture system. The possible potential is seen in clinical applications, as basic research model system or for the progression of bioengineering approaches. The entity of possible applications allows further insight into the BM stem cell niche.

The established system demonstrates a great potential to be used as a culture substrate for expansion of BM progenitor cells. Both cell types, MSC and HSPC, are valuable cell sources

for cellular therapies of degenerative or malignant disorders. For clinical applications large numbers of cells are necessary to achieve curative effects. Further development of this system permits one to achieve of controlled *ex vivo* expansion of stem cells. For example autologous cells could be expanded and applied as direct cellular transplants or in conjunction with intelligent biomaterials that guide the regeneration process. MSC are attractive cell sources for therapeutic applications, given their potential for tissue repair and immunosuppressive properties [275, 276]. Decellularised matrices have shown extensive expansion of MSC over long-term culture periods. To shorten long expansion times, a larger surface area coated with decellularised matrices would allow to expand more cells in a shorter time frame. Since the ECM composition was demonstrated to be largely reproducible between different MSC donors it would be of great assistance for the expansion of patient-MSC if allogeneic MSC from healthy donors could be utilised to generate MDM layers. For example using MDM from young donors could be especially beneficial for the expansion and rejuvenation of MSC from older patients, like it was shown by animal experiments of Sun et al. [246]. Furthermore, the use of immortalised MSC-cell lines for preliminary preparation of ECM substrates might be worth considering. Of course, further investigation needs to be done to analyse the impact of donor age, gender, time-frame for ECM preparation and appropriate MSC yield, before this system could be translated into the clinic. Similar tactics would apply for the expansion of HSPC. Transplantation of HSPC is used for the treatment of a variety of genetic disorders, blood cancers or diseased bone marrow. Here, different cell sources such as peripheral blood, cord blood and bone marrow progenitor cells could be further analysed for their expansion on decellularised matrices in conjunction with growth factor and morphogen supplements.

On the other hand this system is not only valuable for possible future clinical applications, it also holds a great potential for basic research of cell-ECM interactions and ECM-mediated stem cell regulation. Thereby, MDM serve as a model system to probe a multitude of mechanisms and regulatory pathways that are affected by ECM topography, elasticity, adhesion ligands and signalling domains. Specifically, this includes adhesion and integrin activation processes, transduction of extracellular signals into intracellular tensegrity, cell shape regulation of signalling cascades and changes in gene expression and cellular phenotype. One approach could be targeted manipulation of specific ECM molecules by si-RNA knock-down or function blocking experiments and investigation of the cellular response. Others could be the detailed analysis of adhesion receptors involved in cell survival, proliferation and differentiation in contact with MDM. The variability of the model system also lies within the possibility to study uptake and release of soluble growth factors and cytokines. Presentation of soluble ligands via glycosaminoglycans plays an important role for functional cellular interaction. For example biomaterials must also function as a reservoir for growth factors and cytokines that can be released in a timely manner or are presented as a gradient for optimal cellular stimulation. The system might also help to progress the development of serum free culture conditions. Either pre-loaded tissue specific cytokines (for HSPC) or self-secreted growth factors (by MSC) are more effectively presented and preserved by the matrix, minimising the need for undefined

serum supplementation. Another very interesting application of MDM is the use as native environment for the study of cancer cells or cancer stem cells in interaction with extracellular surroundings and in response to chemotherapy.

Third, the system can also serve as a guiding point for ongoing improvement and development of biomaterials for bio- and tissue-engineering applications. Thoroughly characterised MDM are most valuable reference systems for the rational design of multi-biofunctional polymer matrices. The field of bioengineered materials for the control of stem cell behaviour has made great advancements over the last years. Once the underlying mechanisms of stem cell control via ECM interactions are better understood minimal criteria for artificial (man-made and not cell-made) surrogate systems can be refined. Clearly, the native extracellular matrix and recreations of it provide a very fundamental basis for the engineering of scaffolds and cellular substrates. The use of an intelligent combination of the identified crucial BM niche cues can help to accelerate this process. It is not only important that a substrate provides a myriad of adhesion sites for cells and signalling molecules but also the right physical properties that direct cellular maintenance or differentiation into the desired cell type. The presented MDM system can serve as a blueprint for the design of structures that control cellular response. The future complex biomaterial must combine sufficient presentation of adhesion sites, possible via peptide sequences, artificial reconstitution of natural ECM shapes, presentation of functional signalling molecules and elastic 3D properties in a tuneable and cell-interactive manner. Combined efforts of basic research, nanotechnology and chemical engineering will help to approach optimal conditions for *ex vivo* and *in vivo* control of stem and progenitor cell behaviour.

As we progress to appreciate the multi-functionality and complexity of natural extracellular matrices by fabrication of analogous model systems - either as complex as decellularised matrices or by mimicking subsets of selected ECM properties - we can foster and accelerate the intelligent design of new biomaterials for tissue engineering and regenerative medicine.

List of Figures

1.1.1 The extracellular matrix provides an instructive microenvironment	2
1.2.1 Reconstruction of bone marrow stem cell microenvironments <i>ex vivo</i>	6
2.1.1 The extracellular matrix	8
2.1.2 ECM and integrin signalling	12
2.1.3 Elasticity of tissues	13
2.2.1 Multipotency of HSC and MSC	15
2.2.2 HSC niches in trabecular bone cavities	19
2.4.1 Decellularised matrices from tissues/organs and cultured cells	24
2.4.2 Decellularisation techniques for tissues and organs	26
3.1.1 Maleic acid copolymer platform	32
3.1.2 Binding of ECM molecules to POMA-functionalised surfaces	32
3.2.1 Calibration curve of alamarBlue reduction over MSC cell number	36
3.2.2 Isolation of CD34+ HSPC from leukapheresis products	39
3.4.1 Preparation of bone marrow cylinders for ultrastructural and histological analysis	43
4.1.1 Human bone marrow ultrastructure	48
4.1.2 Human bone marrow histology	49
4.2.1 Substrates for stabilisation of secreted ECM to the culture carrier	52
4.2.2 aaECM and osteoECM stabilised on FN/POMA culture carriers	54
4.2.3 Suprastructural appearance of aaECM and osteoECM substrates	56
4.2.4 Characteristics of ECM substrates	58
4.3.1 Extraction and separation of decellularised ECM substrates	61
4.3.2 SDS-PAGE gels and cutting pattern for in-gel digestion	62
4.3.3 Percentage of extracellular matrix annotated proteins in total sample	62
4.4.1 Cell shape of MSC cultured on decellularised matrices	70
4.4.2 MSC culture on decellularised ECM substrates	71

4.4.3 MSC differentiation on ECM and control substrates	75
4.4.4 MSC cytokine secretion	77
4.4.5 HSPC cultured on ECM and PTP substrates	81
4.4.6 Culture of HSPC on ECM substrates	82
4.4.7 Comparison of cytokine-washed and native ECM	83
5.1.1 Stabilisation of MSC-secreted ECM	89
5.1.2 Response of bone marrow stem and progenitor cells to decellularised matrices .	95

List of Tables

2.4.1 Cell-made decellularised matrices <i>in vitro</i>	28
3.1.1 Media formulations for aaECM and osteoECM production	34
3.2.1 Flow cytometry antibodies	40
4.3.1 List of ECM proteins detected in decellularised protein extracts	66
4.4.1 Expansion of MSC	73
4.4.2 Expansion of HSPC on ECM substrates	83

Bibliography

- [1] Niklason LE, Langer R. Prospects for organ and tissue replacement. *JAMA*. 2001 Feb;285(5):573–6.
- [2] Fuchs JR, Nasser BA, Vacanti JP. Tissue engineering: a 21st century solution to surgical reconstruction. *Ann Thorac Surg*. 2001 Aug;72(2):577–91.
- [3] Langer R, Vacanti JP. Tissue engineering. *Science*. 1993 May;260(5110):920–6.
- [4] Bajada S, Mazakova I, Richardson JB, Ashammakhi N. Updates on stem cells and their applications in regenerative medicine. *Journal of tissue engineering and regenerative medicine*. 2008 Jun;2(4):169–83.
- [5] Bottaro DP, Liebmann-Vinson A, Heidaran MA. Molecular signaling in bioengineered tissue microenvironments. *Ann N Y Acad Sci*. 2002 Jun;961:143–53.
- [6] Dvir T, Timko BP, Kohane DS, Langer R. Nanotechnological strategies for engineering complex tissues. *Nat Nanotechnol*. 2011 Jan;6(1):13–22.
- [7] Cancedda R, Bianchi G, Derubeis A, Quarto R. Cell therapy for bone disease: a review of current status. *Stem Cells*. 2003 Jan;21(5):610–9.
- [8] de la Morena MT, Gatti RA. A history of bone marrow transplantation. *Hematol Oncol Clin North Am*. 2011 Feb;25(1):1–15.
- [9] Adams GB. Deconstructing the hematopoietic stem cell niche: revealing the therapeutic potential. *Regenerative medicine*. 2008 Jul;3(4):523–30.
- [10] Yin T, Li L. The stem cell niches in bone. *J Clin Invest*. 2006 May;116(5):1195–201.
- [11] Ehninger A, Trumpp A. The bone marrow stem cell niche grows up: mesenchymal stem cells and macrophages move in. *Journal of Experimental Medicine*. 2011 Mar;208(3):421–8.
- [12] Zandstra PW. The opportunity of stem cell bioengineering. *Biotechnol Bioeng*. 2004 Nov;88(3):263.
- [13] Chai C, Leong KW. Biomaterials approach to expand and direct differentiation of stem cells. *Mol Ther*. 2007 Mar;15(3):467–80.
- [14] Dellatore S, Garcia A, Miller W. Mimicking stem cell niches to increase stem cell expansion. *Current opinion in biotechnology*. 2008;19(5):534–540.
- [15] Place ES, Evans ND, Stevens MM. Complexity in biomaterials for tissue engineering. *Nature Materials*. 2009 Jun;8(6):457–70.

- [16] Lutolf MP, Gilbert PM, Blau HM. Designing materials to direct stem-cell fate. *Nature*. 2009 Nov;462(7272):433–41.
- [17] Lutolf MP, Hubbell JA. Synthetic biomaterials as instructive extracellular microenvironments for morphogenesis in tissue engineering. *Nat Biotechnol*. 2005 Jan;23(1):47–55.
- [18] Peerani R, Zandstra PW. Enabling stem cell therapies through synthetic stem cell-niche engineering. *J Clin Invest*. 2010 Jan;120(1):60–70.
- [19] Hoshiba T, Lu H, Kawazoe N, Chen G. Decellularized matrices for tissue engineering. *Expert Opin Biol Ther*. 2010 Dec;10(12):1717–28.
- [20] Klimanskaya I, Chung Y, Meisner L, Johnson J, West MD, Lanza R. Human embryonic stem cells derived without feeder cells. *Lancet*. 2005 Jan;365(9471):1636–41.
- [21] Datta N, Holtorf HL, Sikavitsas VI, Jansen JA, Mikos AG. Effect of bone extracellular matrix synthesized in vitro on the osteoblastic differentiation of marrow stromal cells. *Biomaterials*. 2005 Mar;26(9):971–7.
- [22] Pham QP, Kasper FK, Baggett LS, Raphael RM, Jansen JA, Mikos AG. The influence of an in vitro generated bone-like extracellular matrix on osteoblastic gene expression of marrow stromal cells. *Biomaterials*. 2008 Jun;29(18):2729–39.
- [23] Klein G. The extracellular matrix of the hematopoietic microenvironment. *Experientia*. 1995 Sep;51(9-10):914–26.
- [24] Uccelli A, Moretta L, Pistoia V. Mesenchymal stem cells in health and disease. *Nature Reviews Immunology*. 2008;8(9):726–736.
- [25] Badylak SF. The extracellular matrix as a biologic scaffold material. *Biomaterials*. 2007 Sep;28(25):3587–93.
- [26] Kreis T, Vale R. Extracellular matrix and adhesion proteins. Oxford University Press. 1993 Jul;p. 1–1.
- [27] Rosso F, Giordano A, Barbarisi M, Barbarisi A. From cell-ECM interactions to tissue engineering. *J Cell Physiol*. 2004 May;199(2):174–80.
- [28] Campbell NA. Biology. Benjamin Cummings. 2004 Jul;.
- [29] Kim SH, Turnbull J, Guimond S. Extracellular matrix and cell signalling: the dynamic cooperation of integrin, proteoglycan and growth factor receptor. *J Endocrinol*. 2011 May;209(2):139–51.
- [30] der Rest MV, Garrone R. Collagen family of proteins. *The FASEB journal*. 1991;5(13):2814.
- [31] Kielty CM, Sherratt MJ, Shuttleworth CA. Elastic fibres. *J Cell Sci*. 2002 Jul;115(Pt 14):2817–28.
- [32] Friedl P, Bröcker EB. The biology of cell locomotion within three-dimensional extracellular matrix. *Cell Mol Life Sci*. 2000 Jan;57(1):41–64.
- [33] Miner J. The Extracellular Matrix: An Overview. *Cell-Extracellular Matrix Interactions in Cancer*. 2010;p. 1–17.

- [34] Ruoslahti E. Fibronectin and its receptors. *Annual review of biochemistry*. 1988;57(1):375–413.
- [35] Schaefer L, Schaefer RM. Proteoglycans: from structural compounds to signaling molecules. *Cell Tissue Res*. 2010 Jan;339(1):237–46.
- [36] Kresse H, Schönherr E. Proteoglycans of the extracellular matrix and growth control. *Journal of cellular physiology*. 2001 Dec;189(3):266–74.
- [37] Sternlicht MD, Werb Z. How matrix metalloproteinases regulate cell behavior. *Annu Rev Cell Dev Biol*. 2001 Jan;17:463–516.
- [38] Yong VW. Metalloproteinases: mediators of pathology and regeneration in the CNS. *Nat Rev Neurosci*. 2005 Dec;6(12):931–44.
- [39] Tang BL. ADAMTS: a novel family of extracellular matrix proteases. *The International Journal of Biochemistry & Cell Biology*. 2001 Jan;33(1):33–44.
- [40] Bruckner-Tuderman L, von der Mark K, Pihlajaniemi T, Unsicker K. Cell interactions with the extracellular matrix. *Cell Tissue Res*. 2010 Jan;339(1):1–5.
- [41] Geiger B, Bershadsky A, Pankov R, Yamada KM. Transmembrane crosstalk between the extracellular matrix–cytoskeleton crosstalk. *Nat Rev Mol Cell Biol*. 2001 Nov;2(11):793–805.
- [42] French Constant C, Colognato H. Integrins: versatile integrators of extracellular signals. *Trends Cell Biol*. 2004 Dec;14(12):678–86.
- [43] Arnaout MA, Goodman SL, Xiong JP. Structure and mechanics of integrin-based cell adhesion. *Curr Opin Cell Biol*. 2007 Oct;19(5):495–507.
- [44] Heinegård D. Proteoglycans and more—from molecules to biology. *International Journal of Experimental Pathology*. 2009 Dec;90(6):575–86.
- [45] Rodgers KD, Antonio JDS, Jacenko O. Heparan sulfate proteoglycans: a GAGgle of skeletal-hematopoietic regulators. *Dev Dyn*. 2008 Oct;237(10):2622–42.
- [46] Rachfal AW, Brigstock DR. Connective tissue growth factor (CTGF/CCN2) in hepatic fibrosis. *Hepatol Res*. 2003 May;26(1):1–9.
- [47] Ingber DE. Mechanical control of tissue growth: function follows form. *Proceedings of the National Academy of Sciences of the United States of America*. 2005 Aug;102(33):11571–2.
- [48] Janmey P, McCulloch C. Cell mechanics: integrating cell responses to mechanical stimuli. *Biomedical Engineering*. 2007;9.
- [49] Yeung T, Georges PC, Flanagan LA, Marg B, Ortiz M, Funaki M, et al. Effects of substrate stiffness on cell morphology, cytoskeletal structure, and adhesion. *Cell Motil Cytoskeleton*. 2005 Jan;60(1):24–34.
- [50] Vogel V, Sheetz M. Local force and geometry sensing regulate cell functions. *Nat Rev Mol Cell Biol*. 2006 Apr;7(4):265–75.
- [51] Discher DE, Mooney DJ, Zandstra PW. Growth factors, matrices, and forces combine and control stem cells. *Science*. 2009 Jun;324(5935):1673–7.

- [52] Bruckner P. Suprastructures of extracellular matrices: paradigms of functions controlled by aggregates rather than molecules. *Cell Tissue Res.* 2010 Jan;339(1):7–18.
- [53] Daley WP, Peters SB, Larsen M. Extracellular matrix dynamics in development and regenerative medicine. *J Cell Sci.* 2008 Feb;121(Pt 3):255–64.
- [54] Weissman IL, Anderson DJ, Gage F. Stem and progenitor cells: origins, phenotypes, lineage commitments, and transdifferentiations. *Annu Rev Cell Dev Biol.* 2001 Jan;17:387–403.
- [55] Morrison SJ, Spradling AC. Stem cells and niches: mechanisms that promote stem cell maintenance throughout life. *Cell.* 2008 Feb;132(4):598–611.
- [56] Travlos GS. Normal structure, function, and histology of the bone marrow. *Toxicol Pathol.* 2006 Jan;34(5):548–65.
- [57] Valtieri M, Sorrentino A. The mesenchymal stromal cell contribution to homeostasis. *Journal of cellular physiology.* 2008;217(2):296–300.
- [58] Wilkins BS. Histology of normal haemopoiesis: bone marrow histology. I. *J Clin Pathol.* 1992 Aug;45(8):645–9.
- [59] Weissman IL. Stem cells: units of development, units of regeneration, and units in evolution. *Cell.* 2000 Jan;100(1):157–68.
- [60] Caplan AI, Bruder SP. Mesenchymal stem cells: building blocks for molecular medicine in the 21st century. *Trends Mol Med.* 2001 Jun;7(6):259–64.
- [61] Bianco P, Robey PG, Simmons PJ. Mesenchymal stem cells: revisiting history, concepts, and assays. *Cell Stem Cell.* 2008 Apr;2(4):313–9.
- [62] Friedenstein AJ, Petrakova KV, Kurolesova AI, Frolova GP. Heterotopic of bone marrow. Analysis of precursor cells for osteogenic and hematopoietic tissues. *Transplantation.* 1968 Mar;6(2):230–47.
- [63] Goshima J, Goldberg VM, Caplan AI. The osteogenic potential of culture-expanded rat marrow mesenchymal cells assayed in vivo in calcium phosphate ceramic blocks. *Clin Orthop Relat Res.* 1991 Jan;(262):298–311.
- [64] Kuhn NZ, Tuan RS. Regulation of stemness and stem cell niche of mesenchymal stem cells: implications in tumorigenesis and metastasis. *Journal of cellular physiology.* 2010 Feb;222(2):268–77.
- [65] Zaragosi LE, Ailhaud G, Dani C. Autocrine fibroblast growth factor 2 signaling is critical for self-renewal of human multipotent adipose-derived stem cells. *Stem Cells.* 2006 Nov;24(11):2412–9.
- [66] Dominici M, Blanc KL, Mueller I, Slaper-Cortenbach I, Marini F, Krause D, et al. Minimal criteria for defining multipotent mesenchymal stromal cells. The International Society for Cellular Therapy position statement. *Cytotherapy.* 2006 Jan;8(4):315–7.
- [67] Jones EA, English A, Kinsey SE, Straszynski L, Emery P, Ponchel F, et al. Optimization of a flow cytometry-based protocol for detection and phenotypic characterization of multipotent mesenchymal stromal cells from human bone marrow. *Cytometry B Clin Cytom.* 2006 Nov;70(6):391–9.

-
- [68] Sacchetti B, Funari A, Michienzi S, Cesare SD, Piersanti S, Saggio I, et al. Self-renewing osteoprogenitors in bone marrow sinusoids can organize a hematopoietic microenvironment. *Cell*. 2007 Oct;131(2):324–36.
- [69] Parekkadan B, Milwid JM. Mesenchymal stem cells as therapeutics. *Annu Rev Biomed Eng*. 2010 Aug;12:87–117.
- [70] Wagner W, Roderburg C, Wein F, Diehlmann A, Frankhauser M, Schubert R, et al. Molecular and secretory profiles of human mesenchymal stromal cells and their abilities to maintain primitive hematopoietic progenitors. *Stem Cells*. 2007 Oct;25(10):2638–47.
- [71] Wagner W, Saffrich R, Ho AD. The Stromal Activity of Mesenchymal Stromal Cells. *Transfusion medicine and hemotherapy : offizielles Organ der Deutschen Gesellschaft fur Transfusionsmedizin und Immunhamatologie*. 2008 Jan;35(3):185–193.
- [72] BECKER AJ, McCULLOCH EA, TILL JE. Cytological demonstration of the clonal nature of spleen colonies derived from transplanted mouse marrow cells. *Nature*. 1963 Feb;197:452–4.
- [73] Osawa M, Hanada K, Hamada H, Nakauchi H. Long-term lymphohematopoietic reconstitution by a single CD34-low/negative hematopoietic stem cell. *Science*. 1996 Jul;273(5272):242–5.
- [74] Kiel MJ, Morrison SJ. Uncertainty in the niches that maintain haematopoietic stem cells. *Nat Rev Immunol*. 2008 Apr;8(4):290–301.
- [75] Wilson A, Trumpp A. Bone-marrow haematopoietic-stem-cell niches. *Nat Rev Immunol*. 2006 Feb;6(2):93–106.
- [76] Yin AH, Miraglia S, Zanjani ED, Almeida-Porada G, Ogawa M, Leary AG, et al. AC133, a novel marker for human hematopoietic stem and progenitor cells. *Blood*. 1997 Dec;90(12):5002–12.
- [77] Terstappen LW, Huang S, Safford M, Lansdorp PM, Loken MR. Sequential generations of hematopoietic colonies derived from single nonlineage-committed CD34+CD38-progenitor cells. *Blood*. 1991 Mar;77(6):1218–27.
- [78] Lapidot T, Kollet O. The essential roles of the chemokine SDF-1 and its receptor CXCR4 in human stem cell homing and repopulation of transplanted immune-deficient NOD/SCID and NOD/SCID/B2m(null) mice. *Leukemia : official journal of the Leukemia Society of America, Leukemia Research Fund, UK*. 2002 Oct;16(10):1992–2003.
- [79] Zon LI. Intrinsic and extrinsic control of haematopoietic stem-cell self-renewal. *Nature*. 2008 May;453(7193):306–13.
- [80] Blank U, Karlsson G, Karlsson S. Signaling pathways governing stem-cell fate. *Blood*. 2008 Jan;111(2):492–503.
- [81] Zhang CC, Lodish HF. Cytokines regulating hematopoietic stem cell function. *Current Opinion in Hematology*. 2008 Jul;15(4):307–11.
- [82] Yoshihara H, Arai F, Hosokawa K, Hagiwara T, Takubo K, Nakamura Y, et al. Thrombopoietin/MPL signaling regulates hematopoietic stem cell quiescence and interaction with the osteoblastic niche. *Cell Stem Cell*. 2007 Dec;1(6):685–97.

- [83] Qian H, Buza-Vidas N, Hyland CD, Jensen CT, Antonchuk J, Månsson R, et al. Critical role of thrombopoietin in maintaining adult quiescent hematopoietic stem cells. *Cell Stem Cell*. 2007 Dec;1(6):671–84.
- [84] Lyman SD, Jacobsen SE. c-kit ligand and Flt3 ligand: stem/progenitor cell factors with overlapping yet distinct activities. *Blood*. 1998 Feb;91(4):1101–34.
- [85] Schofield R. The relationship between the spleen colony-forming cell and the haemopoietic stem cell. *Blood Cells*. 1978 Jan;4(1-2):7–25.
- [86] Jones DL, Wagers AJ. No place like home: anatomy and function of the stem cell niche. *Nat Rev Mol Cell Biol*. 2008 Jan;9(1):11–21.
- [87] Song L, Webb NE, Song Y, Tuan RS. Identification and functional analysis of candidate genes regulating mesenchymal stem cell self-renewal and multipotency. *Stem Cells*. 2006 Jul;24(7):1707–18.
- [88] Meirelles LDS, Caplan AI, Nardi NB. In search of the in vivo identity of mesenchymal stem cells. *Stem Cells*. 2008 Sep;26(9):2287–99.
- [89] Crisan M, Yap S, Casteilla L, Chen CW, Corselli M, Park TS, et al. A perivascular origin for mesenchymal stem cells in multiple human organs. *Cell Stem Cell*. 2008 Sep;3(3):301–13.
- [90] Wilson A, Oser GM, Jaworski M, Blanco-Bose WE, Laurenti E, Adolphe C, et al. Dormant and self-renewing hematopoietic stem cells and their niches. *Annals of the New York Academy of Sciences*. 2007 Jun;1106:64–75.
- [91] Kiel MJ, Yilmaz OH, Iwashita T, Yilmaz OH, Terhorst C, Morrison SJ. SLAM family receptors distinguish hematopoietic stem and progenitor cells and reveal endothelial niches for stem cells. *Cell*. 2005 Jul;121(7):1109–21.
- [92] Calvi LM, Adams GB, Weibrecht KW, Weber JM, Olson DP, Knight MC, et al. Osteoblastic cells regulate the haematopoietic stem cell niche. *Nature*. 2003 Oct;425(6960):841–6.
- [93] Méndez-Ferrer S, Michurina TV, Ferraro F, Mazloom AR, Macarthur BD, Lira SA, et al. Mesenchymal and haematopoietic stem cells form a unique bone marrow niche. *Nature*. 2010 Aug;466(7308):829–34.
- [94] Sugiyama T, Kohara H, Noda M, Nagasawa T. Maintenance of the hematopoietic stem cell pool by CXCL12-CXCR4 chemokine signaling in bone marrow stromal cell niches. *Immunity*. 2006 Dec;25(6):977–88.
- [95] Omatsu Y, Sugiyama T, Kohara H, Kondoh G, Fujii N, Kohno K, et al. The essential functions of adipo-osteogenic progenitors as the hematopoietic stem and progenitor cell niche. *Immunity*. 2010 Sep;33(3):387–99.
- [96] Gordon MY. Extracellular matrix of the marrow microenvironment. *British journal of haematology*. 1988 Sep;70(1):1–4.
- [97] Oguri K, Okayama E, Caterson B, Okayama M. Isolation, characterization, and localization of glycosaminoglycans in rabbit bone marrow. *Blood*. 1987 Aug;70(2):501–10.

-
- [98] Klein G, Müller CA, Tillet E, Chu ML, Timpl R. Collagen type VI in the human bone marrow microenvironment: a strong cytoadhesive component. *Blood*. 1995 Sep;86(5):1740–8.
- [99] Klein G, Beck S, Müller CA. Tenascin is a cytoadhesive extracellular matrix component of the human hematopoietic microenvironment. *J Cell Biol*. 1993 Nov;123(4):1027–35.
- [100] Long MW, Dixit VM. Thrombospondin functions as a cytoadhesion molecule for human hematopoietic progenitor cells. *Blood*. 1990 Jun;75(12):2311–8.
- [101] Dexter TM, Allen TD, Lajtha LG. Conditions controlling the proliferation of haemopoietic stem cells in vitro. *Journal of cellular physiology*. 1977 Jun;91(3):335–44.
- [102] Zuckerman KS, Wicha MS. Extracellular matrix production by the adherent cells of long-term murine bone marrow cultures. *Blood*. 1983 Mar;61(3):540–7.
- [103] Schofield KP, Gallagher JT, David G. Expression of proteoglycan core proteins in human bone marrow stroma. *Biochem J*. 1999 Nov;343 Pt 3:663–8.
- [104] Gupta P, McCarthy JB, Verfaillie CM. Stromal fibroblast heparan sulfate is required for cytokine-mediated ex vivo maintenance of human long-term culture-initiating cells. *Blood*. 1996 Apr;87(8):3229–36.
- [105] Wight TN, Kinsella MG, Keating A, Singer JW. Proteoglycans in human long-term bone marrow cultures: biochemical and ultrastructural analyses. *Blood*. 1986 May;67(5):1333–43.
- [106] Sadovnikova E, Deryugina E, Drize N, Chertkov J. Induction of hematopoietic microenvironment by the extracellular matrix from long-term bone marrow cultures. *Annals of hematology*. 1991;62(5):160–164.
- [107] Sorrentino BP. Clinical strategies for expansion of haematopoietic stem cells. *Nature Reviews Immunology*. 2004 Nov;4(11):878–88.
- [108] Liu SQ, Tay R, Khan M, Ee PLR, Hedrick JL, Yang YY. Synthetic hydrogels for controlled stem cell differentiation. *Soft Matter*. 2009;6(1):67–81.
- [109] Fratzl P, Barth FG. Biomaterial systems for mechanosensing and actuation. *Nature*. 2009 Nov;462(7272):442–8.
- [110] Irvine DJ, Hue KA, Mayes AM, Griffith LG. Simulations of cell-surface integrin binding to nanoscale-clustered adhesion ligands. *Biophys J*. 2002 Jan;82(1 Pt 1):120–32.
- [111] Suzuki T, Yokoyama Y, Kumano K, Takanashi M, Kozuma S, Takato T, et al. Highly efficient ex vivo expansion of human hematopoietic stem cells using Delta1-Fc chimeric protein. *Stem Cells*. 2006 Nov;24(11):2456–65.
- [112] Kertész Z, Vas V, Kiss J, Urbán VS, Pozsonyi E, Kozma A, et al. In vitro expansion of long-term repopulating hematopoietic stem cells in the presence of immobilized Jagged-1 and early acting cytokines. *Cell Biol Int*. 2006 May;30(5):401–5.
- [113] Franke K, Pompe T, Bornhäuser M, Werner C. Engineered matrix coatings to modulate the adhesion of CD133+ human hematopoietic progenitor cells. *Biomaterials*. 2007 Feb;28(5):836–43.

- [114] Oswald J, Steudel C, Salchert K, Joergensen B, Thiede C, Ehninger G, et al. Gene-expression profiling of CD34+ hematopoietic cells expanded in a collagen I matrix. *Stem Cells*. 2006 Mar;24(3):494–500.
- [115] Edlund U, Dänmark S, Albertsson AC. A strategy for the covalent functionalization of resorbable polymers with heparin and osteoinductive growth factor. *Biomacromolecules*. 2008 Mar;9(3):901–5.
- [116] Benoit DSW, Durney AR, Anseth KS. The effect of heparin-functionalized PEG hydrogels on three-dimensional human mesenchymal stem cell osteogenic differentiation. *Biomaterials*. 2007 Jan;28(1):66–77.
- [117] Engler A, Sen S, Sweeney H, Discher D. Matrix elasticity directs stem cell lineage specification. *Cell*. 2006;126(4):677–689.
- [118] McBeath R, Pirone DM, Nelson CM, Bhadriraju K, Chen CS. Cell shape, cytoskeletal tension, and RhoA regulate stem cell lineage commitment. *Dev Cell*. 2004 Apr;6(4):483–95.
- [119] Chua KN, Chai C, Lee PC, Ramakrishna S, Leong KW, Mao HQ. Functional nanofiber scaffolds with different spacers modulate adhesion and expansion of cryopreserved umbilical cord blood hematopoietic stem/progenitor cells. *Exp Hematol*. 2007 May;35(5):771–81.
- [120] Anderson DG, Levenberg S, Langer R. Nanoliter-scale synthesis of arrayed biomaterials and application to human embryonic stem cells. *Nat Biotechnol*. 2004 Jul;22(7):863–6.
- [121] Jongpaiboonkit L, King WJ, Murphy WL. Screening for 3D environments that support human mesenchymal stem cell viability using hydrogel arrays. *Tissue Engineering Part A*. 2009 Feb;15(2):343–53.
- [122] Anderson SB, Lin CC, Kuntzler DV, Anseth KS. The performance of human mesenchymal stem cells encapsulated in cell-degradable polymer-peptide hydrogels. *Biomaterials*. 2011 May;32(14):3564–74.
- [123] Liu SQ, Tian Q, Wang L, Hedrick JL, Hui JHP, Yang YY, et al. Injectable Biodegradable Poly(ethylene glycol)/RGD Peptide Hybrid Hydrogels for in vitro Chondrogenesis of Human Mesenchymal Stem Cells. *Macromol Rapid Commun*. 2010 Jul;31(13):1148–54.
- [124] Batorsky A, Liao J, Lund AW, Plopper GE, Stegemann JP. Encapsulation of adult human mesenchymal stem cells within collagen-agarose microenvironments. *Biotechnol Bioeng*. 2005 Nov;92(4):492–500.
- [125] Yilgor P, Tuzlakoglu K, Reis RL, Hasirci N, Hasirci V. Incorporation of a sequential BMP-2/BMP-7 delivery system into chitosan-based scaffolds for bone tissue engineering. *Biomaterials*. 2009;30(21):3551–3559.
- [126] Kurth I, Franke K, Pompe T, Bornhäuser M, Werner C. Hematopoietic stem and progenitor cells in adhesive microcavities. *Integr Biol*. 2009 Jun;1(5-6):427–34.
- [127] Nichols JE, Cortiella J, Lee J, Niles JA, Cuddihy M, Wang S, et al. In vitro analog of human bone marrow from 3D scaffolds with biomimetic inverted colloidal crystal geometry. *Biomaterials*. 2009 Feb;30(6):1071–9.

-
- [128] Lee J, Kotov NA. Notch ligand presenting acellular 3D microenvironments for ex vivo human hematopoietic stem-cell culture made by layer-by-layer assembly. *Small*. 2009 May;5(9):1008–13.
- [129] Lund AW, Yener B, Stegemann JP, Plopper GE. The natural and engineered 3D microenvironment as a regulatory cue during stem cell fate determination. *Tissue Eng Part B Rev*. 2009 Sep;15(3):371–80.
- [130] Bissell MJ, Aggeler J. Dynamic reciprocity: how do extracellular matrix and hormones direct gene expression? *Progress in clinical and biological research*. 1987;249:251.
- [131] Sellaro TL, Ranade A, Faulk DM, McCabe GP, Dorko K, Badylak SF, et al. Maintenance of human hepatocyte function in vitro by liver-derived extracellular matrix gels. *Tissue Engineering Part A*. 2010 Mar;16(3):1075–82.
- [132] Cortiella J, Niles J, Cantu A, Brettler A, Pham A, Vargas G, et al. Influence of acellular natural lung matrix on murine embryonic stem cell differentiation and tissue formation. *Tissue Engineering Part A*. 2010;16(8):2565–2580.
- [133] Petersen TH, Calle EA, Zhao L, Lee EJ, Gui L, Raredon MB, et al. Tissue-engineered lungs for in vivo implantation. *Science*. 2010 Jul;329(5991):538–41.
- [134] Badylak SF, Taylor D, Uygun K. Whole-Organ Tissue Engineering: Decellularization and Recellularization of Three-Dimensional Matrix Scaffolds. *Annu Rev Biomed Eng*. 2010 Jul;.
- [135] Ott HC, Matthiesen TS, Goh SK, Black LD, Kren SM, Netoff TI, et al. Perfusion-decellularized matrix: using nature's platform to engineer a bioartificial heart. *Nature Medicine*. 2008 Feb;14(2):213–21.
- [136] Singelyn JM, DeQuach JA, Seif-Naraghi SB, Littlefield RB, Schup-Magoffin PJ, Christman KL. Naturally derived myocardial matrix as an injectable scaffold for cardiac tissue engineering. *Biomaterials*. 2009 Oct;30(29):5409–16.
- [137] Funamoto S, Nam K, Kimura T, Murakoshi A, Hashimoto Y, Niwaya K, et al. The use of high-hydrostatic pressure treatment to decellularize blood vessels. *Biomaterials*. 2010 May;31(13):3590–5.
- [138] Badylak SF, Lantz GC, Coffey A, Geddes LA. Small intestinal submucosa as a large diameter vascular graft in the dog. *J Surg Res*. 1989 Jul;47(1):74–80.
- [139] Jungebluth P, Go T, Asnaghi A, Bellini S, Martorell J, Calore C, et al. Structural and morphologic evaluation of a novel detergent-enzymatic tissue-engineered tracheal tubular matrix. *J Thorac Cardiovasc Surg*. 2009 Sep;138(3):586–93; discussion 592–3.
- [140] Wainwright D, Madden M, Luterman A, Hunt J, Monafó W, Heimbach D, et al. Clinical evaluation of an acellular allograft dermal matrix in full-thickness burns. *J Burn Care Rehabil*. 1996 Jan;17(2):124–36.
- [141] Hudson TW, Liu SY, Schmidt CE. Engineering an improved acellular nerve graft via optimized chemical processing. *Tissue Engineering*. 2004 Jan;10(9-10):1346–58.
- [142] Hashimoto Y, Funamoto S, Sasaki S, Honda T, Hattori S, Nam K, et al. Preparation and characterization of decellularized cornea using high-hydrostatic pressurization for corneal tissue engineering. *Biomaterials*. 2010 May;31(14):3941–8.

- [143] Ozeki M, Narita Y, Kagami H, Ohmiya N, Itoh A, Hirooka Y, et al. Evaluation of decellularized esophagus as a scaffold for cultured esophageal epithelial cells. *J Biomed Mater Res*. 2006 Dec;79(4):771–8.
- [144] Uygun BE, Soto-Gutierrez A, Yagi H, Izamis ML, Guzzardi MA, Shulman C, et al. Organ reengineering through development of a transplantable recellularized liver graft using decellularized liver matrix. *Nature Medicine*. 2010 Jul;16(7):814–20.
- [145] Nakayama KH, Batchelder CA, Lee CI, Tarantal AF. Decellularized rhesus monkey kidney as a three-dimensional scaffold for renal tissue engineering. *Tissue Engineering Part A*. 2010 Jul;16(7):2207–16.
- [146] Yang B, Zhang Y, Zhou L, Sun Z, Zheng J, Chen Y, et al. Development of a porcine bladder acellular matrix with well-preserved extracellular bioactive factors for tissue engineering. *Tissue Eng Part C Methods*. 2010 Oct;16(5):1201–11.
- [147] Stapleton TW, Ingram J, Katta J, Knight R, Korossis S, Fisher J, et al. Development and characterization of an acellular porcine medial meniscus for use in tissue engineering. *Tissue Engineering Part A*. 2008 Apr;14(4):505–18.
- [148] Woods T, Gratzer PF. Effectiveness of three extraction techniques in the development of a decellularized bone-anterior cruciate ligament-bone graft. *Biomaterials*. 2005 Dec;26(35):7339–49.
- [149] Flynn LE. The use of decellularized adipose tissue to provide an inductive microenvironment for the adipogenic differentiation of human adipose-derived stem cells. *Biomaterials*. 2010 Jun;31(17):4715–24.
- [150] Trelford JD, Trelford-Sauder M. The amnion in surgery, past and present. *Am J Obstet Gynecol*. 1979 Aug;134(7):833–45.
- [151] Zhang Y, He Y, Bharadwaj S, Hammam N, Carnagey K, Myers R, et al. Tissue-specific extracellular matrix coatings for the promotion of cell proliferation and maintenance of cell phenotype. *Biomaterials*. 2009 Aug;30(23-24):4021–8.
- [152] Gilbert TW, Sellaro TL, Badylak SF. Decellularization of tissues and organs. *Biomaterials*. 2006 Jul;27(19):3675–83.
- [153] Gilbert TW, Freund JM, Badylak SF. Quantification of DNA in biologic scaffold materials. *J Surg Res*. 2009 Mar;152(1):135–9.
- [154] Hoshiba T, Cho CS, Murakawa A, Okahata Y, Akaike T. The effect of natural extracellular matrix deposited on synthetic polymers on cultured primary hepatocytes. *Biomaterials*. 2006 Sep;27(26):4519–28.
- [155] Beacham DA, Amatangelo MD, Cukierman E. Preparation of extracellular matrices produced by cultured and primary fibroblasts. *Curr Protoc Cell Biol*. 2007 Jan;Chapter 10:Unit 10.9.
- [156] Hedman K, Kurkinen M, Alitalo K, Vaheri A, Johansson S, Höök M. Isolation of the pericellular matrix of human fibroblast cultures. *J Cell Biol*. 1979 Apr;81(1):83–91.
- [157] Furuyama A, Mochitate K. Assembly of the exogenous extracellular matrix during basement membrane formation by alveolar epithelial cells in vitro. *J Cell Sci*. 2000 Mar;113 (Pt 5):859–68.

-
- [158] Hosokawa T, Betsuyaku T, Nishimura M, Furuyama A, Katagiri K, Mochitate K. Differentiation of tracheal basal cells to ciliated cells and tissue reconstruction on the synthesized basement membrane substratum in vitro. *Connect Tissue Res.* 2007 Jan;48(1):9–18.
- [159] Hoshiba T, Mochitate K, Akaike T. Hepatocytes maintain their function on basement membrane formed by epithelial cells. *Biochemical and biophysical research communications.* 2007;359(1):151–156.
- [160] Cukierman E, Pankov R, Stevens DR, Yamada KM. Taking cell-matrix adhesions to the third dimension. *Science.* 2001 Nov;294(5547):1708–12.
- [161] Cukierman E, Pankov R, Yamada KM. Cell interactions with three-dimensional matrices. *Curr Opin Cell Biol.* 2002;14(5):633–640.
- [162] Higuchi Y, Shiraki N, Yamane K, Qin Z, Mochitate K, Araki K, et al. Synthesized basement membranes direct the differentiation of mouse embryonic stem cells into pancreatic lineages. *J Cell Sci.* 2010 Aug;123(Pt 16):2733–42.
- [163] Pham MT, Reuther H, Maitz MF. Native extracellular matrix coating on Ti surfaces. *J Biomed Mater Res.* 2003;66(2):310–316.
- [164] Hoshiba T, Kawazoe N, Tateishi T, Chen G. Development of extracellular matrices mimicking stepwise adipogenesis of mesenchymal stem cells. *Adv Mater Weinheim.* 2010 Jul;22(28):3042–7.
- [165] Hoshiba T, Kawazoe N, Tateishi T, Chen G. Development of stepwise osteogenesis-mimicking matrices for the regulation of mesenchymal stem cell functions. *J Biol Chem.* 2009 Nov;284(45):31164–73.
- [166] Amatangelo MD, Bassi DE, Klein-Szanto AJP, Cukierman E. Stroma-derived three-dimensional matrices are necessary and sufficient to promote desmoplastic differentiation of normal fibroblasts. *American Journal of Pathology.* 2005;167(2):475.
- [167] Castelló-Cros R, Cukierman E. Stromagenesis during tumorigenesis: characterization of tumor-associated fibroblasts and stroma-derived 3D matrices. *Methods Mol Biol.* 2009 Jan;522:275–305.
- [168] Pompe T, Zschoche S, Herold N, Salchert K, Gouzy MF, Sperling C, et al. Maleic anhydride copolymers—a versatile platform for molecular biosurface engineering. *Biomacromolecules.* 2003 Jan;4(4):1072–9.
- [169] Salchert K, Pompe T, Sperling C, Werner C. Quantitative analysis of immobilized proteins and protein mixtures by amino acid analysis. *J Chromatogr A.* 2003 Jul;1005(1-2):113–22.
- [170] Salchert K, Streller U, Pompe T, Herold N, Grimmer M, Werner C. In vitro reconstitution of fibrillar collagen type I assemblies at reactive polymer surfaces. *Biomacromolecules.* 2004 Jan;5(4):1340–50.
- [171] Salchert K, Oswald J, Streller U, Grimmer M, Herold N, Werner C. Fibrillar collagen assembled in the presence of glycosaminoglycans to constitute bioartificial stem cell niches in vitro. *J Mater Sci Mater Med.* 2005 Jun;16(6):581–5.

- [172] Lanfer B, Freudenberg U, Zimmermann R, Stamov D, Körber V, Werner C. Aligned fibrillar collagen matrices obtained by shear flow deposition. *Biomaterials*. 2008 Oct;29(28):3888–95.
- [173] Lanfer B, Seib FP, Freudenberg U, Stamov D, Bley T, Bornhäuser M, et al. The growth and differentiation of mesenchymal stem and progenitor cells cultured on aligned collagen matrices. *Biomaterials*. 2009 Oct;30(30):5950–8.
- [174] Kleinman HK, McGarvey ML, Liotta LA, Robey PG, Tryggvason K, Martin GR. Isolation and characterization of type IV procollagen, laminin, and heparan sulfate proteoglycan from the EHS sarcoma. *Biochemistry*. 1982 Nov;21(24):6188–93.
- [175] Reichert JC, Quent VMC, Burke LJ, Stansfield SH, Clements JA, Hutmacher DW. Mineralized human primary osteoblast matrices as a model system to analyse interactions of prostate cancer cells with the bone microenvironment. *Biomaterials*. 2010 Nov;31(31):7928–36.
- [176] Oswald J, Boxberger S, Jørgensen B, Feldmann S, Ehninger G, Bornhäuser M, et al. Mesenchymal stem cells can be differentiated into endothelial cells in vitro. *Stem Cells*. 2004 Jan;22(3):377–84.
- [177] Majumdar MK, Thiede MA, Mosca JD, Moorman M, Gerson SL. Phenotypic and functional comparison of cultures of marrow-derived mesenchymal stem cells (MSCs) and stromal cells. *Journal of cellular physiology*. 1998 Jul;176(1):57–66.
- [178] Pittenger MF, Mackay AM, Beck SC, Jaiswal RK, Douglas R, Mosca JD, et al. Multilineage potential of adult human mesenchymal stem cells. *Science*. 1999 Apr;284(5411):143–7.
- [179] Phinney DG. Building a consensus regarding the nature and origin of mesenchymal stem cells. *J Cell Biochem Suppl*. 2002 Jan;38:7–12.
- [180] Baxter MA, Wynn RF, Jowitt SN, Wraith JE, Fairbairn LJ, Bellantuono I. Study of telomere length reveals rapid aging of human marrow stromal cells following in vitro expansion. *Stem Cells*. 2004 Jan;22(5):675–82.
- [181] Pittenger M, Mbalaviele G, Black M, Mosca J, Marshak D. Mesenchymal stem cells. *Human Cell Culture*, Kluwer Academic Publishers. 2002;Volume V: Primary Mesenchymal Cells:189–207.
- [182] Sen A, Lea-Currie YR, Sujkowska D, Franklin DM, Wilkison WO, Halvorsen YD, et al. Adipogenic potential of human adipose derived stromal cells from multiple donors is heterogeneous. *J Cell Biochem*. 2001 Mar;81(2):312–9.
- [183] Laemmli UK. Cleavage of structural proteins during the assembly of the head of bacteriophage T4. *Nature*. 1970 Aug;227(5259):680–5.
- [184] Ruggeri A, Dell’Orbo C, Quacci D. Electron microscopic visualization of proteoglycans with ruthenium red. *The Histochemical Journal*. 1977;9(2):249–252.
- [185] Krieg M, Arboleda-Estudillo Y, Puech PH, Käfer J, Graner F, Müller DJ, et al. Tensile forces govern germ-layer organization in zebrafish. *Nat Cell Biol*. 2008 Apr;10(4):429–36.
- [186] Weiss L. Haemopoiesis in mammalian bone marrow. 1981;.

- [187] Lüllmann-Rauch R. Taschenlehrbuch Histologie. Thieme. 2006 Jan;p. 637.
- [188] Starborg T, Lu Y, Meadows RS, Kadler KE, Holmes DF. Electron microscopy in cell-matrix research. *Methods*. 2008 May;45(1):53–64.
- [189] Campbell AD, Wicha MS. Extracellular matrix and the hematopoietic microenvironment. *J Lab Clin Med*. 1988 Aug;112(2):140–6.
- [190] Nilsson SK, Debatis ME, Dooner MS, Madri JA, Quesenberry PJ, Becker PS. Immunofluorescence characterization of key extracellular matrix proteins in murine bone marrow in situ. *J Histochem Cytochem*. 1998 Mar;46(3):371–7.
- [191] Pompe T, Markowski M, Werner C. Modulated fibronectin anchorage at polymer substrates controls angiogenesis. *Tissue Engineering*. 2004;10(5-6):841–848.
- [192] Myllyla R, Majamaa K, Günzler V, Hanauske-Abel H, Kivirikko K. Ascorbate is consumed stoichiometrically in the uncoupled reactions catalyzed by prolyl 4-hydroxylase and lysyl hydroxylase. *Journal of Biological Chemistry*. 1984;259(9):5403.
- [193] Sharma S, Poddar R, Sen P, Andrews J. Effect of vitamin C on collagen biosynthesis and degree of birefringence in polarization sensitive optical coherence tomography. *African Journal of Biotechnology*. 2010;7(12).
- [194] Katz BZ, Zamir E, Bershadsky A, Kam Z, Yamada KM, Geiger B. Physical state of the extracellular matrix regulates the structure and molecular composition of cell-matrix adhesions. *Mol Biol Cell*. 2000 Mar;11(3):1047–60.
- [195] Grinnell F, Ho CH, Tamariz E, Lee DJ, Skuta G. Dendritic fibroblasts in three-dimensional collagen matrices. *Mol Biol Cell*. 2003 Feb;14(2):384–95.
- [196] Arnold M, Cavalcanti-Adam EA, Glass R, Blümmel J, Eck W, Kantelehner M, et al. Activation of integrin function by nanopatterned adhesive interfaces. *ChemPhysChem*. 2004 Mar;5(3):383–8.
- [197] Zimmermann B, Wachtel HC, Noppe C. Patterns of mineralization in vitro. *Cell Tissue Res*. 1991 Mar;263(3):483–93.
- [198] Paszek MJ, Zahir N, Johnson KR, Lakins JN, Rozenberg GI, Gefen A, et al. Tensional homeostasis and the malignant phenotype. *Cancer Cell*. 2005 Sep;8(3):241–54.
- [199] Discher DE, Janmey P, Wang YL. Tissue cells feel and respond to the stiffness of their substrate. *Science*. 2005 Nov;310(5751):1139–43.
- [200] Castillo AB, Jacobs CR. Mesenchymal stem cell mechanobiology. *Curr Osteoporos Rep*. 2010 Jun;8(2):98–104.
- [201] Gupta P, Oegema TR, Brazil JJ, Dudek AZ, Slungaard A, Verfaillie CM. Structurally specific heparan sulfates support primitive human hematopoiesis by formation of a multimolecular stem cell niche. *Blood*. 1998 Dec;92(12):4641–51.
- [202] Madhally S, Flake A, Matthew H. Maintenance of CD34 expression during proliferation of CD34+ cord blood cells on glycosaminoglycan surfaces. *Stem Cells*. 1999;17(5):295–305.

- [203] Hackney JA, Charbord P, Brunk BP, Stoeckert CJ, Lemischka IR, Moore KA. A molecular profile of a hematopoietic stem cell niche. *Proceedings of the National Academy of Sciences of the United States of America*. 2002 Oct;99(20):13061–6.
- [204] Charbord P, Moore K. Gene expression in stem cell-supporting stromal cell lines. *Annals of the New York Academy of Sciences*. 2005 Jun;1044:159–67.
- [205] Ren J, Jin P, Sabatino M, Balakumaran A, Feng J, Kuznetsov SA, et al. Global transcriptome analysis of human bone marrow stromal cells (BMSC) reveals proliferative, mobile and interactive cells that produce abundant extracellular matrix proteins, some of which may affect BMSC potency. *Cytotherapy*. 2011 Jul;13(6):661–74.
- [206] Markov V, Kusumi K, Tadesse MG, William DA, Hall DM, Lounev V, et al. Identification of cord blood-derived mesenchymal stem/stromal cell populations with distinct growth kinetics, differentiation potentials, and gene expression profiles. *Stem Cells and Development*. 2007 Feb;16(1):53–73.
- [207] Jeong JA, Hong SH, Gang EJ, Ahn C, Hwang SH, Yang IH, et al. Differential gene expression profiling of human umbilical cord blood-derived mesenchymal stem cells by DNA microarray. *Stem Cells*. 2005 Apr;23(4):584–93.
- [208] Giancotti FG, Comoglio PM, Tarone G. Fibronectin-plasma membrane interaction in the adhesion of hemopoietic cells. *J Cell Biol*. 1986 Aug;103(2):429–37.
- [209] Williams DA, Rios M, Stephens C, Patel VP. Fibronectin and VLA-4 in haematopoietic stem cell-microenvironment interactions. *Nature*. 1991 Aug;352(6334):438–41.
- [210] Balbona K, Tran H, Godyna S, Ingham KC, Strickland DK, Argraves WS. Fibulin binds to itself and to the carboxyl-terminal heparin-binding region of fibronectin. *J Biol Chem*. 1992 Oct;267(28):20120–5.
- [211] Gu YC, Nilsson K, Eng H, Eklom M. Association of extracellular matrix proteins fibulin-1 and fibulin-2 with fibronectin in bone marrow stroma. *British journal of haematology*. 2000 May;109(2):305–13.
- [212] Adams JC, Lawler J. The thrombospondins. *The International Journal of Biochemistry & Cell Biology*. 2004 Jun;36(6):961–8.
- [213] Qian X, Wang TN, Rothman VL, Nicosia RF, Tuszynski GP. Thrombospondin-1 modulates angiogenesis in vitro by up-regulation of matrix metalloproteinase-9 in endothelial cells. *Exp Cell Res*. 1997 Sep;235(2):403–12.
- [214] Lawler J. The functions of thrombospondin-1 and-2. *Curr Opin Cell Biol*. 2000 Oct;12(5):634–40.
- [215] Lawler J, Hynes RO. The structure of human thrombospondin, an adhesive glycoprotein with multiple calcium-binding sites and homologies with several different proteins. *J Cell Biol*. 1986 Nov;103(5):1635–48.
- [216] Emsley J, Knight CG, Farndale RW, Barnes MJ, Liddington RC. Structural basis of collagen recognition by integrin $\alpha 2\beta 1$. *Cell*. 2000 Mar;101(1):47–56.
- [217] Zuckerman KS, Rhodes RK, Goodrum DD, Patel VR, Sparks B, Wells J, et al. Inhibition of collagen deposition in the extracellular matrix prevents the establishment of a stroma supportive of hematopoiesis in long-term murine bone marrow cultures. *J Clin Invest*. 1985 Mar;75(3):970–5.

-
- [218] Tsai KS, Kao SY, Wang CY, Wang YJ, Wang JP, Hung SC. Type I collagen promotes proliferation and osteogenesis of human mesenchymal stem cells via activation of ERK and Akt pathways. *J Biomed Mater Res*. 2010 Sep;94(3):673–82.
- [219] Boutboul S, Black GCM, Moore JE, Sinton J, Menasche M, Munier FL, et al. A subset of patients with epithelial basement membrane corneal dystrophy have mutations in TGFBI/BIGH3. *Hum Mutat*. 2006 Jun;27(6):553–7.
- [220] Reinboth B, Thomas J, Hanssen E, Gibson MA. Beta ig-h3 interacts directly with biglycan and decorin, promotes collagen VI aggregation, and participates in ternary complexing with these macromolecules. *J Biol Chem*. 2006 Mar;281(12):7816–24.
- [221] Thapa N, Lee BH, Kim IS. TGFBIp/betaig-h3 protein: a versatile matrix molecule induced by TGF-beta. *The International Journal of Biochemistry & Cell Biology*. 2007 Jan;39(12):2183–94.
- [222] Coutu DL, Wu JH, Monette A, Rivard GE, Blostein MD, Galipeau J. Periostin, a member of a novel family of vitamin K-dependent proteins, is expressed by mesenchymal stromal cells. *J Biol Chem*. 2008 Jun;283(26):17991–8001.
- [223] Kim JE, Kim SJ, Jeong HW, Lee BH, Choi JY, Park RW, et al. RGD peptides released from beta ig-h3, a TGF-beta-induced cell-adhesive molecule, mediate apoptosis. *Oncogene*. 2003 Apr;22(13):2045–53.
- [224] Seiffert M, Beck SC, Schermtzki F, Müller CA, Erickson HP, Klein G. Mitogenic and adhesive effects of tenascin-C on human hematopoietic cells are mediated by various functional domains. *Matrix Biol*. 1998 Apr;17(1):47–63.
- [225] Anstrom KK, Tucker RP. Tenascin-C lines the migratory pathways of avian primordial germ cells and hematopoietic progenitor cells. *Dev Dyn*. 1996 Aug;206(4):437–46.
- [226] Mongiat M, Otto J, Oldershaw R, Ferrer F, Sato JD, Iozzo RV. Fibroblast growth factor-binding protein is a novel partner for perlecan protein core. *J Biol Chem*. 2001 Mar;276(13):10263–71.
- [227] Tu H, Sasaki T, Snellman A, Göhring W, Pirilä P, Timpl R, et al. The type XIII collagen ectodomain is a 150-nm rod and capable of binding to fibronectin, nidogen-2, perlecan, and heparin. *J Biol Chem*. 2002 Jun;277(25):23092–9.
- [228] Mongiat M, Fu J, Oldershaw R, Greenhalgh R, Gown AM, Iozzo RV. Perlecan protein core interacts with extracellular matrix protein 1 (ECM1), a glycoprotein involved in bone formation and angiogenesis. *J Biol Chem*. 2003 May;278(19):17491–9.
- [229] Iozzo RV, Cohen IR, Grässel S, Murdoch AD. The biology of perlecan: the multifaceted heparan sulphate proteoglycan of basement membranes and pericellular matrices. *Biochem J*. 1994 Sep;302 (Pt 3):625–39.
- [230] Iozzo RV. Matrix proteoglycans: from molecular design to cellular function. *Annual review of biochemistry*. 1998 Jan;67:609–52.
- [231] Roberts R, Gallagher J, Spooncer E, Allen TD, Bloomfield F, Dexter TM. Heparan sulphate bound growth factors: a mechanism for stromal cell mediated haemopoiesis. *Nature*. 1988 Mar;332(6162):376–8.

- [232] Bruno E, Luikart SD, Long MW, Hoffman R. Marrow-derived heparan sulfate proteoglycan mediates the adhesion of hematopoietic progenitor cells to cytokines. *Exp Hematol*. 1995 Oct;23(11):1212–7.
- [233] Hidalgo-Bastida LA, Cartmell SH. Mesenchymal stem cells, osteoblasts and extracellular matrix proteins: enhancing cell adhesion and differentiation for bone tissue engineering. *Tissue Eng Part B Rev*. 2010 Aug;16(4):405–12.
- [234] Riddle RC, Taylor AF, Genetos DC, Donahue HJ. MAP kinase and calcium signaling mediate fluid flow-induced human mesenchymal stem cell proliferation. *Am J Physiol, Cell Physiol*. 2006 Mar;290(3):C776–84.
- [235] Klein EA, Yin L, Kothapalli D, Castagnino P, Byfield FJ, Xu T, et al. Cell-cycle control by physiological matrix elasticity and in vivo tissue stiffening. *Curr Biol*. 2009 Sep;19(18):1511–8.
- [236] Lindner U, Kramer J, Behrends J, Driller B, Wendler NO, Boehrnsen F, et al. Improved proliferation and differentiation capacity of human mesenchymal stromal cells cultured with basement-membrane extracellular matrix proteins. *Cytherapy*. 2010 Dec;12(8):992–1005.
- [237] Seib FP, Müller K, Franke M, Grimmer M, Bornhäuser M, Werner C. Engineered extracellular matrices modulate the expression profile and feeder properties of bone marrow-derived human multipotent mesenchymal stromal cells. *Tissue Engineering Part A*. 2009 Oct;15(10):3161–71.
- [238] Seib FP, Prewitz M, Werner C, Bornhäuser M. Matrix elasticity regulates the secretory profile of human bone marrow-derived multipotent mesenchymal stromal cells (MSCs). *Biochemical and Biophysical Research Communications*. 2009 Nov;389(4):663–7.
- [239] Rosenkilde MM, Schwartz TW. The chemokine system – a major regulator of angiogenesis in health and disease. *APMIS*. 2004 Jan;112(7-8):481–95.
- [240] Alford AI, Terkhorn SP, Reddy AB, Hankenson KD. Thrombospondin-2 regulates matrix mineralization in MC3T3-E1 pre-osteoblasts. *Bone*. 2010 Feb;46(2):464–71.
- [241] Reilly GC, Engler AJ. Intrinsic extracellular matrix properties regulate stem cell differentiation. *Journal of Biomechanics*. 2010 Jan;43(1):55–62.
- [242] Gregory CA, Ylostalo J, Prockop DJ. Adult bone marrow stem/progenitor cells (MSCs) are preconditioned by microenvironmental "niches" in culture: a two-stage hypothesis for regulation of MSC fate. *Science's STKE*. 2005 Jul;2005(294):pe37.
- [243] Chen XD. Extracellular matrix provides an optimal niche for the maintenance and propagation of mesenchymal stem cells. *Birth Defects Res C Embryo Today*. 2010 Mar;90(1):45–54.
- [244] Chen XD, Dusevich V, Feng JQ, Manolagas SC, Jilka RL. Extracellular matrix made by bone marrow cells facilitates expansion of marrow-derived mesenchymal progenitor cells and prevents their differentiation into osteoblasts. *J Bone Miner Res*. 2007 Dec;22(12):1943–56. References 16 to 20 about ECM in the bone marrow.
- [245] Lai Y, Sun Y, Skinner CM, Son EL, Lu Z, Tuan RS, et al. Reconstitution of marrow-derived extracellular matrix ex vivo: a robust culture system for expanding large-scale

- highly functional human mesenchymal stem cells. *Stem Cells and Development*. 2010 Jul;19(7):1095–107.
- [246] Sun Y, Li W, Lu Z, Chen R, Ling J, Ran Q, et al. Rescuing replication and osteogenesis of aged mesenchymal stem cells by exposure to a young extracellular matrix. *FASEB J*. 2011 Jan;25.
- [247] Jing D, Fonseca AV, Alakel N, Fierro FA, Muller K, Bornhauser M, et al. Hematopoietic stem cells in co-culture with mesenchymal stromal cells—modeling the niche compartments in vitro. *Haematologica*. 2010 Apr;95(4):542–50.
- [248] Mishima S, Nagai A, Abdullah S, Matsuda C, Taketani T, Kumakura S, et al. Effective ex vivo expansion of hematopoietic stem cells using osteoblast-differentiated mesenchymal stem cells is CXCL12 dependent. *Eur J Haematol*. 2010 Jun;84(6):538–46.
- [249] Bhatia M, Bonnet D, Kapp U, Wang JC, Murdoch B, Dick JE. Quantitative analysis reveals expansion of human hematopoietic repopulating cells after short-term ex vivo culture. *J Exp Med*. 1997 Aug;186(4):619–24.
- [250] Conneally E, Cashman J, Petzer A, Eaves C. Expansion in vitro of transplantable human cord blood stem cells demonstrated using a quantitative assay of their lympho-myeloid repopulating activity in nonobese diabetic-scid/scid mice. *Proceedings of the National Academy of Sciences of the United States of America*. 1997 Sep;94(18):9836–41.
- [251] Gammaitoni L, Bruno S, Sanavio F, Gunetti M, Kollet O, Cavalloni G, et al. Ex vivo expansion of human adult stem cells capable of primary and secondary hemopoietic reconstitution. *Experimental Hematology*. 2003 Mar;31(3):261–70.
- [252] Ueda T, Tsuji K, Yoshino H, Ebihara Y, Yagasaki H, Hisakawa H, et al. Expansion of human NOD/SCID-repopulating cells by stem cell factor, Flk2/Flt3 ligand, thrombopoietin, IL-6, and soluble IL-6 receptor. *J Clin Invest*. 2000 Apr;105(7):1013–21.
- [253] Tsuji K, Ueda T, Ebihara Y. Cytokine-mediated expansion of human NOD-SCID-repopulating cells. *Methods Mol Biol*. 2003 Jan;215:387–95.
- [254] Ohishi K, Varnum-Finney B, Bernstein ID. Delta-1 enhances marrow and thymus repopulating ability of human CD34(+)CD38(-) cord blood cells. *J Clin Invest*. 2002 Oct;110(8):1165–74.
- [255] Delaney C, Varnum-Finney B, Aoyama K, Brashem-Stein C, Bernstein ID. Dose-dependent effects of the Notch ligand Delta1 on ex vivo differentiation and in vivo marrow repopulating ability of cord blood cells. *Blood*. 2005 Oct;106(8):2693–9.
- [256] Delaney C, Heimfeld S, Brashem-Stein C, Voorhies H, Manger RL, Bernstein ID. Notch-mediated expansion of human cord blood progenitor cells capable of rapid myeloid reconstitution. *Nature Medicine*. 2010 Feb;16(2):232–6.
- [257] Verfaillie CM. Adhesion receptors as regulators of the hematopoietic process. *Blood*. 1998 Oct;92(8):2609–12.
- [258] Hurley RW, McCarthy JB, Verfaillie CM. Direct adhesion to bone marrow stroma via fibronectin receptors inhibits hematopoietic progenitor proliferation. *J Clin Invest*. 1995 Jul;96(1):511–9.



































































































- [259] Dao MA, Hashino K, Kato I, Nolta JA. Adhesion to fibronectin maintains regenerative capacity during ex vivo culture and transduction of human hematopoietic stem and progenitor cells. *Blood*. 1998 Dec;92(12):4612–21.
- [260] Sagar BMM, Rentala S, Gopal PNV, Sharma S, Mukhopadhyay A. Fibronectin and laminin enhance engraftability of cultured hematopoietic stem cells. *Biochemical and Biophysical Research Communications*. 2006 Dec;350(4):1000–5.
- [261] Driessen RL, Johnston HM, Nilsson SK. Membrane-bound stem cell factor is a key regulator in the initial lodgment of stem cells within the endosteal marrow region. *Exp Hematol*. 2003 Dec;31(12):1284–91.
- [262] Roark EF, Keene DR, Haudenschild CC, Godyna S, Little CD, Argraves WS. The association of human fibulin-1 with elastic fibers: an immunohistological, ultrastructural, and RNA study. *Journal of Histochemistry & Cytochemistry*. 1995;43(4):401.
- [263] Duncan AW, Rattis FM, DiMascio LN, Congdon KL, Pazianos G, Zhao C, et al. Integration of Notch and Wnt signaling in hematopoietic stem cell maintenance. *Nat Immunol*. 2005 Mar;6(3):314–22.
- [264] Fleming HE, Janzen V, Celso CL, Guo J, Leahy KM, Kronenberg HM, et al. Wnt signaling in the niche enforces hematopoietic stem cell quiescence and is necessary to preserve self-renewal in vivo. *Cell Stem Cell*. 2008 Mar;2(3):274–83.
- [265] Lengerke C, Schmitt S, Bowman TV, Jang IH, Maouche-Chretien L, McKinney-Freeman S, et al. BMP and Wnt specify hematopoietic fate by activation of the Cdx-Hox pathway. *Cell Stem Cell*. 2008 Jan;2(1):72–82.
- [266] Holst J, Watson S, Lord MS, Eamegdool SS, Bax DV, Nivison-Smith LB, et al. Substrate elasticity provides mechanical signals for the expansion of hemopoietic stem and progenitor cells. *Nat Biotechnol*. 2010 Oct;28(10):1123–8.
- [267] Hines M, Nielsen L, Cooper-White J. The hematopoietic stem cell niche: what are we trying to replicate? *Journal of Chemical Technology & Biotechnology*. 2008;83(4):421–443.
- [268] Takada T, Katagiri T, Ifuku M, Morimura N, Kobayashi M, Hasegawa K, et al. Sulfated polysaccharides enhance the biological activities of bone morphogenetic proteins. *J Biol Chem*. 2003 Oct;278(44):43229–35.
- [269] Mauney JR, Kaplan DL, Volloch V. Matrix-mediated retention of osteogenic differentiation potential by human adult bone marrow stromal cells during ex vivo expansion. *Biomaterials*. 2004 Jul;25(16):3233–43.
- [270] Sekiya I, Larson BL, Smith JR, Pochampally R, Cui JG, Prockop DJ. Expansion of human adult stem cells from bone marrow stroma: conditions that maximize the yields of early progenitors and evaluate their quality. *Stem Cells*. 2002 Jan;20(6):530–41.
- [271] Brooke G, Cook M, Blair C, Han R, Heazlewood C, Jones B, et al. Therapeutic applications of mesenchymal stromal cells. *Semin Cell Dev Biol*. 2007 Dec;18(6):846–58.
- [272] Bi Y, Stuelten CH, Kilts T, Wadhwa S, Iozzo RV, Robey PG, et al. Extracellular matrix proteoglycans control the fate of bone marrow stromal cells. *J Biol Chem*. 2005 Aug;280(34):30481–9.

- [273] Pei M, He F, Kish V. Expansion on extracellular matrix deposited by human bone marrow stromal cells facilitates stem cell proliferation and tissue-specific lineage potential. *Tissue Engineering Part A*. 2011 Jul;.
- [274] Lau TT, Wang DA. Stromal cell-derived factor-1 (SDF-1): homing factor for engineered regenerative medicine. *Expert Opin Biol Ther*. 2011 Feb;11(2):189–97.
- [275] Abdallah BM, Kassem M. The use of mesenchymal (skeletal) stem cells for treatment of degenerative diseases: current status and future perspectives. *J Cell Physiol*. 2009 Jan;218(1):9–12.
- [276] Blanc KL, Ringdén O. Immunomodulation by mesenchymal stem cells and clinical experience. *J Intern Med*. 2007 Nov;262(5):509–25.




























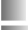






































































Appendix A

Full list of MS-identified proteins



































































































APPENDIX A. FULL LIST OF MS-IDENTIFIED PROTEINS

log (MS2 count) aaECM	log (MS2 count) osteoECM	Protein IDs	MW [kDa]	Descriptions
	0.52		0.90	P62258 29.174 14-3-3 protein epsilon
	0.52		0.45	P27348 27.764 14-3-3 protein theta
	0.92		1.53	P63104 27.745 14-3-3 protein zeta/delta
	0.62		0.00	P17980 49.203 26S protease regulatory subunit 6A
	0.54		0.45	P35998 48.633 26S protease regulatory subunit 7
	0.54		0.65	Q99460 105.84 26S proteasome non-ATPase regulatory subunit 1
	1.06		0.78	O00231 47.463 26S proteasome non-ATPase regulatory subunit 11
	0.54		0.24	Q9UNM6 42.945 26S proteasome non-ATPase regulatory subunit 13
	0.65		0.76	Q13200 100.2 26S proteasome non-ATPase regulatory subunit 2
	0.66		0.63	O43242 60.977 26S proteasome non-ATPase regulatory subunit 3
	0.56		0.45	Q99714 26.923 3-hydroxyacyl-CoA dehydrogenase type-2
	0.00		0.00	P09110 44.292 3-ketoacyl-CoA thiolase, peroxisomal
	0.56		0.54	Q9Y3B7 20.683 39S ribosomal protein L11, mitochondrial
	2.00		1.69	P46783 18.898 40S ribosomal protein S10
	1.43		1.40	P62280 18.431 40S ribosomal protein S11
	1.37		0.48	P25398 14.515 40S ribosomal protein S12
	1.72		1.38	P62277 17.222 40S ribosomal protein S13
	1.40		1.41	P62263 16.273 40S ribosomal protein S14
	0.59		0.30	P62841 17.04 40S ribosomal protein S15
	0.65		0.65	P62244 14.839 40S ribosomal protein S15a
	2.02		1.77	P62249 16.445 40S ribosomal protein S16
	1.71		1.22	P08708 15.55 40S ribosomal protein S17
	1.84		1.64	P62269 17.718 40S ribosomal protein S18
	1.74		1.41	P39019 16.06 40S ribosomal protein S19
	0.70		0.72	P15880 31.324 40S ribosomal protein S2
	0.77		1.11	P60866 13.373 40S ribosomal protein S20
	1.37		0.81	P62266 15.807 40S ribosomal protein S23
	1.01		0.94	P62847 15.423 40S ribosomal protein S24
	1.47		1.55	P62851 13.742 40S ribosomal protein S25
	1.09		0.85	P62854 13.015 40S ribosomal protein S26
	0.65		0.45	P42677 9.461 40S ribosomal protein S27
	0.85		0.15	P62273 6.6767 40S ribosomal protein S29
	2.15		1.92	P23396 26.688 40S ribosomal protein S3
	1.71		1.54	P61247 29.945 40S ribosomal protein S3a
	2.06		1.89	P62701 29.597 40S ribosomal protein S4, X isoform
	1.37		1.15	P46782 22.876 40S ribosomal protein S5
	2.09		1.69	P62081 22.127 40S ribosomal protein S7
	0.63		0.74	P62241 24.205 40S ribosomal protein S8
	0.70		1.09	P08865 32.854 40S ribosomal protein SA
	1.54		1.91	P21589 63.367 5-nucleotidase
	0.88		0.81	Q01813 85.595 6-phosphofructokinase type C
	0.59		0.78	P52209 53.139 6-phosphogluconate dehydrogenase, decarboxylating
	1.34		1.63	P10809 61.054 60 kDa heat shock protein, mitochondrial
	0.99		1.39	P05388 34.273 60S acidic ribosomal protein P0
	0.39		0.63	P05387 11.665 60S acidic ribosomal protein P2
	0.63		0.69	P27635 24.604 60S ribosomal protein L10
	0.52		0.86	P62906 24.831 60S ribosomal protein L10a
	1.10		1.07	P62913 20.252 60S ribosomal protein L11
	1.08		1.11	P30050 17.818 60S ribosomal protein L12



































































































APPENDIX A. FULL LIST OF MS-IDENTIFIED PROTEINS

log (MS2 count) aaECM	log (MS2 count) osteoECM	Protein IDs	MW [kDa]	Descriptions
	0.69		0.39	P26373 24.261 60S ribosomal protein L13
	0.42		0.48	P40429 23.577 60S ribosomal protein L13a
	0.87		0.48	P50914 23.432 60S ribosomal protein L14
	0.70		0.87	P18621 21.397 60S ribosomal protein L17
	0.48		0.24	Q07020 21.634 60S ribosomal protein L18
	0.35		0.24	Q02543 20.762 60S ribosomal protein L18a
	0.77		0.80	P46778 18.565 60S ribosomal protein L21
	1.43		1.26	P35268 14.787 60S ribosomal protein L22
	0.87		0.96	P62829 14.865 60S ribosomal protein L23
	1.26		1.03	P62750 17.695 60S ribosomal protein L23a
	0.85		1.21	P83731 17.779 60S ribosomal protein L24
	0.60		0.78	P61353 15.798 60S ribosomal protein L27
	0.54		0.72	P46776 16.561 60S ribosomal protein L27a
	0.71		0.65	P39023 46.108 60S ribosomal protein L3
	0.96		0.76	P62888 12.784 60S ribosomal protein L30
	1.25		0.98	P62899 14.463 60S ribosomal protein L31
	0.24		0.30	P18077 12.538 60S ribosomal protein L35a
	1.94		1.48	P63173 8.2178 60S ribosomal protein L38
	0.70		0.15	Q02878 32.728 60S ribosomal protein L6
	0.69		0.50	P18124 29.225 60S ribosomal protein L7
	0.85		0.60	P62424 29.995 60S ribosomal protein L7a
	0.96		0.78	P62917 28.024 60S ribosomal protein L8
	1.63		1.20	P32969 21.863 60S ribosomal protein L9
	1.81		1.75	P11021 72.332 78 kDa glucose-regulated protein
	0.59		1.09	Q9UHI8 105.36 A disintegrin and metalloproteinase with thrombospondin motifs 1
	0.69		1.30	Q9Y2D5 94.659 A-kinase anchor protein 2
	0.35		0.54	P24752 45.199 Acetyl-CoA acetyltransferase, mitochondrial
	0.56		0.78	Q99798 85.424 Aconitate hydratase, mitochondrial
	0.96		1.44	P61160 44.76 Actin-related protein 2
	0.48		0.90	O15143 40.949 Actin-related protein 2/3 complex subunit 1B
	0.52		1.08	O15144 34.333 Actin-related protein 2/3 complex subunit 2
	0.72		1.21	O15145 20.546 Actin-related protein 2/3 complex subunit 3
	0.63		1.32	P59998 19.667 Actin-related protein 2/3 complex subunit 4
	0.30		0.60	O15511 16.32 Actin-related protein 2/3 complex subunit 5
	0.81		0.54	Q9BPX5 16.941 Actin-related protein 2/3 complex subunit 5-like protein
	1.39		0.84	P61158 47.371 Actin-related protein 3
	2.40		2.30	P62736 42.009 Actin, aortic smooth muscle
	3.82		3.56	P63261 41.792 Actin, cytoplasmic 2
	0.35		0.65	Q9Y305 49.901 Acyl-coenzyme A thioesterase 9, mitochondrial
	0.00		0.45	Q6UY14 116.54 ADAMTS-like protein 4
	0.60		0.54	P07741 19.608 Adenine phosphoribosyltransferase
	0.45		0.78	P23526 47.716 Adenosylhomocysteinase
	0.69		0.45	P00568 21.635 Adenylate kinase isoenzyme 1
	0.42		0.74	Q01518 51.901 Adenyl cyclase-associated protein 1
	1.54		0.63	Q8IUX7 130.93 Adipocyte enhancer-binding protein 1
	0.57		0.93	Q10588 35.724 ADP-ribosyl cyclase 2
	0.72		0.42	P61204 20.601 ADP-ribosylation factor 3
	0.45		0.45	P18085 20.511 ADP-ribosylation factor 4
	0.56		0.92	P05141 32.852 ADP/ATP translocase 2



































































































APPENDIX A. FULL LIST OF MS-IDENTIFIED PROTEINS

log (MS2 count) aaECM	log (MS2 count) osteoECM	Protein IDs	MW [kDa]	Descriptions
		P12236	32.866	ADP/ATP translocase 3
		P43652	69.068	Afamin
		P49588	106.81	Alanyl-tRNA synthetase, cytoplasmic
		P14550	36.573	Alcohol dehydrogenase [NADP+]
		P30837	57.206	Aldehyde dehydrogenase X, mitochondrial
		P05186	57.304	Alkaline phosphatase, tissue-nonspecific isozyme
		P02765	39.324	Alpha-2-HS-glycoprotein
		P01023	163.29	Alpha-2-macroglobulin
		P12814	103.06	Alpha-actinin-1
		O43707	104.85	Alpha-actinin-4
		P35611	80.954	Alpha-adducin
		P04745	57.767	Alpha-amylase 1
		P02511	20.159	Alpha-crystallin B chain
		P06733	47.168	Alpha-enolase
		P02771	68.677	Alpha-fetoprotein
		Q16352	55.39	Alpha-internexin
		Q9NVD7	42.243	Alpha-parvin
		P15144	109.54	Aminopeptidase N
		Q9P0K7	110.04	Ankycorbin
		P04083	38.714	Annexin A1
		P50995	54.389	Annexin A11
		P07355	38.604	Annexin A2
		P08758	35.936	Annexin A5
		P08133	75.872	Annexin A6
		P01008	52.602	Antithrombin-III
		O95782	107.54	AP-2 complex subunit alpha-1
		P63010	104.55	AP-2 complex subunit beta
		O00203	121.32	AP-3 complex subunit beta-1
		O14617	130.16	AP-3 complex subunit delta-1
		Q9Y2T2	46.939	AP-3 complex subunit mu-1
		P04114	515.6	Apolipoprotein B-100
		P02649	36.154	Apolipoprotein E
		P05089	34.735	Arginase-1
		P25705	59.75	ATP synthase subunit alpha, mitochondrial
		P24539	28.908	ATP synthase subunit b, mitochondrial
		P06576	56.559	ATP synthase subunit beta, mitochondrial
		O75947	18.491	ATP synthase subunit d, mitochondrial
		P36542	32.996	ATP synthase subunit gamma, mitochondrial
		P48047	23.277	ATP synthase subunit O, mitochondrial
		Q8NE71	95.925	ATP-binding cassette sub-family F member 1
		P53396	120.84	ATP-citrate synthase
		O76031	69.223	ATP-dependent Clp protease ATP-binding subunit clpX-like, mitochondrial
		Q08211	140.96	ATP-dependent RNA helicase A
		Q92499	82.431	ATP-dependent RNA helicase DDX1
		Q9NVI7	71.368	ATPase family AAA domain-containing protein 3A
		O95816	23.772	BAG family molecular chaperone regulator 2
		O75531	10.058	Barrier-to-autointegration factor
		P98160	468.83	Basement membrane-specific heparan sulfate proteoglycan core protein
		Q13425	57.949	Beta-2-syntrophin



































































































APPENDIX A. FULL LIST OF MS-IDENTIFIED PROTEINS

log (MS2 count) aaECM	log (MS2 count) osteoECM	Protein IDs	MW [kDa]	Descriptions
	2.18		1.90	Q562R1 42.003 Beta-actin-like protein 2
	0.15		0.15	P13929 46.931 Beta-enolase
	1.08		0.69	P31939 64.615 Bifunctional purine biosynthesis protein PURH
	3.02		2.56	P21810 41.654 Biglycan
	0.52		0.15	P53004 33.428 Biliverdin reductase A
	0.98		0.52	Q13867 52.562 Bleomycin hydrolase
	0.63		0.60	P13497 111.25 Bone morphogenetic protein 1
	0.57		0.70	Q96CX2 35.7 BTB/POZ domain-containing protein KCTD12
	0.69		1.01	P11586 101.56 C-1-tetrahydrofolate synthase, cytoplasmic
	0.60		1.36	P55290 78.286 Cadherin-13
	0.63		0.30	O75746 74.761 Calcium-binding mitochondrial carrier protein Aralar1
	0.81		0.72	Q9UJS0 74.175 Calcium-binding mitochondrial carrier protein Aralar2
	2.33		2.30	Q05682 93.249 Caldesmon
	0.00		0.63	P62158 16.837 Calmodulin
	0.30		1.05	Q9NZT1 15.892 Calmodulin-like protein 5
	0.45		0.50	P27824 67.567 Calnexin
	0.67		0.60	P04632 28.315 Calpain small subunit 1
	1.23		1.14	P51911 33.17 Calponin-1
	0.75		0.54	Q99439 33.697 Calponin-2
	1.32		1.31	Q15417 36.413 Calponin-3
	0.69		0.39	P27797 48.141 Calreticulin
	0.89		0.39	P10644 42.981 cAMP-dependent protein kinase type I-alpha regulatory subunit
	0.52		0.30	P16152 30.375 Carbonyl reductase [NADPH] 1
	0.00		0.60	P14384 50.513 Carboxypeptidase M
	0.71		1.18	P35221 100.07 Catenin alpha-1
	0.45		0.54	P35222 85.496 Catenin beta-1
	0.35		0.72	P07339 44.552 Cathepsin D
	1.15		1.36	Q03135 20.471 Caveolin-1
	0.50		0.84	P51636 18.291 Caveolin-2
	1.13		1.88	Q6YHK3 161.69 CD109 antigen
	0.00		0.85	Q13740 65.102 CD166 antigen
	0.35		0.60	P16070 81.537 CD44 antigen
	0.15		0.45	P43121 71.607 Cell surface glycoprotein MUC18
	0.39		0.54	Q9H444 24.95 Charged multivesicular body protein 4b
	1.36		1.35	O00299 26.922 Chloride intracellular channel protein 1 =CLIC1 PE=1 SV=4
	0.72		0.97	Q9Y696 28.772 Chloride intracellular channel protein 4
	0.00		0.15	Q6UVK1 250.53 Chondroitin sulfate proteoglycan 4
	0.45		0.59	O75390 51.712 Citrate synthase, mitochondrial
	1.68		1.94	Q00610 191.61 Clathrin heavy chain 1
	1.32		1.76	P12259 251.7 Coagulation factor V
	0.74		1.11	P00742 54.731 Coagulation factor X
	0.65		1.20	P00488 83.266 Coagulation factor XIII A chain
	0.89		0.93	P53621 138.34 Coatomer subunit alpha
	0.69		0.72	P35606 102.49 Coatomer subunit beta
	0.69		0.78	P53618 107.14 Coatomer subunit beta
	0.78		0.42	Q9Y678 97.717 Coatomer subunit gamma
	1.77		1.38	P23528 18.502 Cofilin-1
	0.15		0.45	Q9Y281 18.736 Cofilin-2
	1.40		1.70	Q76M96 108.17 Coiled-coil domain-containing protein 80




















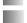














































































APPENDIX A. FULL LIST OF MS-IDENTIFIED PROTEINS

log (MS2 count) aaECM	log (MS2 count) osteoECM	Protein IDs	MW [kDa]	Descriptions
	0.52		0.42	Q9NX63 26.152 Coiled-coil-helix-coiled-coil-helix domain-containing protein 3, mitochondrial
	2.26		2.05	P02452 138.94 Collagen alpha-1(I) chain
	1.11		0.81	P02461 138.56 Collagen alpha-1(III) chain
	1.06		0.99	P02462 160.61 Collagen alpha-1(IV) chain
	1.82		1.54	P20908 183.56 Collagen alpha-1(V) chain
	3.16		2.76	P12109 108.53 Collagen alpha-1(VI) chain
	2.05		2.27	P27658 73.363 Collagen alpha-1(VIII) chain
	1.12		1.91	P12107 181.06 Collagen alpha-1(XI) chain
	3.08		3.22	Q99715 333.14 Collagen alpha-1(XII) chain
	2.74		0.85	Q05707 193.51 Collagen alpha-1(XIV) chain
	1.00		0.48	P39059 141.72 Collagen alpha-1(XV) chain
	0.66		0.99	Q07092 157.75 Collagen alpha-1(XVI) chain
	1.54		1.37	P39060 178.19 Collagen alpha-1(XVIII) chain
	2.33		2.33	P08123 129.31 Collagen alpha-2(I) chain
	1.71		1.70	P08572 167.55 Collagen alpha-2(IV) chain
	1.40		1.33	P05997 144.91 Collagen alpha-2(V) chain
	2.86		2.49	P12110 108.58 Collagen alpha-2(VI) chain
	1.17		0.57	P25940 172.12 Collagen alpha-3(V) chain
	3.52		3.35	P12111 343.67 Collagen alpha-3(VI) chain
	0.39		0.39	Q96CG8 26.224 Collagen triple helix repeat-containing protein 1
	1.12		1.59	P01024 187.15 Complement C3
	0.63		1.40	P0C0L4 192.77 Complement C4-A
	0.00		0.60	P01031 188.3 Complement C5
	0.00		0.30	P02748 63.173 Complement component C9
	0.92		1.24	P29279 38.091 Connective tissue growth factor
	0.24		0.92	Q9NZB2 121.89 Constitutive coactivator of PPAR-gamma-like protein 1
	0.42		0.30	Q99829 59.058 Copine-1
	0.35		0.78	O75131 60.13 Copine-3
	0.00		0.00	Q86YQ8 63.107 Copine-8
	1.49		1.46	O75367 39.617 Core histone macro-H2A.1
	0.15		0.48	Q15517 51.522 Comeodesmosin
	0.68		0.80	Q9BR76 54.234 Coronin-1B
	1.08		0.78	Q9ULV4 53.248 Coronin-1C
	0.62		0.89	Q9UQ03 54.953 Coronin-2B
	0.48		0.78	P12277 42.644 Creatine kinase B-type
	0.52		0.72	P17812 66.69 CTP synthase 1
	1.17		1.24	Q7Z408 380.03 CUB and sushi domain-containing protein 2
	0.77		0.93	Q86VP6 136.37 Cullin-associated NEDD8-dissociated protein 1
	0.15		0.56	P04080 11.139 Cystatin-B
	0.52		0.50	P22695 48.442 Cytochrome b-c1 complex subunit 2, mitochondrial
	0.15		0.69	O75462 46.301 Cytokine receptor-like factor 1
	0.94		1.36	Q14204 532.4 Cytoplasmic dynein 1 heavy chain 1
	1.49		1.07	Q8NCM8 492.62 Cytoplasmic dynein 2 heavy chain 1
	0.42		0.30	Q7L576 145.18 Cytoplasmic FMRI-interacting protein 1
	1.48		1.61	Q07065 66.022 Cytoskeleton-associated protein 4
	0.62		0.93	O00154 41.796 Cytosolic acyl coenzyme A thioester hydrolase
	0.24		0.30	Q69YQ0 124.6 Cytospin-A
	0.92		0.76	O43175 56.65 D-3-phosphoglycerate dehydrogenase
	0.52		0.54	O43293 52.535 Death-associated protein kinase 3






























































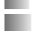




































APPENDIX A. FULL LIST OF MS-IDENTIFIED PROTEINS

log (MS2 count) aaECM	log (MS2 count) osteoECM	Protein IDs	MW [kDa]	Descriptions
		P07585	39.746	Decorin
		P54886	87.301	Delta-1-pyrroline-5-carboxylate synthase
		P81605	11.284	Dermcidin
		Q08554	99.986	Desmocollin-1
		Q02413	113.75	Desmoglein-1
		P15924	331.77	Desmoplakin
		P60981	18.506	Destrin
		P10515	68.996	Dihydrolipoyllysine-residue acetyltransferase component
		P36957	48.755	Dihydrolipoyllysine-residue succinyltransferase component
		Q16555	62.293	Dihydropyrimidinase-related protein 2
		Q5VWQ8	131.62	Disabled homolog 2-interacting protein
		P11387	90.725	DNA topoisomerase 1
		Q02880	183.26	DNA topoisomerase 2-beta
		O75165	254.41	DnaJ homolog subfamily C member 13
		P39656	50.8	Dolichyl-diphosphooligosaccharide--protein glycosyltransferase 48 kDa subunit
		P04843	68.569	Dolichyl-diphosphooligosaccharide--protein glycosyltransferase subunit 1
		P04844	69.283	Dolichyl-diphosphooligosaccharide--protein glycosyltransferase subunit 2
		Q16643	71.428	Drebrin
		Q9UJU6	48.207	Drebrin-like protein
		Q14203	141.69	Dynactin subunit 1
		P50570	98.063	Dynammin-2
		Q03001	860.65	Dystonin
		P11532	426.74	Dystrophin
		Q9UNE7	34.856	E3 ubiquitin-protein ligase CHIP
		O43854	53.764	EGF-like repeat and discoidin I-like domain-containing protein 3
		Q9H4M9	60.626	EH domain-containing protein 1
		Q9NZN4	61.161	EH domain-containing protein 2
		Q9H223	61.174	EH domain-containing protein 4
		P15502	68.468	Elastin
		P13804	35.079	Electron transfer flavoprotein subunit alpha, mitochondrial
		P68104	50.14	Elongation factor 1-alpha 1
		P29692	31.121	Elongation factor 1-delta
		P26641	50.118	Elongation factor 1-gamma
		P13639	95.337	Elongation factor 2
		P49411	49.541	Elongation factor Tu, mitochondrial
		Q9Y6C2	106.67	EMILIN-1
		P17813	70.577	Endoglin
		Q9Y371	40.796	Endophilin-B1
		Q9NR46	43.973	Endophilin-B2
		P14625	92.468	Endoplasmin
		P30084	31.387	Enoyl-CoA hydratase, mitochondrial
		P58107	555.61	Epiplakin
		P23284	23.742	eptidyl-prolyl cis-trans isomerase B
		O75477	38.925	Erlin-1
		O94905	37.839	Erlin-2
		P27105	31.73	Erythrocyte band 7 integral membrane protein
		Q53GQ0	34.324	Estradiol 17-beta-dehydrogenase 12
		P60842	46.153	Eukaryotic initiation factor 4A-I
		P05198	36.112	Eukaryotic translation initiation factor 2 subunit 1



































































































APPENDIX A. FULL LIST OF MS-IDENTIFIED PROTEINS

log (MS2 count) aaECM	log (MS2 count) osteoECM	Protein IDs	MW [kDa]	Descriptions
	0.57		1.76	Q14152 166.57 Eukaryotic translation initiation factor 3 subunit A
	0.52		1.56	P55884 92.48 Eukaryotic translation initiation factor 3 subunit B
	0.65		1.34	Q99613 105.34 Eukaryotic translation initiation factor 3 subunit C
	0.45		1.00	P60228 52.22 Eukaryotic translation initiation factor 3 subunit E
	0.39		0.72	O00303 37.563 Eukaryotic translation initiation factor 3 subunit F
	0.15		0.69	O75821 35.611 Eukaryotic translation initiation factor 3 subunit G
	0.24		1.10	O15372 39.93 Eukaryotic translation initiation factor 3 subunit H
	0.30		0.95	Q13347 36.501 Eukaryotic translation initiation factor 3 subunit I
	0.35		0.95	Q9Y262 66.726 Eukaryotic translation initiation factor 3 subunit L
	0.15		0.54	Q7L2H7 42.502 Eukaryotic translation initiation factor 3 subunit M
	0.78		0.56	P78344 102.36 Eukaryotic translation initiation factor 4 gamma 2
	0.80		0.78	P63241 16.832 Eukaryotic translation initiation factor 5A-1
	0.30		0.72	Q96A65 110.5 Exocyst complex component 4
	0.35		0.99	O00471 81.852 Exocyst complex component 5
	1.63		0.96	P55060 110.42 Exportin-2
	0.62		0.74	Q9BSJ8 122.85 Extended synaptotagmin-1
	1.10		0.80	Q16610 60.673 Extracellular matrix protein 1
	0.84		1.62	Q81WU6 101.03 Extracellular sulfatase Sulf-1
	1.14		1.15	P52907 32.922 F-actin-capping protein subunit alpha-1
	1.29		1.31	P47755 32.949 F-actin-capping protein subunit alpha-2
	0.35		0.80	P47756 31.35 F-actin-capping protein subunit beta
	0.39		1.32	Q9Y5B9 119.91 FACT complex subunit SPT16
	0.39		0.67	Q08945 81.074 FACT complex subunit SSRP1
	1.10		0.59	Q16658 54.529 Fascin
	0.24		0.24	P49327 273.42 Fatty acid synthase
	0.30		0.48	Q01469 15.164 Fatty acid-binding protein, epidermal
	0.39		0.45	Q96AC1 77.86 Fermitin family homolog 2
	0.60		0.15	P02792 20.019 Ferritin light chain
	0.82		0.76	P35555 312.24 Fibrillin-1
	0.00		0.39	P02679 51.511 Fibrinogen gamma chain
	4.09		3.97	P02751 262.62 Fibronectin
	1.84		2.13	P23142 77.213 Fibulin-1
	1.74		1.97	P98095 126.57 Fibulin-2
	0.52		0.69	Q9UBX5 50.18 Fibulin-5
	0.45		0.80	Q5D862 248.07 Filaggrin-2
	3.00		3.01	P21333 280.74 Filamin-A
	1.97		1.79	O75369 278.16 Filamin-B
	1.75		1.53	Q14315 291.02 Filamin-C
	0.90		1.73	O75955 47.355 Flotillin-1
	0.71		1.40	Q14254 47.064 Flotillin-2
	0.78		0.74	Q13642 36.263 Four and a half LIM domains protein 1
	0.92		0.78	Q14192 32.193 Four and a half LIM domains protein 2
	1.42		1.34	P04075 39.42 Fructose-bisphosphate aldolase A
	0.00		0.30	P05062 39.473 Fructose-bisphosphate aldolase B
	0.45		0.39	P07954 54.636 Fumarate hydratase, mitochondrial
	1.79		1.56	P09382 14.716 Galectin-1
	1.15		1.35	P47929 15.075 Galectin-7
	0.59		0.30	Q16666 88.255 Gamma-interferon-inducible protein 16
	2.49		2.30	P06396 85.696 Gelsolin































































































APPENDIX A. FULL LIST OF MS-IDENTIFIED PROTEINS

log (MS2 count) aaECM	log (MS2 count) osteoECM	Protein IDs	MW [kDa]	Descriptions
	0.88		1.62	P78347 112.42 General transcription factor II-I
	0.60		0.24	O60763 107.89 General vesicular transport factor p115
	1.78		1.50	P07093 44.002 Glia-derived nexin
	0.00		0.57	P14314 59.425 Glucosidase 2 subunit beta
	0.63		0.67	O94925 73.46 Glutaminase kidney isoform, mitochondrial
	1.09		1.23	P09211 23.356 Glutathione S-transferase P
	2.48		2.13	P04406 36.053 Glyceraldehyde-3-phosphate dehydrogenase
	0.42		0.35	P43304 80.852 Glycerol-3-phosphate dehydrogenase, mitochondrial
	0.72		1.22	P11216 96.695 Glycogen phosphorylase, brain form
	1.49		1.26	P41250 83.165 Glycyl-tRNA synthetase
	0.65		0.65	O75487 62.411 Glypican-4
	0.15		0.30	Q9H4G4 17.218 Golgi-associated plant pathogenesis-related protein 1
	0.24		0.24	Q9H772 19.32 Gremlin-2
	0.56		2.10	Q14393 79.676 Growth arrest-specific protein 6
	0.97		0.81	Q99988 34.14 Growth/differentiation factor 15
	0.52		0.83	P62826 24.423 GTP-binding nuclear protein Ran
	1.33		1.48	P04899 40.45 Guanine nucleotide-binding protein G(i) subunit alpha-2
	1.09		0.71	P62873 37.377 Guanine nucleotide-binding protein G(I)/G(S)/G(T) subunit beta-1
	0.50		0.81	P63244 35.076 Guanine nucleotide-binding protein subunit beta-2-like 1
	1.01		1.46	P00738 45.205 Haptoglobin
	0.91		1.48	P08107 70.051 Heat shock 70 kDa protein 1A/1B
	0.66		1.13	P34932 94.33 Heat shock 70 kDa protein 4
	0.63		0.57	P17066 71.027 Heat shock 70 kDa protein 6
	2.16		2.15	P11142 70.897 Heat shock cognate 71 kDa protein
	0.39		0.39	Q92598 96.864 Heat shock protein 105 kDa
	1.85		1.92	P04792 22.782 Heat shock protein beta-1
	1.71		1.85	P07900 84.659 Heat shock protein HSP 90-alpha
	2.20		2.03	P08238 83.263 Heat shock protein HSP 90-beta
	2.51		2.53	P69905 15.257 Hemoglobin subunit alpha
	2.10		2.07	P02042 16.055 Hemoglobin subunit delta
	0.52		1.08	P02790 51.676 Hemopexin
	0.30		0.69	P09038 30.77 Heparin-binding growth factor 2
	1.07		0.65	Q5SSJ5 61.206 Heterochromatin protein 1-binding protein 3
	1.09		0.71	P38159 42.331 Heterogeneous nuclear ribonucleoprotein
	0.59		0.30	Q13151 30.84 Heterogeneous nuclear ribonucleoprotein A0
	0.52		0.39	P51991 39.594 Heterogeneous nuclear ribonucleoprotein A3
	1.07		0.95	P52272 77.515 Heterogeneous nuclear ribonucleoprotein M
	0.81		0.65	O60506 69.602 Heterogeneous nuclear ribonucleoprotein Q
	1.45		1.00	O43390 70.942 Heterogeneous nuclear ribonucleoprotein R
	2.41		2.10	Q00839 90.583 Heterogeneous nuclear ribonucleoprotein U
	0.71		1.02	Q1KMD3 85.104 Heterogeneous nuclear ribonucleoprotein U-like protein 2
	1.98		1.68	P07910 33.67 Heterogeneous nuclear ribonucleoproteins C1/C2
	0.94		1.00	P19367 102.48 Hexokinase-1
	0.15		1.16	P09429 24.893 High mobility group protein B1
	1.24		0.88	P16403 21.364 Histone H1.2 =HIST1H1C PE=1 SV=2
	2.54		2.23	P16402 22.35 Histone H1.3
	0.89		0.90	P04908 14.135 Histone H2A type 1-B/E
	1.25		0.63	P0C0S5 13.553 Histone H2A.Z
	2.66		2.10	O60814 13.89 Histone H2B type 1-K Histone H2B type 1-D



































































































APPENDIX A. FULL LIST OF MS-IDENTIFIED PROTEINS

log (MS2 count) aaECM	log (MS2 count) osteoECM	Protein IDs	MW [kDa]	Descriptions
		P68431	15.404	Histone H3.1
		P62805	11.367	Histone H4
		P50502	41.331	Hsc70-interacting protein
		P10915	40.165	Hyaluronan and proteoglycan link protein 1
		Q96S86	40.894	Hyaluronan and proteoglycan link protein 3
		Q9Y4L1	111.33	Hypoxia up-regulated protein 1
		Q14974	97.169	Importin subunit beta-1
		O00410	123.63	Importin-5
		O95373	119.52	Importin-7
		Q70UQ0	39.309	Inhibitor of nuclear factor kappa-B kinase-interacting protein
		P12268	55.804	Inosine-5-monophosphate dehydrogenase 2
		Q9Y6M1	66.121	Insulin-like growth factor 2 mRNA-binding protein 2
		P01344	20.14	Insulin-like growth factor II
		P17936	31.674	Insulin-like growth factor-binding protein 3
		Q9UKX5	133.47	Integrin alpha-11
		P08648	114.54	Integrin alpha-5
		P06756	116.04	Integrin alpha-V
		P05556	88.414	Integrin beta-1
		P18084	88.053	Integrin beta-5
		P19823	106.46	Inter-alpha-trypsin inhibitor heavy chain H2
		Q06033	99.848	Inter-alpha-trypsin inhibitor heavy chain H3
		Q12906	95.337	Interleukin enhancer-binding factor 3
		P50213	39.591	Isocitrate dehydrogenase [NAD] subunit alpha, mitochondrial
		P48735	50.909	Isocitrate dehydrogenase [NADP], mitochondrial
		P41252	144.5	Isoleucyl-tRNA synthetase, cytoplasmic
		Q9NSE4	113.79	Isoleucyl-tRNA synthetase, mitochondrial
		P14923	81.744	Junction plakoglobin
		Q15323	47.237	Keratin, type I cuticular Ha1
		Q14532	50.343	Keratin, type I cuticular Ha2
		Q14525	46.213	Keratin, type I cuticular Ha3-II
		O76011	49.423	Keratin, type I cuticular Ha4
		Q92764	50.36	Keratin, type I cuticular Ha5
		O76013	52.247	Keratin, type I cuticular Ha6
		P13645	58.826	Keratin, type I cytoskeletal 10
		P13646	49.588	Keratin, type I cytoskeletal 13
		P02533	51.561	Keratin, type I cytoskeletal 14
		P08779	51.267	Keratin, type I cytoskeletal 16
		Q04695	48.105	Keratin, type I cytoskeletal 17
		P05783	48.057	Keratin, type I cytoskeletal 18
		P35527	62.064	Keratin, type I cytoskeletal 9
		Q9NSB4	56.652	Keratin, type II cuticular Hb2
		P78386	55.802	Keratin, type II cuticular Hb5
		O43790	53.5	Keratin, type II cuticular Hb6
		P04264	66.038	Keratin, type II cytoskeletal 1
		Q7Z794	61.901	Keratin, type II cytoskeletal 1b
		P35908	65.432	Keratin, type II cytoskeletal 2
		P19013	57.285	Keratin, type II cytoskeletal 4
		P13647	62.378	Keratin, type II cytoskeletal 5
		P02538	60.044	Keratin, type II cytoskeletal 6A






























































































APPENDIX A. FULL LIST OF MS-IDENTIFIED PROTEINS

log (MS2 count) aaECM	log (MS2 count) osteoECM	Protein IDs	MW [kDa]	Descriptions
	1.98		1.85	P04259 60.066 Keratin, type II cytoskeletal 6B
	2.28		1.78	P08729 51.385 Keratin, type II cytoskeletal 7
	0.00		0.42	Q14CN4 55.877 Keratin, type II cytoskeletal 72
	1.07		1.11	O95678 59.56 Keratin, type II cytoskeletal 75
	0.95		0.78	Q8N1N4 56.865 Keratin, type II cytoskeletal 78
	0.95		1.03	Q5T749 64.135 Keratinocyte proline-rich protein
	0.50		0.74	Q86UP2 156.27 Kinectin
	1.33		1.42	P33176 109.68 Kinesin-1 heavy chain
	0.35		1.34	Q63ZY3 91.173 KN motif and ankyrin repeat domain-containing protein 2
	0.50		1.24	P00338 36.688 L-lactate dehydrogenase A chain
	0.24		0.70	P07195 36.638 L-lactate dehydrogenase B chain
	1.29		1.16	P07864 36.311 L-lactate dehydrogenase C chain
	0.78		1.63	Q08431 43.122 Lactadherin
	0.84		1.17	P02788 78.181 Lactotransferrin
	1.05		0.68	P20700 66.408 Lamin-B1
	0.81		0.67	Q03252 67.688 Lamin-B2
	0.35		0.24	Q16363 202.52 Laminin subunit alpha-4
	0.24		0.66	P07942 198.04 Laminin subunit beta-1
	0.00		0.56	P55268 195.98 Laminin subunit beta-2
	0.39		1.17	P11047 177.6 Laminin subunit gamma-1
	0.72		0.45	Q14766 186.79 Latent-transforming growth factor beta-binding protein 1
	0.92		1.38	Q14767 195.05 Latent-transforming growth factor beta-binding protein 2
	0.70		0.45	P29536 67.042 Leiomodulin
	0.42		0.30	O95202 83.353 LETM1 and EF-hand domain-containing protein 1, mitochondrial
	1.29		1.50	Q86V48 120.27 Leucine zipper protein 1
	0.69		0.39	P42704 157.9 Leucine-rich PPR motif-containing protein, mitochondrial
	0.35		0.94	Q8TF66 64.396 Leucine-rich repeat-containing protein 15
	0.60		0.89	Q96AG4 34.93 Leucine-rich repeat-containing protein 59
	0.63		0.57	Q9PJ25 134.46 Leucyl-tRNA synthetase, cytoplasmic
	0.48		1.13	Q9UPQ0 121.87 LIM and calponin homology domains-containing protein 1
	0.30		0.39	P48059 37.251 LIM and senescent cell antigen-like-containing domain protein 1
	0.74		0.76	Q14847 29.717 LIM and SH3 domain protein 1
	2.54		2.36	Q9UHB6 85.225 LIM domain and actin-binding protein 1
	2.25		2.40	Q8WWI1 192.69 LIM domain only protein 7
	0.00		0.65	O14495 35.116 Lipid phosphate phosphohydrolase 3
	0.63		0.57	P36776 106.49 Lon protease homolog, mitochondrial
	1.85		1.10	P51884 38.429 Lumican
	0.30		0.69	P11279 44.882 Lysosome-associated membrane glycoprotein 1
	0.24		0.98	P61626 16.537 Lysozyme C
	1.88		1.58	Q9Y4K0 86.724 Lysyl oxidase homolog 2
	0.35		0.84	P58215 83.166 Lysyl oxidase homolog 3
	0.65		1.16	Q96JB6 84.483 Lysyl oxidase homolog 4
	2.32		2.39	Q14764 99.326 Major vault protein
	1.02		0.72	Q13724 91.916 Mannosyl-oligosaccharide glucosidase
	0.77		1.04	P43243 94.622 Matrin-3
	0.00		0.89	P08493 12.353 Matrix Gla protein
	1.41		0.56	Q9NR99 312.15 Matrix-remodeling-associated protein 5
	0.90		0.24	Q8NEH6 60.571 Meiosis-specific nuclear structural protein 1
	0.24		0.30	O15173 23.818 Membrane-associated progesterone receptor component 2






























































































APPENDIX A. FULL LIST OF MS-IDENTIFIED PROTEINS

log (MS2 count) aaECM	log (MS2 count) osteoECM	Protein IDs	MW [kDa]	Descriptions
	1.45		1.18	P35625 24.145 Metalloproteinase inhibitor 3
	0.45		0.77	O14880 16.516 Microsomal glutathione S-transferase 3
	0.54		1.18	P78559 305.48 Microtubule-associated protein 1A
	0.77		1.46	P46821 270.63 Microtubule-associated protein 1B
	0.80		1.15	P27816 121 Microtubule-associated protein 4
	0.60		0.95	Q9Y6C9 33.331 Mitochondrial carrier homolog 2
	1.82		1.78	Q16891 83.677 Mitochondrial inner membrane protein
	0.56		0.15	P28482 41.389 Mitogen-activated protein kinase 1
	1.66		1.61	P26038 67.819 Moesin
	1.15		0.65	Q6UB35 105.79 Monofunctional C1-tetrahydrofolate synthase, mitochondrial
	1.26		1.47	Q96S97 35.273 Myeloid-associated differentiation marker
	0.68		1.22	Q9NZM1 234.71 Myoferlin
	1.29		1.01	P08590 21.932 Myosin light chain 3
	2.37		1.87	P60660 16.93 Myosin light polypeptide 6
	1.96		2.04	Q6WCQ1 116.53 Myosin phosphatase Rho-interacting protein
	1.23		1.40	P24844 19.827 Myosin regulatory light polypeptide 9
	2.07		2.18	P35580 229 Myosin-10
	1.17		1.60	P35749 227.34 Myosin-11
	2.10		1.96	Q7Z406 228 Myosin-14
	0.30		0.24	P13535 222.76 Myosin-8
	3.78		3.58	P35579 226.53 Myosin-9
	1.74		1.90	O43795 131.98 Myosin-Ib
	2.35		2.48	O00159 121.68 Myosin-Ic
	0.87		1.43	O94832 116.2 Myosin-I d
	0.82		1.26	Q12965 127.06 Myosin-I e
	0.65		0.93	Q9Y4I1 215.4 Myosin-Va
	1.36		2.02	Q9UM54 149.69 Myosin-VI
	0.50		0.72	Q96KG9 89.63 N-terminal kinase-like protein
	0.60		0.71	O75489 30.241 NADH dehydrogenase [ubiquinone] iron-sulfur protein 3, mitochondrial
	0.83		1.26	P00387 34.234 NADH-cytochrome b5 reductase 3
	0.73		1.34	P28331 79.467 NADH-ubiquinone oxidoreductase 75 kDa subunit, mitochondrial
	0.39		0.85	Q13765 23.384 Nascent polypeptide-associated complex subunit alpha
	0.39		0.60	Q9Y2A7 128.79 Nck-associated protein 1
	0.45		1.00	Q8NF91 1011 Nesprin-1
	0.56		0.59	Q6ZMZ3 112.22 Nesprin-3
	0.71		0.77	Q96SB3 89.191 Neurabin-2
	1.96		2.57	Q09666 629.09 Neuroblast differentiation-associated protein AHNAK
	0.00		0.50	Q7Z3B1 38.719 Neuronal growth regulator 1
	0.87		1.22	Q14697 106.87 Neutral alpha-glucosidase AB
	2.14		2.44	Q0ZGT2 80.657 Nexilin
	0.59		0.77	P40261 29.574 Nicotinamide N-methyltransferase
	0.50		1.32	P14543 136.38 Nidogen-1
	1.43		1.98	Q14112 151.25 Nidogen-2
	0.30		0.00	Q5JPE7 139.44 Nodal modulator 2
	0.54		0.45	Q15233 54.231 Non-POU domain-containing octamer-binding protein
	0.77		0.69	Q14980 238.26 Nuclear mitotic apparatus protein 1
	0.54		0.69	P57740 106.37 Nuclear pore complex protein Nup107
	0.35		1.02	Q14686 219.14 Nuclear receptor coactivator 6
	0.45		0.00	P67809 35.924 Nuclease-sensitive element-binding protein 1

APPENDIX A. FULL LIST OF MS-IDENTIFIED PROTEINS

log (MS2 count) aaECM	log (MS2 count) osteoECM	Protein IDs	MW [kDa]	Descriptions
	0.52		0.39	Q9NR30 87.343 Nucleolar RNA helicase 2
	0.00		1.62	P19338 76.613 Nucleolin
	1.14		1.16	P06748 32.575 Nucleophosmin
	0.15		0.00	P12270 267.29 Nucleoprotein TPR
	0.39		0.48	Q9BSD7 20.713 Nucleoside-triphosphatase C1orf57
	1.19		1.87	Q8WX93 150.56 Palladin
	0.65		0.00	O75475 60.103 PC4 and SFRS1-interacting protein
	0.66		0.80	O00151 36.071 PDZ and LIM domain protein 1
	0.30		0.30	Q96JY6 37.458 PDZ and LIM domain protein 2
	1.47		1.28	P50479 35.398 PDZ and LIM domain protein 4
	0.78		1.20	Q96HC4 63.944 PDZ and LIM domain protein 5
	0.62		0.52	Q9NR12 49.844 PDZ and LIM domain protein 7
	1.43		1.65	P26022 41.975 Pentraxin-related protein PTX3
	1.35		1.46	P62937 18.012 Peptidyl-prolyl cis-trans isomerase A
	0.69		0.39	Q96AY3 64.244 Peptidyl-prolyl cis-trans isomerase FKBP10
	0.65		0.42	O60664 47.074 Perilipin-3
	2.99		2.33	Q15063 93.313 Periostin
	1.34		1.48	Q92626 165.27 Peroxidasin homolog
	1.37		1.47	Q06830 22.11 Peroxiredoxin-1
	0.92		0.84	P32119 21.892 Peroxiredoxin-2
	0.45		0.50	Q13162 30.54 Peroxiredoxin-4
	0.64		0.74	P30044 22.086 Peroxiredoxin-5, mitochondrial
	0.30		0.60	P30041 25.035 Peroxiredoxin-6
	0.62		0.85	P51659 79.685 Peroxisomal multifunctional enzyme type 2
	0.57		0.59	Q00325 40.094 Phosphate carrier protein, mitochondrial
	0.54		0.00	Q16822 70.729 Phosphoenolpyruvate carboxykinase [GTP], mitochondrial
	0.65		0.63	P36871 61.448 Phosphoglucosmutase-1
	1.63		1.66	P00558 44.614 Phosphoglycerate kinase 1
	1.36		1.30	Q6NYC8 67.942 Phostensin
	1.44		1.54	P36955 46.312 Pigment epithelium-derived factor
	0.00		0.87	Q13835 82.86 Plakophilin-1
	1.52		1.43	P05121 45.059 Plasminogen activator inhibitor 1
	0.90		0.95	P13797 70.81 Plastin-3
	0.83		0.39	P68402 25.569 Platelet-activating factor acetylhydrolase IB subunit beta
	2.79		3.16	Q15149 531.78 Plectin
	1.17		1.35	Q7Z5L7 68.975 Podocan
	0.24		0.65	Q9UKK3 192.59 Poly [ADP-ribose] polymerase 4
	0.57		0.80	Q15365 37.497 Poly(rC)-binding protein 1
	0.60		0.76	Q15366 38.58 Poly(rC)-binding protein 2
	0.73		0.50	P11940 70.67 Polyadenylate-binding protein 1
	0.71		0.65	Q9BY77 46.089 Polymerase delta-interacting protein 3
	2.11		2.23	Q6NZI2 43.476 Polymerase I and transcript release factor
	0.42		0.39	P26599 57.221 Polypyrimidine tract-binding protein 1
	2.34		2.25	P0CG48 77.028 Polyubiquitin-C
	0.48		0.57	O60831 19.258 PRA1 family protein 2
	1.25		1.39	Q2NL82 91.809 Pre-rRNA-processing protein TSR1 homolog
	0.54		0.88	P20742 163.86 Pregnancy zone protein
	2.52		2.39	P02545 74.139 Prelamin-A/C
	0.24		0.30	Q96IZ0 36.567 PRKC apoptosis WT1 regulator protein





























































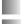




































APPENDIX A. FULL LIST OF MS-IDENTIFIED PROTEINS

log (MS2 count) aaECM	log (MS2 count) osteoECM	Protein IDs	MW [kDa]	Descriptions
	0.75		1.50	Q3SY69 101.74 Probable 10-formyltetrahydrofolate dehydrogenase ALDH1L2
	0.85		0.78	P17844 69.147 Probable ATP-dependent RNA helicase DDX5
	0.88		0.39	Q02809 83.549 Procollagen-lysine,2-oxoglutarate 5-dioxygenase 1
	1.48		1.18	P07737 15.054 Profilin-1
	1.00		1.36	Q8WUM4 96.022 Programmed cell death 6-interacting protein
	0.65		0.78	P35232 29.804 Prohibitin
	0.56		0.97	Q99623 33.296 Prohibitin-2
	0.00		0.85	P12273 16.572 Prolactin-inducible protein
	2.15		2.52	P51888 43.809 Prolargin
	0.59		0.96	Q07954 504.6 Prolow-density lipoprotein receptor-related protein 1
	0.35		0.30	Q32P28 83.393 Prolyl 3-hydroxylase 1
	0.00		0.39	P49720 22.949 Proteasome subunit beta type-3
	1.32		1.95	O00622 42.026 Protein CYR61
	1.62		1.63	P07237 57.116 Protein disulfide-isomerase
	0.91		1.29	P30101 56.782 Protein disulfide-isomerase A3
	0.45		0.00	Q15084 48.121 Protein disulfide-isomerase A6
	0.42		0.30	Q8NCA5 55.4 Protein FAM98A
	0.30		0.60	Q86VS8 83.125 Protein Hook homolog 3
	0.50		0.30	P17252 76.749 Protein kinase C alpha type
	1.18		1.41	Q969G5 27.701 Protein kinase C delta-binding protein
	0.35		0.67	Q86UE4 63.836 Protein LYRIC
	0.15		0.30	Q9HAS0 44.621 Protein Njmu-R1
	0.00		0.30	Q8IWE2 60.741 Protein NOXP20
	0.93		1.52	O14974 115.28 Protein phosphatase 1 regulatory subunit 12A
	1.22		0.86	Q14690 208.7 Protein RRP5 homolog
	0.57		1.00	P60903 11.203 Protein S100-A10
	0.59		0.93	P31949 11.74 Protein S100-A11
	0.15		0.35	P05109 10.834 Protein S100-A8
	0.00		0.65	P06702 13.242 Protein S100-A9
	0.74		0.50	Q9H3U1 103.08 Protein unc-45 homolog A
	0.50		0.80	Q9H1J7 40.323 Protein Wnt-5b
	2.54		2.19	P21980 77.328 Protein-glutamine gamma-glutamyltransferase 2
	0.15		0.62	Q08188 76.631 Protein-glutamine gamma-glutamyltransferase E
	0.62		0.75	P28300 46.944 Protein-lysine 6-oxidase
	0.57		1.20	P00734 70.036 Prothrombin
	0.48		0.74	Q14517 506.27 Protocadherin Fat 1
	0.57		0.24	Q58FF8 44.348 Putative heat shock protein HSP 90-beta 2
	1.13		0.70	Q2TB90 102.54 Putative hexokinase HKDC1
	0.68		0.57	P46087 89.301 Putative ribosomal RNA methyltransferase NOP2
	0.30		0.15	P08559 43.295 Pyruvate dehydrogenase E1 component subunit alpha, somatic form, mitochondrial
	2.32		2.20	P14618 57.936 Pyruvate kinase isozymes M1/M2
	1.95		1.86	P46940 189.25 Ras GTPase-activating-like protein IQGAP1
	0.24		0.54	P63000 21.45 Ras-related C3 botulinum toxin substrate 1
	0.56		0.59	P61026 22.541 Ras-related protein Rab-10
	0.96		1.09	Q15907 24.488 Ras-related protein Rab-11B
	0.54		0.75	P61106 23.897 Ras-related protein Rab-14
	0.69		0.87	P62820 22.677 Ras-related protein Rab-1A
	0.50		0.89	P51148 23.482 Ras-related protein Rab-5C
	0.45		0.63	P51149 23.489 Ras-related protein Rab-7a











































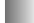













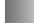

























APPENDIX A. FULL LIST OF MS-IDENTIFIED PROTEINS

log (MS2 count) aaECM	log (MS2 count) osteoECM	Protein IDs	MW [kDa]	Descriptions
<div></div> 0.57	<div></div> 0.84	P61224	20.825	Ras-related protein Rap-1b
<div></div> 0.30		Q96D15	37.493	Reticulocalbin-3
<div></div> 0.50	<div></div> 0.54	Q9NQC3	129.93	Reticulon-4
<div></div> 0.54	<div></div> 0.59	P52565	23.207	Rho GDP-dissociation inhibitor 1
<div></div> 0.80	<div></div> 0.42	Q07960	50.435	Rho GTPase-activating protein 1
<div></div> 0.45	<div></div> 0.15	P08134	22.006	Rho-related GTP-binding protein RhoC RhoB =RHO
<div></div> 1.36	<div></div> 1.38	P13489	49.973	Ribonuclease inhibitor
<div></div> 0.59	<div></div> 0.39	Q9Y3A5	28.763	Ribosome maturation protein SBDS
<div></div> 1.57	<div></div> 1.56	Q9P2E9	152.47	Ribosome-binding protein 1
<div></div> 0.80	<div></div> 1.22	Q96PK6	69.491	RNA-binding protein 14
<div></div> 0.45	<div></div> 0.69	P49756	100.18	RNA-binding protein 25
<div></div> 0.52	<div></div> 0.72	Q9UKM9	32.463	RNA-binding protein Raly
<div></div> 0.89	<div></div> 0.85	A6NHQ2	34.675	rRNA/tRNA 2-O-methyltransferase fibrillarin-like protein 1
<div></div> 1.18	<div></div> 0.42	Q9Y265	50.227	RuvB-like 1
<div></div> 0.00	<div></div> 0.54	Q92765	36.254	Secreted frizzled-related protein 3
<div></div> 0.70	<div></div> 1.19	Q13228	52.39	Selenium-binding protein 1
<div></div> 0.42	<div></div> 0.87	Q99985	85.206	Semaphorin-3C
<div></div> 0.30	<div></div> 0.30	O75326	74.823	Semaphorin-7A
<div></div> 0.57	<div></div> 0.39	Q9NVA2	49.398	Septin-11
<div></div> 1.06	<div></div> 0.67	Q15019	41.487	Septin-2
<div></div> 1.15	<div></div> 0.48	Q16181	50.679	Septin-7
<div></div> 0.60	<div></div> 0.87	Q9UHD8	65.401	Septin-9
<div></div> 0.81	<div></div> 0.30	P34897	55.992	Serine hydroxymethyltransferase, mitochondrial
<div></div> 2.02	<div></div> 2.07	O95084	43.001	Serine protease 23
<div></div> 2.53	<div></div> 2.53	Q92743	51.286	Serine protease HTRA1
<div></div> 0.00	<div></div> 0.63	P84103	19.329	Serine/arginine-rich splicing factor 3
<div></div> 0.30	<div></div> 0.54	P62140	37.186	Serine/threonine-protein phosphatase PP1-beta catalytic subunit
<div></div> 0.39	<div></div> 0.39	Q96P63	46.276	Serpin B12
<div></div> 0.15	<div></div> 0.24	P29508	44.564	Serpin B3
<div></div> 2.25	<div></div> 1.96	P50454	46.44	Serpin H1
<div></div> 3.21	<div></div> 3.20	P02768	69.366	Serum albumin
<div></div> 0.35	<div></div> 0.45	A1X283	101.58	SH3 and PX domain-containing protein 2B
<div></div> 0.39	<div></div> 0.50	Q9BWM7	35.978	Sideroflexin-3
<div></div> 1.51	<div></div> 1.72	Q8IX30	109.28	Signal peptide, CUB and EGF-like domain-containing protein 3
<div></div> 0.69	<div></div> 0.59	P42224	87.334	Signal transducer and activator of transcription 1-alpha/beta
<div></div> 0.15	<div></div> 0.54	O43166	200.03	Signal-induced proliferation-associated 1-like protein 1
<div></div> 0.72	<div></div> 0.89	P53814	99.461	Smoothelin
<div></div> 0.39	<div></div> 0.45	P05023	112.89	Sodium/potassium-transporting ATPase subunit alpha-1
<div></div> 0.99	<div></div> 0.91	P09486	34.632	SPARC
<div></div> 0.00	<div></div> 0.80	Q9H4F8	48.162	SPARC-related modular calcium-binding protein 1
<div></div> 1.95	<div></div> 1.92	Q13813	284.54	Spectrin alpha chain, brain
<div></div> 1.47	<div></div> 1.50	Q01082	274.61	Spectrin beta chain, brain 1
<div></div> 0.45	<div></div> 0.54	P19623	33.824	Spermidine synthase
<div></div> 0.30	<div></div> 0.45	Q13435	100.23	Splicing factor 3B subunit 2
<div></div> 0.59	<div></div> 0.91	P23246	76.149	Splicing factor, proline- and glutamine-rich
<div></div> 1.03	<div></div> 1.32	Q7KZF4	102	Staphylococcal nuclease domain-containing protein 1
<div></div> 0.59	<div></div> 0.59	Q9UJZ1	38.534	Stomatin-like protein 2
<div></div> 1.62	<div></div> 1.59	P38646	73.68	Stress-70 protein, mitochondrial
<div></div> 0.84	<div></div> 0.15	P48061	10.666	Stromal cell-derived factor 1

APPENDIX A. FULL LIST OF MS-IDENTIFIED PROTEINS

log (MS2 count) aaECM	log (MS2 count) osteoECM	Protein IDs	MW [kDa]	Descriptions
	0.35		0.59	Q9UQE7 141.54 Structural maintenance of chromosomes protein 3
	0.00		1.46	P02814 8.1875 Submaxillary gland androgen-regulated protein 3B
	0.45		0.35	Q9Y6N5 49.96 Sulfide:quinone oxidoreductase, mitochondrial
	0.52		0.24	Q9UH99 80.31 SUN domain-containing protein 2
	0.65		0.24	O95425 247.74 Supervillin
	0.45		0.54	O15260 30.394 Surfeit locus protein 4
	0.56		0.72	Q99536 41.92 Synaptic vesicle membrane protein VAT-1 homolog
	0.42		0.77	Q8N3V7 99.462 Synaptopodin
	1.34		1.64	Q9UMS6 117.51 Synaptopodin-2
	0.87		1.35	P17987 60.343 T-complex protein 1 subunit alpha
	1.58		0.87	P78371 57.488 T-complex protein 1 subunit beta
	0.87		1.20	P50991 57.924 T-complex protein 1 subunit delta
	1.03		0.85	P48643 59.67 T-complex protein 1 subunit epsilon
	0.98		1.09	Q99832 59.366 T-complex protein 1 subunit eta
	0.73		0.65	P49368 60.533 T-complex protein 1 subunit gamma
	0.83		1.03	P50990 59.62 T-complex protein 1 subunit theta
	1.07		1.21	P40227 58.024 T-complex protein 1 subunit zeta
	2.31		2.42	Q9Y490 269.76 Talin-1
	0.56		1.13	Q7Z7G0 118.64 Target of Nesh-SH3
	3.32		2.84	P24821 240.85 Tenascin
	0.65		0.50	Q9HBL0 185.7 Tensin-1
	0.15		0.85	Q9UGI8 47.996 Testin
	0.35		0.74	P30048 27.692 Thioredoxin-dependent peroxide reductase, mitochondrial
	0.82		0.84	P26639 83.434 Threonyl-tRNA synthetase, cytoplasmic
	0.45		1.03	Q6ZMP0 112.45 Thrombospondin type-1 domain-containing protein 4
	3.25		3.03	P07996 129.38 Thrombospondin-1
	1.21		0.63	P35442 129.99 Thrombospondin-2
	1.36		1.40	P04216 17.935 Thy-1 membrane glycoprotein 2
	0.39		0.93	P05543 46.324 Thyroxine-binding globulin
	0.30		0.15	Q8WZ42 3816.1 Titin
	0.42		0.48	Q5JTV8 66.248 Torsin-1A-interacting protein 1
	0.65		0.50	P37837 37.54 Transaldolase
	0.87		0.66	O43294 49.814 Transforming growth factor beta-1-induced transcript 1 protein
	3.00		2.58	Q15582 74.68 Transforming growth factor-beta-induced protein ig-h3
	1.76		1.62	Q01995 22.611 Transgelin
	1.00		1.14	P37802 22.391 Transgelin-2
	1.68		1.57	P55072 89.321 Transitional endoplasmic reticulum ATPase
	0.48		0.54	P13693 19.595 Translationally-controlled tumor protein
	0.30		0.30	P43307 32.235 Translocon-associated protein subunit alpha
	0.39		0.30	P51571 18.998 Translocon-associated protein subunit delta
	0.24		0.15	P57088 27.978 Transmembrane protein 33
	0.66		0.59	Q9BTV4 44.875 Transmembrane protein 43
	0.67		0.89	Q92973 102.35 Transportin-1
	0.39		0.45	P53007 34.012 Tricarboxylate transport protein, mitochondrial
	1.19		1.71	P40939 82.999 Trifunctional enzyme subunit alpha, mitochondrial
	1.31		1.52	P55084 51.294 Trifunctional enzyme subunit beta, mitochondrial
	0.62		0.98	Q9H2D6 261.37 TRIO and F-actin-binding protein
	0.72		1.09	P60174 26.669 Triosephosphate isomerase
	0.54		0.15	Q9NZR1 39.595 Tropomodulin-2

APPENDIX A. FULL LIST OF MS-IDENTIFIED PROTEINS

log (MS2 count) aaECM	log (MS2 count) osteoECM	Protein IDs	MW [kDa]	Descriptions		
	0.93		1.18	Q9NYL9	39.594	Tropomodulin-3
	2.35		2.14	P09493	32.708	Tropomyosin alpha-1 chain
	0.52		0.42	P67936	28.521	Tropomyosin alpha-4 chain
	1.51		1.25	P07951	32.85	Tropomyosin beta chain
	2.15		1.78	P07437	49.67	Tubulin beta chain
	1.18		1.10	Q13885	49.906	Tubulin beta-2A chain
	2.28		2.09	P68371	49.83	Tubulin beta-2C chain
	1.00		0.39	Q13509	50.432	Tubulin beta-3 chain
	0.88		0.99	Q9BUF5	49.857	Tubulin beta-6 chain
	0.52		0.84	Q9GZM7	52.387	Tubulointerstitial nephritis antigen-like
	0.48		0.50	P54578	56.068	Ubiquitin carboxyl-terminal hydrolase 14
	0.81		1.23	P22314	117.85	Ubiquitin-like modifier-activating enzyme 1
	1.35		1.24	O60701	55.023	UDP-glucose 6-dehydrogenase
	0.45		0.54	Q16222	58.768	UDP-N-acetylhexosamine pyrophosphorylase
	0.56		0.81	P30085	22.222	UMP-CMP kinase
	0.30		0.15	Q8N766	111.76	Uncharacterized protein KIAA0090
	0.30		0.42	Q9P266	148.35	Uncharacterized protein KIAA1462
	0.74		0.84	P46939	394.46	Utrophin
	1.26		1.07	Q9BZF9	162.5	Uveal autoantigen with coiled-coil domains and ankyrin repeats
	0.00		0.87	Q5VU13	43.89	V-set and immunoglobulin domain-containing protein 8
	0.66		1.00	P61421	40.329	V-type proton ATPase subunit d 1
	0.79		0.98	P36543	26.145	V-type proton ATPase subunit E 1
	0.30		0.24	O75436	38.169	Vacuolar protein sorting-associated protein 26A
	0.65		1.08	Q96QK1	91.706	Vacuolar protein sorting-associated protein 35
	0.35		0.24	P50552	39.829	Vasodilator-stimulated phosphoprotein
	1.20		1.48	P13611	372.82	Versican core protein
	0.15		0.42	P51809	24.935	Vesicle-associated membrane protein 7
	0.67		0.50	P46459	82.593	Vesicle-fusing ATPase
	1.20		0.98	Q00341	141.45	Vigilin
	3.50		3.20	P08670	53.651	Vimentin
	1.97		2.02	P18206	123.8	Vinculin
	0.00		0.71	P02774	52.963	Vitamin D-binding protein
	2.16		2.01	P04004	54.305	Vitronectin
	1.31		1.28	P21796	30.772	Voltage-dependent anion-selective channel protein 1
	1.62		1.50	P45880	31.566	Voltage-dependent anion-selective channel protein 2
	0.54		0.72	Q9Y277	30.658	Voltage-dependent anion-selective channel protein 3
	0.75		1.36	P54289	124.57	Voltage-dependent calcium channel subunit alpha-2/delta-1
	0.39		0.60	Q6PCB0	46.804	von Willebrand factor A domain-containing protein 1
	0.94		1.39	O75083	66.193	WD repeat-containing protein 1
	0.98		0.63	Q86UP3	393.73	Zinc finger homeobox protein 4
	0.24		0.65	Q15942	61.277	Zyxin

Selbstständigkeitserklärung

Hiermit versichere ich, dass ich die vorliegende Arbeit ohne unzulässige Hilfe Dritter und ohne Benutzung anderer als der angegebenen Hilfsmittel angefertigt habe; die aus fremden Quellen direkt oder indirekt übernommenen Gedanken sind als solche kenntlich gemacht. Die Arbeit wurde bisher weder im Inland noch im Ausland in gleicher oder ähnlicher Form einer anderen Prüfungsbehörde vorgelegt.

Die vorliegende Dissertation wurde am Leibniz-Institut für Polymerforschung Dresden e.V. in der Arbeitsgruppe Biofunktionelle Polymermaterialien am Max Bergmann Zentrum für Biomaterialien unter der Betreuung von Herrn Prof. Dr. Carsten Werner angefertigt.

Bei der Auswahl und Auswertung des Materials sowie bei der Herstellung des Manuskripts habe ich Unterstützungsleistungen von folgenden Personen erhalten:

- Prof. Dr. Carsten Werner
- Dr. Philipp Seib
- Dr. Uwe Freudenberg
- Dr. Jens Friedrichs
- Christian Niehage

Die Promotionsordnung der Fakultät Mathematik und Naturwissenschaften der Technischen Universität Dresden vom 23. Februar 2011 erkenne ich hiermit an.

Dresden, den 29.07.2011

Marina Prewitz